SURFACE PROPERTY MODIFICATION OF COATINGS VIA SELF-STRATIFICATION

A Dissertation
Submitted to the Graduate Faculty
of the
North Dakota State University
of Agriculture and Applied Science

By

Robert Joseph Pieper

In Partial Fulfillment of the Requirements
for the Degree of
DOCTOR OF PHILOSOPHY

Major Department:
Coatings and Polymeric Materials

September 2010

Fargo, North Dakota

North Dakota State University
Graduate School

Title

Surface Property of Coatings via Self-Stratification

By

Robert Joseph Pieper

The Supervisory Committee certifies that this ***disquisition*** complies with North Dakota State University's regulations and meets the accepted standards for the degree of

DOCTOR OF PHILOSOPHY

SUPERVISORY COMMITTEE:

Dr. Dean C. Webster
Chair

Dr. Stuart Croll

Dr. Sanku Mallik

Dr. Linda Helstern

Approved:

7th Sept 2010
Date

Dr. Stuart Croll
Department Chair

ABSTRACT

Pieper, Robert Joseph, Ph.D., Department of Coatings and Polymeric Materials, College of Science and Mathematics, North Dakota State University, September 2010. Surface Property Modification of Coatings via Self-Stratification. Major Professor: Dr. Dean C. Webster.

Biological fouling occurs everywhere in the marine environment and is a significant problem for marine vessels. Anti-fouling coatings have been used effectively to prevent fouling; however, these coatings harm non-targeted sea-life. Fouling-release coatings (FRC) appear to be an alternative way to combat fouling. FRC do not necessarily prevent the settlement of marine organisms but rather allow their easy removal with application of shear to the coatings surface. These coatings must be non-toxic, non-leaching, have low surface energy, low modulus, and durability to provide easy removal of marine organisms. Here the goal is to develop FRC based on thermosetting siloxane-polyurethane, amphiphilic polyurethane, and zwitterionic/amphiphilic polyurethane systems. A combinatorial high-throughput approach has been taken in order to explore the variables that may affect the performance of the final coatings. Libraries of acrylic polyols were synthesized using combinatorial high-throughput techniques by either batch or semi-batch processes. The design of the experiments for the batch and semi-batch processes were done combinatorially to explore a range of compositions and various reaction process variables that cannot be accomplished or are not suitable for single reaction experiments. Characterization with Rapid-GPC, high-throughput DSC, and gravimetrically calculated percent solids verified the effects of different reaction conditions on the MW, glass transition temperatures, and

percent conversion on the different compositions of acrylic polyols. Coatings were characterized for their surface energy, pseudobarnacle pull-off adhesion, and were subjected to bioassays including marine bacteria, algae, and barnacles. From the performance properties results the acrylic polyol containing 20% hydroxyethyl acrylate and 80% butyl acrylate was selected for further siloxane-polyurethane formulation and were subjected to the same physical, mechanical, and performance testing. Amphiphilic copolymers based on PDMS molecular weight and the addition of PEG based polymer blocks on the properties of acrylic-polyurethane coatings were explored. The key properties screened were surface energy, determined by contact angle measurements using water and methylene iodide, dynamic water contact angle, and pseudo-barnacle adhesion properties. Coatings were generally stable and showed an increase in water contact angle following water immersion. After water immersion the coatings, in general, had lower pseudo-barnacle adhesion due to possible surface rearrangement. Coatings were also evaluated against several marine bacteria, algae, and barnacles. The synthesis of a new amphiphilic macroinitiator via Michael Addition reaction of APT-PDMS and PEA-6 and subsequent reaction with ATRP initiator produced the macroinitiator for the synthesis of a novel zwitterionic/amphiphilic penta-block copolymer. The penta-block copolymer was reacted with an acrylic polyol (80% butyl acrylate, 20% 2-hydroxyethyl acrylate) and an aliphatic isocyanate to form a crosslinked coating system. The data from all of the biological assays indicates that the novel coatings are able to resist fouling and have low fouling adhesion for the broad variety of fouling organisms tested.

ACKNOWLEDGEMENTS

Though only my name appears on the cover of this dissertation, a great many people have contributed to its production. I owe my gratitude to all those people who have made this dissertation possible and because of whom my graduate experience has been one that I will cherish forever.

My deepest gratitude is to my advisor, Dr. Dean C. Webster. I have been amazingly fortunate to have an advisor who gave me the freedom to explore on my own and at the same time the guidance to recover when my steps faltered. Dr. Webster taught me how to question thoughts and express ideas. His patience and support helped me overcome many crises and finish this dissertation. I would like to thank my committee members, Dr. Stuart G. Croll, Dr. Sanku Mallik, and Dr. Linda Helstern for their guidance and time over the years.

I am also indebted to the past and present members of the Webster Group with whom I have interacted during the course of my graduate years. Particularly, I would like to acknowledge Dr. Abdullah Ekin, Dr. Partha Majumdar, Dr. Mohammed J. Nasrullah, Stacy Sommer, Rajan Bodkhe, and Dr. Alex Kugel for the many valuable discussions that helped me understand my research area better. I appreciate the efforts of my undergraduate students, Scott Ennis and Hanna Fischer, my sincere thanks for their contributions to my research. I would like to thank David Christianson for assistance with the use of the high-throughput instruments; all members of the CNSE biology lab; Heidi Docktor for assistance in the instrument lab; Carol Johnson, Jacinda Wollan, and Kathy Backen-Andersen for their constant effort to make life easier in the department. Thanks go out to my

friends that I have made at UWSP and NDSU, thank you for all the support through the years.

Special thanks go out to my closest friend John Sheski; you helped me stay sane through all of these difficult years. Your support and care helped me overcome setbacks and stay focused on my graduate study and I greatly value your friendship and I deeply appreciate your belief in me. To my friend Sean Essinger, whose life was tragically ended short, but I will forever be grateful of the time we had together and I look forward to someday seeing you again. Last but not least, I would like to thank my fiancé and best friend, Alexis Pegram. You saw me struggle through the years but never stopped believing in me. You stood by me and gave me encouragement and I will be forever grateful.

DEDICATION

I would like to dedicate this dissertation to my parents Joseph and Judy Pieper, my sister Megan Pieper, and my Grandparents. Words can not thank you enough for all the sacrifices you made to get me to this point in my life. Thank you for your constant support, encouragement, love and belief in me even during the difficult years. Even though you, Grandma and Grandpa Pieper and Grandma Mueller, have passed on I know that you have been watching over me, smiling and are proud of me.

TABLE OF CONTENTS

LIST OF TABLES

LIST OF FIGURES

LIST OF SCHEMES

CHAPTER 1. GENERAL INTRODUCTION

The research presented in this dissertation involves the development and synthesis of fouling-release siloxane acrylic-polyurethanes, amphiphilic acrylic-polyurethanes, and zwitterionic/amphiphilic acrylic-polyurethane coating systems for marine application. Experimental coatings were characterized by surface energy and pseudo-barnacle adhesion and the promising candidates were used for further analysis with analytical tools and biological workflows to understand their different structure-property behaviors and their interactions as well as performance against marine organisms.

1.1. Overview of Anti-fouling and Fouling-Release Coatings

Biological fouling occurs everywhere in the marine environment and is a significant problem for marine vessels. Some of the most common biological fouling sites are ship hulls, propellers, heat exchangers, water cooling pipes and even ballast water. All of which results in a large number of undesirable effects on the ships' operational performance and capabilities. Biological fouling results in frictional resistance and increased hull roughness which leads to increased fuel consumption decreased maximum attainable speed and promotion of corrosion. The increase in roughness and weight may result in an increase of fuel consumption by as much as 40% and overall voyage cost of up to 70%.[1] Another consequence of biological fouling is the frequency of cleaning and dry-docking, resulting in wasted time and natural resources. In addition, during hull repair and during dry-docking, much chemical waste is produced and pollutes the environment. One other consequence of biological fouling is the introduction of

invasive and non-invasive species into environments where they do not actually belong.[1-3]

1.1.1. The process of marine biofouling

The marine environment is very complex and still not well understood. More than 4,000 species have been identified as foulants that are involved in biological fouling processes, which is a small number in comparison to the known marine species. Temperature, salinity, water flow, and type of micronutrients in the water control the type and number of foulants and only those foulants that have the ability to adapt to the varying environment can adhere strong enough to avoid being washed off. The fouling process has been considered to consist of four main stages as shown in Figure 1.1.

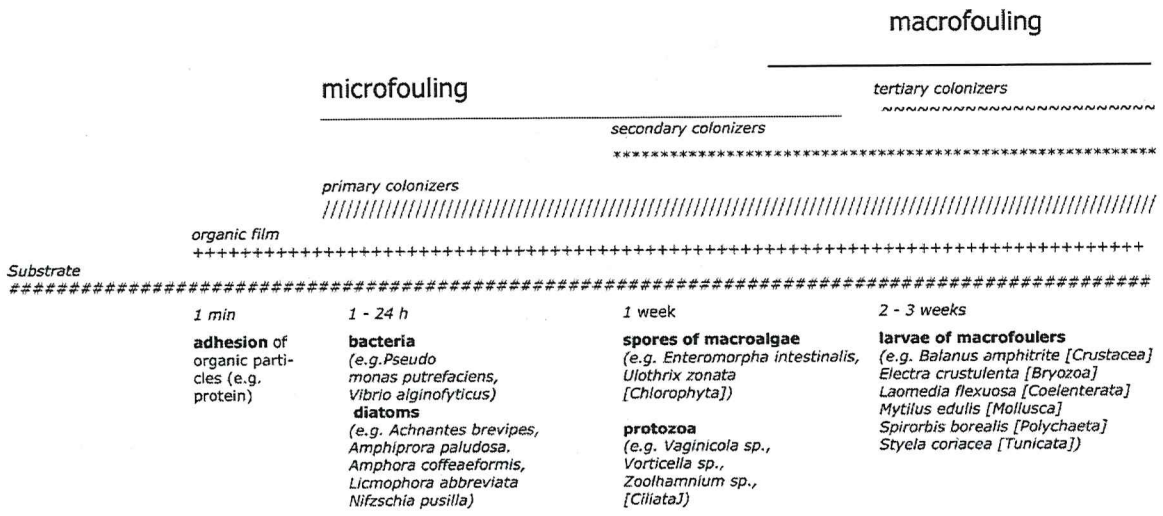

Figure 1.1. The process of biofouling (Reproduced from Reference 1)

The first stage is the adsorption, formation and growth of a conditioning film by dissolved organic molecules, such as proteins and polysaccharides that are present in the marine environment. In around a minute these organic molecules

quickly accumulate on the surface forming the conditioning film. The second stage is the settlement and growth of microorganisms, such as bacteria and diatoms to the conditioning film, producing a primary slime film; this film takes 1-24 hours to develop. The third stage is the addition of algal spores and marine fungi, which continue to attach to the slime film and create a foundation for the macrofoulers to attach, usually occurring within the first week immersion. The final stage is adhesion of tertiary colonizers which are marine invertebrate larvae of macrofoulers such as barnacle cyprids, tube worms, mollusks, and bryozoans, which take place after 2-3 weeks of immersion. However, different species of marine organisms appear to respond differently when considering settlement, which does not make this initial fouling process develop in a random fashion. Instead, conditions must be favorable for the settlement of the primary and secondary colonizers, including proper pH, humidity and nutrient availability.

1.1.2. Development of anti-fouling coatings

For more than 2000 years the disadvantages of marine biofouling have been recognized and attempts at combating biofouling have been divided into two main approaches: anti-fouling coatings and fouling-release coatings. Anti-fouling coatings prevent the growth of marine organisms by typically using toxic compounds, whereas, fouling-release coatings do not necessarily inhibit settlement of marine organisms, but limit the ability of the fouling organism to form a strong adhesive bond to the coating surface. Ideally the speed of the vessel would create enough shear to dislodge the organisms from the coating.[4]

The best solution to combat biological fouling has been the use of tributyltin (TBT) containing compounds and tributyltin self-polishing copolymer (TBT-SPC) anti-fouling coatings. The binders for these paints are primarily acrylic copolymers containing pendant side chains of tin acrylate coupled to the backbone by an ester linkage, which are hydrolyzed by water to form carboxylic groups causing the copolymer to become soluble and release tin-containing toxins. Self-polishing behavior of the paints is achieved through the erosion process of the polymeric binder, enabling the release of incorporated biocides at a constant rate. When in contact with seawater, the coatings exhibit a thin surface erosion zone controlled by hydrolysis/erosion that leads to a constantly polished surface. TBT-SPC's have been very effective in combating marine fouling by the slow release of TBT compounds slowly into the surrounding marine environment.[5] However, the release of TBT compounds persists in the water and cause deformations of non-targeted sea-life by entering into their food chains. Therefore, The Marine Environmental Protection Committee (MEPC) of The International Maritime Organization (IMO) proposed the deadline of January 1, 2003, prohibiting the application of new TBT containing coatings and the second deadline of January 1, 2008, for complete removal of TBT containing coatings from all marine vessels.[4,6]

Another approach in anti-fouling marine coatings industry is the use of tin-free ablative coatings technology. Ablative binder systems that incorporate cuprous oxide have been used because it is a more environmentally friendly coating. Similar to self-polishing coatings, the composition of these ablative tin-free coatings consists of crosslinked polymeric networks made from polymers with

hydrolyzable functional groups. Once hydrolyzed, these functional groups release small molecules and create a hydrophilic site on the polymer backbone. Once the polymer backbone accumulates an adequate number of hydrophilic sites, it becomes water soluble and is washed away from the coatings surface, taking with it any marine organisms attached. Cu-acrylate coatings where the copper complex is bound to an acrylic matrix have shown to be active up to three years.[1] The advantage of copper compounds when compared with other pigments is its low solubility, because of this insolubility, the copper precipitates rapidly decreasing its toxicity.

Another research area in anti-fouling marine coatings is the use of co-biocides or booster biocides to prevent marine fouling. Biocides can be classified under two main categories: booster biocides and natural biocides. The basis of the use of booster biocides comes from their biocidal activates towards organisms such as bacteria and to kill marine organisms that cuprous oxide does not. The most commonly used booster biocides are the non-metal based herbicides Irgarol 1051, Diuron, Sea-nine 211, Kathon 5287, Chlorothalonil, Dichlofluanid, Thiram, and metal-based biocides Zinc pyrithione, Ziram, Maneb, and Zineb. The booster biocides antifouling coatings have been formulated directly with the paint ingredients, adsorbed on to a carrier (nanoparticles), and sometimes attached to a polymer backbone.[1] The concept of natural biocides comes from observations in nature where the surface of some marine organisms maybe completely fouled while other organism's surfaces are fouling-free. This natural anti-fouling concept has created interest in categorizing the secondary metabolites that might repel or

inhibit fouling organisms. Researchers have directed efforts into extracting compounds from numerous marine organisms such as marine algae,[7-9] sponges,[10,11] and mussels.[12] Studies suggest that many marine organisms release metabolites that deter settlement of other fouling organisms. The secondary metabolites include terpenoids, steroids, fatty acids, aminoacids, heterocyclics, aceogenins, alkaloids, and polyphenolics which, if extracted, could be used as natural, environmentally benign biocides to prevent marine fouling. One of the challenges to incorporate natural biocides into anti-fouling coatings is the addition of them without affecting their biocidal activity and, all the while, keeping the integrity of the anti-fouling coating.[1,13]

1.1.3. Development of fouling-release coatings

One promising technology currently commercialized in the response to the need for a nontoxic coating alternative to toxic anti-fouling paints is that of fouling-release coatings. The advantages of using fouling-release coatings over anti-fouling coatings are; "direct fuel savings of 4% due to improved smoothness and less fouling, extended dry-docking intervals, improved plant utilization, and savings on the reduced transport of fuel to the bunkering ports".[14,15]

Brady has reported the desirable factors in a fouling-release coating as

- "A flexible, linear backbone which introduces no undesirable interactions;
- A sufficient number of surface-active groups which are free to move to the surface, there to impart a surface energy in a desired range;
- Low elastic modulus;

- A surface which is smooth at the molecular level, to avoid infiltration of a biological adhesive leading to mechanical interlocking;
- High molecular mobility in the backbone and surface active sidechains;
- A thickness which controls the fracture mechanics of the interface;.
- Molecules which combine all of the above factors, and are physically and chemically stable for prolonged periods in the marine environment".[6,16]

These factors are needed to better understand and apply the underlying principles of the composition and structure to improve on the design and manufacturing of fouling-release coatings.

The mechanisms by which marine organisms initiate adhesion is by producing an adhesive that wets the substrate that allows the organism to spread upon it, either singly or in combination of chemical bonding, electrostatic interaction, mechanical interlocking, and/or diffusion.[6] So, when developing fouling release coatings it's important to keep marine organism adhesive from wetting the surface and spreading over it. The Baier curve illustrated in Figure 1.2 demonstrates the generalized observation between the critical surface free energy and the relative amount of bioadhesion. This curve shows that surfaces with a surface free energy of 23-25 mN/m are least prone to foul, which is equal to the curves minimum. This minimum of the curve occurs close to the surface energy of polydimethylsiloxane (PDMS).[16]

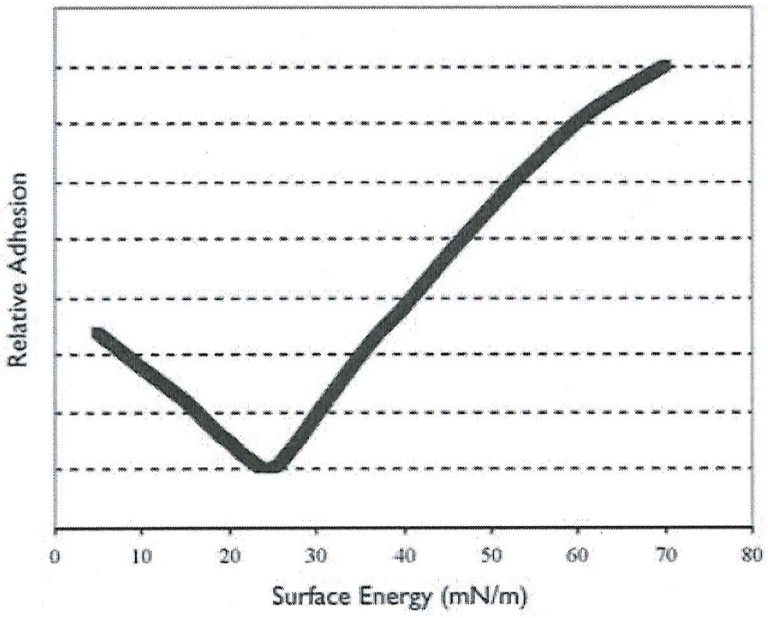

Figure 1.2. The empirical relationship between surface energy and relative bioadhesion. (Reproduced from Reference 16)

For this reason, PDMS has low bioadhesion as a result of the capability of the marine adhesive to slip on the polymer surface. It has been demonstrated that relative bioadhesion does not correlate with surface energy or modulus alone; it does, however, correlate better as a function of the square root of the product of critical surface free energy (γ_c) and elastic modulus (*E*), as shown in Figure 1.3. The minimum in adhesion corresponds with the lowest value of the elastic modulus, but does not correspond with the lowest surface energy, confirming that modulus is, at the very least, as important as surface energy in determining the performance of fouling-release coatings.[4] A very important concept in foulant removal is the fracture mechanics of the foulant at the interface.

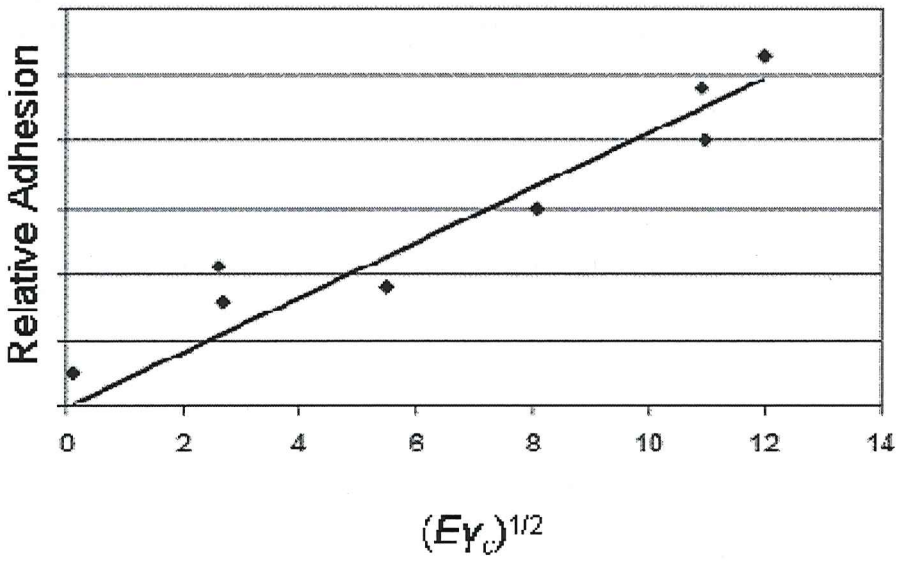

Figure 1.3. Relative adhesion as a function of the square root of the product of elastic modulus and surface energy. (Reproduces from Reference 4)

An important model in measuring the mechanism of removal of marine coatings is the pseudo-barnacle adhesion test illustrated in Figure 1.4. The pseudo-barnacle adhesion test is different from the conventional pull-off adhesion test by attempting to mimic barnacle adhesion and release.[17]

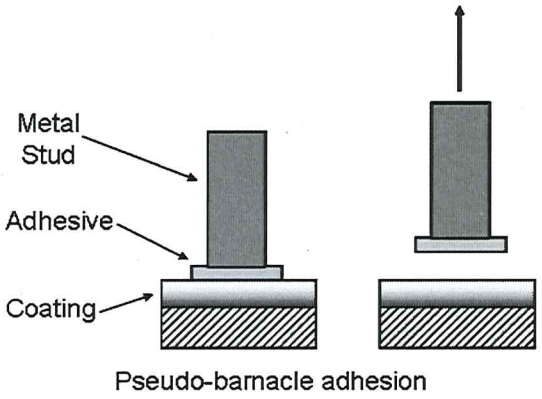

Figure 1.4. Schematic representation of the pseudo-barnacle adhesion test.

The important concepts regarding fouling-release coatings have been identified by early work done by Kendall. Kohl and Singer have investigated the relationship between pull-off force and coating thickness based on Kendall's equation and emphasized the important factors in a fouling-release coating as coating thickness, surface energy, and elastic modulus which all contribute to lower adhesion.[17] Since thickness is not an intrinsic property and easy to adjust depending on application method, the important concepts to focus on when formulating a fouling-release coating are low surface energy and low elastic modulus.

$$P_c = \pi a^2 \left(\frac{2 w_a K_t}{t^*} \right)^{1/2}$$

Where P_c is pull off force, K is bulk modulus of the coating, a is radius of the stud, t is the thickness of the coating, and w_a is Dupre's work of adhesion between the epoxy and the top coat.

Elastic modulus, also known as Young's modulus, is a measure of the stiffness of the material. The higher the value of Young's modulus, the more resistant the material is to mechanical stretching. Young's modulus is measured by the stress applied to the material divided by the strain of the material:

$$E = \sigma / \varepsilon ,$$

where σ is tensile stress and ϵ is tensile strain.

When the material is exposed to cyclical or repetitive of stress and strain, Young's modulus has two components which are storage modulus and loss

modulus. Storage modulus is the energy stored during deformation, and the loss modulus is a measure of the energy converted to heat.[18]

$$E^* = E' + iE'',$$

Where E^* is Young's modulus, E' is the storage modulus, and E'' is the loss modulus.

Surface energy can be defined as the work required to increase the surface area of a substance by unit area. In other words, when a surface is created, the disruption of chemical bonds at that surface is the measure of surface energy. At the molecular level, being present on the surface is less favorable. Bulk material would not exist if being on the surface were more favorable. Every material has different surface energies because each material has different bond strength. Surface energy of solid materials is usually measured by contact angle method using Young's equation as seen in Figure 1.5.

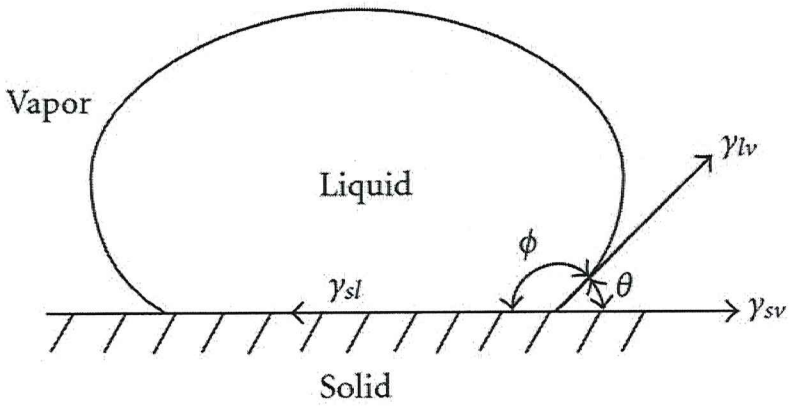

$$\gamma_{lv}\cos\theta = \gamma_{sv} - \gamma_{sl}$$

Figure 1.5. Young's equation for the static contact angle of a liquid drop on a surface.

In Figure 1.5, γ_{lv}, γ_{sv} and γ_{sl} are the surface tension of the solid, liquid and solid-liquid interface, respectively. θ is the so-called contact angle and is the angle drawn from the tangent line from the surface. There are several common methods to calculate surface energy including Zisman, Lewis acid base/van Oss-Good-Chaudhury, Wu, and Owens-Wendt, to name a few. The most widely used method in industrial research to calculate surface energy of the solid polymer is the Owens-Wendt method. In the Owens-Wendt method, contact angles of water and methylene iodide are used to calculate surface energies. Contact angle is measured from the tangent to the solid interface at the contact line. Surface energy usually has two components; polar/hydrogen bonding component and London-Van der Waals/non-polar/dispersive forces component. For the Owens-Wendt method the polar/hydrogen bonding component is measured with the water contact angle and the London-Van der Waals/non-polar/dispersive force component is measured with methylene iodide contact angle:[19]

$$\gamma = \gamma^d + \gamma^h$$

where γ is surface energy, γ^d is the surface energy component from dispersion forces and γ^h is the surface energy component of hydrogen bonding.

The understanding of contact angle can be very difficult when it comes to the measurement on real surfaces. Experimentally, as the contact liquid volume is increased the contact angle value that is seen increases and ultimately reaches a maximum value. This maximum contact angle value is called the advancing contact angle. Similarly, when the contact liquid volume is decreases the contact

angle value that is seen decreases and ultimately reaches a minimum value. The minimum contact angle value is called the receding contact angle. The difference between advancing and receding contact angles is called the contact angle hysteresis.[20]

Advancing contact angle using water (as the test liquid) to the surface measures the hydrophobicity of the surface because water is dispensed on the surface. In contrast, receding contact angle using water (as test liquid) measures the hydrophilicity of the surface because water is aspirated from the surface. The contact angle hysteresis gives information about the difference between hydrophobicity and the hydrophilicity of the surface. Therefore, contact angle hysteresis gives an idea about the stability of the surfaces.[21,22] It has been reported that the lower the contact angle hysteresis of a coating, the better the coatings performance in terms of fouling-release properties, this is because hysteresis appears to be a direct indication of the resistance to liquid or adhesive surface penetration and reconstruction.[23]

The complexities of the surfaces, roughness, impurities in medium, and type of contact angle to be used depending on the surface contact angle measurement and interpretation have not been understood. Wynne et al. and others have reported that impurities present in the test liquid can reduce the contact angle and skew the information about the contact angle as well as surface energy.[24, 25] The most common and practical method to measure contact angle is taking a side view picture of a drop and evaluating the contact angle from the picture.[26] The understanding of the relationship between the advancing/receding

contact angles, the dependence of the interfacial tension of the solid-liquid interface on the surface tensions of the solid and the liquid, and the need to develop standard surfaces for comparing and calibrating contact angle measurements. A lot of progress is still needed in measurement and interpretation of contact angles for complete understanding of surface energies of solid materials.

As previously stated, the performance of fouling-release coatings depends on the surface energy, elastic modulus, and thickness of the coating based on the Kendal equation. Coatings with lower surface energies demonstrate better release because the lower surface energy results in reduced intermolecular attractive forces. Lower elastic modulus also results in lower adhesive strength. Lower pseudo-barnacle adhesion can also result from the lowering of the coatings modulus due to an increase in temperature since modulus is a function of temperature.[27] Also, according to the Kendall equation, an increase in film thickness results in a decrease in pseudo-barnacle adhesion since coating thickness is a function of pull-off force.

Recent studies have shown that pseudo-barnacle adhesion not only depends on the elastic properties of the coating but the geometric properties as well. Chung and researches presented a model where the film thickness was denoted as h and the radius of the stud was denoted as a.[28] A thick film was described as film thickness being much greater than radius of the stud ($a/h \ll 1$). From this model it was found that in thick coatings, pseudo-barnacle adhesion depends on elastic modulus and the radius of the stud:

$$P_c \sim (E/a)^{1/2},$$

where P_c is pseudo-barnacle adhesion, E is elastic modulus, and a is the radius of the stud.

The model also looked at thin coatings which were described as film thickness being much less than radius of the stud (a/h »1). In thin coatings, pseudo-barnacle adhesion depends on elastic modulus and the thickness of the coatings:[28]

$$P_c \sim (E/h)^{1/2},$$

where P_c is pseudo-barnacle adhesion, E is elastic modulus, and h is the thickness of the coating.

Several studies have been reported on the release behavior of coatings. It has been stated that permanent adhesive bonding can be reduced by increasing the mobility of the surface which results in lower pseudo-barnacle adhesion. Additionally, release properties can be enhanced by creating a smooth coating surface. Coatings with rough surfaces have voids were the adhesive can penetrate resulting in mechanical interlocking. Poly(dimethsiloxane) (PDMS) has a very low glass transition temperature, so at normal temperatures the molecules on the surface slide over one another. The sliding molecules result in surface instability and it's because of this surface instability that helps to lower the pseudo-barnacle adhesion.[29]

PDMS is one of the most widely used silicon based polymers. PDMS has received a lot of attention since its commercial introduction in the 1940s and industrially, one billion kg of silicones are produced each year. PDMS has several

unique properties including its particularly low glass transition temperature (-120 °C), good oxidative, thermal, and UV stability, hydrophobicity, biocompatibility, high gas permeability, chemical compatibly, and low surface energy. The most distinctive property of PDMS is its viscoelastic behavior over a range of temperatures. These unique properties of PDMS have resulted in a broad set of applications, which include electrical insulation, biomaterials, and aerospace research.[30,31] The chemical structure of PDMS can be seen in Figure 1.6.

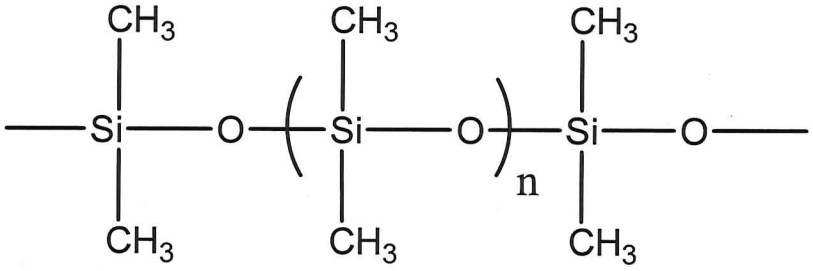

Figure 1.6. Chemical structure of poly(dimethylsiloxane).

PDMS has found widespread use in marine coating applications due to its specific properties including its low surface energy and low modulus. Studies on PDMS have been concentrated on filled and crosslinked PDMS and thermoplastic PDMS-polyurethanes. However, there have been problems encountered with PDMS such low adhesion to primer, insufficient mechanical properties, and the changes of properties especially in PDMS-polyurethanes. In thermoplastic PDMS-polyurethane, good initial properties have been obtained, but after water immersion, the properties changed because of migration of the hydrophobic urethane groups to the surface, changing the materials from a hydrophilic silicone-like surface to a hydrophobic polyurethane-like surface.[32-34] It is because of these

problems that PDMS is usually modified to get practical properties.[35,36] Studies have been conducted in order to combine the fantastic properties of PDMS with other polymeric systems by functionalizing,[37] block copolymerizing,[38] grafting,[39] blending,[40] and crosslinking.[41]

1.2. Summary of Self-stratified, Siloxane-urethane, Amphiphilic, and Zwitterionic/amphiphilic Coatings

1.2.1. Self-stratified coatings

Self-stratifying coatings are coatings that are applied in a single step but phase separate into two or more distinct layers that have different functions within the coating.[42] The concept of self-stratification was first introduced in 1976 by W. Funke. The coatings used for the study consisted of incompatible polymer blends which were dissolved in either solvents or melted on a substrate.[43] The coatings then stratified into a double or multilayer coating where each layer was formed with a distinct polymer.[43-45] There are several factors that affect self-stratification including the degree of incompatibility, glass transition temperature, molecular weight, type of solvent, and surface energy.

Self-stratified coating structures can occur via two possible actions. They can form two sharply separated homophase layers or partially separated when one layer overlaps with the other.[46] Another self-stratification system observed occurred during the crosslinking reaction of a semi-compatible resin with a thermosetting component.[47]

Self-stratifying coatings have two main advantages. The first one is the economic advantage where the application of two-coats can be achieved in one

process. In this manner, considerable time and labor cost savings can be achieved. In addition, the amount of the losses during paint application can also be reduced. This can be very significant in exposed or hazardous operations. The second advantage is the formation of bonding between two layers. The bonding between the two layers should be stronger in the self-stratification approach than that between separately applied coatings because of the possibility of interlocking during stratification. Thus, use of self-stratified coatings ultimately eliminates the risk of intercoat adhesion failure. One route to self-stratification is a self-stratifying coating in which primer and top-coat are applied in one single step but then phase separate into two layers. The bottom layer will provide good adhesion to substrate as well as corrosion resistance. The top layer will provide decorative properties and environmental protection. It has been shown that self-stratifying coatings provide a number of properties such as improvement of corrosion protection by adhesion durability, selective penetration into porous substrates, and finally upgrading a number of surface properties including gloss, wear-resistance, and anti-friction.[42, 48-51]

1.2.2. Siloxane-polyurethane coatings

Siloxane-polyurethane coating systems were developed to combine the physical and mechanical properties of both polysiloxane and polyurethanes in a hybrid coating system. In this case, the thermoplastic polyurethane elastomers are based on soft segments (polysiloxanes) and hard segments (polyurethanes) which results in heterogeneous microstructures due to the thermodynamic incompatibility of the soft and hard segments. The combination of the two

segment properties into one system have many advantages over their individual segment properties including low temperature flexibility and superior heat resistance, as well as an increase in abrasion resistance.[52] Applications for such coatings were quickly found in the areas of antithrombogenic coatings, biocompatible materials, flexible paper coatings, and water and oil repellent coatings for textiles, glass, and ceramics due in part to the siloxane enriched coating surface.[52,53]

Crosslinked siloxane-polyurethane coatings exhibited a self-stratifying mechanism via various driving forces (molecular weight, surface energy, type of solvent, etc.) during film formation. A key driving force in the siloxane-polyurethane self-stratification was the low surface energy of the siloxane phase separating into a low surface energy, low modulus PDMS top layer, and a tough, durable polyurethane lower layer.[48-51,54-62]

Siloxane-polyurethane copolymers are also being evaluated for use as anti-fouling and fouling-release coating systems. Several studies have used low surface energy poly(dimethyl siloxane) (PDMS) elastomers in fouling-release marine coatings, where fouling organisms adhere weakly and under suitable hydrodynamic conditions or by water jet cleaning "release" from the coating. [54-62] However, due to the amphiphilic nature of the adhesives produced by biofoulers, these types of coatings are not always effective in preventing adsorption of marine organism. While some species, such as *Ulva*, are easily removed from hydrophobic surfaces,[63,64] others, such as diatoms show strong adhesion to hydrophobic surfaces.[65,66] Thus, it appears that a single substrate chemistry

cannot be utilized single-handedly in designing multipurpose marine coatings for all forms of biofouling, including *Ulva* and diatoms.[16]

1.2.3. Poly(ethylene glycol) and zwitterionic polymers and coatings

Amphiphilic substances are designed to have both hydrophobic and hydrophilic moieties on one compound. It has been recognized in the research community that poly(ethylene glycol) (PEG) and zwitterionic based materials are commonly used as nonfouling materials because of their protein resistance properties. They have gained popularity for use in non-fouling biomaterials based on the idea that surfaces with amphiphilic compounds will form nanoscale heterogeneities, creating a surface topography that is unsuitable for the proliferation and adsorption of proteins and marine micro-foulers.[67-77]

Prior research suggests that the protein resistance of PEG may possibly relate to its hydrophilicity or hydration. In truth, the mechanism of the protein resistance of PEG remains unclear. In a steric repulsion model, the protein resistance is attributed to the compression or the conformational entropy loss of PEG chains as the protein approaches the surface, which leads to repulsive protein-PEG interactions. The protein resistance of short PEG chains can be interpreted in terms of the water barrier theory, where PEG chains are assumed to create a strong surface hydration layer via hydrogen bonds, forming a physical barrier to prevent direct contact between the protein and the surface.[65,75-77]

The realization that there are desirable surface properties associated with both extremes of wettability has led several groups of researchers to the development of amphiphilic coating materials incorporating both hydrophobic and

hydrophilic moieties. Motivation has been driven by the desire to produce a universal antifouling and/or fouling-release coating capable of resisting settlement (attachment) as well as the ability to readily release a wide a range of fouling organisms. With this in mind, Gudipati and coworkers produced surface-tethered hyperbranched polymers containing both fluorinated and PEGylated groups.[70] These materials were characterized by both low protein adsorption and high fouling release at an optimal composition of hydrophobic and hydrophilic monomers. More recently, Ober and co-workers reported on the development of a polystyrene block-poly(acrylic acid)-derived surface-active block copolymer with amphiphilic ethoxylated fluoroalkyl side chains capable of both resisting settlement (attachment) and enhancing the release of zoospores as well as improving the release of sporelings (young plants) of the green alga *Ulva* and the diatom *Navicula* and also deterring the settlement of barnacles.[71-73] Additionally, a similar functionalized amphiphilic polystyrene block copolymer containing ethoxylated fluoroalkyl side chains has been reported by Martinelli and coworkers to have the potential to control algal settlement and release.[65] The antifouling and fouling release properties of these coatings are attributed to the very low interfacial energy with water because of the PEG groups, the nonadhesive nature due to the fluoroalkyl groups, and the environmentally responsive dynamic switch in surface wettability due to conformational changes in the amphiphilic side chains.[65,71-73]

In addition to PEG-based materials, it has also been recognized in the research community that zwitterionic based materials are also commonly used as nonfouling materials because of their protein resistance properties.[66,67,78-86] One

type of zwitterionic material that belongs to the polybetaine polymers is sulfobetaine (SBMA) polymers, in which both cationic and anionic groups are on the same monomer residue.[79] It is believed that the nonfouling properties of a surface are from their functional groups and their surface packing.[66,67,79,80] Chang and coworkers have designed diblock copolymers with fixed polypropylene backbones and a range of chain lengths of polysulfobetaine poly(SBMA) synthesized via ATRP.[79] The copolymers were absorbed on to methyl (CH_3) - terminated self-assembled monolayers (SAM) and nonspecific protein absorption was compared.[66] In another study done by Cheng and coworkers, long chain poly(SBMA) were grafted on to SAMs via ATRP and studied for long term and short term protein adsorption as well as biological evaluation of SAMs surface properties over time.[67] It was found that the longer chain length of the zwitterionic moiety greatly effected the reduction of protein adsorption due to surface packing.[67] It should be pointed out that previous studies have focused on materials and surfaces to resist nonspecific protein adsorption from single-protein solutions or human plasma. However, controlling biofouling in marine environments poses great challenges because of the variety of fouling organisms (which all have different mechanisms of adhesion), the complexity of the environment, and the need for a long-life coating.

1.3. The Combinatorial/High-throughput Approach to Polymer Synthesis, Coating Formulation, and Their Characterization

Combinatorial/ high-throughput experimentation can be defined as a technique to design and execute a large number of experiments very quickly and

screen them for useful properties. Another definition of combinatorial/high-throughput experimentation (CHTE) is the rapid execution of experiments using integrated robotic systems, data processing, and control software to screen libraries of candidate compounds. Recently, researchers' demonstrated a CHTE process using drop-based microfluidics allowing 1,000 times faster screening (100 million reactions in 10 hours) at 1 millionth the cost using 10^{-7} times the reagent volume than conventional techniques.[86] CHTE has been used widely in pharmaceutical research for over three decades, however, presently the use of CHTE has found application in materials chemistry and coatings science.[88-93] Due to the complexity of coating systems that might include more than one crosslinker, polyol, catalyst, solvent, surface modifier, pigment, pigment dispersants, and other additives, the use of CHTE can help to understand the role of these individual components, their interactions with each other, and provide a better understanding of structure-property relationships. CHTE has the potential to accelerate research in coatings science by increasing the number of screened coating formulations in a short period of time by exploring a large compositional space resulting in targeted properties. In addition, the use of CHTE can generate an enormous amount of data to help better understand the coatings structure-property relationships. Because of the large amount of data that can be produced using CHTE, it is imperative that the initial step to any CHTE is the design of experiment (DoE). A proper DoE not only provides a lot of information but can also save an enormous amount of time. Just as important is the analysis of the data, and a number of different approaches have been reported in data analysis including software

packages such as Spotfire and DesignExpert which are available to assist data analysis. Recently, several examples have been reported where CHTE have been used in polymer synthesis and coatings formulations and analysis, from controlled free-radical polymerization, and synthesis of nanoscale material to photo degradable material and kinetic studies of heterocyclic chemical compounds.[94-99] Overall all, the main goals of CHTE in a research setting are to speed up the design of new materials, faster optimization and characterization of materials, and to have a better understanding of structure-property relationships.

The scope of the research reported in this dissertation was to explore the synthesis of tough and durable fouling-release marine coatings for underwater marine applications. For this reason, siloxane-polyurethane, amphiphilic-polyurethane and zwitterionic/ amphiphilic-polyurethane systems were studied in detail. The formulations have then been applied in array format to substrates, some which use CHTE to deposit the coating. The coatings systems in general, used an isocyanate crosslinker, functional siloxane oligmers, acrylic polyol, pot-life extender, and a blend of solvents. PEG was crosslinked into the functional PDMS for the amphiphilic system, which was then used as a macroinitiator for the controlled free-radical copolymerization of the sulfobetaine, resulting in the zwitterionic/amphiphilic coating system. The siloxane-polyurethane system is thought to self-stratify after application resulting in PDMS top-layer and polyurethane under-layer. This self-stratification mechanism was further studied using a copolymer of PDMS/PEG, were the copolymer was chemically crosslinked in the hopes that the PDMS would bring the hydrophilic PEG moiety to the surface

resulting in amphiphilic surface heterogeneities. The amphiphilic coating system was systematically studied by adjusting the molecular weight of both the PDMS and PEG using CHTE. The zwitterionic moiety was chemically bound to the amphiphilic copolymer (adjusted PDMS molecular weights) with the same self-stratification mechanism in mind where the resulting coating surface would now have both zwitterionic and amphiphilic complexities. The resulting coatings were analyzed for their surface energy and pseudo-barnacle adhesion and the promising candidates were used as candidates for further analysis with analytical tools and biological workflows to understand their different structure-property behaviors and their interactions as well as performance against marine organisms.

1.4. References

1. Yebra, D. M.; Kiil, S.; Dam-Johansen, K. *Prog. Org. Coat.* **2004**, 50, 75-104.
2. Rascio, V. J. D. *Corros. Rev.* **2000**, 18(2-3), 133-154.
3. Meyer, A. E.; Baier, R. E.; King, R. W. *Can. J. Chem. Eng.* **1998**, 66, 55-32.
4. Brady, R. F. Jr. *J. Coat. Technol.* **2000**, 72(900), 44-56.
5. Milne, A.; Hails, G. (The International Paint Company Limited, London, England) US Patent 4,021,392, May 3, **1977**.
6. Champ, M. A. *Sci. Total Environ.* **2000**, 258, 21-71.
7. Hellio, C.; Berge, J. P.; Beaupoil, C.; Le Gal, Y.; Bourgougnon, N. *Biofouling* **2002**, 18(3), 205-215.
8. Cho, J. Y.; Kowon, E.-H.; Choi, J.-S., *et. al. J. Appl. Phycol.* **2001**, 13, 117-125.

9. Da Gamma, B. A. P.; Pereira, R. C.; Carvalho, A. G.V.; Coutinho, R.; Yoneshigue-Valentin, Y. *Biofouling* **2002**, 18(1), 13-20.

10. Yang, L. H.; Lee, O. O.; Jin, T.; Li, X. C.; Qian, P. Y. *Biofouling* **2006**, 22(1-2), 23-32.

11. Faimali, M.; Sepcic, K.; Turk, T.; Geraci, S. *Biofouling* **2003**, 19(1), 47-56.

12. Bers, A. V.; D'Souza, F.; Klijnstra, J. W.; Willemsen, P. R.; Wahl, M. *Biofouling* **2006**, 22(4), 251-259.

13. Thouvenin, M.; Peron, J. J.; Langlois, V.; Guerin, P.; Langlois, J. Y.; Vallee-Rehel, K. *Prog. Org. Coat.* **2002**, 44, 85-92.

14. Anderson, C.; Atlar, M.; Callow, M.; Candries, M.; Milne, A.; Townsin, R. L. *Maine Des. Oper., Part B4* **2004**, 11-23.

15. Candries, M.; Atlar, M. Mesbahi, E.; Pazouki, K. *Biofouling* **2003**, 19 (Suppl 1), 27-36.

16. Brady, R. F. Jr. *J. Coat. Technol.* **1999**, 35, 31-35.

17. Kohl, J. G.; Singer, I. L. *Prog. Org. Coat.* **1999**, 36, 15-20.

18. Sperling, L. H. Introduction to Physical Polymer Science, Wiley-Interscience: New York, **2001**.

19. Owens, D. K.; Wendt. R. K. *J. Appl. Polym. Sci.* **1969**, 13, 1741-1747.

20. Marmur, A. *Soft. Matter* **2006**, 2, 12-17.

21. Dettre, R. H.; Johnson, R. E. Jr. *J. Phys. Chem.*, **1965**, 69(5), 1507-1515.

22. Gao, L.; McCarthy, T. J. *Langmuir* **2006**, 22, 6234-6237.

23. Schmidt, D. L.; Brady, R. F. Jr.; Lam, K. L.; Schmidt, D. C.; Chaudhury, M. K. *Langmuir* **2004**, 20, 2830-2836.

24. Wynne, K. J.; Uilk, J.; Bertolucci, M.; Makal, U. *Polym. Prep. (Am. Chem. Soc., Polym. Chem.)* **2002**, 43(2), 663-664.

25. Kalantarian, A.; David, R.; Neumann, A. W. *Langmuir* **2009**, 25(24), 14146-14154.

26. Marmur, A. *Colloids Surf., A.* **1998**, 136, 209.

27. Berglin, M.; Lonn, N.; Gatenholm, P. *Biofouling* **2003**, 19 (Supplement.), 63-69.

28. Chung, J. Y.; Chaudhury, M. K. *J. Adhes.* **2005**, 81, 1119-1145.

29. Critchlow, G. W.; Litchfield, R. E.; Sutherland, I.; Grandy, D. B.; Wilson, S. *Int. J. Adhes. Adhesiv.* **2006**, 26, 577-599.

30. Yilgor, I.; McGrath, J. E. *Adv. Polym. Sci.* **1988**, 86, 1-86.

31. Mark, J. E. ACS Symposium Series 729; American Chemical Society: Washington DC, **2000**, p1-10.

32. Pike, J. K.; Ho, T.; Wynne, K. *J. Chem. Mater.* **1996**, 8, 856-860.

33. Tezuka, T.; Kazama, H.; Imai, K. *J. Chem. Soc., Faraday Trans.* **1991**, 87(1), 147-152.

34. Tezuka, T.; Ono, T.; Imai, K. *J. Colloid Interface Sci.* **1990**, 136(2), 408-414.

35. Kavanagh, C. J.; Swain, G. W.; Kovach, B. S.; Stein, J.; Darkangelo-Wood, C.; Truby, K; Holm, E.; Montemarano, J.; Meyer, A.; Wiebe, D. *Biofouling* **2003**, 19(6), 381-390.

36. Stein, J.; Truby, K.; Darkangelo-Wood, C.; Stein, J.; Gardner, M.; Swain, G.; Kavanagh, C.; Kovach, B.; Schultz, M.; Wiebe, D.; Holm,

E.; Montemarano, J.; Wendt, D.; Smith, C.; Meyer, A. *Biofouling* **2003**, 19(1), Supplement 1, 71-82.

37. Kojima, K.; Gore, C. R.; Marvel, C. S. *J. Polym. Sci.* **1966**, 4(9), 2325-2327.
38. Yilgor, I.; Steckle, W. P. Jr.; Yilgor, E.; Freelin, R. G.; Riffle, J. S. *J. Polym. Sci. Part A: Polym. Chem.* **1989**, 27, 3673-3690.
39. Smith, S. D.; DeSimone, J. M.; Huang, H.; York, G.; Dwight, D. W.; Wilkes, G. L.; McGrath, J. E. *Macromolecules* **1992**, 25, 2575-2581.
40. Patel, N. M.; Dwight, D. W.; Hedrick, J. L.; Webster, D. C.; McGrath, J. E. *Macromolecules* **1988**, 21, 2689-2696.
41. Riffle, J. S.; Yilgor, I.; Banthia, A. K.; Wilkes, G. L.; McGrath, J. E. *Org. Coat. Appl. Polym. Sci. Proc.* **1981**, 46, 397-400.
42. Walbridge, D. J. *Prog. Org. Coat.* **1996**, 28, 155-159.
43. Funke, W. *J. Oil Colour Chem. Assoc.* **1976**, 59(11), 398-403.
44. Verkholanstev, V. *Prog. Org. Coat.* **1985**, 13(2), 71-96.
45. Verkholanstev, V. *Prog. Org. Coat.* **1990**, 18(1), 43-77.
46. Verkholanstev, V. *Prog. Org. Coat.* **1995**, 26(1), 31-52.
47. Misev, T. A. *J. Coat. Tech.* **1991**, 63, 23.
48. Vink, P.; Bots, T. L. *Prog. Org. Coat.* **1996**, 28(3), 173-181.
49. Carr, C.; Wallstrom, E. *Prog. Org. Coat.* **1996**, 28(3),161-171
50. Benjamin, S.; Carr, C.; Walbridge, D. J. *Prog. Org. Coat.* **1996**, 28(3),197-207.
51. Verkholanstev, V.; Flavian, M. *Prog. Org. Coat.* **1996**, 29(1-4), 239-246.
52. Kozakiewicz, J. *Prog. Org. Coat.* **1996**, 27, 123-131.

53. Benrashid, R.; Nelson, G. L.; Linn, J. H.; Hanley, K. H.; Wade, W. R. *J. Appl. Polym. Sci.* **1993**, 49(3), 523-537.

54. Ho, T.; Wynne, K. J.; Nissan, R. A. *Macromolecules* **1993**, 26, 7029-7036.

55. Chen, J.; Gardella, J. A. Jr. *Macromolecules* **1998**, 31, 9328-9336.

56. Johnston, E.; Bullock, S.; Uilk, J.; Gatenholm, P.; Wynne, K. J. *Macromolecules* **1999**, 32, 8173-8182.

57. Bullock, S.; Johnston, E.; Willson, T.; Gatenholm, P.; Wynne, K. J. *Colloid Interface. Sci.* **1999**, 210, 18-36.

58. Majumdar, P.; Ekin, A.; Webster, D. C. *ACS Symposium Series* **2007**, 957, 61-75.

59. Ekin, A.; Webster, D. C. *J. Combinatorial Chemistry*, **2007**, 9, 178-188.

60. Ekin, A.; Webster, D. C.; Daniels, J. W.; Stafslien, S. J.; Casse, F.; Callow, J. A.; Callow, M. E. *J. Coatings Tech. & Res.* **2007**, 4(4),435-451.

61. Majumdar, P.; Webster, D. C. *Macromolecules*, **2005**, 38, 5857-5859.

62. Majumdar, P.; Webster, D. C. *Polymer*, **2006**, 47, 4172-4181.

63. Schultz, M. P.; Finaly, J. A.; Callow, M. E.; Callow, J. A. *Biofouling* **2003**, 19 (Supplement), 17-26.

64. Chaudhury, M. K.; Finlay, J. A.; Chung, J. Y.; Callow, M. E.; Callow, J. A. *Biofouling*, **2005** 21, 41-48.

65. Martinelli, E.; Agostini, S.; Galli, G.; Chiellini, E.; Glisenti, A.; Pettitt, M. E.; Callow, M. E.; Callow, J. A.; Graf, K.; Bartels, F. W. *Langmuir*, **2008**, 24(22) 13138-13147.

66. Chang, Y.; Shengfu, C.; Zheng, Z.; Jiang, S. *Langmuir*, **2006**, 22, 2222-2226.

67. Cheng, G.; Zheng, Z.; Shengfu, C.; Bryers, J. D.; Jiang, S. *Biomaterials*, **2007**, 28, 4192-4199.

68. Holland, R.; Dugdale, T. M.; Wetherbee, R., Brennan, A. B.; Finaly, J. A.; Callow, J. A.; Callow, M. E. *Biofouling* **2004**, 20, 323-329.

69. Terlizzi, A.; Conte, E.; Zupo, V.; Mazzella, L. *Biofouling*, **2000**, 15, 327-342.

70. Gudipati, C. S., Finlay, J. A., Callow, J. A., Callow, M. A., Wooley, K. L. *Langmuir*, **2005**, 21, 3044-3053.

71. Finlay, J.A.; Sitaraman, K.; Callow, M. A.; Callow, J. A.; Rong, D.; Asgill, N.; Wong, K.; Kramer, E. J.; Ober, C. K. *Langmuir*, **2008**, 24(20), 503-510.

72. Krishnan, S.; Ayothi, R.; Finlay, J. A.; Sohn, K. E.; Perry, R.; Ober, C. K.; Kramer, E. J.; Callow, M. E.; Callow, J. A.; Fischer, D. A. *Langmuir*, **2006**, 22(11), 5075-5086.

73. Krishnan, S.; Wang, N.; Ober, C. K.; Finlay, J. A.; Callow, M. E.; Callow, J. A.; Hexemer, A.; Kramer, E. J.; Fischer, D. A. *Biomacromolecules,* **2006**, 7(5), 1449-1462..

74. Chen, S.; Zheng, J..; Li, L.; Jiang, S. *J. Am. Chem. Soc.* **2005**, 127, 14473-14478. Chen, S.; Zheng, J..; Li, L.; Jiang, S. *J. Am. Chem. Soc.* **2005**, 127, 14473-14478.

75. Unsworth, L. D.; Sheardown, H.; Brash, J. L. *Langmuir* **2005**, 21, 1036.

76. Chen, S.; Zheng, J.; Ratner, B. D.; Jiang, S. *J. Phys. Chem. B*, **2005,** 109, 2934.

77. Luk, Y.-Y.; Kato, M.; Mrksich, M. *Langmuir*, **2000**, 16, 9604.

78. Lewis, A. L. *Colloids Surf., B* **2000**, 18, 261-275.

79. Chang, Y.; Shengfu, C.; Yu, Q; Zhang, Z.; Bernards, M; Jiang, S. *Biomacromolecules* **2007**, 8, 122-127.

80. Cho, W. K.; Kong, B.; Choi, I. S. *Langmuir* **2007**, 23, 5678-5682.

81. West, S. L.; Salavage, J. P.; Lobb, E. J.; Armes, S. P.; Billingham, N. C.; Lewis, A. L.; Hanoln, G. W.; Lloyd, A. W. *Biomaterials* **2004**, 25, 1195-1204.

82. Zheng, Z.; Chao, T.; Chen, S.; Jiang, S. *Langmuir* **2006**, 22, 10072-10077.

83. Zheng, Z.; Finlay, J. A.; Wang, L.; Gao, Y.; Callow, J. A.; Callow, M. E.; Jiang, S. *Langmuir* **2009**, 25(23), 13516–13521.

84. Lowe, A. B.; McCormick, C. L. *Chem. Rev.* **2002**, 102, 4177.

85. Zheng, J.; Li, L.; Jiang, S.; Chen, S. *Langmuir*, **2004**, 20, 8931-8938.

86. Ostuni, E.; Champman, R. G.; Holmlin, R. E.; Takayama, S.; Whitesides, G. M. *Langmuir,* **2001**, 17, 5605-5620.

87. Agrestia, J. J.; Antipovc, E.; Abatea, A. R.; Ahna, K.; Rowata, A. C.; Barete, J. C.; Marquezf, M.; Klibanovc, A. M.; Griffiths, A. D., Weitz, D. A. *Proceedings of the National Academy of Sciences*, **2010**, 107(9), 4004-4009.

88. Potyrailo, R. A.; Olson, D. R.; Medford, G.; Brennan, M. J. *Anal. Chem.* **2002**, 74, 5676-5680.

89. Webster, D. C.; Bennett, J.; Kuebler, S.; Kossuth, M. B.; Jonasdottir, S. *JCT Coatings Tech.* **2004**, 1, 34-39.

90. Webster, D. C. *JCT Coatings Tech.* **2005**, 2, 24-29.

91. Cawse, J. N. *Acc. Chem. Res.* **2001**, 34, 213-221.

92. Cawse, J. N. Experimental Design for Combinatorial and High-Throughput Materials Development, Wiley-Interscience, New York, NY **2003**.

93. Chisholm, B. J.; Webster, D. C. *J. Coat. Technol. Res.* **2007**, 4(1), 1–12.

94. Anderson, D. G.; Tweedie, C. A.; Hossain, N.; Navarro, S. M.; Brey, D. M.; Van Vliet, K. J.; Langer, R.; Burdick, J. A. *Adv. Mater.* **2006**, 18, 2614-2618.

95. Boseman, A. W.; Heuman, A.; Klaerner, G.; Benoit, D.; Frechet, J. M. J.; Hawker, C. J. *J. Am. Chem. Soc.* **2001**, 123, 6461-6462.

96. Fijten, M. W. M.; Paulus, R. M.; Shubert, U. S. *J. Polym. Sci. Part A: Polym. Chem.* **2005**, 43, 3831-3839.

97. Hoogenboom, R.; Fijten, M. W. M.; Shubert, U. S. *J. Polym. Sci. Part A: Polym. Chem.* **2004**, 42, 1830-1840.

98. Adams, N.; Shubert, U. S. *Macromol. Rapid Commun.* **2004**, 25, 48-58.

99. Adams, N.; Shubert, U. S. *J. Comb. Chem.* **2004**, 6, 12-23.

CHAPTER 2. SYNTHESIS AND CHARACTERIZATION OF ACRYLIC POLYOL LIBRARIES BY HIGH THROUGHPUT METHODS

2.1. Introduction

Known since the 1970's with the onset of hydroxy functional acrylates, acrylic polyols are a special group of amorphous polymers obtained by radical copolymerization of acrylic monomers, such as acrylic and methacrylic acids and esters, which have been known since the middle of the nineteenth century.[1] Acrylic monomers and their analogous methacrylic monomers are highly reactive which results from unsaturated terminal sites within their structure. The source of hydroxyl groups in these acrylic polyols was the utilization of hydroxyethyl acrylate as the comonomer. Figure 2.1 illustrates the acrylic and methacrylic monomers used to obtain desired properties in the synthesis of the acrylic polyols for the experiments in this chapter.

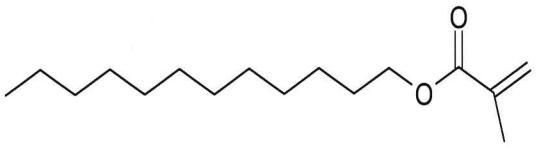

Lauryl Methacrylate T_g= 208 K (-65°C)

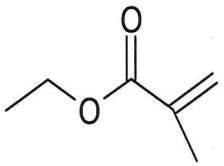

Ethyl Methacrylate

T_g = 338 K (65°C)

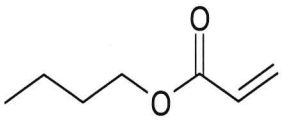

Butyl Acrylate

T_g = 219 K (-54°C)

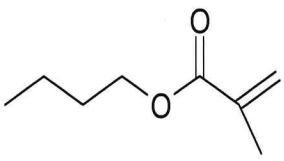

Butyl Methacrylate

T_g = 293 K (20°C)

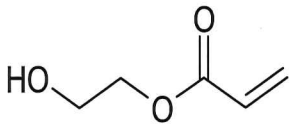

Hyroxyethyl Acrylate

T_g = 258 K (-15°C)

Figure 2.1. Monomers used as raw materials in acrylic polyol syntheses, labeled by name and glass transition temperatures of the homopolymers.

These monomers offer significant advantages as an additive in copolymer-based finishes in coatings including flexibility, weatherability, internal plasticization, and abrasion resistance. Hydroxyethyl acrylate monomer adds important properties on the polyol products including improved adhesion to substrates, and sites for crosslinking.

A process for industrial production of acrylate esters[2] and methyl methacrylate[3] was developed by researchers at Röhm and Haas in 1928 and 1927, respectively. The use of these polyacrylates and polymethacrylates increased rapidly in many fields of application as new methods were developed for producing (meth)acrylic acid and (meth)acrylic esters.[4] The polymerization of acrylates and methacryaltes can be carried out easily due to their carbonyl groups being adjacent to a vinyl group. Radical polymerization is almost exclusively used to produce polyacrylates and polymethacrylates, however, polymerization can also be initiated photochemically by ultraviolet radiation (UV) or electron beams (EB), as well as ionic (particularly anionic) polymerization.[5] Due to the exothermic nature of the polymerization of acrylates and methacrylates, the heat of the reaction must be removed in order for the process to be controlled effectively.[6,7]

Another factor (and just as important) in understanding the polymerization of acrylates and methacrylate is the familiarity of the radical and monomer reactivity. Despite the fact that great progress has been made since the early 1980s in understanding radical and monomer reactivity, researchers continue to use models about radical and monomer reactivity from the sixties and seventies.[8,9] The typical convention to study the reactivities of monomers and radicals have

been the use of copolymerization data. It was these studies, as well as earlier work that have led to the current structure in which researchers think about radical and monomer reactivities. There are four factors that govern the reactivity: (1) polar effects, (2) steric effects, (3) (resonance) stabilization effects, and (4) thermodynamic effects.[8] First, polar effects are very important in radical reactions due to nucleophilic radicals reacting with electrophilic monomers (and vice versa). Next, the most obvious observation that steric effects play an important role in radical reactions is in the most common propagation reaction, the head-to-tail addition; whereas the head –to-head addition hardly ever occurs. Additionally, several studies have indicated, with few exceptions, that 1,2-disubstituted alkenes do not homopolymerize, but easily copolymerize, which may be attributed to steric hindrance.[10] However, it has been shown that cycloalkenes readily polymerize due to the relief of ring strain by either ring opening metathesis polymerization (ROMP) or through the double bond.[11-15] Subsequently, stabilization effects can arise if the unpaired electron in the monomer radical is delocalized, the radical will be relatively stable and thus will lead to relatively low reactivity. Alternatively, the monomer will be more reactive if the addition of a monomer will lead to a radical that has a highly delocalized electron. Finally, the thermodynamic effects can be attributed to the lowering or increasing of the reaction barriers due to differences in the relative energy barriers between monomer and polymer.[16,17]

The free radical polymerization of acrylic and methacrylic monomers which occurs in a chain reaction consisting of three steps: initiation, propagation and termination, illustrated in Figure 2.2.[8] The initiation step involves two reactions.

The first step, a radical is produced by the homolytic decomposition of **I** to yield a pair of primary radicals where k_d is the rate constant for the initiator dissociation. The second step involves the addition of this radical I• to the first monomer molecule (M) to produce the initiating radical I-M• where k_i is the rate constant for

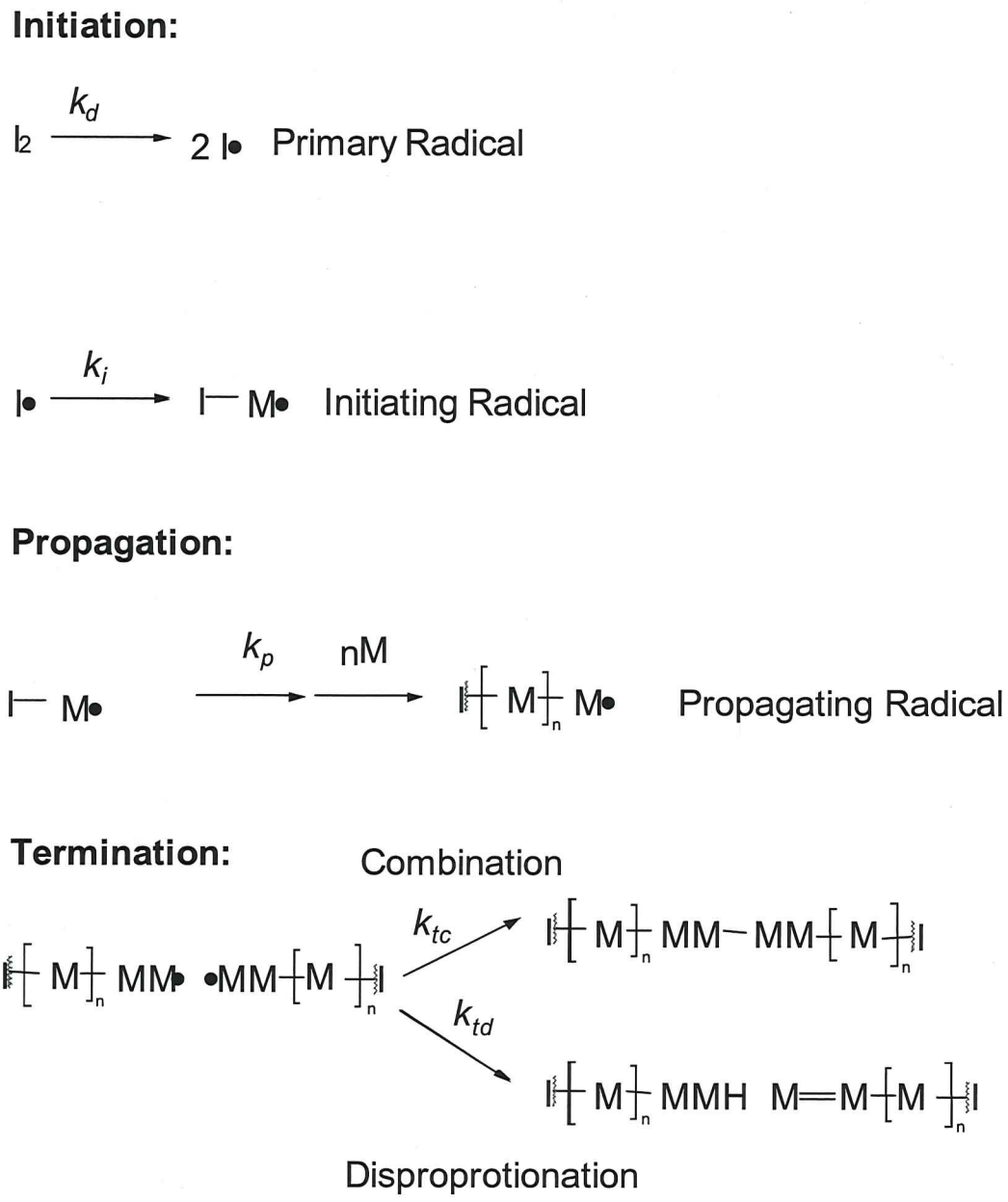

Figure 2.2. General schematic of free radical polymerization mechanism.

the second step in the initiation process. In general, chain propagation consists of the growth of I-M• by the successive addition of monomer molecules (M) where k_p is the propagation rate constant. Rapid chain propagation produces high molecular weight polymer, but at some point the propagating polymer chain stops growing and terminates. Deactivation of the propagating chain occurs by the bimolecular reaction of propagating radicals by combination or disproportionation. In termination by combination, two propagating radicals react with each other, where k_{tc} is the combination termination rate constant, to form a dead polymer. Termination by disproportionation involves an abstractable β-hydrogen from one radical center to another radical center to form two dead polymer chains, one saturated and one unsaturated, where k_{td} is the rate constant for termination by disproportionation.

Chain transfer (CT) can also occur in conventional free radical polymerization. In general, chain transfer is a chain-stopping reaction. It occurs during the reaction of a propagating radical with a transfer agent to yield a dead polymer and a new radical, and this new radical can reinitiate polymerization During this process, the degree of polymerization decreases and the number of polymer molecules increases, however, the effect on the polymerization rate is dependent on whether the rate of reinitiation is comparable to that of the original propagating radical. It should be noted that chain transfer can occur to all the substances present in the polymerization system (initiator, monomer, polymer, and solvent). Depending on the initiator, chain transfer can accelerate the generation of initiating radicals by induced decomposition, such CT occurs with peroxide

initiator, as well as azo initiators (azobisisobutyronitrile, AIBN), however, CT to aliphatic azo initiators are believed to be insignificant.[10,18-20] Chain transfer to monomer involves a propagating polymer chain transferring a β-proton to monomer, resulting in the formation of terminal saturation in the polymer.[21] The chain is not terminated by this since a new propagating species is regenerated, however, CT to monomer is the principle reaction that limits the maximum molecular weight that can be achieved by a given monomer. Chain transfer to polymer results in the formation of a radical site (backbone radical center) on a polymer chain that may be capable of polymerizing monomers to produce a branched polymer. If the reactivity of the polymer radical is high, intramolecular chain transfer or backbiting may occur as well. Previous studies have shown that chain transfer to polymer plus termination by combination, can lead to gelation under certain circumstances. Consequently, the properties of the polymer can be greatly reduced because of the possibility of branching.[22,23] Another possible chain transfer reaction is the chain transfer to solvent in solution polymerizations.[24-26] Here, the polymer radical removes a proton from a solvent molecule yielding a terminated polymer molecule and a new free radical. If the free radical formed in the chain transfer reaction adds readily to the monomer, then a new chain is immediately begun. These chain transfer reactions do not affect the over-all rate of polymerization, they simply reduce the average molecular weight of the polymer formed, and the solvent acts as a "regulator" of polymerization. However, if the free radicals formed from the solvent molecule do

not add readily to monomer, then they will accumulate in solution, destroy reaction chains and reduce the over-all rate of polymerization.

Due to the exothermic nature of conventional acrylic free radical polymerization, an uncontrolled acceleration in the rate of polymerization at high conversion, better known as the "Trommsdorff effect", can occur. This effect can cause problems within both an industrial and scientific context ranging from product mixture to reactor explosion.[27,28] The actual cause of the gel (or Trommsdorff) effect has been debated over the last 50 years and various theories have emerged [29,30], however, it is believed that the gel effect is due to a reduction in the termination rate coefficient at higher conversion because of an increase in viscosity (chain entanglements hinder diffusion of macroradicals through the reaction mixture). Since the concentration of radicals is determined by balancing the rates of initiation and termination, a decrease in the termination rate will increase the concentration of radicals and accelerate propagation. As stated previously, free radical polymerizations are exothermic and cause increases in the reaction temperature which further enhances the initiation and can result in an uncontrolled process.

Among all the issues/problems that can occur in free radical polymerization, controlling polymer composition and molecular weight or molecular weight distribution is of primary importance. From an industrial standpoint, many of these polymer products are prepared via heterogeneous (emulsion, suspension) [31-35] or homogeneous (bulk, solution) [36-40] polymerization in a wide range of process configurations from tubular to well-mixed tanks that may be continuous, batch, or

semi-batch. (continuous, batch, or semi-batch are the three major classifications of chemical processes based on the method in which reactants are added to the reaction vessel).

In a batch process, all of the reactants are added to the reaction vessel prior to starting the polymerization. During the polymerization, no material is added or removed from the reaction vessel. Although batch polymerizations are the simplest to run, they offer the least amount of control. It is important to keep in mind those polymerizations with more than one monomer that the consumption rates of the different monomers will be governed by the monomers respective reactivities. The resulting products may have broad polydispersities and become inhomogeneous. Also, in batch polymerization, reactant concentrations change throughout the polymerization causing the phenomenon of molecular weight distribution (MWD) drift leading to very broad distributions in the final product. An advantage of batch polymerization is the ability to be flexible and readily adaptable to new products for operations where changes to the formulation or polymerization conditions are common.

Semi-batch processes (also known as semicontinuous) are similar to batch processes, the only difference is that reactants and/or products can be added or removed during the polymerization. At the beginning of a semi-batch polymerization, a portion of the total reactants are charged to the reaction vessel. Once the polymerization is started, reactants are added systematically to control the desired properties or the reaction rate. Usually, monomer(s) or initiators are fed to the reaction vessel at a finite time or over the course of the polymerization;

this addition can be stopped or started at any desired time. This technique is used most commonly to control product composition or reaction rate, which leads to reduced composition drift because the concentration ratio of the respective monomers are held nearly constant by a predetermined feeding rate.[36,37]

The molecular weight and composition ratio can also be controlled by adding initiator and monomers at starved conditions. "Starved" conditions refer to a reaction system where the concentration of reactants is very low and the reactant consumption rate is equal to the addition rate. This is achieved by selecting a readily decomposing initiator, while the monomers are fed in the desired ratio to provide composition control which leads to the mean chain length being a ratio of monomer to initiator. The initiator used in the solution polymerizations of the monomers in this chapter was Vazo 67, illustrated in Figure 2.3. Vazo 67 has a decomposition half-life (t=1/2) of 10 hours at 67°C.[41-43] Polymerizations are often conducted at temperatures within 10°C of the half-life temperature of the initiator, but can be operated at higher temperatures. Commonly, only a small amount of initiator is required in most chain reactions

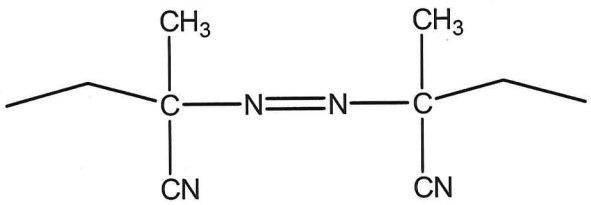

2-azobis (2-methylbutanenitrile)

Vazo 67

Figure 2.3. Initiator used in free radical polymerization of acrylic polyol libraries.

typically 1-5 wt% relative to the total charge of reactants.

Since some free radical polymerizations are fast, larger scale operations can lead to the heat of polymerization not being transferred out of the reaction vessel safely. To help eliminate this problem usually a portion of the total monomer charge is initially fed into the reactor vessel and the remainder of the monomer is added at a rate that is compatible with the heat removal capacity of the cooling system. At starved conditions, the monomer concentration is low at any given time which minimizes the event of a thermal runaway reaction. However, there is a potential concern while operating at starved conditions that the polymer concentrations may become high resulting in chain transfer to polymer reactions which can have a significant effect on the overall product properties.

The final industrial chemical process is called a continuous process. During this process all reactants are fed continuously to the reactor vessel and any unconsumed reactants and products are removed continuously. Most continuous processes are operated at "steady state" conditions. Steady state generally means that all reactant concentrations and process conditions are independent of time, thus, it is an autonomous system. This has a huge benefit on certain properties. Since concentrations are held constant throughout the process, there is no MWD drift or composition drift, which leads to the narrowest possible molecular weight and MWD.

The work done in this chapter will focus primarily on acrylic polyol solution free radical polymerization using a Symyx batch reactor system and a semi-batch automated parallel reactor system. The use of parallel and combinatorial

experiments are ideal areas for polymer research due to the fact that many parameters, both composition and process variables, can be varied during the synthesis resulting in the identification of compositions having unique properties and possible structure-properties relationships.[44-50] The rationale for the batch polymerizations was to explore the use of high throughput methods for the synthesis of polymers using free radical polymerization. Another reason was to select acrylic polyols for use as candidates in the siloxane-polyurethane coatings systems. In contrast, using conventional laboratory methods, only a few selected compositions can be explored, which might result in missing important properties of those polymers. The objective of using the Chemspeed experiments was to demonstrate how this reactor system can be used in the exploration of acrylics synthesized using a semi-batch process, which is the process commonly used in industry. As stated previously, there are some advantages to running acrylic free radical polymerizations at a semi-batch process such as better MWD control, as well as enhanced reactor temperature control which eliminates possible runaway reactions. With the use of the Chemspeed Autoplant A100™ process variables can be explored simultaneously in one experiment or in just a few experiments. This gives the ability to do reactions much more efficiently and possibly do experiments that would not be possible if the time and resources were not available. Another advantage of using a computer-controlled, automated reactor system is that every experiment is carried out using a programmed set of process steps and conditions, avoiding human variability.

By using the Symyx batch reactor system and the semi-batch automated parallel reactor system, large amounts of data can characterized and collected where the data can then be stored and one can begin to create a database of important polymer properties as a function of composition. The database of structure-property relationships on multiple (co)polymers systems can be of great importance to the scientific community, giving important information that can be used to further develop new polymer systems or optimize systems already present. For researchers in the field, it can help by eliminating compositional space in their respective experimental design and focus (or narrow) their screening of tailor-made polymer systems for certain structure-property relationships.

Overall, the aim of this study was the design, synthesis via batch and semi-batch solution free radical polymerization and characterization of acrylate polymers using combinatorial/ high-throughput and automated parallel reactor methods. With the use of the Chemspeed Autoplant 100™ for the polymerization, variations in process parameters, i.e. – reaction temperature, rate of monomer and initiator addition, agitation speed, etc were conducted. It was demonstrated that acrylic polyols can be synthesized by free radical polymerization with combinatorial/high-throughput and automated parallel reactor system and that there was good correlation among the replicates. The progress of the polymerization could be followed by sampling the reactor contents periodically, providing valuable information regarding conversion and molecular weight as a function of time. The acrylic polyols were characterized by Rapid-Gel Permeation

Chromatography (RGPC) for molecular weight and polydispersity information, Differential Scanning Calorimetry (DSC) was used for glass transition temperature data, and percent solids and percent conversion was used for tracking completion of the reaction.

2.2. Experimental

2.2.1. Chemicals and reagents

Butyl methacrylate (BMA), n-butyl acrylate (BA), ethyl methacrylate (EMA), 2-hydroxyethyl acrylate (HEA), and lauryl methacrylate (LMA) were obtained from Aldrich and used as received. Toluene was obtained from VWR and purified by a solvent purification system. The free radical initiator, 2-azobis (2-methylbutanenitrile) (Vazo 67) was obtained from DuPont.

2.2.2. Polymer characterization

A TA Instruments Q1000 DSC with an autosampler accessory was used for the T_g determinations. The samples were dried and then subjected to heat-cool-heat cycle from -65 °C to +150 °C by ramping 20 °C per minute for both heating and cooling. The second heating cycle was used to determine the T_g. T_g was determined from the midpoint of the inflection. Symyx Rapid GPC with an evaporative light scattering detector (PL-ELS 1000) equipped with two PLgel mixed-B columns (10 µm particle size) was used for molecular weight analysis. Solutions of 1 mg/mL sample in THF were prepared before the run; calibration was carried out with polystyrene standards and THF was used as the eluent at 45 °C at a flow rate of 2.0 mL/min. The molecular weight and PDI were determined with Epoch software (Symyx, Inc.) using polystyrene or poly(methyl methacrylate)

standards. Percent solids were determined gravimetrically and the percent conversion was then calculated from the percent solids results. Library Studio was used for designing acrylic polyol polymer libraries for the Symyx combinatorial synthesis. The software allows for both full factorial and statistical experimental design. The library designs are stored in a common database. For the Symyx polyol polymerization study, 6x4 arrays of experiments were designed.[50,51]

2.2.3. Symyx combinatorial polymer synthesis

Synthesis library designs were done using Library Studio software (Symyx, Inc.). The software allows both statistical and full factorial experiment designs and these designs are stored in a common database. All solution polymerizations were carried out in a Symyx batch reactor system.[51] The Symyx batch reactor system is comprised of a dual-arm liquid dispensing robot housed inside a glove box under dry nitrogen. The robot dispenses liquids according to Library Studio designs. The three center wells in the synthesis platform holds arrays of reaction vials, and up to 288 simultaneous 1-mL reactions could be run in the batch mode with magnetic stirring and heating up to 120 °C. 8-mL vials in 6 X 4 arrays were used for the synthesis of the acrylic polyols. A stock solution of Vazo 67 (10%) in purified toluene was prepared for the synthesis experiments. Acrylate monomers, solvent and initiator were dispensed into 24 vials (with magnetic stirbars) using a dual-arm liquid robotic pipette, sealed, and heated for 500 minutes. The samples were cooled to room temperature inside the glove box, taken out and characterized.

2.2.4. Automated parallel polymer synthesis

Automated acrylic polyol synthesis was done using a Chemspeed Autoplant A100™, shown in Figure 2.4.[52-54] The system used in this study consists of 12 Process Development (PD) units. (The system can be fitted with up to 20 PD units.) Each PD unit contains two 100 mL stainless steel reactors mechanical stirring up to 600 rpm and reflux cooling.

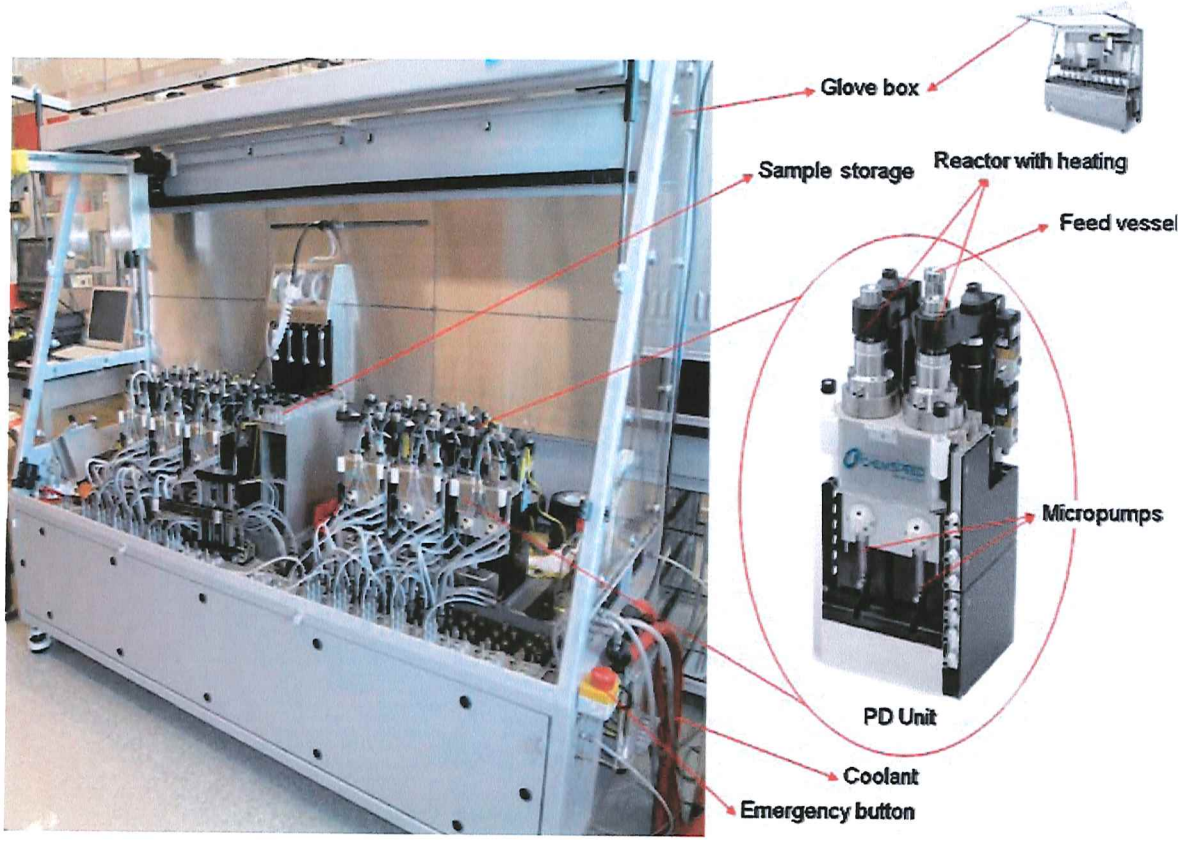

Figure 2.4. Chemspeed Autoplant A100™ (left) and PD Unit (right)

The temperature in each reactor can be controlled independently over a range of -10 to 250 °C. Solid and liquid reagents can be automatically charged to each reactor by an overhead gravimetric solid and powder dispenser and a 4-channel liquid handling needle head. In these experiments, the system was setup

to operate in semicontinuous mode. Thus, one of the 100 mL vessels in the PD unit is designated as the reactor and the other as the feed vessel. A third 50 mL feed vessel is also present in each PD unit. Prior to the beginning of the polymerization the reactor vessel is charged initially with solvent and the other 100 ml feed vessel is charged with the monomers and the 50 ml feed vessel is charged with the initiator solution. The contents of the two feed vessels are then fed slowly to the reactor using two syringe pumps on the PD unit. In this mode, up to 12 reactions can be conducted simultaneously and both compositional variations as well as process variations can be explored. Several different inline real-time data analysis factors, such as temperature and stirring, can be monitored for all of the 12 PD units. Gas supply for inertization using nitrogen can be done up to 20 bar working pressure. The synthesizer is equipped with a four-needle liquid handling system with four syringes (1–10 mL) to accurately dispense different volumes of stock solutions and samples. The entire system is self-contained inside a pseudo-glove box.

2.3. Results and Discussion

There are two parts to this study; the first part was to investigate molecular weight, polydispersity, and glass transitions temperatures of the combinatorial free radical polymerization of libraries (one library = 24 unique acrylic polyol compositions) of acrylic polyols with different mole ratios of HEA, BA, EMA, BMA, and LMA, the second part investigated the use of parallel reactors in the polymerization of acrylic polyols adjusting processes variables such as reaction temperature, monomer and initiator feed times, adjusting percent solids and

initiator concentration, and oscillating reactor temperature in real-time. The second study is important from an industrial perspective because the use of the parallel reactors can mimic the processes of large scale industrial reactors and the results can be useful in better understanding the reaction kinetics of the acrylic polyol polymerization under those conditions.

2.3.1. Solvent and initiator study on the batch free radical polymerization of an acrylic polyol using combinatorial methods

This objective of this study was to better understand the molecular weight effects by changing the amount of solvent (effects on % solids) in the composition of the acrylic polyol and changing the concentration of initiator, which can then be used to set the solvent and initiator levels for the other batch/semi-batch polymerization experiments. The range of the amount of solvent used was 50-70% and the initiator concentration ranged from 1-4%/wt. The acrylic polyol composition (20% HEA, 20:80 (BA:EMA)) was held constant for all initiator/solvent combinations in this study, thus eliminating the composition variable and strictly focusing on the effects of the different solids levels and initiator concentration. This is true for the constant reaction temperature as well. The acrylic polyols were produced by free radical polymerization using combinatorial techniques resulting in 12 acrylic polyols with the same compositions. The polymerization consisted of 1-4%/wt initiator, 50-70% solvent resulting in 30-50% (theoretical) solids, and the reaction temperature was set to 95°C. Samples from each reactor were characterized by RGPC to obtain the MW and PDI and percent conversion was determined gravimetrically. It is readily known that adjusting the initiator and

solvent content of the solution polymerization of acrylic polyols can greatly affect the molecular weight. The RGPC molecular weight results for the acrylic polyol library can be seen in Figure 2.5.

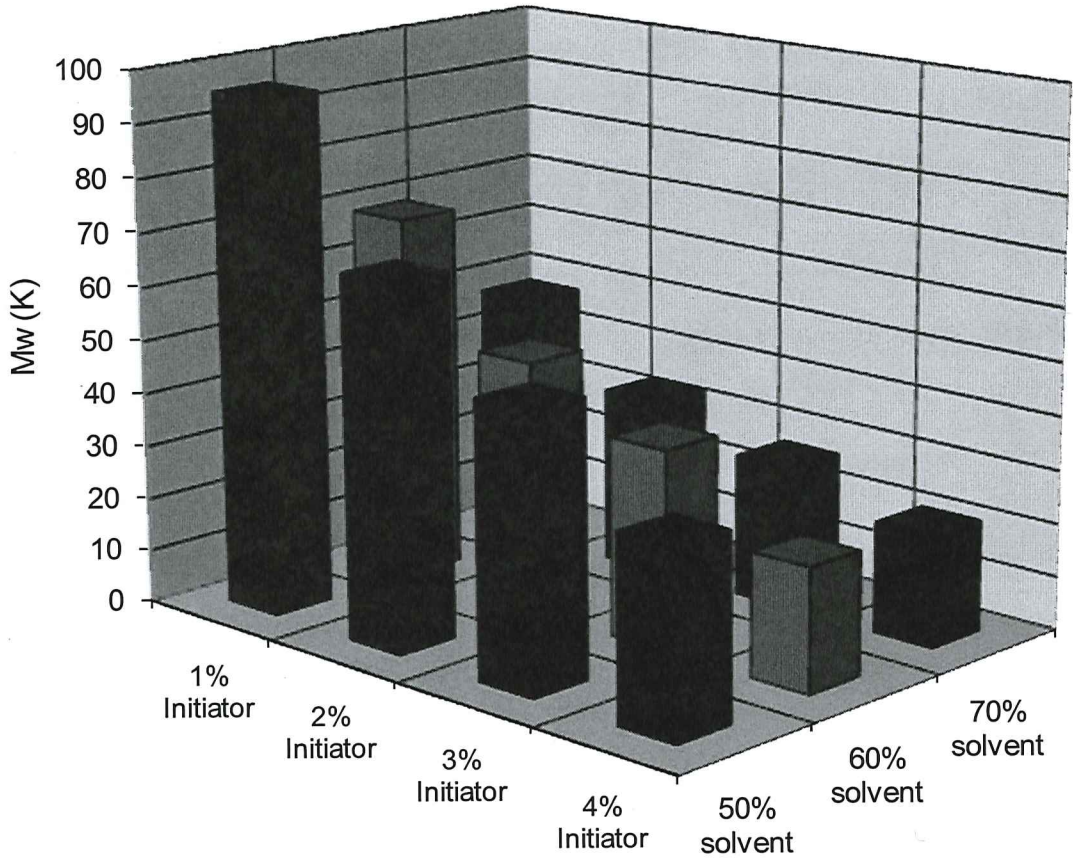

Figure 2.5. Rapid GPC molecular weight data from the batch solvent/initiator study for the acrylic polyol library comprised of 20% HEA and 20:80 (BA:EMA) with a range of 1-4%/wt initiator and 30-50% solids.

The overall trend seen from the MW data is the decrease in the acrylic polyol MW with the increase in both the level of initiator and amount of solvent. The decrease in MW with the increase in initiator level occurs with the increase in

free radicals in solution, thus creating more propagating radical chains that create lower MW chains before terminating. In the same regards, increasing the amount of solvent in the polymerization also lowered the MW. This occurred because of the chain transfer to solvent effect where the radical on the propagating polymer chain removed a proton from the solvent molecule yielding a terminated polymer chain and a new radical essentially regulating the polymerization and reducing the overall MW. The highest MW of 96 kDa was observed with 1% initiator and 50% solvent. The lowest MW of 20 kDa was shown with 4% initiator and 70% solvent. A linear trend in MW is shown going from the lowest percent of initiator to the highest, as well as going from the lowest percent solvent to the highest percent solvent. The 50% solvent acrylic polyols had the highest overall MW, ranging from 96 kDa to 34 kDa. Subsequently, the 70% solvent acrylic polyols had the lowest overall MW, ranging from 48 kDa to 20 kDa.

Analyzing the data closer reveals that the largest change in MW was due to the initiator rather than the percent solvent. With an increase from 1% initiator to 2% initiator, a decrease in MW from 96 kDa to 68 kDa for the 50% solvent polyols, a difference of 28 kDa, the 60% solvent polyols showed a difference of 22 kDa, and the 70% solvent polyols showed a difference of 15 kDa. The MW difference from the increase in initiator from 2% to 3% and 3% to 4%, regardless of percent solvent, greatly decreased. The difference in MW for the 50% solvent polyols for 2% to 3% and 3% to 4% initiator were both 17 kDa. The difference in MW for the 60% solvent polyols for 2% to 3% initiator was 10 kDa and 3% to 4% initiator was 14 kDa, similarly with the 70% solvent polyols showed a difference in MW of 6 kDa

and 7 kDa for 2% to 3% and 3% to 4% initiator, respectively. However, the 1% initiator row going from 50% solvent to 70% solvent showed a decrease in MW with a difference of 48 kDa, the difference in MW decreased as the percent initiator was increased for the other initiator percents; 2% initiator was 35 kDa difference, 3% initiator was 24 kDa, and 4% initiator was 13 kDa for the difference in MW when observing the increase in percent solvent according to Figure 2.5.

Polydispersity data for the study illustrated in Figure 2.6 showed that all acrylic polyols were within the range of 2.0 to 2.8. The polyols polymerized using 1% and 2% initiator had the lowest PDIs at 50% solvent of ~2.

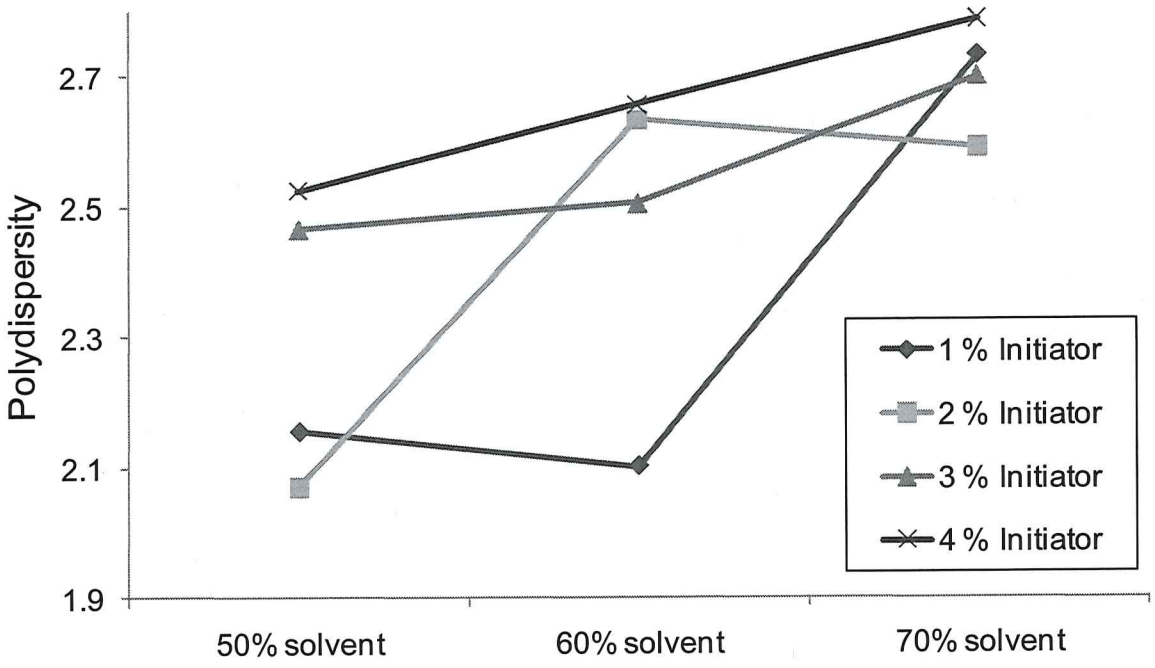

Figure 2.6. Polydispersity data from the batch solvent/initiator study for the acrylic polyol library comprised of 20% HEA and 20:80 (BA:EMA) with a range of 1-4%/wt initiator and 30-50% solids.

When the solvent was increased for the 2% initiator polyols, PDI increased to 2.5. Polyols polymerized using 3% and 4% initiator had PDIs of 2.3-2.7 regardless of the amount of solvent. An interesting trend observed was at 70% solvent all polyols had the same PDI of ~2.5. The MW data from the solvent /initiator study indisputably shows the effects of initiator concentration and percent solvent on the MW for the solution polymerization of acrylic polyols.

It shows that both the increase in percent initiator and percent solvent lowers the MW of the acrylic polyols polymerized by a batch-type method considerably.

2.3.2. Free radical polymerization study of acrylic polyols comprised of HEA, BA, and EMA using combinatorial methods

The first acrylic polyol library comprised of three monomers, HEA, BA, and EMA, were produced by batch free radical polymerization using combinatorial techniques resulting in 24 unique acrylic polyol compositions. The polymerization conditions consisted of 4%/wt initiator, 50% solids, and a reaction temperature of 75°C. HEA was varied from 5 to 20 percent to provide a range of hydroxyl equivalent weight from 488 g/mol to 2324 g/mol. A combination of BA and EMA were varied by a range of ratios from 100:0 (BA:EMA) to 0:100 (BA:EMA). The acrylic polyol composition is illustrated in Figure 2.7 in a 4X6 array library format. The 24 acrylic polyols were synthesized in a single experiment using the Symyx automated batch synthesis system. The RGPC molecular weight data for the library can be seen in Figure 2.8. As the amount of EMA is increased, the MW

values of the acrylic polyols decreased as expected due to BA terminating primarily by combination.[55]

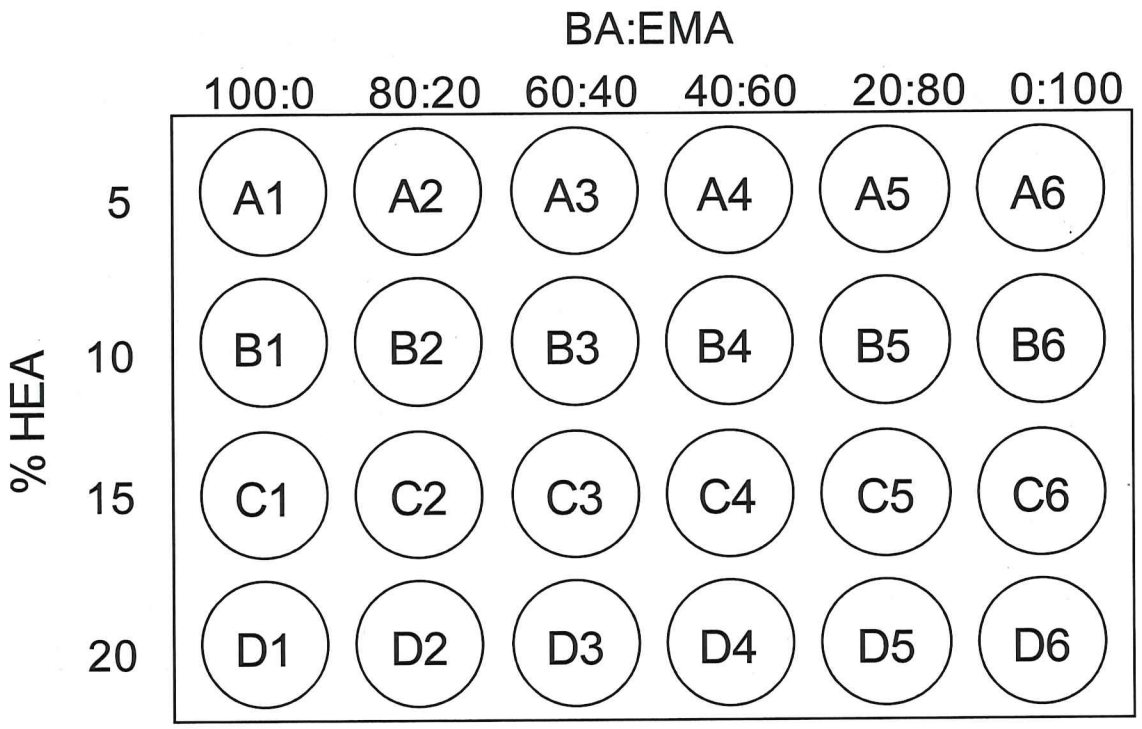

Figure 2.7. 4X6 array library format of acrylic polyol composition consisting of HEA, BA and EMA.

The termination reactions of the acrylic polyols play a large factor in the MW as is evident by the copolymers comprised of BA and HEA having MW of 160-180 kDa, while the polyols consisting of EMA and HEA have MW of 70-100 kDa, almost a decrease of 100 kDa. The lower amounts of HEA in the acrylic polyols have very little effect on the overall molecular weight, however at 20% HEA and a higher amount of BA there is a significant drop in the MW, this may be due in part to the higher degree of hydrogen bonding with HEA resulting in lower MW gelled particles which can sometimes result in a false MW reading from the RGPC. Also, due to the higher percent of HEA the viscosity of the polyol increased which may

contribute to the higher MW seen for all the acrylic polyols with the 20% HEA composition, this phenomenon is known as the autoacceleration effect, where the increase in viscosity reduces the termination rate coefficient. Since the reaction temperature was 75°C, the half-life of the free radical initiator (Vazo 67) is 2.31 minutes, which results in higher MW due to the propagating radical to remain active longer (before terminating) than it would at higher temperatures. This is due to the stability of the free radicals at lower temperatures which induce the decomposition of the initiator thus; the decomposition rate is dependent on the lifetime of the radicals in the system.[56-60]

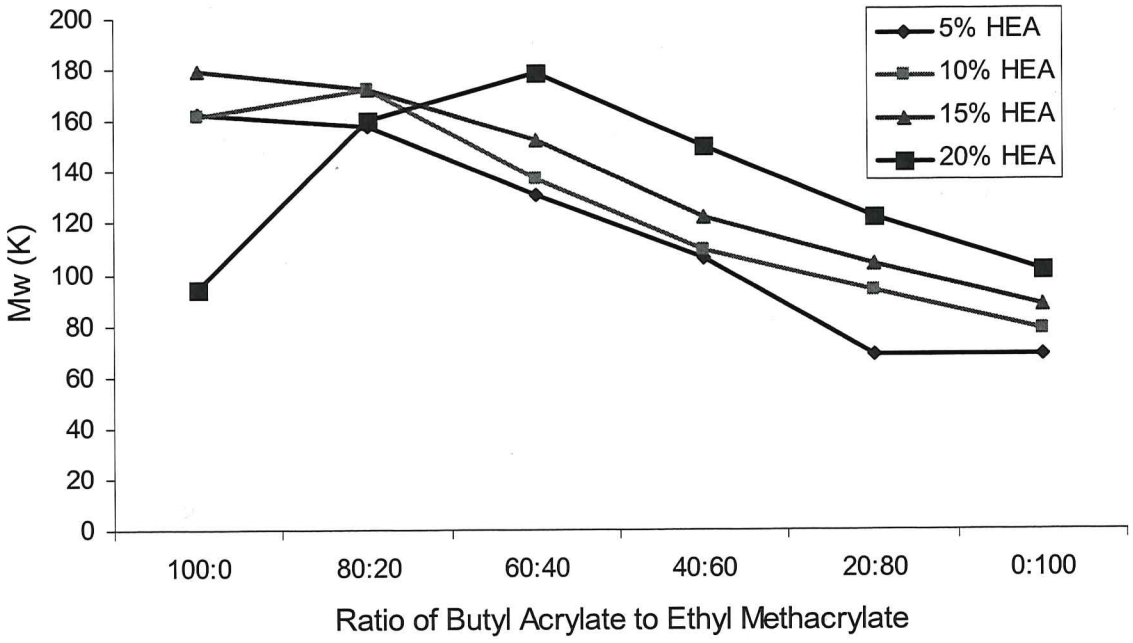

Figure 2.8. Rapid GPC molecular weight data for acrylic polyol library comprised of HEA, BA, and EMA.

This gel effect phenomenon can be seen more apparent in the polydispersity data shown in Figure 2.9. Similar to the molecular weight data in

Figure 2.8 for the BA and HEA acrylic polyol compositions, the higher amounts of BA and HEA polyols result in considerably higher polydispersities compared to the acrylic polyols with the composition of EMA instead of BA. This is possible due to the same reason the MW's are higher for those acrylic polyols, where chain entanglements hinder the diffusion of macroradicals leading to gelled products with large polydispersities.[61,62]

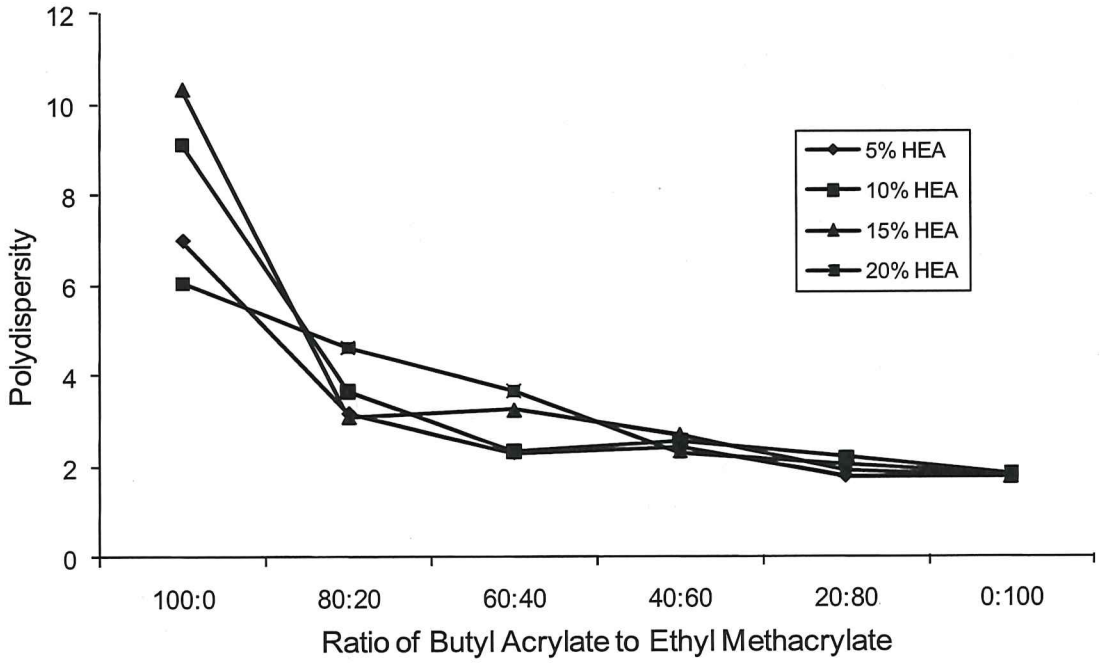

Figure 2.9. Rapid GPC polydispersity data for acrylic polyol library comprised of HEA, BA, and EMA.

The impurities and ethylene glycol diacrylates present in HEA can causes the formation of gelled and branched products which contain a wide range of molecular weights in each of those specific acrylic polyols. When characterizing the gelled polyols via RGPC, only the soluble portion of the polymer is being characterized resulting in lower MW and higher polydispersity shown in Figure 2.8

and 2.9, respectively. As the ratio of EMA is increased the polydispersity decreased, a similar trend seen with the molecular weight data.

DSC measurements of the acrylic polyol library were made for further characterization. In Figure 2.10, the glass transition temperatures of the theoretical acrylic polyols (based on the Fox equation)[63] and experimental acrylic polyols of HEA, BA, and EMA are shown. Overall, there is a general trend of increasing T_gs with increase of EMA in the acrylic polyol composition. The experimental acrylic polyols with the composition ratio of 100:0 (BA:EMA) produced the lowest T_gs, ranging from -43°C with 5% HEA to -30°C with 20% HEA. The increase in the amount of HEA causes a slight increase in T_gs due to the increase in hydrogen bonding. As the amount of EMA is increased in the composition of the acrylic polyol, the T_g increases in a rather systematic way, however, there is a convergence of the T_gs at the ratio 40:60 (BA:EMA) indicating that at this point, regardless of the amount of HEA, all have the same relative T_gs (similar convergence was observed for the theoretical T_gs). Another interesting trend observed from Figure 2.10 is after the convergent point the acrylic polyols with the lower HEA content have higher T_gs than those with higher percents of HEA, which is the opposite of what was seen before the convergence point. The T_g values of the experimental polyols showed correlation with the theoretical T_gs. There were some differences at the 0:100 (BA:EMA) where the theoretical T_gs were slightly lower than the experimental T_gs. This may be due to molecular weight effects and/or the heating rate on the DSC which can have significant effects on the T_g. If a slower heating rate was set on the DSC it might

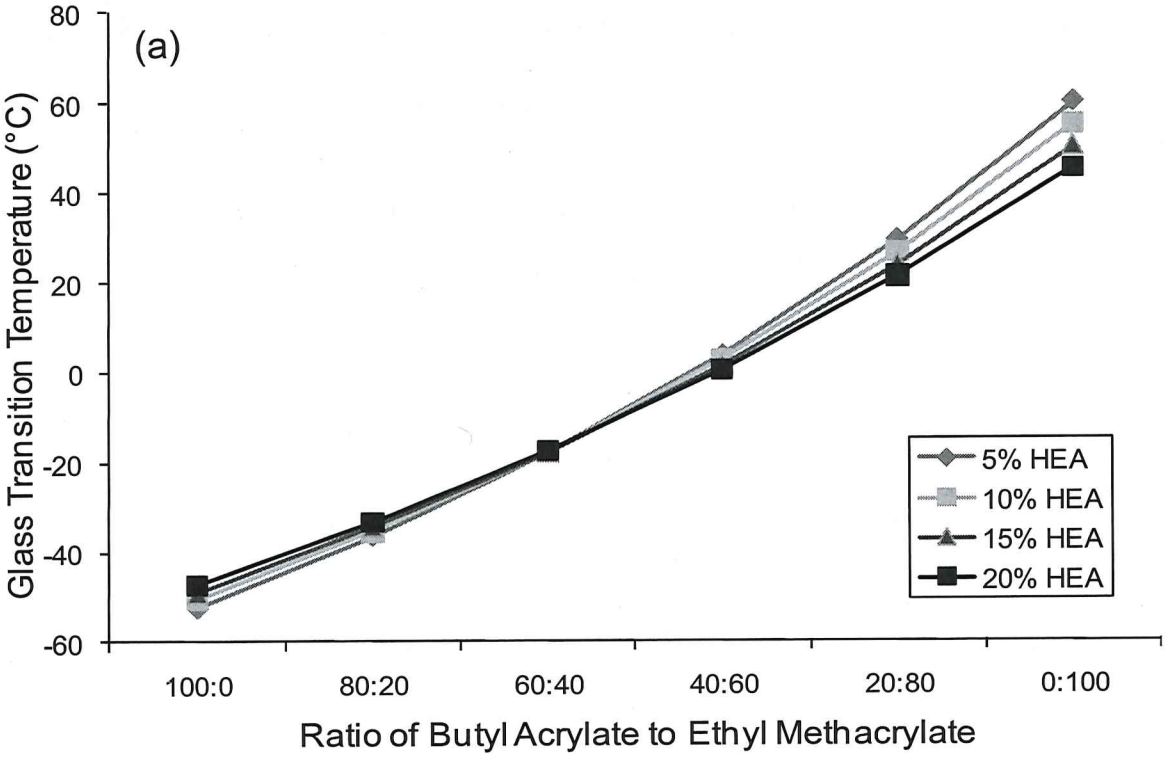

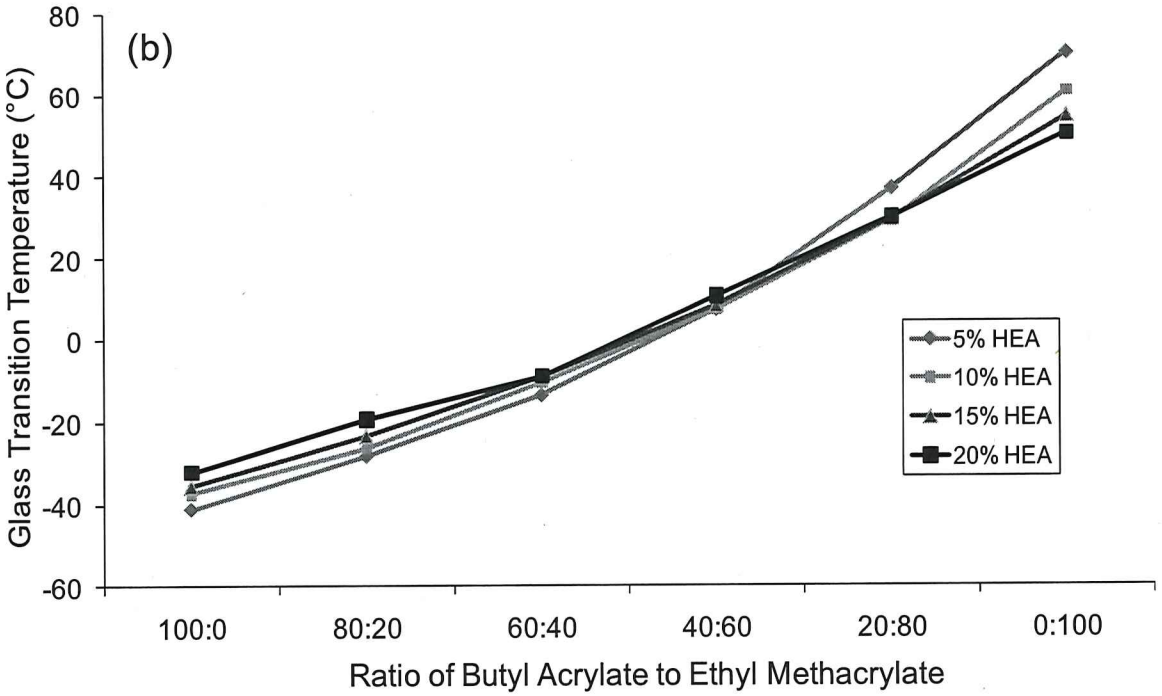

Figure 2.10. DSC (a) theoretical and (b) experimental glass transition temperature data for acrylic polyol library comprised of HEA, BA, and EMA.

be possible to get lower T_g values that might correlate better with the theoretical T_g values. Percent conversion was determined from the results of the percent solids which was calculated gravimetrically and showed that all acrylic polyols had conversions above 95%, with a range of 95.3%-99.1%.

2.3.3. Free radical polymerization study of acrylic polyols comprised of HEA, BA, and BMA using combinatorial methods

The next acrylic polyol library comprised of three monomers, HEA, BA, and BMA, were produced by free radical polymerization using combinatorial techniques resulting in 24 unique acrylic polyol compositions. The acrylic polyol composition is illustrated in Figure 2.11 in a 4X6 array library format.

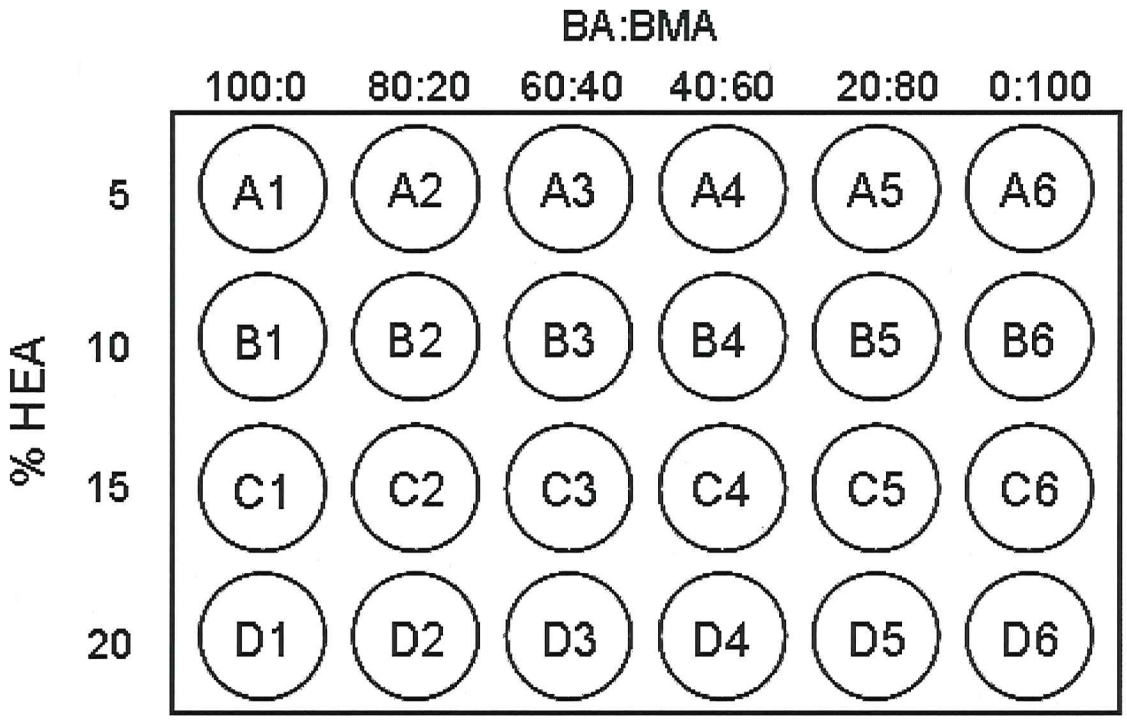

Figure 2.11. 4X6 array library format of acrylic polyol composition consisting of 5-20 % HEA, and ratio of 100:0 to 0:100 (BA: BMA).

The change from EMA to BMA was done with the understanding that this would modify the T_gs of the library since the T_g of BMA is 45°C less than EMA due to the longer alkyl chain increasing mobility of the polymer thus, decreasing the T_g. The polymerization conditions consisted of 4%/wt initiator, 50% solids, and a reaction temperature of 95°C, which was increased from 75°C to look at the effects of temperature on the MW. HEA was varied from 5 to 20 percent to provide a range of hydroxyl equivalent weight from 581 g/mol to 2324 g/mol. A combination of BA and BMA were varied by a range of ratios from 100:0 (BA:EMA) to 0:100 (BA:EMA). The 24 acrylic polyols were synthesized in a single experiment using the automated batch synthesis system.

The RGPC molecular weight results for the library can be seen in Figure 2.12. As the amount of BMA is increased, the MW values of the acrylic polyols decreased as expected due to BA terminating by combination and BMA terminating predominantly by disportionation.[16] Similar to the pervious study, the termination reactions of the acrylic polyols play a large factor in the MW evident by the copolymers comprised of BA and HEA having MW of 110-125 kDa. The polyols consisting of BMA and HEA have MW of 20-30 kDa, a decrease of 100 kDa is observed over the compositional space, this is once again similar to the acrylic polyol library study using EMA. Overall, the amount of HEA in the acrylic polyols has a small effect on the overall molecular weight, however there is a slight increase in MW (~10K/ BA:BMA composition) as the HEA is increased, which seems to be a common trend throughout the acrylic polyol library. Also,

comparing the GPC results of 100:0 (BA:BMA) to Figure 2.6 of a similar composition (EMA v. BMA) showed a significant drop in MW due to the higher reaction temperature and thus a lower half-life (1.13 min) of the Vazo 67 indicating the termination of the propagating species sooner than in the previous acrylic polyol study.

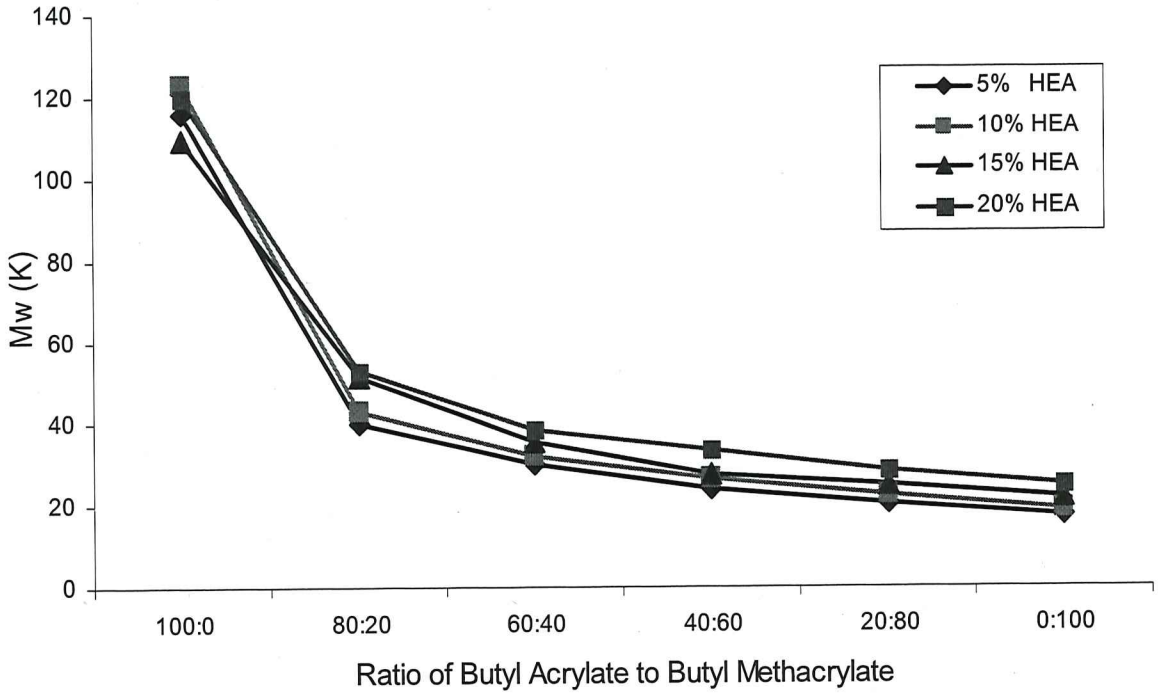

Figure 2.12. Rapid GPC molecular weight data for acrylic polyol library comprised of 5-20 % HEA, and ratio of 100:0 to 0:100 (BA: BMA).

The polydispersity data for the acrylic polyol library is illustrated in Figure 2.13. Similar to the molecular weight data in Figure 2.12, the BA and HEA acrylic polyol compositions have considerably higher polydispersities compared to the acrylic polyols with the composition of BMA and HEA. PDIs for the BA and HEA compositions ranged from 13-16, significantly higher than the composition with 80:20 (BA:BMA) which had a PDI range of 5-7. This may be due to the increase in

viscosity due to the hydrogen bonding of HEA and the high molecular weight of the acrylic polyol. With the addition of BMA, even in a small amount, allowed for the lowering of the viscosity of the solution polymerization thus allowing for better control of the MW and as a result the PDI was much lower. As the amount of BMA was increased the PDI eventually reached a minimum of ~3 and showed a rather tight grouping regardless of the amount of HEA throughout the entire library compositional space.

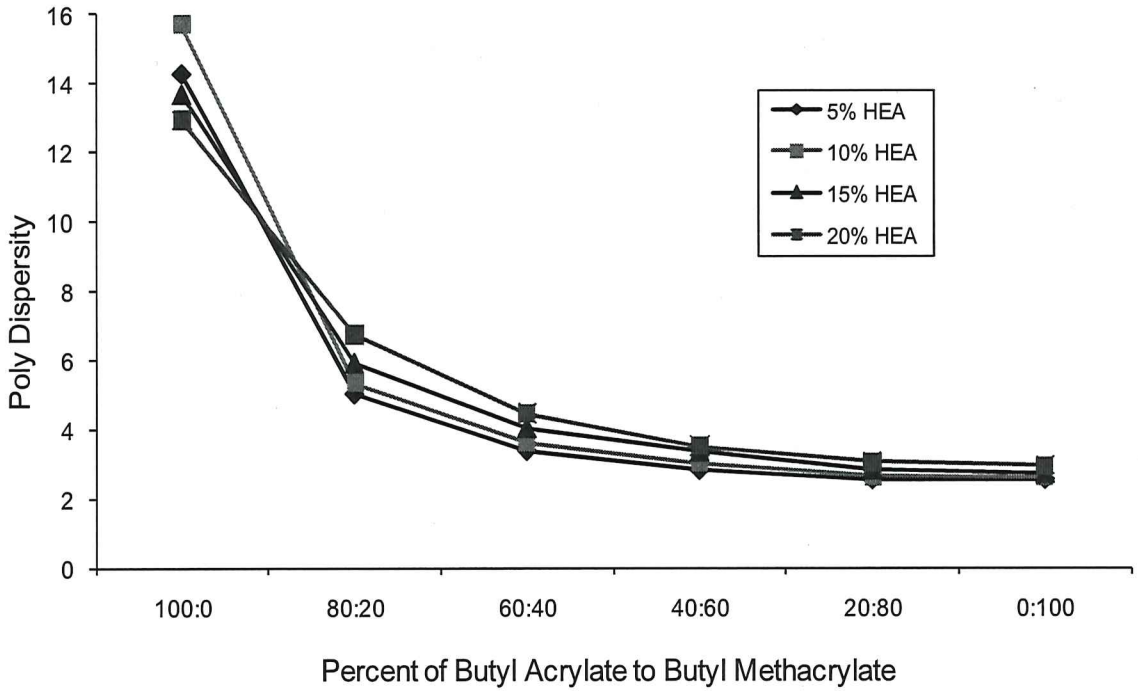

Figure 2.13. Rapid GPC polydispersity data for acrylic polyol library comprised of 5-20 % HEA, and ratio of 100:0 to 0:100 (BA: BMA).

In Figure 2.14, both theoretical and experimental glass transition temperatures were calculated for the acrylic polyols comprised of HEA, BA, and BMA. Overall, there is a general trend of a linear increasing of the T_gs with an increase of BMA in the acrylic polyol composition. Acrylic polyols with the

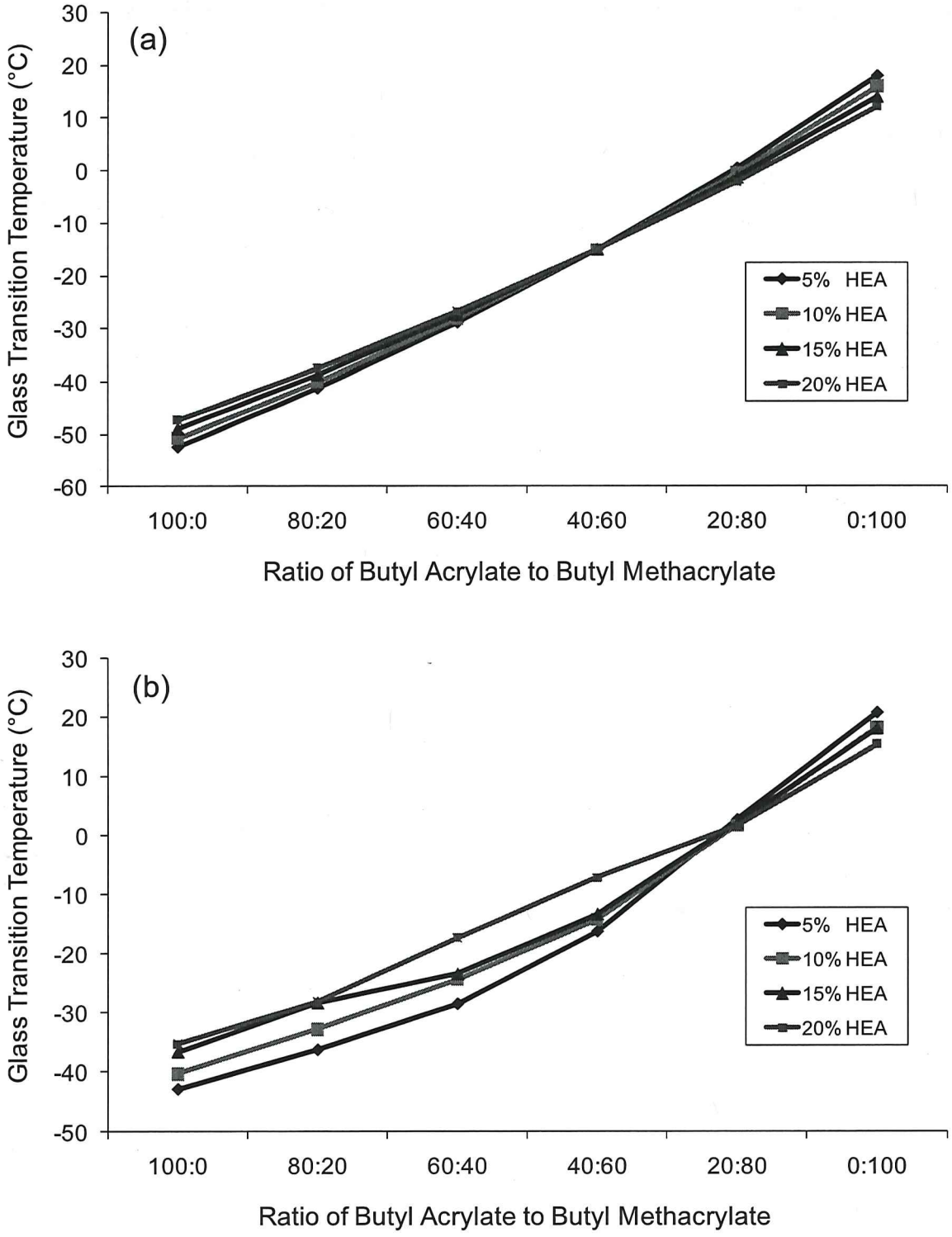

Figure 2.14. DSC (a) theoretical and (b) experimental glass transition temperature data for acrylic polyol library comprised of 5-20 % HEA, and ratio of 100:0 to 0:100 (BA: BMA).

composition ratio of 100:0 (BA:BMA) produced the lowest T_gs, ranging from -45°C to -35°C with 5% HEA through 20% HEA, respectively. The increase in HEA causes a slight increase in T_gs due to the increase in hydrogen bonding. As the amount of BMA is increased in the composition of the acrylic polyol, the T_gs increase in a generally linear way, however, there is a convergence of the T_gs at the ratio 20:80 (BA:BMA) indicating that at this point (~0°C), regardless of the amount of HEA, all have the same relative T_gs. Another interesting trend observed from Figure 2.14 is after the convergent point the acrylic polyols with the lower HEA content have higher T_gs than those with higher amount of HEA, which is the opposite of what was seen before the convergence point. These similar trends are also seen in the previous acrylic polyol library using EMA instead of BMA. The most interesting trend is the convergence point of 0°C, which was the same for the previous library. An observation when comparing the theoretical T_gs to the experimental T_gs was the convergence point was -20°C for the theoretical polyols and was once again 0°C for the experimental polyols. Also, the experimental T_gs for the higher ratios of BA were lower than the theoretical values. Similar to the previous study, this may possibly be from the molecular weight or structure of the experimental acrylic polyols resulting in higher values. These higher values may also be from the speed of the heating rate of the DSC experiment.

Percent conversion for the experimental acrylic polyols were determined from the results of the percent solids which was calculated gravimetrically and

showed that all acrylic polyols had conversions above 96%, with a range of 96.4%-98.7%.

A similar library was designed using the same three monomers (HEA, BA and BMA). In this acrylic polyol library the percent HEA was increased to a range of 15-40% and the BA:BMA ratio was changed to the range of 100:0 to 50:50 as shown in the 4X6 array library format in Figure 2.15. The objective of this study was to better understand the effects of an increase of HEA in composition and also to give another acrylic polyol library with a range of T_gs and modulus.

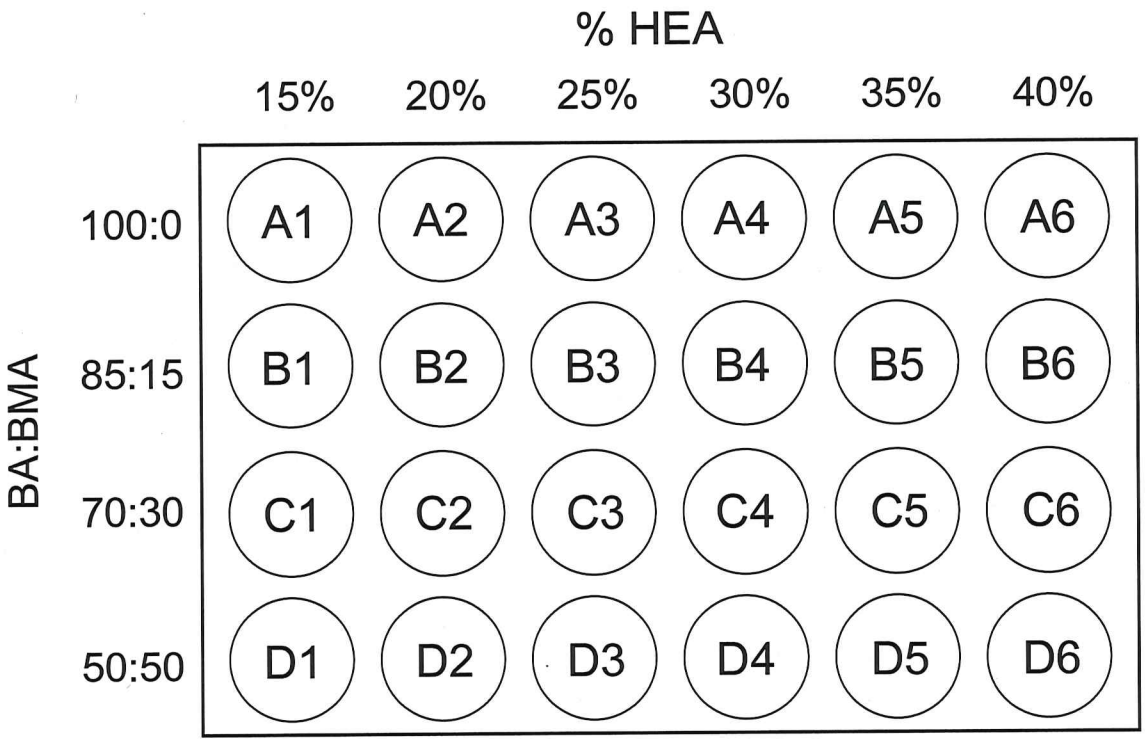

Figure 2.15. 4X6 array library format of acrylic polyol composition consisting of 15-40 % HEA, and ratio of 100:0 to 50:50 (BA: BMA).

The polymerization conditions consisted of 4%/wt initiator, 50% solids, and a reaction temperature of 95°C. HEA was varied from 15 to 40 percent to provide

a range of hydroxyl equivalent weight from 290 g/mol to 775 g/mol. A combination of BA and BMA were varied by a range of ratios from 100:0 (BA:BMA) to 50:50 (BA:BMA). The 24 acrylic polyols were synthesized in a single experiment using automated batch synthesis system. The results of this acrylic polyol library are explained in Chapter 3 of this dissertation.

2.3.4. Free radical polymerization study of acrylic polyols comprised of HEA, BA, and LMA using combinatorial methods

The next acrylic polyol library comprised of three monomers, HEA, BA, and LMA, was produced by free radical polymerization using combinatorial techniques resulting in 24 unique acrylic polyol compositions. The acrylic polyol composition is illustrated in Figure 2.16 in a 4X6 array library format. The polymerization conditions consisted of 4%/wt initiator, 50% solids, and a reaction temperature of 95°C. HEA was varied from 5 to 20 percent to provide a range of hydroxyl equivalent weight from 581 g/mol to 2324 g/mol. A combination of BA and LMA were varied by a range of ratios from 100:0 (BA:LMA) to 0:100 (BA:LMA). LMA was chosen for this study to better understand the effect of using a monomer with a much lower T_g on the overall acrylic polyol compositions T_gs.

The RGPC molecular weight results for the acrylic polyol library can be seen in Figure 2.17. As the amount of LMA is increased, the MW values of the acrylic polyols decreased as expected due to BA terminating by combination.[16] Similar to the pervious study, the termination reactions of the acrylic monomers play a large factor in the MW evident by the copolymers comprised of BA and HEA having MW of 90-145 kDa.

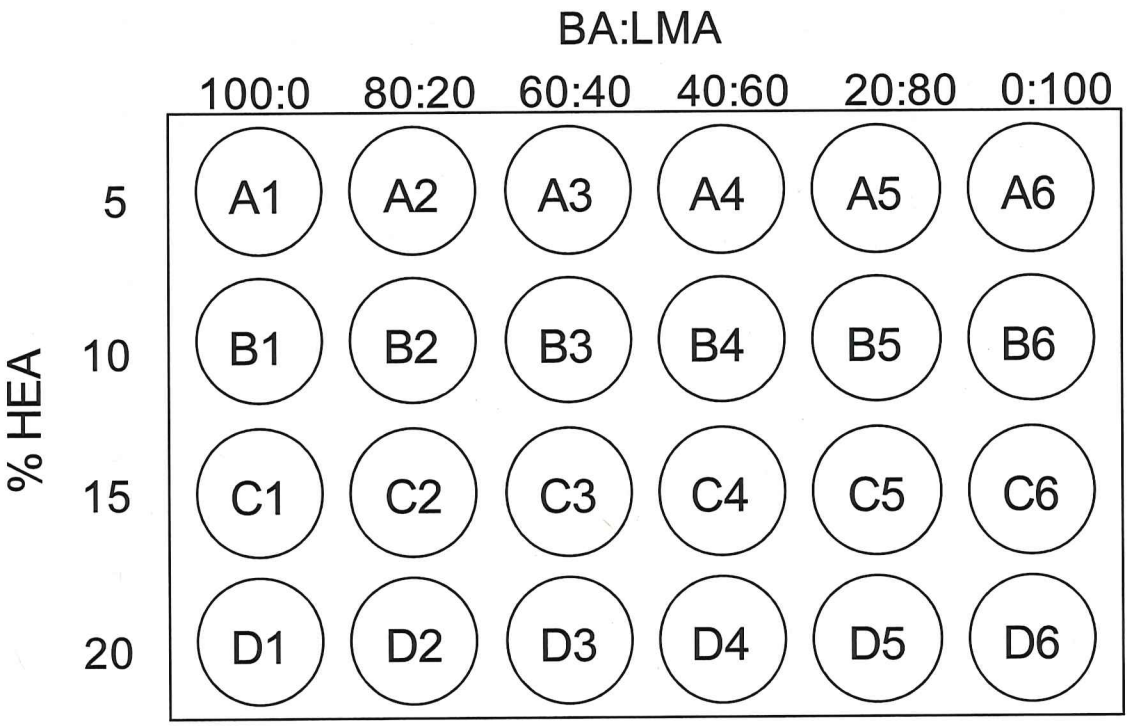

Figure 2.16. 4X6 array library format of acrylic polyol composition consisting of 5-20 % HEA, and ratio of 100:0 to 0:100 (BA: LMA).

The polyols consisting of LMA and HEA have MW of 30-70 kDa, a decrease of 60 kDa is observed over the compositional space, this is once again similar to the acrylic polyol library study using EMA and BMA. Overall, the amount of HEA in the acrylic polyols has a larger effect on the overall molecular weight than the previous studies. The 20% HEA seems to have the largest effect by having the larger of the MWs in comparison to the rest of the library which has a common trend of a tighter MW grouping throughout the acrylic polyol library with the 5-15% HEA compositions.

The polydispersity data for the acrylic polyol library is illustrated in Figure 2.18. Showing a similar trend to the molecular weight data in Figure 2.17, the BA and HEA acrylic polyol compositions have considerably higher polydispersities

compared to the acrylic polyols with the composition of LMA and HEA. PDIs for the BA and HEA compositions ranged from 12-14, significantly higher than the first composition with 80:20 (BA:LMA) which had a PDI range of 6-8. This may be due to the increase in viscosity due to the hydrogen bonding of HEA and thus the high molecular weight of the acrylic polyol.

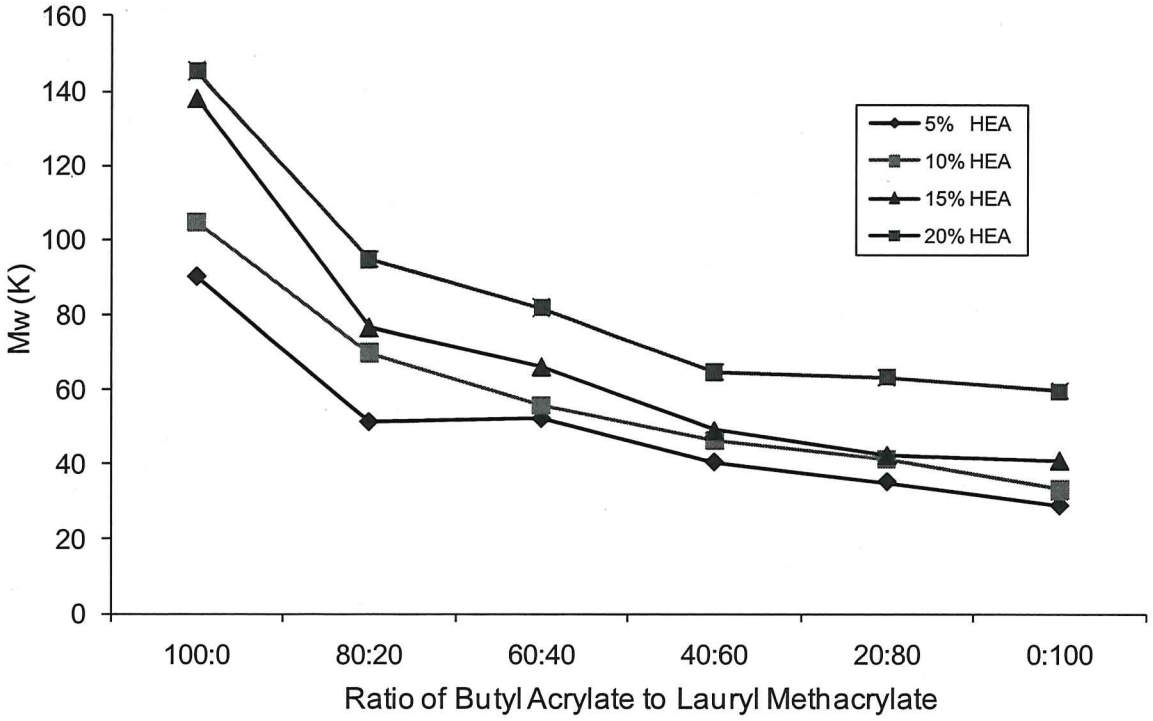

Figure 2.17. Rapid GPC molecular weight data for acrylic polyol library comprised of 5-20 % HEA, and ratio of 100:0 to 0:100 (BA: LMA).

With the addition of BMA, even in a small amount, allowed for the lowering of the viscosity of the solution polymerization thus allowing for better control of the MW and as a result the PDI was much lower. As the amount of LMA was increased in the acrylic polyol compositions the PDIs eventually reached a minimum convergence of ~3 and showed a rather tight grouping regardless of the amount of HEA throughout the entire library compositional space. The exception

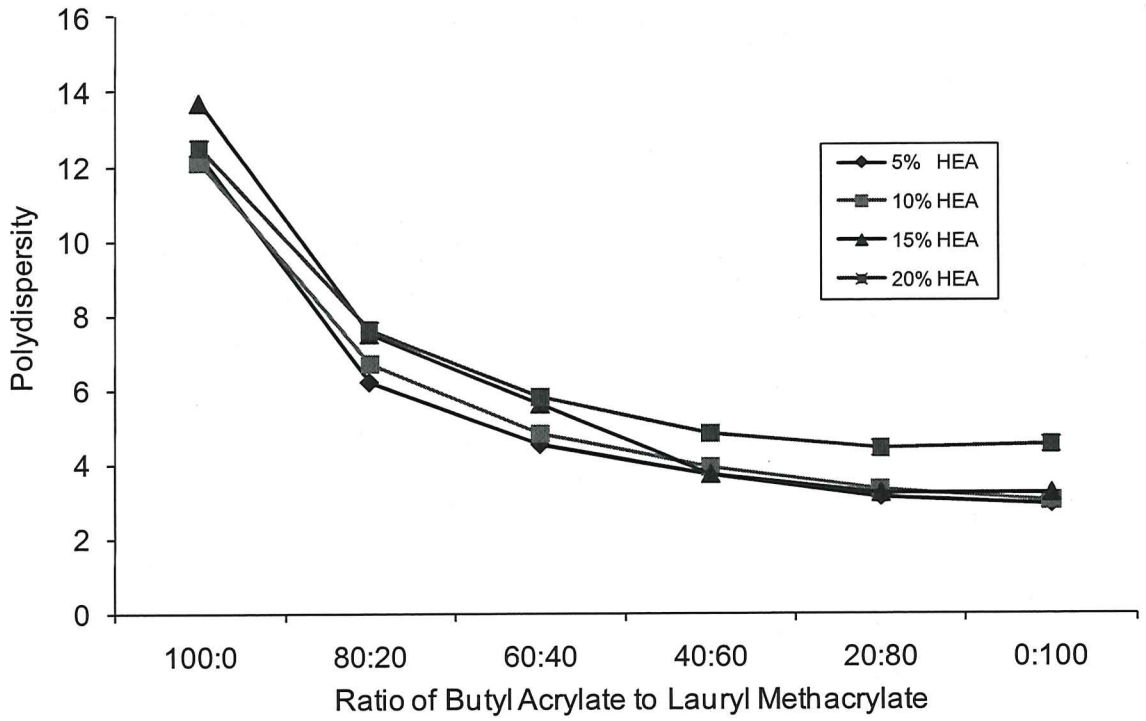

Figure 2.18. Rapid GPC polydispersity data for acrylic polyol library comprised of 5-20 % HEA, and ratio of 100:0 to 0:100 (BA: LMA).

being similar to the results seen in Figure 2.18, in which the polyols with 20% HEA showed a minimum PDI of ~5.

Figure 2.19 illustrates the DSC measurements of the glass transition temperatures of the theoretical and experimental acrylic polyols comprised of HEA, BA, and LMA. Overall, there is a general trend of a linear decrease of the T_gs with an increase of LMA in the acrylic polyol composition which is expected since the T_g of LMA is -65°C compared to BA which has a T_g of -54°C. Acrylic polyols with the composition ratio of 0:100 (BA:LMA) produced the lowest T_gs, ranging from -56°C to -64°C with 5% HEA through 20% HEA, respectively. The

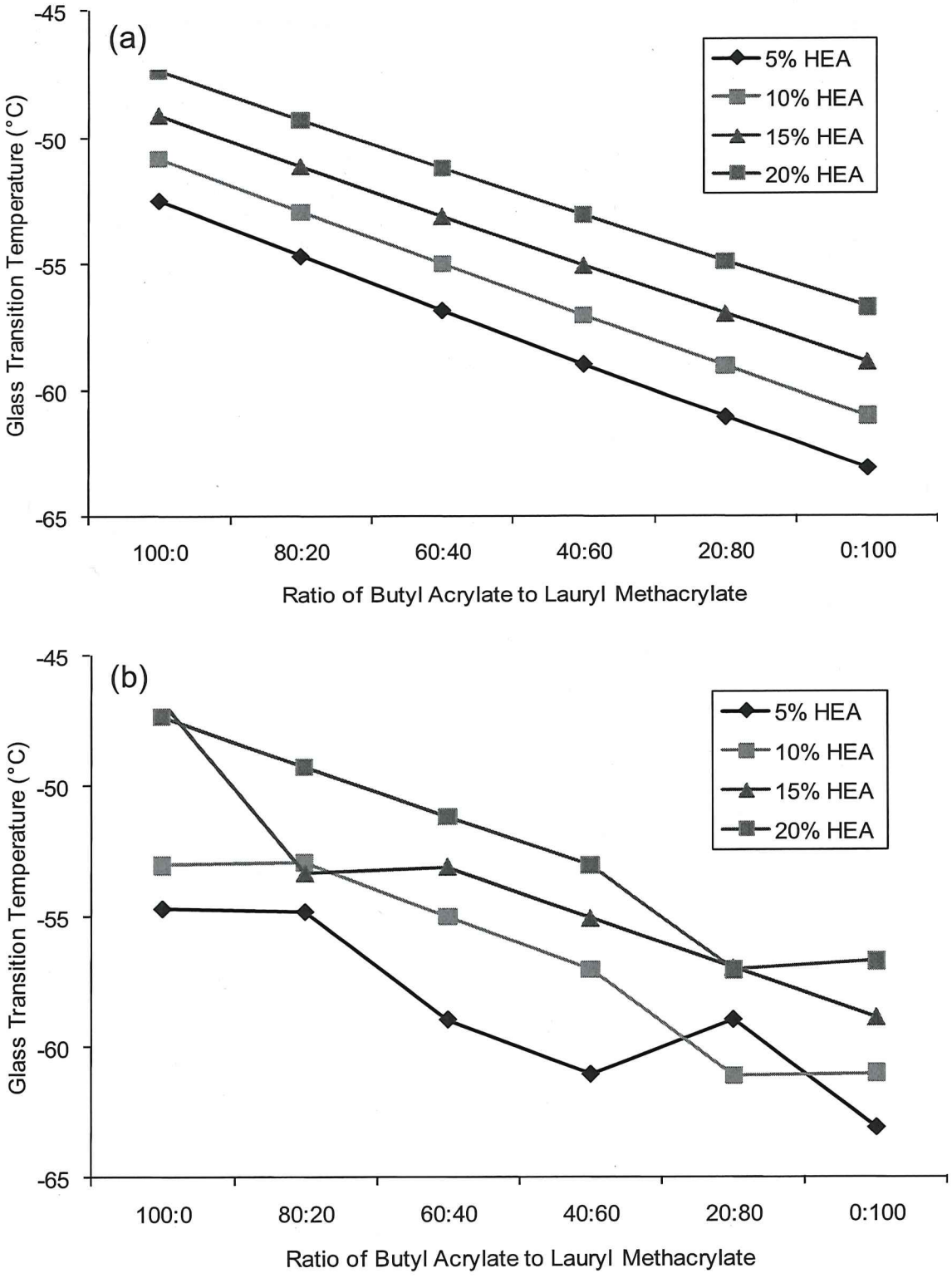

Figure 2.19. DSC theoretical (a) and experimental (b) glass transition temperature data for acrylic polyol library comprised of 5-20 % HEA, and ratio of 100:0 to 0:100 (BA: LMA).

increase in percent HEA causes a slight increase in T_gs due to the increase in hydrogen bonding and having the highest of the homopolymer T_gs of -15°C. This can be seen with the 5% HEA acrylic polyol compositions having an average of 10°C lower T_gs than the compositions with 20% HEA indicating that the BA and LMA have a much larger effect on the overall T_gs. Also observed is that as the percent of LMA is increased in the composition of the acrylic polyol, the T_gs decrease as expected. The theoretical T_gs for the acrylic polyol showed a linear decrease with an increase in the ratio of LMA. Compared to the results from the experimental T_gs, there was a similar decrease in the T_gs, however due to possible molecular weight effects, structure of the acrylic polyol, and the heating rate of the DSC, the experimental T_gs slightly different than the theoretical values.

A similar acrylic polyol library to the previous study was comprised of the same three monomers, HEA, BA, and LMA, and was produced by free radical polymerization using combinatorial techniques resulting in 24 unique acrylic polyol compositions. The acrylic polyol composition is illustrated in Figure 2.20 in a 4X6 array library format. The polymerization conditions consisted of 4%/wt initiator, 50% solids, and a reaction temperature of 95°C. HEA was increased in this study providing a range of 10 to 40% percent thus; provide a range of hydroxyl equivalent weight from 290 g/mol to 1162 g/mol. A combination of BA and LMA were varied by a range of ratios from 100:0 (BA:LMA) to 0:100 (BA:LMA). By increasing the HEA percent for this study the objective was to better understand the effects on the overall T_gs of the acrylic polyol library. Illustrated in Figure 2.21 are the RGPC molecular weight results for the acrylic polyol library.

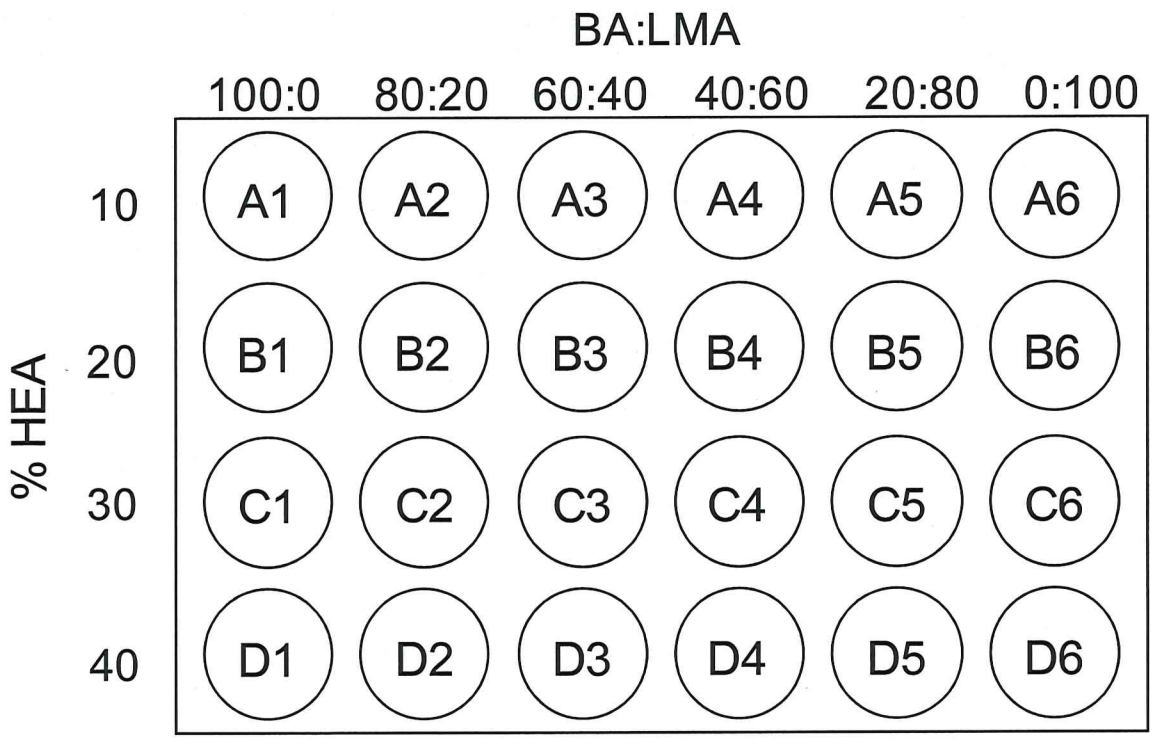

Figure 2.20. 4X6 array library format of acrylic polyol composition consisting of 10-40 % HEA, and ratio of 100:0 to 0:100 (BA: LMA).

As the amount of LMA is increased, the MW values of the acrylic polyols decreased as expected due to BA terminating by combination[16] however, due to the significant amount of hydrogen bonding with the higher percent HEA compositions and subsequent increase in viscosity the acrylic polyols have lower MW. The acrylic polyols with said compositions actually formed gels so only the soluble fraction was analyzed, which may have contributed to the lower MWs. The gelled polymer did not allowing for adequate mixing during the reaction and thus retarding the radical species during the propagation step of the polymerization and terminating the polymer resulting in lower MW acrylic polyols. As described, the termination reactions of the acrylic polyols play a large factor in the MW evident by the copolymers comprised of 30% and 40% HEA having MW of 80 and 90 kDa,

respectively. The acrylic polyols consisting of 10% and 20% HEA and 100:0 (BA:LMA) resemble the same MWs from the previous study as expected with values of 120 kDa for 10% HEA and 165 kDa for 20% HEA. With the addition of LMA into the compositions the acrylic polyols the general trend of decreasing MW was observed, similar to pervious study with LMA, as well as the study with EMA and BMA. Overall, the amount of HEA in the acrylic polyols has a larger effect on the overall molecular weight than the previous studies. The 40% HEA seems to have the largest effect by having the larger of the MWs ranging from 230 kDa to 125 kDa as the amount of LMA is increased to 0:100 (BA:LMA). Another observation is the larger separation of MWs between the percentages of HEA in the acrylic polyol compositions when compared to Figure 2.17 from the previous study.

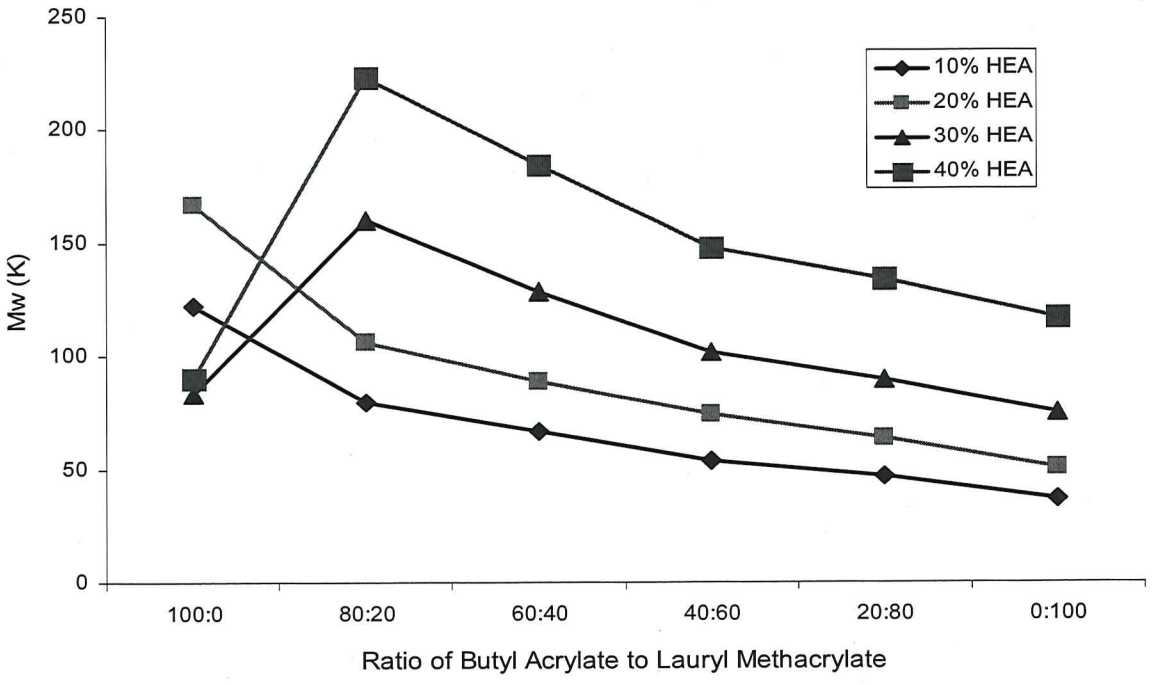

Figure 2.21. Rapid GPC molecular weight data for acrylic polyol library comprised of 10-40 % HEA, and ratio of 100:0 to 0:100 (BA: LMA).

The polydispersity data for the acrylic polyol library is illustrated in Figure 2.22. Showing a similar trend to the molecular weight data in Figure 2.21, the BA and HEA acrylic polyol compositions have considerably higher polydispersities compared to the acrylic polyols with the composition of LMA and HEA. PDIs for the BA and HEA compositions ranged from 12-14, significantly higher than the first composition with 80:20 (BA:LMA) which had a PDI range of 6-8. This may be due to the increase in viscosity due to the hydrogen bonding of HEA and thus the high molecular weight of the acrylic polyol. With the addition of BMA, even in a small

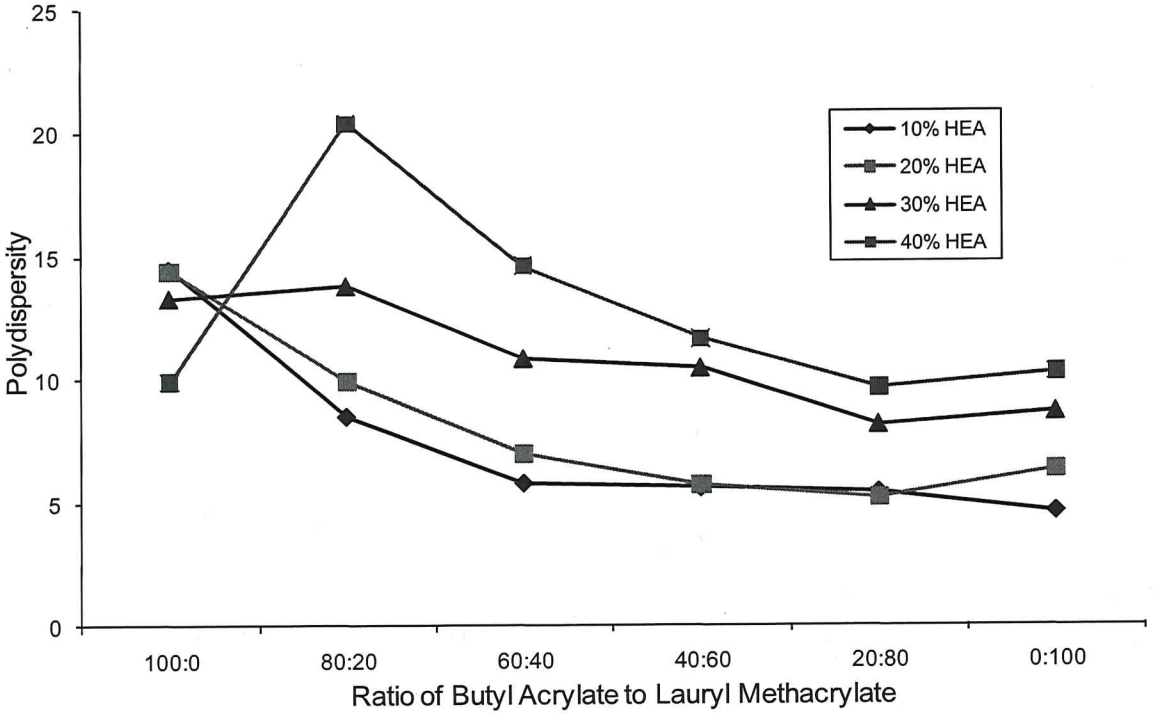

Figure 2.22. Rapid GPC polydispersity data for acrylic polyol library comprised of 10-40 % HEA, and ratio of 100:0 to 0:100 (BA: LMA).

amount, allowed for the lowering of the viscosity of the solution polymerization thus allowing for better control of the MW and as a result the PDI was much lower.

As the amount of LMA was increased in the acrylic polyol compositions the PDIs eventually reached a minimum convergence of ~3 and showed a rather tight grouping regardless of the amount of HEA throughout the entire library compositional space. The exception being similar to the results seen in Figure 2.15, in which the polyols with 20% HEA showed a minimum PDI of ~5.

Figure 2.23 illustrates the DSC theoretical and experimental measurements of the glass transition temperatures of the acrylic polyols comprised of HEA, BA, and LMA. Overall, there is a general trend of a linear decrease of the T_gs with an increase of LMA in the acrylic polyol composition which is expected since the T_g of LMA is -65°C compared to BA which has a T_g of -54°C. Acrylic polyols with the composition ratio of 0:100 (BA:LMA) produced the lowest T_gs, ranging from -56°C to -64°C with 5% HEA through 20% HEA, respectively. The increase in percent HEA causes a slight increase in T_gs due to the increase in hydrogen bonding and having the highest of the homopolymer T_gs of -15°C. This can be seen with the 5% HEA acrylic polyol compositions having an average of 10°C lower T_gs than the compositions with 20% HEA indicating that the BA and LMA have a much larger effect on the overall T_gs. Another observed trend is that as the percent of LMA is increased in the composition of the acrylic polyol, the T_gs decrease as expected. The overall change in T_gs are all $\trianglelefteq$0°C from 100:0 to 0:100 (BA:LMA) for 10, 20 30, and 40% HEA this is due to both BA and LMA having very low T_gs, thus there isn't a dramatic effect on the acrylic polyols T_gs from 100 wt% BA to 100 wt% LMA. The theoretical T_gs for this study followed the same trend seen in Figure

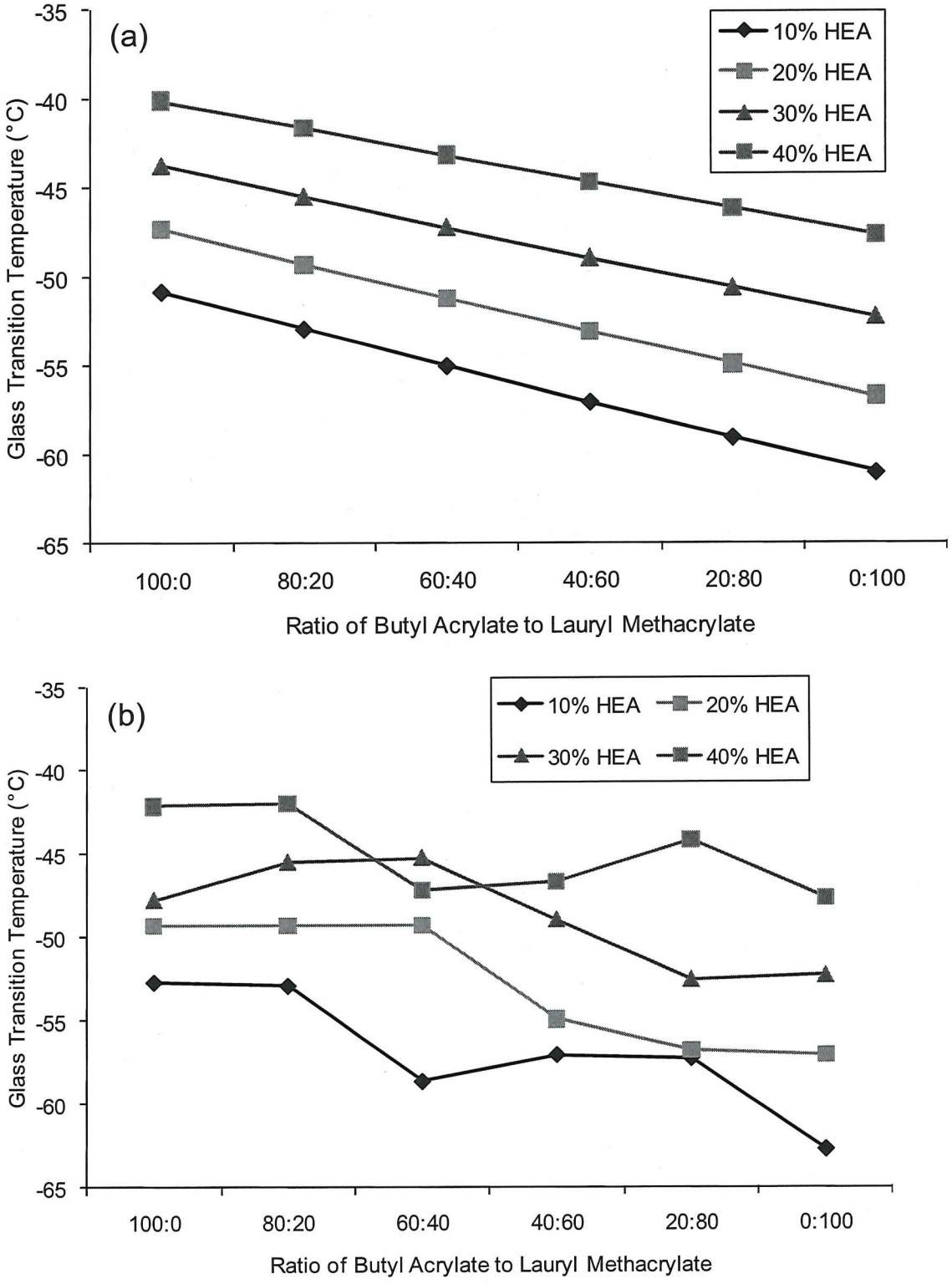

Figure 2.23. DSC theoretical (a) and experimental (b) glass transition temperature data for acrylic polyol library comprised of 10-40 % HEA, and ratio of 100:0 to 0:100 (BA: LMA).

2.19, with a decrease in T_gs with the increase in LMA. An observation when comparing the experimental T_gs to the theoretical T_gs is the values are similar. The major differences seen with the experimental values are most like due to molecular weight effects, structure of the acrylic polyols, and the heating rate of the DSC. These variables would lead to variations in the experimental T_gs when compared to theoretical values that were calculated by use of the Fox equation.

Overall the acrylic polyols comprised of HEA, BA, and LMA showed a decrease in MW with an increase in LMA in the composition consistent with previous findings due to the termination reaction of BA by combination. The data supports these observations for polydispersity as well. The DSC data indicates that BA and LMA had little effect on the overall T_gs; HEA played a much larger role in the determination of the polyols T_gs due to its higher T_g when compared to the T_gs of BA and LMA.

The characterization results from the FRP of the various acrylic polyols done on this first part of the study were useful in selecting the acrylic polyol libraries to be used in the formulations of the siloxane-acrylic-polyurethane coatings systems described in the next chapter.

2.3.5. Systematic measuring of percent conversion and MW of acrylic polyols using the Chemspeed Autoplant A100™

The second part of the study consisted of using the Chemspeed Autoplant 100™ for the free radical polymerization of acrylic polyols using a semi-batch process, which is the process most commonly used in industry. The main objective of this study was to better understand the capabilities of the Chemspeed

by exploring the effects of key process variables on the outcome of the acrylic polyol polymerizations. Several experiments were conducted to test these process variables. The first experiment consisted of measuring the PDI and MW systematically throughout the course of the semi-batch FRP of the acrylic polyols. The second experiment comprised of varying the percent solvent and percent initiator in the FRP of acrylic polyols, similar to the batch process experiment done in the first part of this study. Since the Chemspeed has the ability to be programmed to automatically adjust the feed time of the reactants into the reactor vessel The third experiment involved adjusting the monomer feed time during the FRP while keeping the initiator feed time constant. The fourth experiment was similar to the previous experiment except the initiator feed time was adjusted and the monomer feed time was held constant. The final experiment incorporated the ability of the Chemspeed to be programmed to oscillate the reaction temperature of each PD unit separately. In this case the reaction temperatures were oscillated at either 95±5°C, 105±5°C, 95±10°C or 105±10°C during the FRP of the acrylic polyols.

The experiments used in this study consist of the use of 12 Process Development (PD) units located on the Chemspeed platform. Each PD unit contains two 100 mL stainless steel reactors one utilized for the polymerization and the other for holding the monomer feed solution. A third 50 mL feed vessel is also present in each PD unit and was used for the initiator solution, which was cold when dispensed into the feed vessel. All PD units were set to a mechanical stirring of 200 rpm and in order to keep the monomer solution cold, reflux cooling

was incorporated for the monomer feed vessel and set at -10°C. The liquid reagents (toluene, monomer solution, and initiator solution) were automatically charged to each reactor and feed vessels via the 4-channel needle head. Several different real-time data analysis factors, such as temperature and stirring, were monitored for all of the 12 PD units. Nitrogen was used to purge the reactor vessel after the toluene was charged into each reactor vessel.

In this study the acrylic polyol free radical polymerization comprised of 20% HEA and 80% BA, initiator (Vazo 67) concentration of 4%, and 50% solids, was done using a Chemspeed Autoplant A100™. Illustrated in Figure 2.24 is the design of the experiment (DOE). The study was duplicated with reactors 1-6 being the exact same reactions as reactors 7-12, respectively. Essentially the Chemspeed platform was split in half so that six reaction temperatures could be reproduced twice in one run. The temperature in each reactor was programmed and controlled independently ranging from 70°C to 120°C.

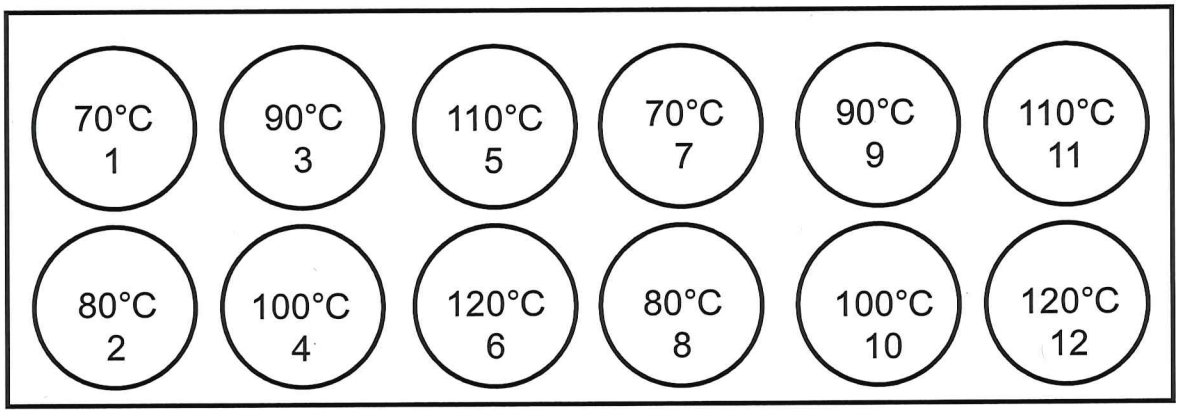

Figure 2.24. Schematic representation of the Chemspeed Autoplant A100™ platform indicating reaction temperature and miniplant location for the acrylic polyol "kinetics study."

The PD units are labeled with their respective locations and reaction temperatures depending on programmed location on the Chemspeed platform. The contents of the two feed vessels were then fed into the reactor vessel at a rate of 0.18 ml/min for the monomer and 0.04 ml/min for the initiator solutions using the two syringe pumps on the PD unit. Depicted in Figure 2.25. is a graphical timeline of events for the FRP of the acrylic polyols. After the toluene was charged to the reactor vessels, heating and stirring was started and a wait time of ten minutes was incorporated so that each reactor could reach and maintain the stability of the respective reaction temperature. Once the temperature was stable the pumps began to feed both the monomer and initiator solutions into the reactor vessel. The feed time for both feed vessels were set to 180 minutes with a total reaction time of 300 minutes.

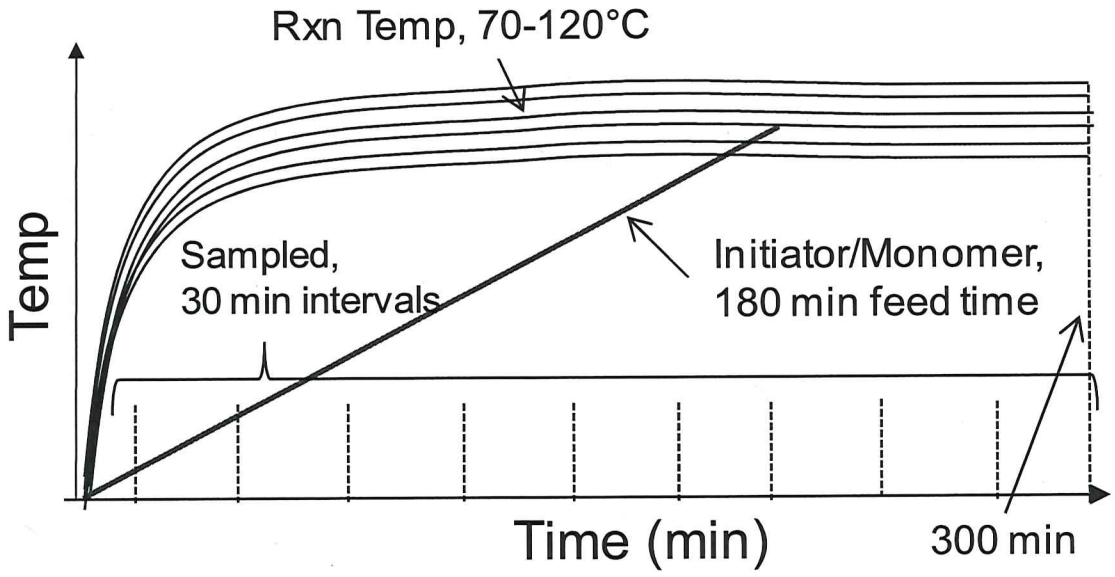

Figure 2.25. Graphical timeline of events for the systematic measuring of PDI and MW for the FRP of acrylic polyols.

For each polymerization, aliquots were taken from the reactor vessels every 30 minutes during the reaction and continued at that interval until the reaction time was complete.

The samples were characterized by RGPC and percent conversion. The RGPC molecular weight results of the acrylic polyols from reactors 1-6 can be seen in Figure 2.26. The y-axis was set to match the MW data from reactors 7-12 illustrated in Figure 2.27 for a better comparison on the reproducibility of the study. A general trend that is observed is the decrease in MW with an increase in reaction temperature. This trend is consistent with the free radical initiators half-life at the given reaction temperatures.

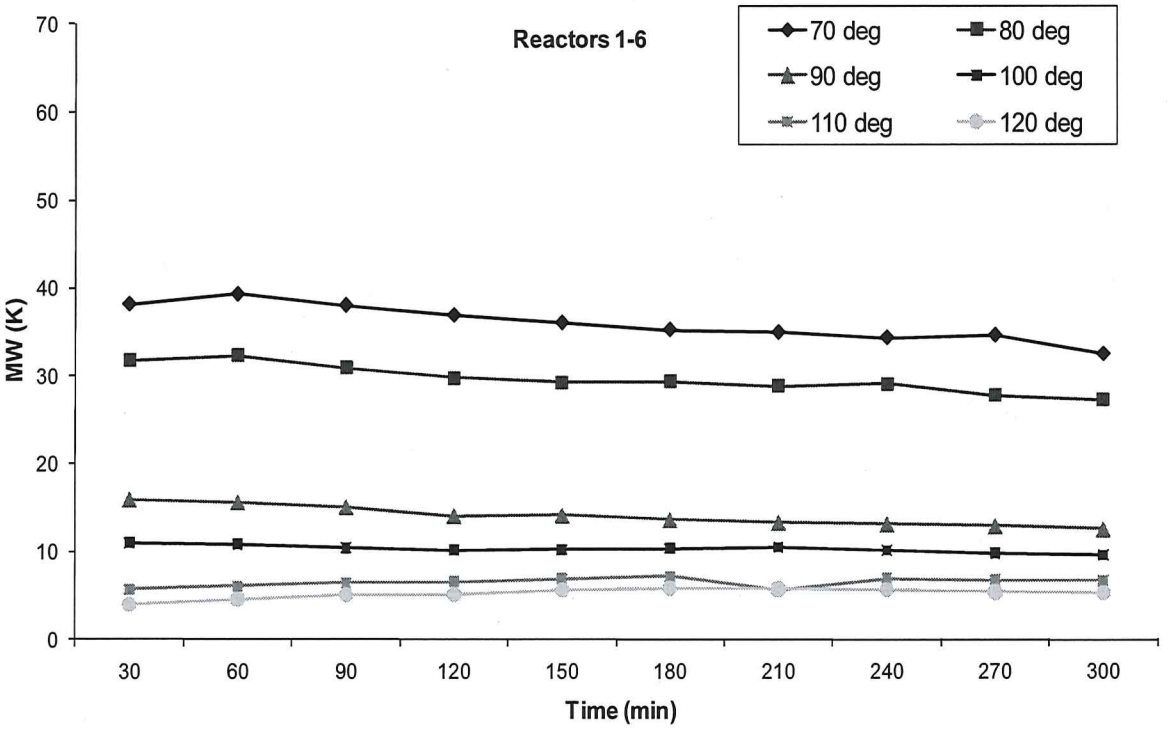

Figure 2.26. Rapid GPC molecular weight data from kinetics study of the acrylic polyol library indicating miniplant reactors 1-6, reaction temperature, and 30 minute sample intervals over the entire reaction time.

At 70°C the half-life of the free radical initiator (289 min) is the longest compared to the other reaction temperatures; because of this the initiator generates radicals at a slower rate, so there are less radical to initiate the monomer, leading to higher MW. Another trend observed is the large MW difference between the reaction temperatures of 80°C and 90°C.

There is a drop-off of nearly 20 kDa between 80°C and 90°C. This indicates that between 80°C and 90°C the half-life of the initiator is much lower causing the radicals to persist for a much shorter time, thus creating much lower MW acrylic polyols. The half-life of the initiator at 80°C is 74 minutes compared to 21 minutes for 90°. It can be observed from the graph from Figure 2.27 that Vazo

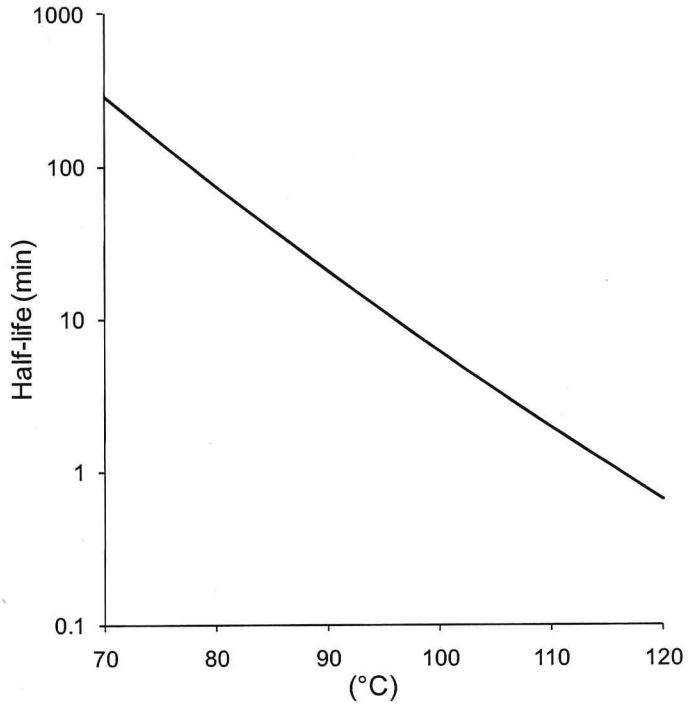

Figure 2.27. Half-life of Vazo 67 at various reaction temperatures.

67 readily decomposes at higher temperatures leading to a shorter half-life, which can have a great effect on the molecular weight of the polymer. Since this polymerization is done in a semi-batch mode the polymer MW is well controlled due to the constant control of the concentration ratio of the reactants through predetermined feeding times. Since this study was to better understand the MW and PDI effects using a semicontinuous process on the FRP of acrylic polyols, an observation can be seen in the MW results; already seen after 30 minutes into the polymerization, the acrylic polyols have essentially the same MW throughout the rest of the reaction time. This observation suggests that the monomer consumption rate is equal to the addition rate resulting in a mean chain length being a ratio of monomer to initiator providing constant composition control.[64]

Taking a closer look at this trend of a consistent MW throughout the entire reaction shows that the MW for the reaction temperatures ranging from 70°C to 90°C actually decrease as the reaction progressed to the end. The most dramatic Mw change came from the 70°C temperature. At 70°C, the MW at 30 minutes was 38 kDa, over time the MW decreased to 22 kDa; this trend is most likely due to the amount of solids in the reactor at any given time. Illustrated in Figure 2.28 are the theoretical percent solids as a function of time assuming 100 percent conversion. This observation is consistent with the MW results from the solvent/initiator study previously analyzed in 2.3.1. This same trend can be seen at 80°C, where the MW decreased from 32 kDa to 27 kDa. At the higher reaction temperature of 110°C and 120°C, the MW stayed the same throughout the entire reaction. The MWs were within the variability of the RGPC.

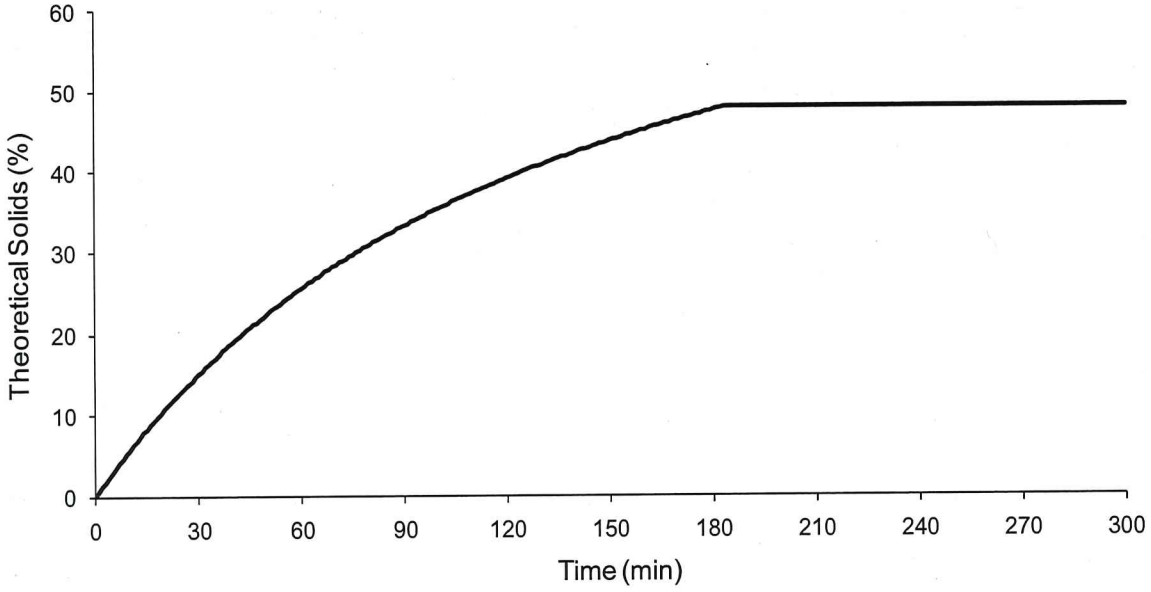

Figure 2.28. Graphical representation of the acrylic polyol theoretical percent solids as a function of time.

The RGPC molecular weight results of the acrylic polyols from reactors 7-12 can be seen in Figure 2.29. A general trend that is observed is the decrease in MW with an increase in reaction temperature, similar to Figure 2.26. Once again, at 70°C the MW is the highest from all other reaction temperatures. Another trend observed is the large MW difference between the reaction temperatures of 70°C and 80°C. There is a drop-off of nearly 24 kDa between those temperatures, which is an even larger MW difference than what was found in Figure 2.26. This indicates that between 70°C and 80°C there is a large influence on the reaction temperature control and thus the half-life of the initiator, as a result, creating much lower MW acrylic polyols. The same observation that was seen in Figure 2.26 was seen with Figure 2.29 in the MW results; already seen after 30 minutes into the polymerization, the acrylic polyols have essentially the same MW throughout the

rest of the reaction time. This general observation should be consistent for both MW results since they are replicates of the same reactions.

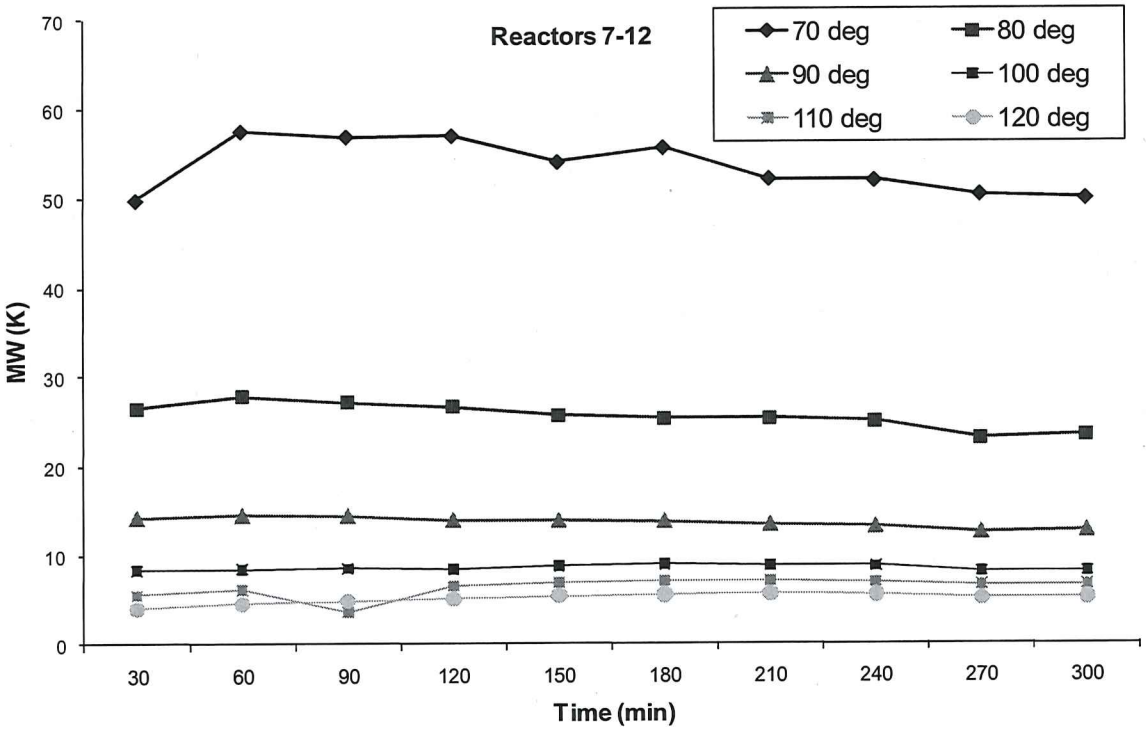

Figure 2.29. Rapid GPC molecular weight data from kinetics study of the acrylic polyol library indicating miniplant reactors 7-12, reaction temperature, and 30 minute sample intervals over the entire reaction time.

Figure 2.30 shows the temperature log for the PD unit at 80°C at position 8. The fluctuation in MW could be due to the poor temperature control of the reactor vessel where the temperature drastically lost control at ~ 180 minutes and continued to fluctuate until ~270 minutes. At 80°C and 90°C the MW decreased slightly, starting at 26 kDa and decreasing to 23 kDa at 80°C and 14 kDa

decreasing to 12 kDa at 90°C, a trend that is consistent with the MW data from Figure 2.26.

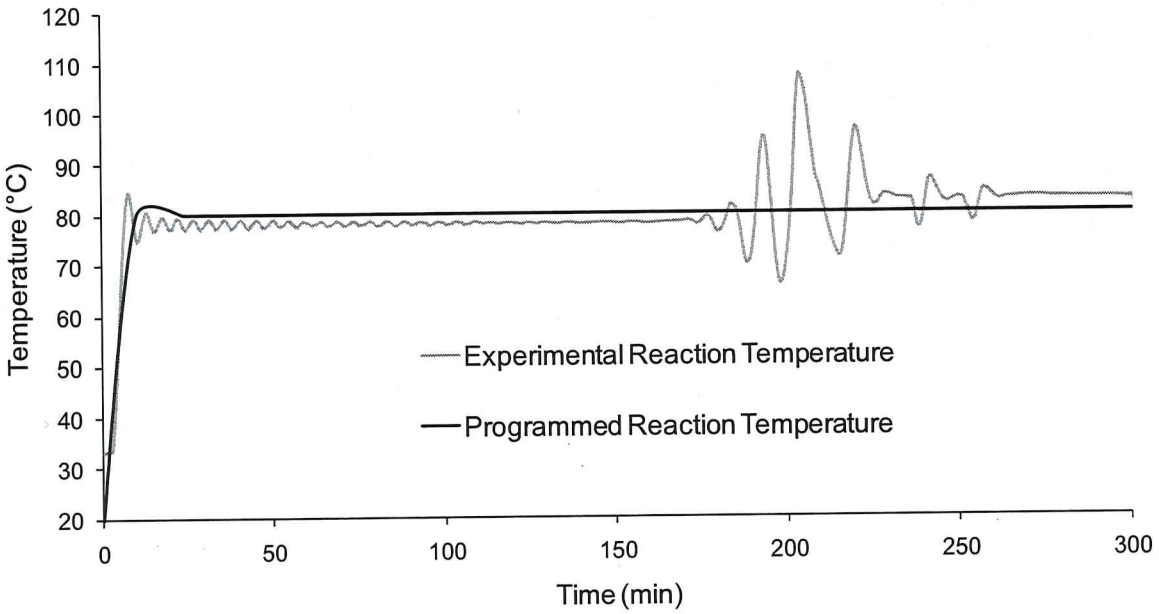

Figure 2.30. Representation of Chemspeed experimental and programmed reaction temperatures for the 80°C PD unit #8 over the course of the FRP of acrylic polyols.

If the MW data from Figure 2.26 and 2.29 are compared a noticeable difference is observed. The most obvious trend, or difference, is the overall MW for most reaction temperatures in Figure 2.26 are noticeably lower. Starting with the MW data at 70°C, there is a difference of 28 kDa between miniplant 1 and miniplant 7 (Chemspeed platform illustrated in Figure 2.24). As the reaction temperature is increased the difference in MW between the replicates become smaller; 80°C had a difference of 4 kDa, 90°C was almost the same, 100°C was 1.5 kDa, 110°C was almost the same, 120°C was exactly the same. These differences indicate that "tuning constants" (based on internal algorithms in the hardware of the Chemspeed) for temperature control for the reactor vessels were

correctly tuned at the higher temperatures reactors. It may be necessary to tune the lower temperatures reactors. The graphs representing the temperature logs in Figure 2.31 better clarify this finding.

As observed in Figure 2.31, the reactors 7-12 are closest to the cryostat (cooling system) for the Chemspeed which could make controlling the lower

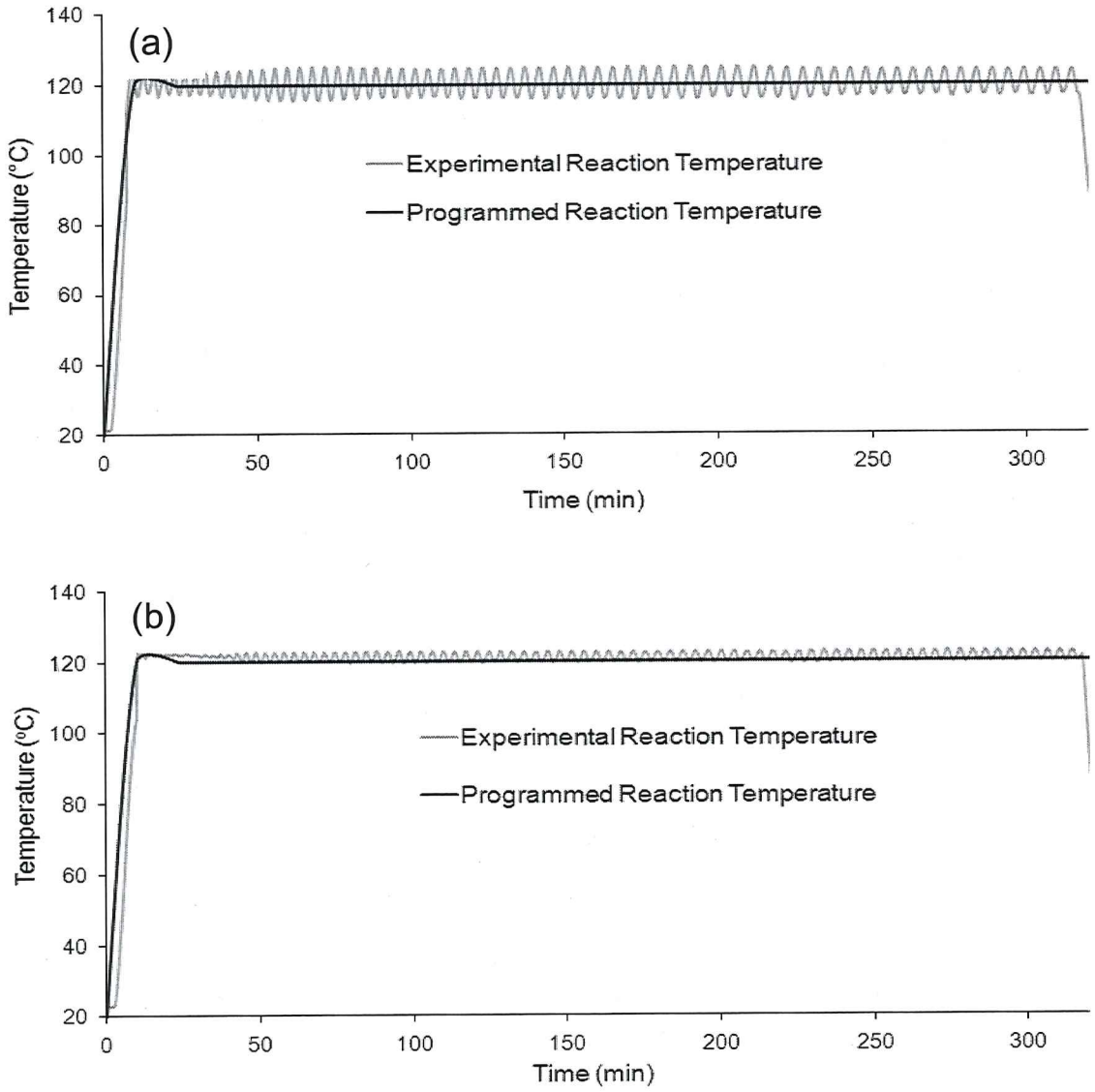

Figure 2.31. Graphical representation of reaction temperature logs for PD unit 6 (a) and PD unit 12 (b) at 120°C.

temperature reactions easier than compared to reactors 1-6, which are further from the cryostat and the reactors may require tuning. This evident from the tight temperature control on PD unit 12 was compared to the control on PD unit 6. A possible reason for the lacking control is once the liquid used in the reflux cooling reaches the 1-6 those reactors it was already warmed due to previously cooling reactors 7-12. If this is true, than reactors 7-12 in this study give the most reliable data since the internal reactor vessel temperature was probably much closer to the original reaction temperature set for the study.

The conversions (based on theoretical solids, Figure 2.28) of monomer to polymer are represented in Figure 2.32 and 2.33 for reactors 1-6 and reactors 7-12, respectively. A general trend observed from both graphs is the almost linear increase of percent conversion over time. At approximately 180 minutes for both graphs the percent conversion reaches a plateau around the range of 88-100% conversion, where it maintained that conversion or increases slightly until the reaction was over, at this point the percent solids is theoretically 50%. Coincidentally the feed time for the initiator and monomer solutions was 180 minutes which is why the high conversion was reached at that time interval, since the total volume of both solutions were dispensed and the temperature was maintained for another 120 minutes for a total reaction time of 300 minutes. At the first sample interval of 30 minutes conversion was in the range of 10-30% conversion, lower percent conversions were obtained with the lower reaction temperatures and increased with the increase in reaction temperature. This percent conversion/ reaction temperature trend continues to the next sample

interval at 60 minutes, but the sample intervals thereafter don't follow that same observed trend. The exception is seen In Figure 2.33, where the polymerization at 70°C does, in fact, continue that trend. Overall, the percent conversion for the data in Figure 2.31 has a tighter grouping of the sample intervals for each reaction temperature when compared to the data in Figure 2.33. This may be due to the temperature control of the reactor vessels 1-6, as previously reported in this study.

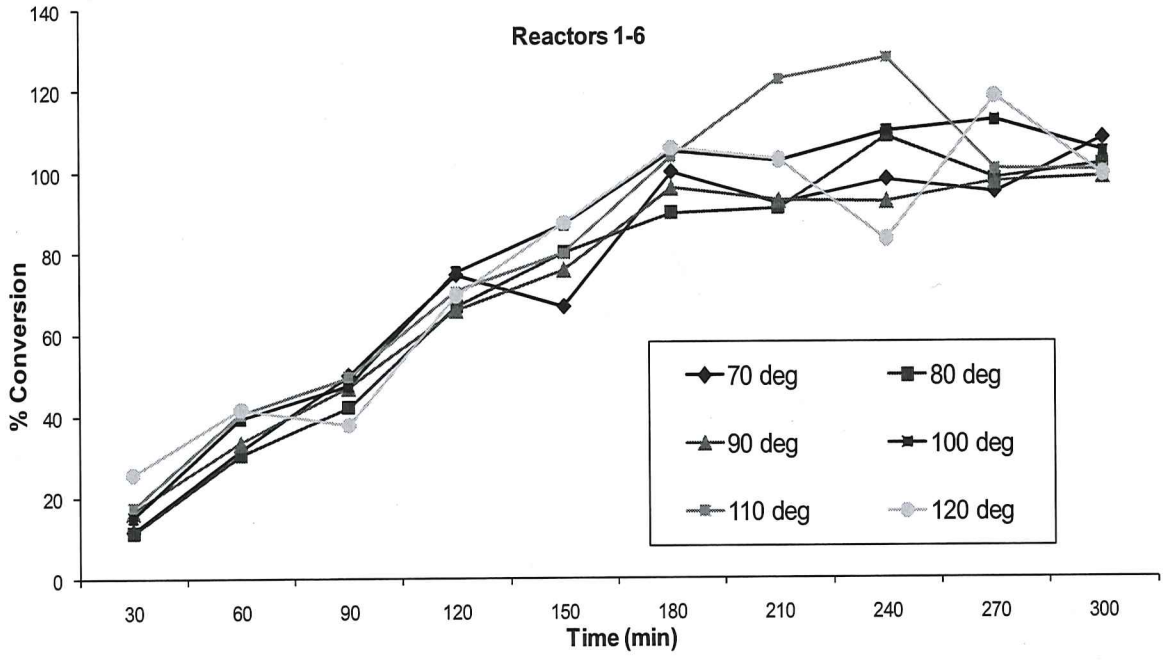

Figure 2.32. Monomer conversion data from kinetics study of the acrylic polyol library indicating miniplant reactors 1-6, reaction temperature, and 30 minute sample intervals over the entire reaction time.

Illustrated in both Figure 2.32 and 2.33, after the completion of the dispensing of both the initiator and monomer solution into the reactor vessel some of the conversions happen to increase above 100%, which is theoretically impossible.

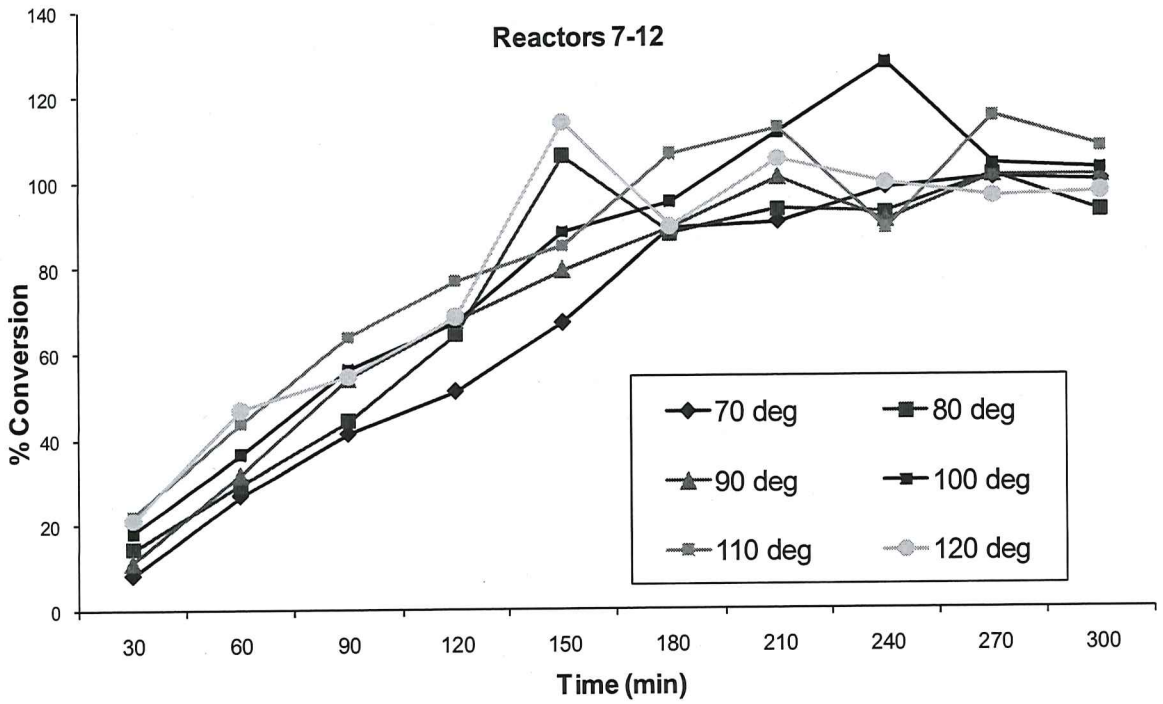

Figure 2.33. Monomer conversion data from kinetics study of the acrylic polyol library indicating miniplant reactors 7-12, reaction temperature, and 30 minute sample intervals over the entire reaction time.

This may be due to solvent leaking out of the reactor over the course of the reaction. The MW and percent conversion data from this kinetics study demonstrated that using the Chemspeed Autoplant A100™ could create the appropriate conditions for a true starved-feed reaction. MW for all acrylic polyols was rather constant throughout the entire reaction time. The conversion increased linearly until the feed times of the monomer and initiator solutions were completed, at that point the conversion reached a maximum and leveled off until the reaction was complete.

2.3.6. Solvent and initiator study on the semi-batch free radical polymerization of an acrylic polyol

This study was used to better understand the molecular weight effects by

changing the percent of solvent (effects on % solids) in the composition of the acrylic polyol and changing the concentration of the percent of initiator. The range of the percent of solvent used was 50-70% and the initiator concentration ranged from 1-4%/wt. The acrylic polyol composition (20% HEA, 80% BA) was held constant for all initiator/solvent combinations in this study, thus eliminating the composition variable and strictly focusing on the effects of the different percent solids and initiator concentration, this is true for the constant reaction temperature through the entire polymerization as well. The polymerization conditions consisted of 1-4%/wt initiator, 50-70% solvent resulting in 50-30% solids, respectively, and the reaction temperature was set to 95°C.

The temperature in each reaction reactor was controlled independently at 95°C. Depending on location on the Chemspeed platform the locations of the PD units and their respective percent initiator and percent solvent are illustrated in the DOE of this study in Figure 2.34.

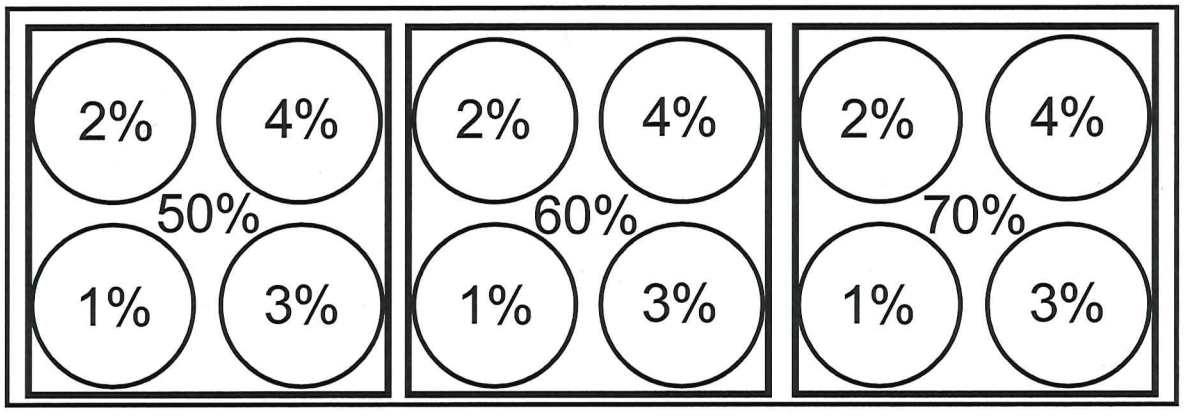

Figure 2.34. Schematic representation of the Chemspeed Autoplant A100™ platform indicating location of percent initiator and percent solvent for the acrylic polyol semi-batch "solvent/initiator study."

The contents of the two feed vessels were then fed into the reactor vessel at a rate of 0.18 ml/min for the monomer and 0.01, 0.02, 0.03, or 0.04 ml/min for the 1, 2, 3, 4% initiator solutions, respectively using the two syringe pumps on the PD unit. After the toluene was charged to the reactor vessels depending on the percent solvent, heating and stirring was started and a wait time of ten minutes was incorporated so that each reactor could reach and maintain stability of 95°C.

Once the temperature was stable the pumps began to feed both the monomer and initiator solutions into the reactor vessel. The feed time for both feed vessels were set to 180 minutes with a total reaction time of 300 minutes. Samples from each reactor were obtained at the end of the reaction and were characterized by RGPC to obtain the MW and PDI and percent solids was determined from the percent solids calculated gravimetrically.

This solvent/initiator study explores the difference between batch and semicontinuous reactions comparing the results seen in section 2.3.1. Illustrated in Figure 2.35 are the MW results from the study using the Chemspeed Autoplant A100™. The overall trend seen from the MW data is the decrease in the acrylic polyol MW with the increase in both the percent initiator and percent solvent similar to what was observed in section 2.3.1. This follows the FRP theory where the $MW \propto 1/\sqrt{(I)}$, where I is the initiator concentration. The highest MW of 92 kDa was observed with 1% initiator and 50% solvent. The lowest MW of 41 kDa was shown with 4% initiator and 70% solvent. The 50% solvent row of the acrylic polyols had the highest overall MW, ranging from 92 kDa to 55 kDa.

Subsequently, the 70% solvent row acrylic polyols had the lowest overall MW, ranging from 78 kDa to 41 kDa.

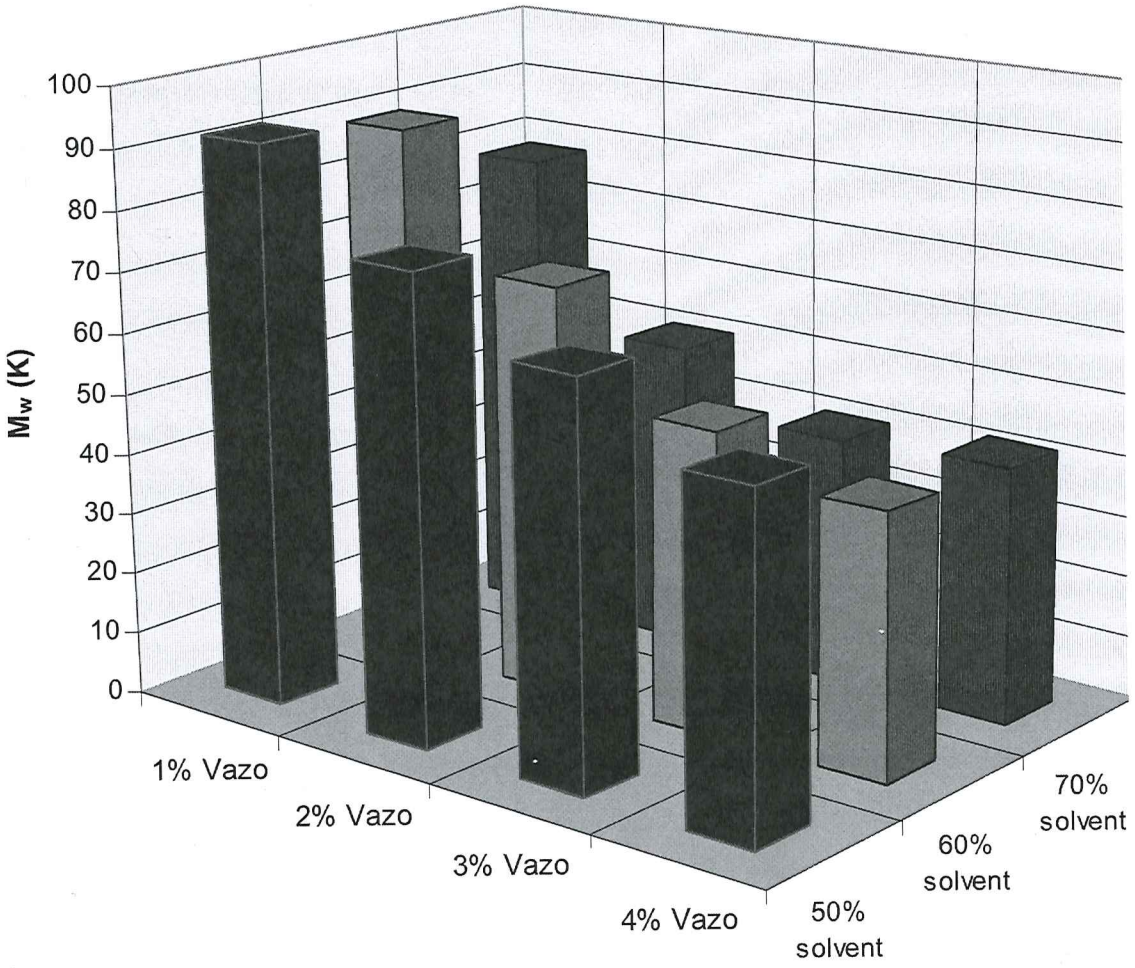

Figure 2.35. Rapid GPC molecular weight data from the semi-batch solvent/initiator study for the acrylic polyol library comprised of 20% HEA and 80% BA with a range of 1-4%/wt initiator and 50-70% solvent.

It was observed that the largest change in MW was due to the solvent. This trend is due to the chain transfer to solvent effect where the radical on the propagating polymer chain removed a proton from the solvent molecule yielding a terminated polymer chain and a new radical essentially regulating the polymerization and reducing the overall MW.

The MW difference from the increase in initiator from 2% to 3% and 3% to 4%, regardless of percent solvent, decreased, similar to the results found in Figure 2.22.

Unlike the results of the batch experiment, this study found that the MW difference when looking at the solvent amount, as the variable, was much less in the decrease of MW. The 1% initiator row going from 50% solvent to 70% solvent showed a decrease in MW with a difference of 14 kDa, this is a drastically lower change in MW than what was previously seen in Figure 2.22.

The polydispersity data from this study is illustrated in Figure 2.36 shows that all acrylic polyols ranged from 1.54-1.85.

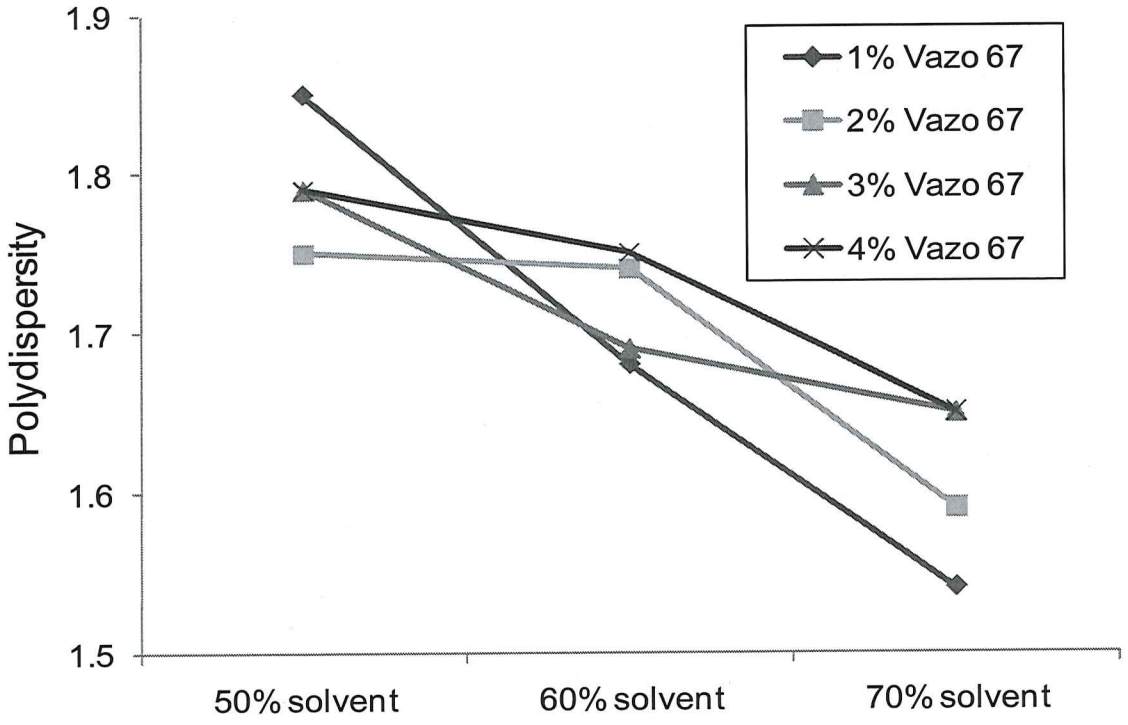

Figure 2.36. Polydispersity data from the semi-batch solvent/initiator study for the acrylic polyol library comprised of 20% HEA and 80% BA with a range of 1-4%/wt initiator and 50-70% solvent.

The overall trend that is seen is the slight decrease in PDI with the increase in solvent amount. The polyols polymerized using 1% initiator had the highest PDI of 1.85 at 50% solvent; this was also the highest MW polyol as well. As the solvent was increased the PDI decreased to 1.68 using 60% solvent and 1.54 using 70% solvent. This was consistent with the other levels of initiator. The reason for the overall decrease in PDIs with the increase in solvent amount for all the polyols is due to a possible combination of chain transfer to solvent, which would result in lower Mw and the FRP being performed using a semi-batch process which would control the Mw by holding the concentration ratio of monomer nearly constant. Figure 2.37 illustrates the difference in PDIs, comparing the difference from the batch process to the semi-batch process.

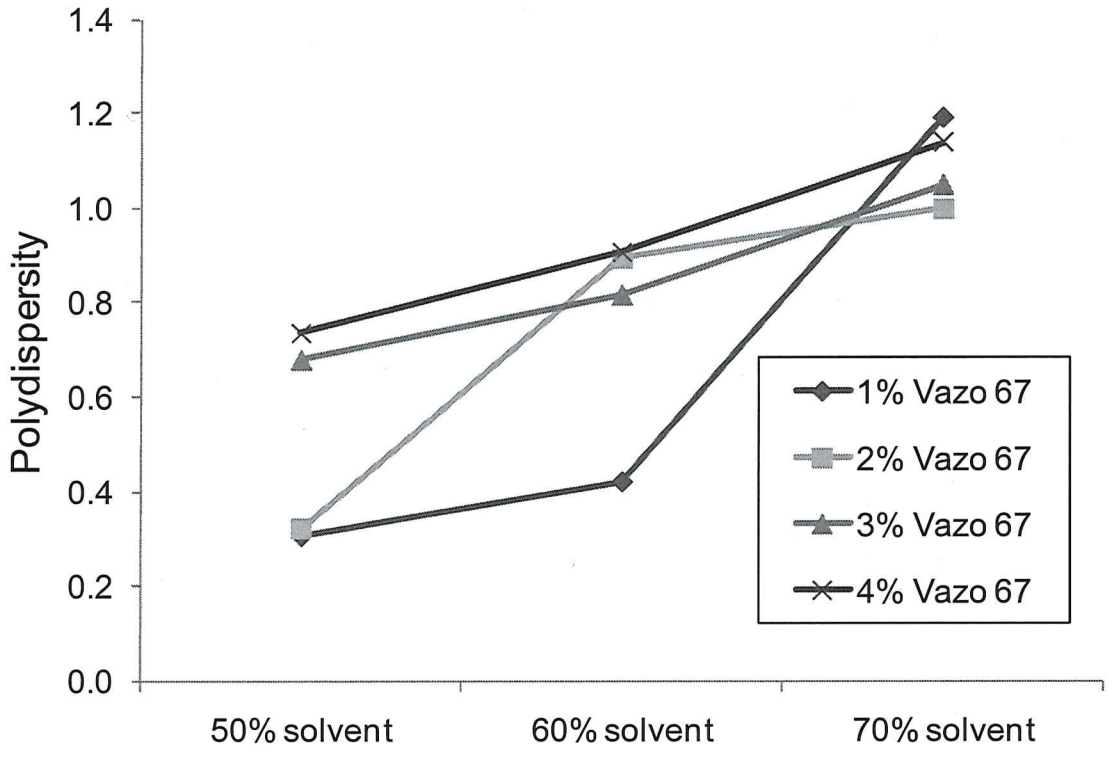

Figure 2.37. Difference in PDIs for the batch versus semi-batch process for the solvent/initiator study.

An initial observation seen in Figure 2.36 is the significant difference in PDIs for the 70% solvent reactions; this is mostly due to the lack of reactant concentration control of the polymerization during the batch process. There was also the possibility of chain transfer side reactions occurring during the batch process which would lead to higher PDIs as well.

However, because of the low concentration of reactants there is another concern that arises from higher solvent content in free radical polymerization of the acrylic polyols and that concern is the conversion of monomer to polymer. The percent conversion data from the acrylic polyols are illustrated in Figure 2.38.

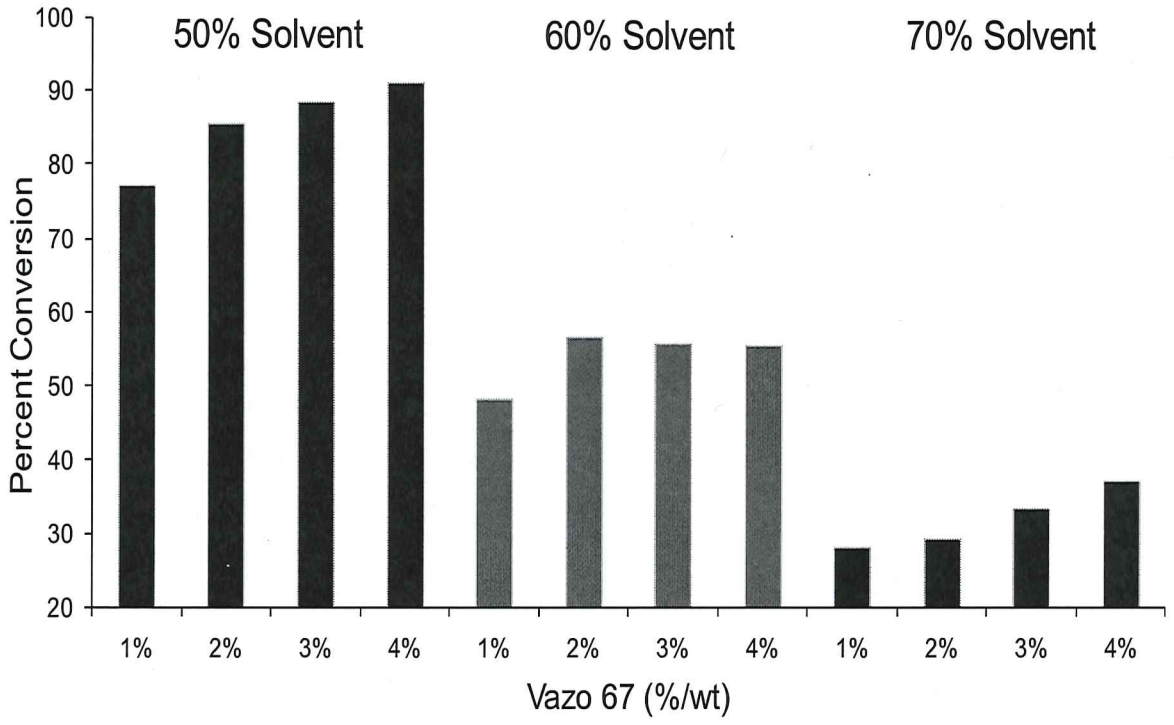

Figure 2.38. Conversion data from the semi-batch solvent/initiator study for the acrylic polyol library comprised of 20% HEA 80% BA with a range of 1-4%/wt initiator and 50-70% solvent.

The general trend observed from the percent conversion data is with the increase in amount of solvent there is a dramatic decrease in conversion. At 50% solvent (50% solids) the acrylic polyols showed the highest percent conversion due to a concentration effect of reactants within the reactor vessel; less solvent will give a higher overall concentration of reactants since the concentration of reactants were constant for all reactions, but the amount of initial solvent was not. A trend within the 50% solvent reactions was an increase in percent conversion with the acrylic polyols as the amount of initiator was increased. This increase is due to the higher concentration of radicals formed, thus, converting more monomer to polymer. A significant decrease in conversion was seen with the 60% solvent reactions. The conversion stayed the same with 3% and 4% initiator, resulting in a 56% conversion for both. The 70% solvent gave the lowest overall percent conversion ranging from 28% to 37%, based on the amount of initiator. The same conversion trend seen with the 50% solvent was also seen with 70% solvent, were the conversion increased with the increase in initiator concentration. The conversion results illustrated in Figure 2.38 prove that low solids content results in low conversion of the acrylic polyols in a semi-batch free radical polymerization.

Even though the acrylic polyol composition was slightly different than the study illustrated in section 2.3.1, the MW data from the solvent/initiator study shows, without a doubt the effects of initiator concentration and percent solvent for the solution polymerization of acrylic polyols and this study shows good correlation and reproducibly of the MWs when compared to the batch study (2.3.1) from the

results in Figure 2.24. Also, using the semi-batch method had better control of the MW compared to the batch method used in study 2.3.1, but because of this, the percent conversion for the higher solvent content reactions resulted in very low conversion.

2.3.7. Monomer feed time study on the semi-batch free radical polymerization of acrylic polyols

This study was used to look at the molecular weight effects and percent conversion by having a range of feed times of the monomer solution (while keeping the initiator feed time constant) of the acrylic polyol and incorporating a range of reaction temperature within each monomer feed time.

The locations of the PD units and their respective reaction temperatures and monomer feed times are illustrated in the DOE in Figure 2.39 and further explained in the graphical timeline of the study in Figure 2.40.

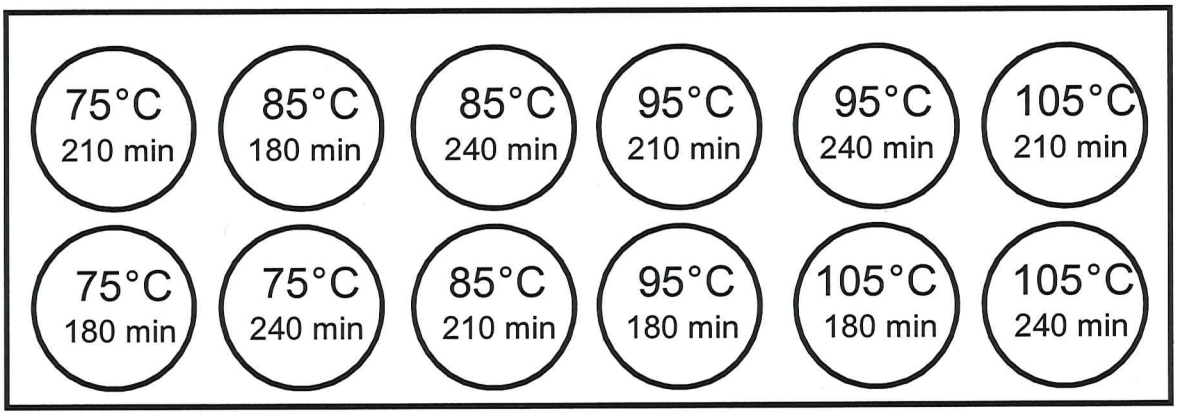

Figure 2.39. Schematic representation of the Chemspeed Autoplant A100™ platform indicating location of reaction temperature and monomer feed time for the acrylic polyol semi-batch "monomer feed time" study.

The feed times of the monomer were varied either to 180, 210, or 240

minutes, while the initiator solution (4%) feed time was kept at 180 minutes for all reactions in this study. The reaction temperatures were programmed to 75°C, 85°C, 95°C, or 105°C depending on the programmed location of the reactors on the Chemspeed platform.

The acrylic polyol composition (20% HEA, 80% BA, 50% solids) was held constant for this study, thus elevating the composition variable and strictly focusing on the effects of the monomer feed time and reaction temperature.

The contents of the two feed vessels were then fed into the reactor vessel at a rate of 0.18, 0.16, or 0.14 ml/min for the monomer feed times of 180, 210, or 240 minutes, respectively and 0.04 ml/min for the initiator solution using the two syringe pumps on the PD unit.

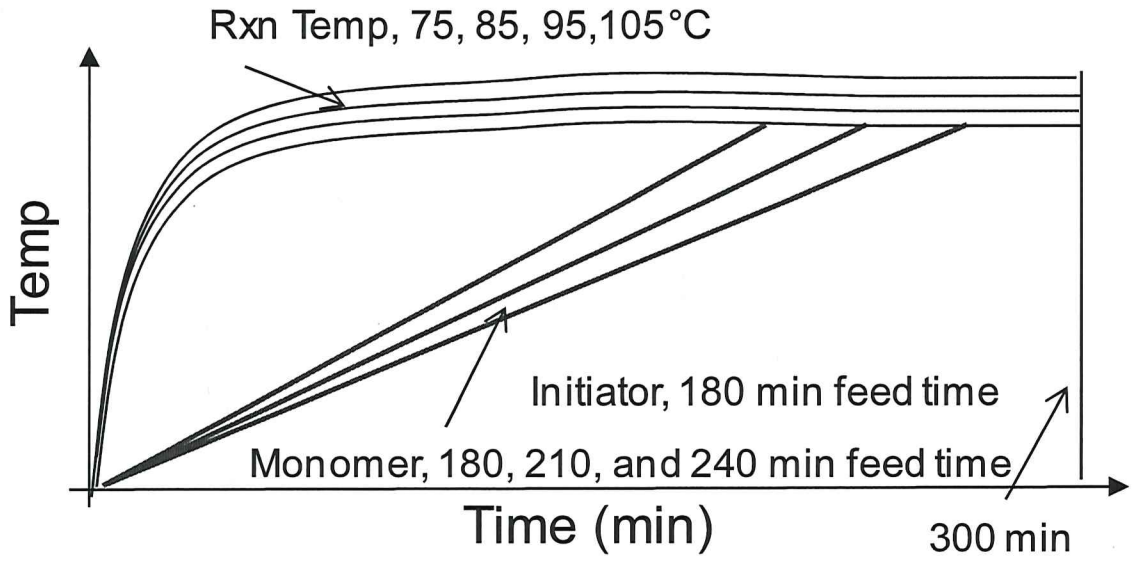

Figure 2.40. Graphical timeline of events for the FRP monomer feed time study of acrylic polyols.

Once the toluene was charged to the reactor vessels and nitrogen purged the headspace of the reactor vessel, heating and stirring was started and a wait

time of ten minutes was incorporated so that each reactor could reach and maintain stability at the reactors respective reaction temperature. Once the temperature was stable the pumps began to feed both the monomer and initiator solutions into the reactor vessel at their respective feed times; the total reaction time was set to 300 minutes. Samples from each reactor were obtained at the end of the reaction and were characterized by RGPC to obtain the MW and percent conversion was calculated gravimetrically.

The MW results of the acrylic polyols from the monomer feed time study is illustrated in Figure 2.41. The overall trend observed from the MW results is the decrease in MW with the increase in reaction temperature. The lowest reaction temperature of 75°C showed the highest overall MW of the acrylic polyols when comparing reaction temperatures. The feed time of 180 minutes at 75°C resulted in a MW of 59 kDa, which is similar to the MW obtained in the study in section 2.3.5 with similar acrylic polyol composition and reaction conditions. However, when the feed time of the monomer was increased to 210 minutes and 240 minutes, remembering that the initiator feed time was held constant at 180 minutes, the MW increased significantly to 100 kDa and 104 kDa, respectively. This is due to the decrease in monomer concentration during the longer feed times. Also, since the reaction temperature is lower the half-life of the initiator is longer than at the higher temperatures. This temperature dependence on the MW is shown when the temperature is increased to 85°C. This trend was also observed in Figure 2.41, with a significant drop in MW compared to 75°C, the

monomer feed time of 180 minutes gave a MW of 44 kDa, when the feed time was increased to 210 minutes the MW decreased to 36 kDa but increased when the feed time was increased to 240 minutes to 39 kDa.

The small variation in MW regardless of the feed times is due to the higher reaction temperature reducing the half-life of the initiator consequently consuming the monomer resulting in lower MW polyols. This observation continued to holds true when the reaction temperature was increased to 95°C and 105°C. MW of the acrylic polyols at 95°C were 25 kDa, 24 kDa, and 22 kDa for the 180 minutes, 210 minutes, and 240 minutes monomer feed times, respectively. The MW was the lowest at 105°C, showing a slight decrease from 17 kDa at 180 minutes to 15 kDa at 240 minutes.

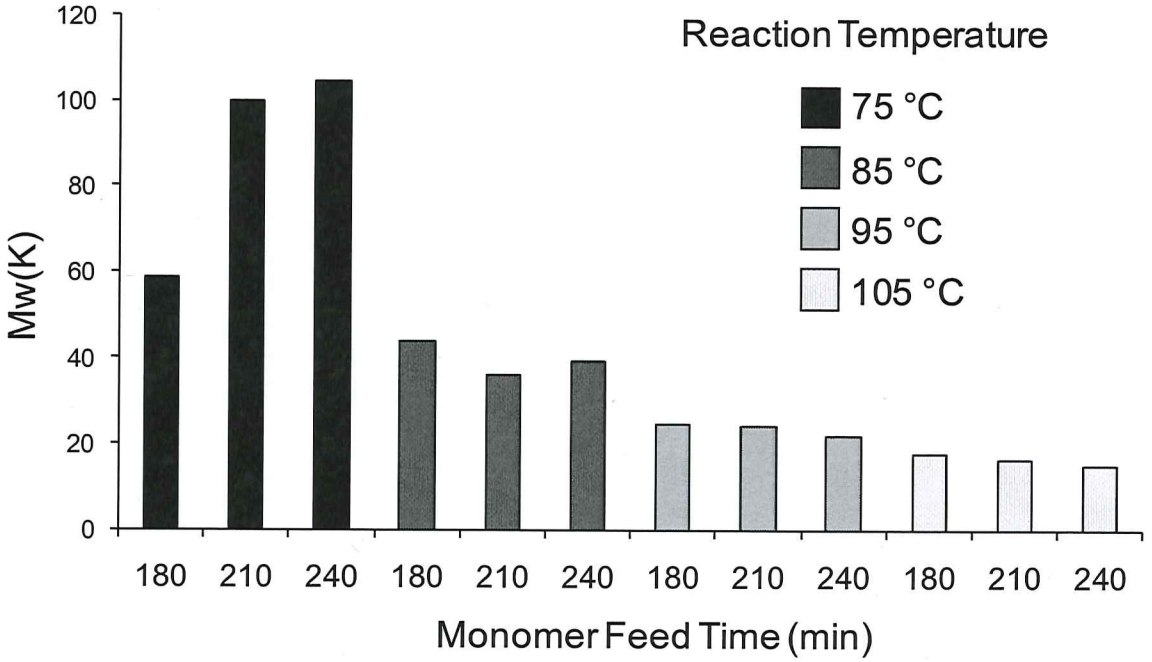

Figure 2.41. Rapid GPC molecular weight data from the semi-batch monomer feed time study for the acrylic polyol library comprised of 20% HEA and 80% BA.

The percent conversion data from the monomer feed time study for the acrylic polyols are illustrated in Figure 2.42. The general trend observed from the percent conversion data is with the increase in the monomer feed time there is a decrease in conversion regardless of the reaction temperature. The 180 minutes monomer feed time for acrylic polyols showed the highest conversion most likely due to the feed rates of both the monomer and initiator solutions were the same leading to similar concentrations of both in the reactor at any given time.

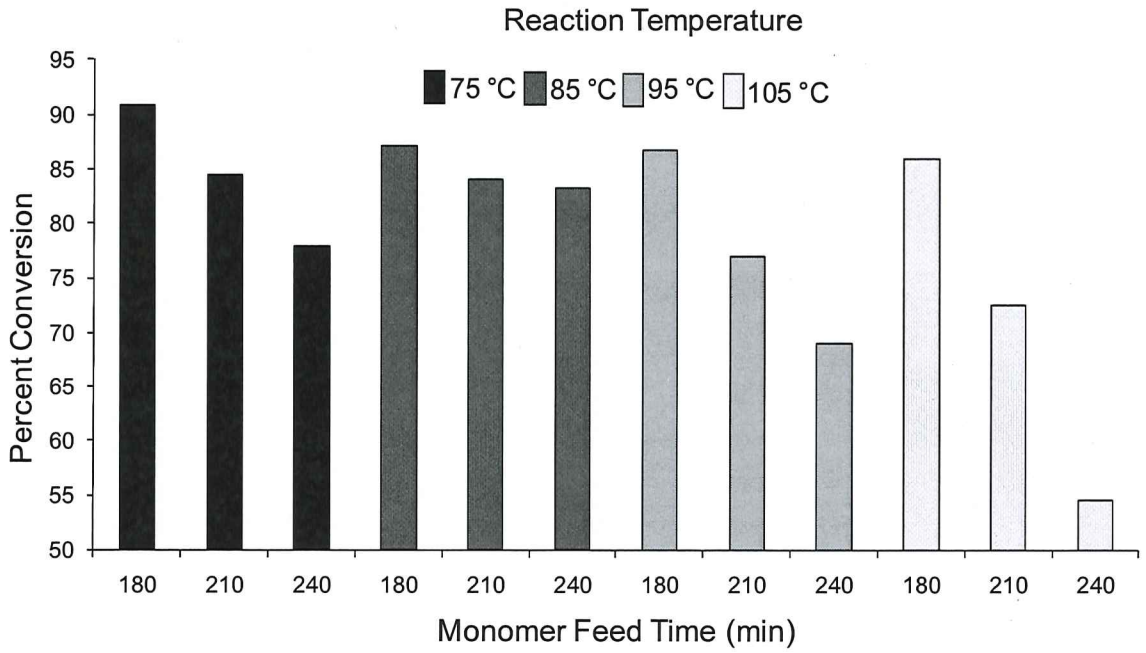

Figure 2.42. Conversion data from the semi-batch monomer feed time study for the acrylic polyol library comprised of 20% HEA and 80% BA.

For example, the reaction temperature of 75°C and monomer feed time of 180 minutes showed the highest percent conversion of 91%. The percent conversion for the polyols at 75°C decreased to 85% at 210 minutes feed time and

78% at 240 minutes feed time, the decrease in conversion is due to the amount of initiator available to decompose into new radicals with the extended monomer feed and thus an increase in the monomer concentration, resulting in not all monomer being converted to polymer.

MW for all acrylic polyols followed similar trends seen previously when reaction temperatures are increased and the conversion decreased linearly with the increase in feed times of the monomer.

2.3.8. Initiator feed time study on the semi-batch free radical polymerization of acrylic polyols

This study was used to look at the molecular weight effects and percent conversion by having a range of feed times of the initiator solution (while keeping the monomer feed time constant) of the acrylic polyol and changing the reaction temperature within each initiator feed time. The locations of the PD units and their respective reaction temperatures and initiator feed times are illustrated in the experimental design in Figure 2.43. The feed times of the initiator were varied either to 180, 210, or 240 minutes, while the monomer solution feed time was kept at 180 minutes for all reactions in this study. The reaction temperatures were varied as well, 75°C, 85°C, 95°C, or 105°C depending on the programmed location of the reactors on the Chemspeed platform. The acrylic polyol composition (20% HEA, 80% BA) was held constant for this study, thus elevating the composition variable and strictly focusing on the effects of the monomer feed time and reaction temperature.

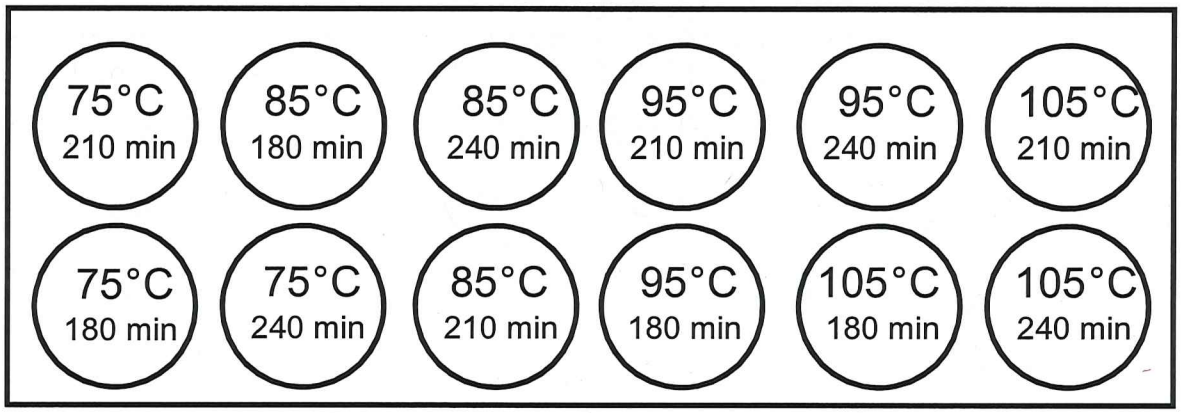

Figure 2.43. Schematic representation of the Chemspeed Autoplant A100™ platform indicating location of reaction temperature and initiator feed time for the acrylic polyol semi-batch "initiator feed time" study.

Figure 2.44 illustrates the graphical timeline of the initiator feed time study reaction. The contents of the two feed vessels were then fed into the reactor vessel at a rate of 0.18, 0.16, or 0.14 ml/min for the initiator feed times of 180, 210, or 240 minutes, respectively and 0.018 ml/min for the monomer solution using the two syringe pumps on the PD unit. Several different inline real-time data analysis factors, such as temperature and stirring, were monitored for all of the 12 PD units. Once the toluene was charged to the reactor vessels and nitrogen purged the headspace of the reactor vessel, heating and stirring was started and a wait time of ten minutes was incorporated so that each reactor could reach and maintain stability at the reactors respective reaction temperature. Once the temperature was stable the pumps began to feed both the monomer and initiator solutions into the reactor vessel at their respective feed times; the total reaction time was set to 300 minutes. Samples from each reactor were obtained at the end of the reaction and were characterized by RGPC to obtain the MW and percent conversion was calculated gravimetrically.

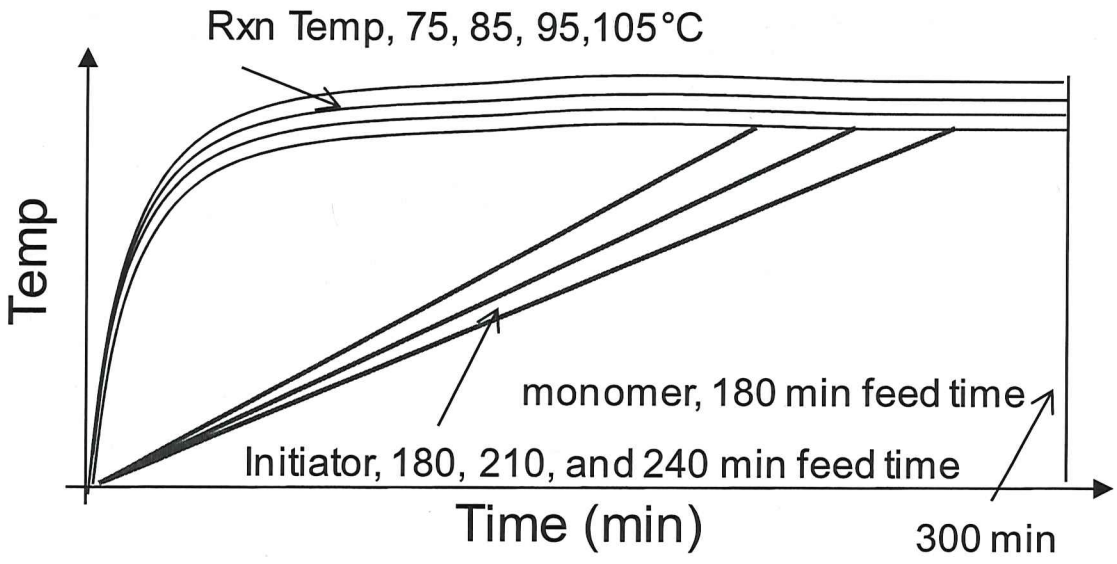

Figure 2.44. Graphical timeline of events for the FRP monomer feed time study of acrylic polyols.

The MW results of the acrylic polyols from the initiator feed time study is illustrated in Figure 2.45. The overall trend observed from the MW results is the significant decrease in MW with the increase in reaction temperature. The lowest reaction temperature of 75°C showed the highest overall MW of the acrylic polyols when comparing the other reaction temperatures. The feed time of 180 minutes at 75°C resulted in a MW of 87 kDa, which is similar to the MW obtained in the study of similar acrylic polyol composition and reaction conditions (section 2.3.5). However, when the feed time of the initiator was increased to 210 minutes, remembering that the monomer feed time was held constant at 180 minutes, the MW increased to 940 kDa and at the 240 minutes initiator feed time a significant increase in MW was observed at 144 kDa. This is due to the decrease in initiator concentration during the longer feed times because as the initiator is consumed by the monomer any radical chains still propagating will increase the MW by possibly

grafting onto already formed polymer. Also, since the reaction temperature is lower the half-life of the initiator is longer than at the higher temperatures.

The results are consistent with what was observed with the same reaction temperature from the monomer feed time study shown in Figure 2.41. The small variation in MW regardless of the feed times is due to the higher reaction temperature reducing the half-life of the initiator.

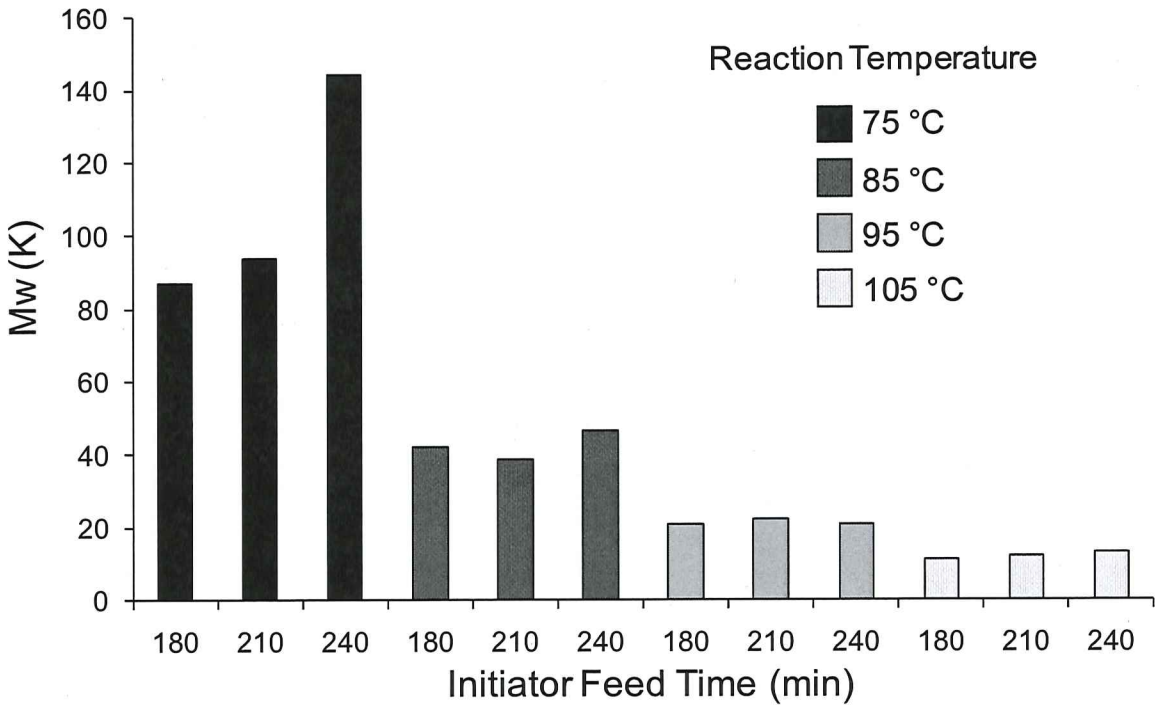

Figure 2.45. Rapid GPC molecular weight data from the semi-batch initiator feed time study for the acrylic polyol library comprised of 20% HEA and 80% BA.

The initiator forms free radicals upon decomposition from heating at the higher reaction temperatures and instantly forms low MW propagating chains or the possibility of chain transfer from solvent or polymer could occur as well as other side reactions from impurities in the monomer.

The percent conversion data from the initiator feed time study for the acrylic polyols are illustrated in Figure 2.46. The general trend observed from the percent conversion data is with the increase in the initiator feed time there is a linear decrease in conversion regardless of the reaction temperature. The 180 minutes monomer feed time for acrylic polyols regardless of reaction temperature showed the highest percent conversion (83% at 85°C, 87% at 95°C , and 86% at 105°C) which is due to the proper conditions for a starved-feed reaction. The reaction temperature of 75°C and monomer feed time of 180 minutes showed the highest percent conversion at 98%.

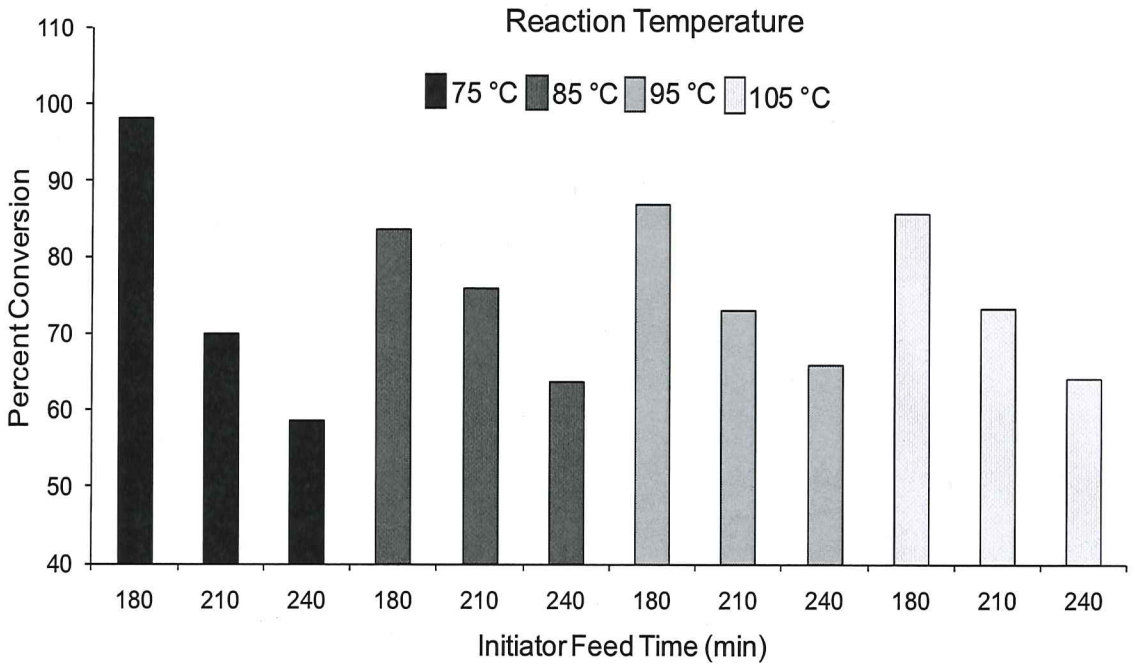

Figure 2.46. Percent conversion data from the semi-batch initiator feed time study for the acrylic polyol library comprised of 20% HEA and 80% BA.

The percent conversion for the polyols at 75°C decreased to 70% at 210 minutes feed time and 59% at 240 minutes feed time, the decrease in conversion

is due to the lower concentration of initiator versus monomer concentration at the extended feed times resulting in not all monomer being converted to polymer. The highest percent conversion was seen once again with the 180 minutes monomer feed time for all reaction temperatures which is consistent with previous studies of similar composition and reaction conditions. The decrease in conversion with the increase in monomer feed time were similar for 85°C, 95°C, and 105°C reaction temperatures. At the 210 minutes feed time the conversion decreased similarly for the those reactions and was reported at 76% for 85°C, 73% for 95°C, and 73% for 105°C. When the feed time was increased to 240 minutes the conversion decreased again to 64% for 85°C, 66% for 95°C, and 64% for 105°C.

If the results from the similar reactions conditions are compared to the monomer feed time study from Figure 2.42, its observed that the initiator feed time study has higher overall conversion, this is due to the higher concentration of monomer in the reactor vessels being converted to polymer, where the monomer feed time study had opposite results due to the higher concentration of initiator in the reactor vessels. However, the low conversion percentage is not all that surprising when comparing radical lifetimes to the composition rates of the reaction. As stated previously, at longer feed times for the initiator the concentration will be low and there is a possibility that the reaction is operating at or near starved conditions. If that is the case there is the concern that the polymer concentration may become high which would result in chain transfer to polymer at longer feed times and higher temperatures. Another possibility for the low conversion is the rates of initiation and termination are not balanced, so if the

termination rate increases a decrease in the concentration of radicals would slow down the propagation rate.

The MW and percent conversion data from the initiator feed time study demonstrated that using the Chemspeed Autoplant A100™ confirmed that an increase in initiator concentration compared to monomer concentration in the same reaction results in low percent conversion.

MW for most acrylic polyols followed similar trends seen previously when reaction temperatures are increased, the exception was the 240 minutes feed time at 75°C where there was a large increase in MW. The conversion decreased linearly with the increase in feed times of the initiator consistent with previous results.

2.3.9. Oscillating reaction temperature study on the semi-batch free radical polymerization of acrylic polyols

This study was used to look at the molecular weight effects and conversion of acrylic polyols by introducing oscillating reaction temperatures during the polymerization, mimicking the possible temperature variation of industrial large scale acrylic polyol synthesis. Illustrated in Figure 2.47 is a graphical timeline of FRP events for the oscillation reaction temperature study.

The feed times of the monomer and initiator solutions were kept at 180 minutes for all reactions in this study. The reaction temperatures were oscillated by either ±5°C or ±10°C for 95°C and 105°C in the reactors on the Chemspeed platform as depicted in Figure 2.47. The acrylic polyol composition (20% HEA, 80% BA) was held constant for this study, thus elevating the composition variable

and strictly focusing on the effects of the oscillating reaction temperatures The experiment was done in triplicate, which can be seen in the DOE in Figure 2.48. The temperature in each reaction reactor was programmed and controlled independently from 95°C±5, 95°C ±10°C, 105°C ±5°C or 105°C ±10°C depending on location on the Chemspeed platform. The oscillating frequency was set to either increase or decrease to the respective programmed temperature every 30 minutes.

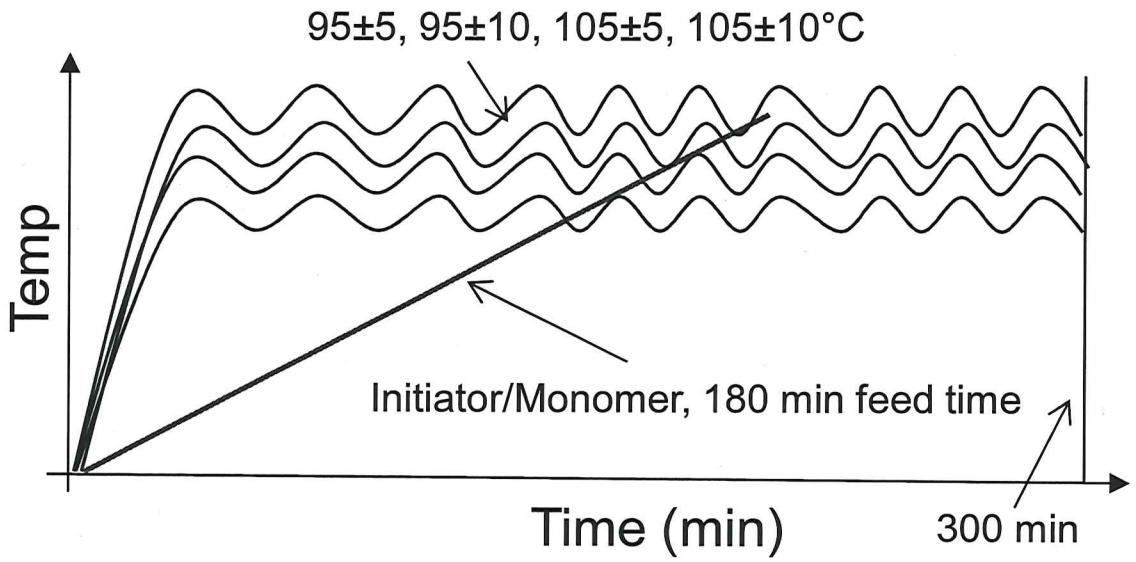

Figure 2.47. Graphical timeline of events for the FRP oscillation reaction temperature study of acrylic polyols.

The contents of the two feed vessels were then fed into the reactor vessel at a rate of 0.18 ml/min for the monomer and 0.04 ml/min for the initiator solution using the two syringe pumps on the PD unit. Once the toluene was charged to the reactor vessels and nitrogen purged the headspace of the reactor vessels, heating and stirring was started and a wait time of ten minutes was incorporated so that

each reactor could reach and maintain stability at the reactors respective reaction temperature.

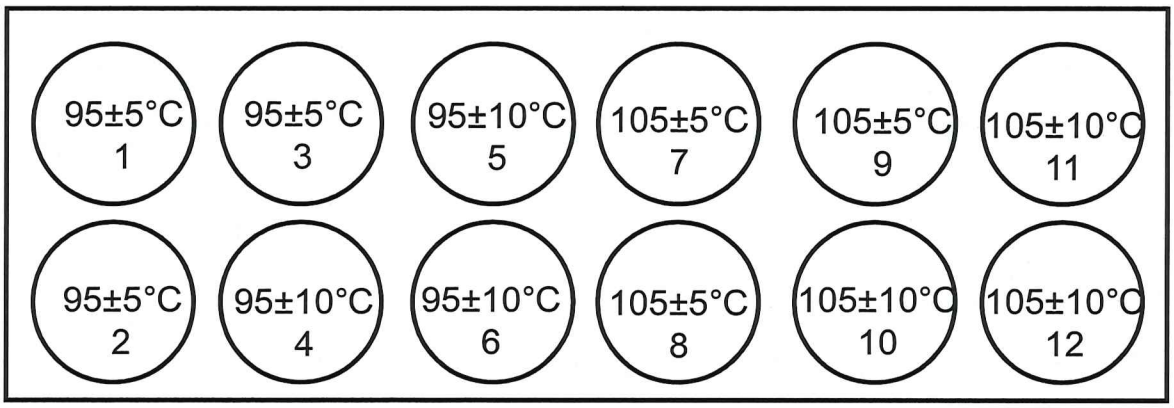

Figure 2.48. Schematic representation of the Chemspeed Autoplant A100™ platform indicating location of oscillating reaction temperature for the acrylic polyol "oscillating reaction temperature study."

Once the temperature was stable the pumps began to feed both the monomer and initiator solutions into the reactor vessel at their respective feed times and the oscillation of the respective temperatures began; the total reaction time was set to 300 minutes. The oscillating temperatures were set to change at 30 minute intervals. Samples of each reactor were characterized by RGPC to obtain the MW and percent conversion was determined by the percent solids results calculated gravimetrically.

The MW results of the acrylic polyols from the oscillating reaction temperatures study is illustrated in Figure 2.50. The overall trend observed from the MW results is the decrease in MW with the increase in reaction temperature. The lowest reaction temperature of 95°C±5°C showed the highest overall MW of the acrylic polyols when comparing the other oscillating reaction temperatures. The reaction temperature of 95°C±5°C resulted in an average MW of 60 kDa.

However, there was an increase in the MW from PD unit 2 and 3 at that same reaction temperature. A graphical representation of the temperature log for PD unit 3 is depicted in Figure 2.49. This MW variation is most likely due to the reactor vessels having less temperature control during the lower oscillating temperatures (±5°C), where the theoretical temperature was undershot during the reaction, thus a lower reaction temperature resulted in higher MW polyols as the result. The temperature was undershot most likely because those PD units need to be tuned. When the temperature log of the Chemspeed was analyzed, the average temperature of PD unit 1 was 95.1°C, however, PD unit 2 had an average temperature of 94.6°C, and PD unit 3 had a slightly less average temperature of 93.8°C, these results would be in agreement with the increase in MW for those reactions.

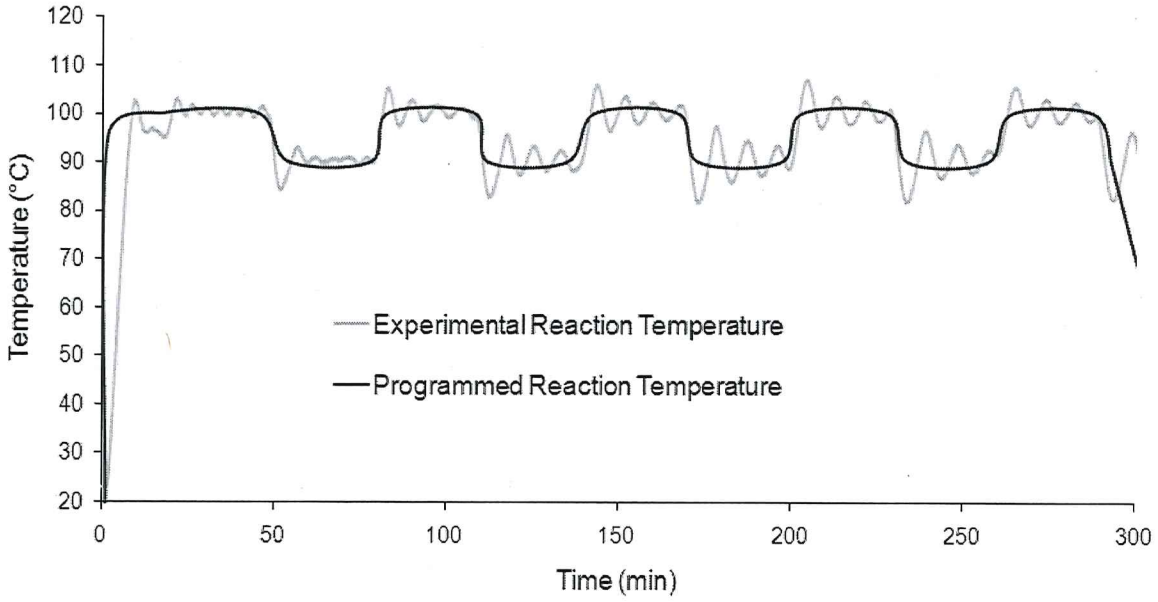

Figure 2.49. Temperature log for PD unit 3 at 95±5°C comparing the programmed temperature oscillation to the experimental temperature oscillation.

Figure 2.50 depicts the RGPC results for the oscillating temperature study. The reaction temperature of 95°C±10°C resulted in an average Mw of 52 kDa, which is reasonable because the oscillating temperature is set +5°C warmer than the previous oscillating temperature resulting in a higher end temperature, which lowers the half-life of the initiator and consequently lowers the MW of the polyol. At 105°C±5°C the average MW was 37 kDa, which was lower than the previous reaction temperature MW results, consistent with the higher reaction temperature conditions result in lower MWs. However, when looking at the MW data from 105°C±10°C the average MW increased to 42.5 kDa. This was unexpected since all previous studies show an increase in reaction temperature should decrease the MW. This increase in MW was possibly due to the Chemspeed temperature control undershooting the low end of the oscillation as depicted in Figure 2.48.

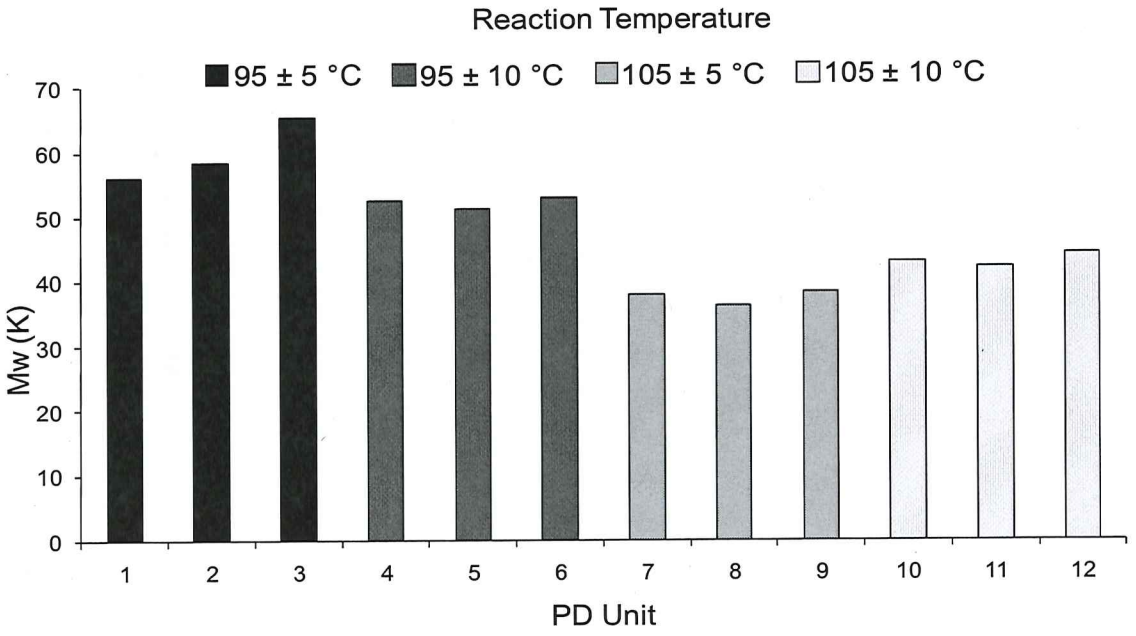

Figure 2.50. Rapid GPC molecular weight data from the semi-batch oscillating reaction temperature study for the acrylic polyol library comprised of 20% HEA and 80% BA.

Table 2.1 describes the average reaction temperatures analyzed form the temperature logs. It was evident that the average temperature of the reactions involving the 105°C±10°C study showed an average of 104°C, while the average temperature of the reactions involving the 105°C±5°C study showed an average of 107°C.

Table 2.1. Average reaction temperatures from the oscillating reaction temperature study, described by PD unit location and overall average per reaction temperature.

95±5°C	**95±10°C**	**105±5°C**	**105±10°C**
1=95.1°C	4=95.7°C	7=107.8°C	10=104.7°C
2=94.6°C	5=94.8°C	8=107.2°C	11=104.2°C
3=93.8°C	6=95.3°C	9=106.7°C	12=103.6°C
Average temp.=94.5°C	Average temp.=95.3°C	Average temp.=107.2°C	Average temp.=104.2°C

These results are consistent with the finding in Figure 2.50, where the MW was lower for 105°C±5°C compared to the MWs for 105°C±10°C. Figure 2.51 depicts the graphical representation of the temperature log files for PD unit 7 from the 105°C±5°C experiment and PD unit 12 from the 105°C±10°C experiment.

The percent conversion data from the oscillating temperature study for the acrylic polyols are illustrated in Figure 2.52. The general trend observed from the percent conversion data for this study was that all PD units had relatively similar percent conversions regardless of the oscillating reaction temperature. The acrylic polyols from the 95°C±5°C reaction temperature had an average percent conversion of 93%. There was a slight increase in percent conversion from PD unit 1 to PD unit 3, which correlates with the MW data from Figure 2.41.

The acrylic polyols polymerized under the 95°C±10°C reaction temperature

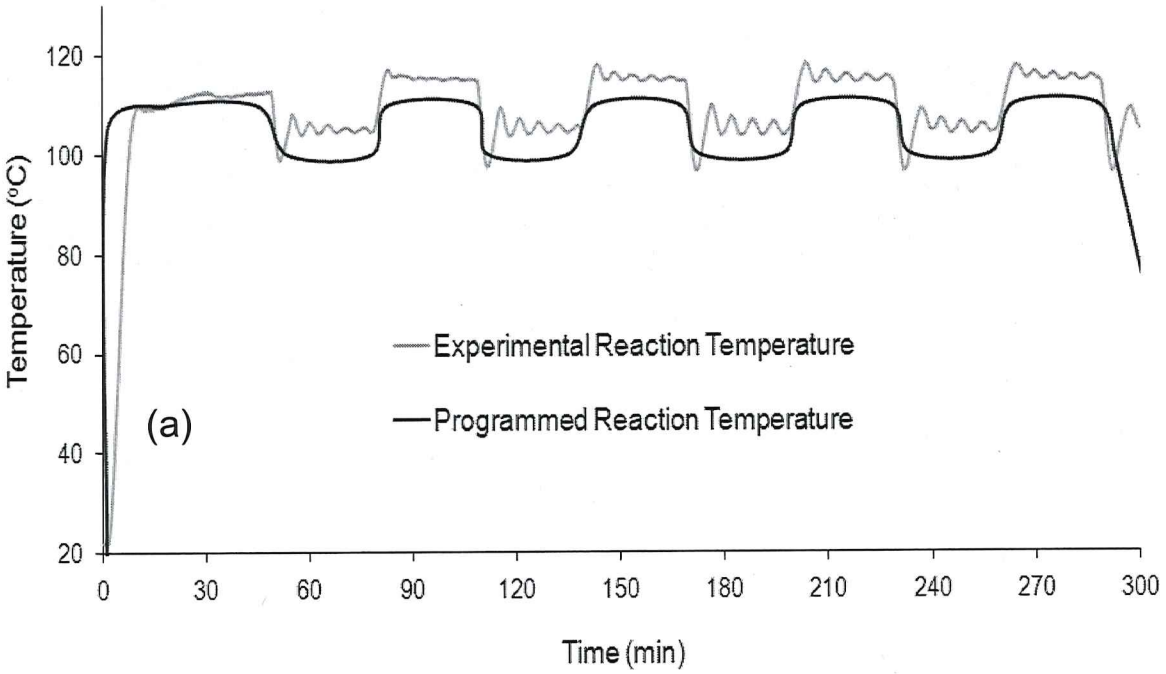

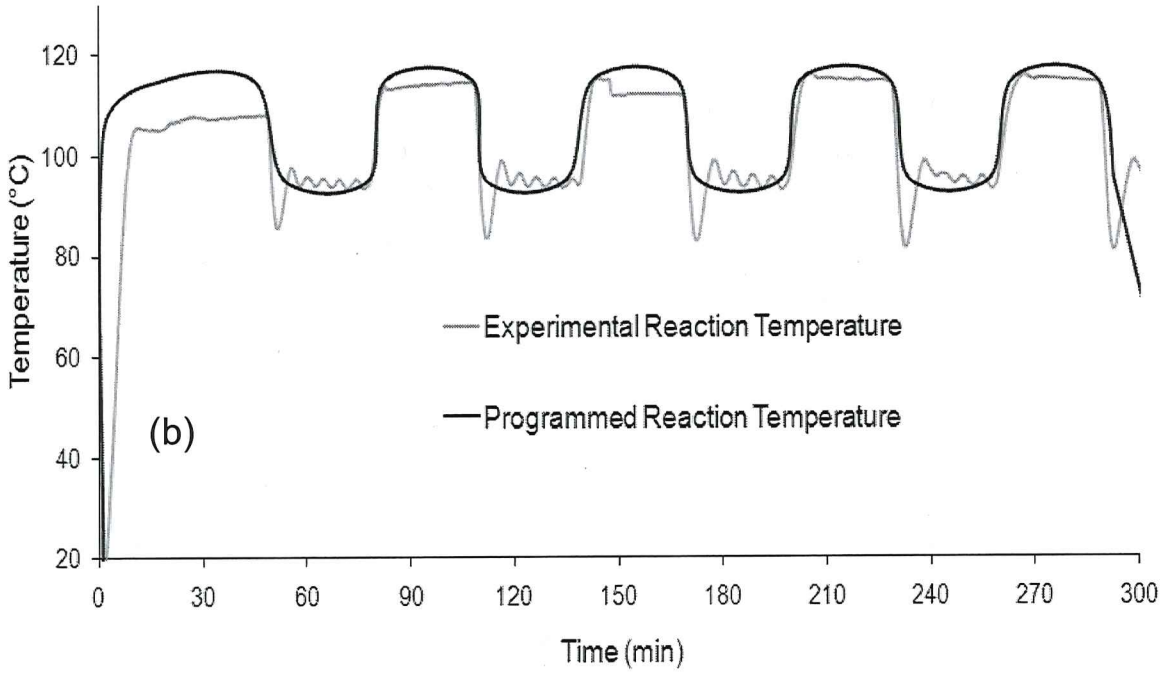

Figure 2.51. Graphical representation of the temperature log files for (a) PD unit 7 from the 105°C±5°C experiment and (b) PD unit 12 from the 105°C±10°C experiment.

conditions had an average percent conversion of 95% with not much derivation from the average from PD units 4-5; a slight increase in percent conversion from the previous oscillating temperature conditions possibly due to the better temperature control between PD units 4-6.

The polymerization of the acrylic polyols with the 105°C±5°C reaction temperature conditions also had an average percent conversion of 95%. A slight difference in conversion of the acrylic polyols is observed between PD units 7-9 possibly due to the difference in average temperature for each of the PD units. The acrylic polyols prepared under the 105°C±10°C reaction temperature conditions had an average percent conversion of 93%.

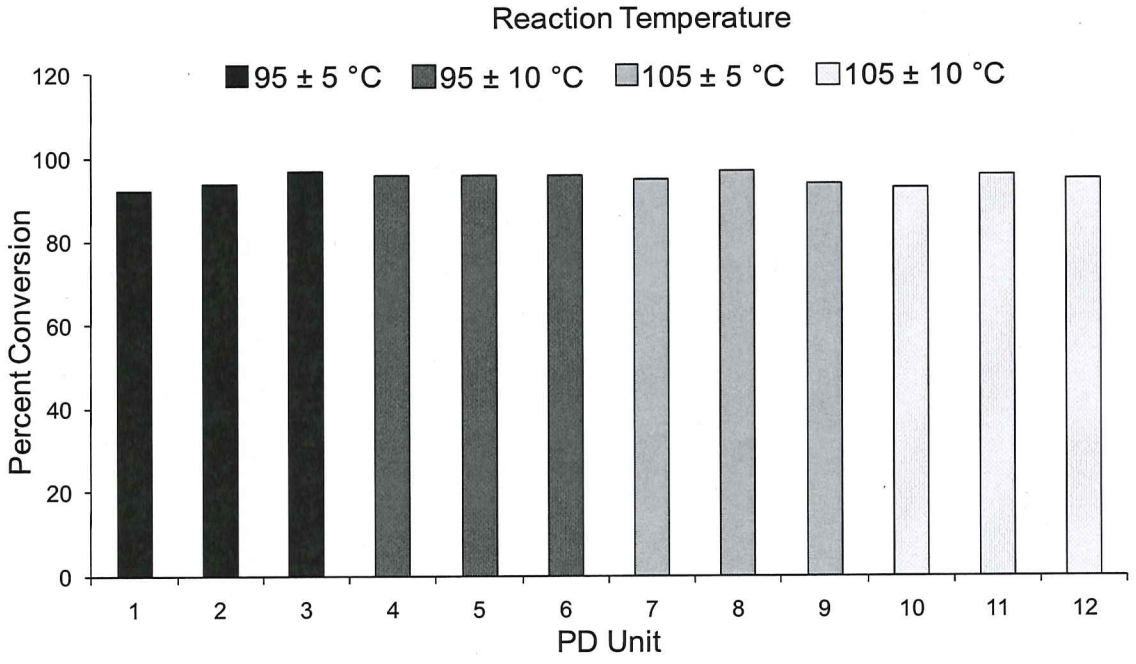

Figure 2.52. Conversion data from the semi-batch oscillating reaction temperature study for the acrylic polyol library comprised of 20% HEA and 80% BA.

Overall, the percent conversion for this study had a range from 91% to 98% with

an average of 94%, which demonstrated that, regardless of the oscillating temperatures, good conversion was maintained.

The oscillating temperature study demonstrated that using the Chemspeed Autoplant A100™ for temperature process variation could be achieved effectively. The MW data confirmed the temperature effects on the polymerization of the acrylic polyols by decreasing the MW with the increase in temperature. The experiment demonstrated good conversion for the entire study regardless of the oscillating temperatures. This study also showed that the Chemspeed has some difficulty controlling and maintaining a stable temperature when the set temperatures are oscillating at small intervals (±5°C), but showed better control with larger intervals (±10°C), tuning of the reactors is needed. This study also showed that even slight variations in process temperature can have an effect on the resulting molecular weight of the polymer produced.

2.4. Conclusions

Libraries of acrylic polyols were synthesized using combinatorial high-throughput techniques by either batch or semi-batch processes. The experiments for the batch and semi-batch processes were done combinatorially to explore a range of compositions and various reaction process variables that cannot be accomplished or are not suitable for single reaction experiments. Characterization with Rapid-GPC, high-throughput DSC, and gravimetrically calculated percent solids verified the effects of different reaction conditions (temperature, initiator and monomer concentration, and percent solids) on the MW, glass transition temperatures, and percent conversion on the different compositions of acrylic

polyols. Using the combinatorial high-throughput approach, several different studies of the synthesis of the acrylic polyols were done in a very short amount of time (24 unique acrylic polyol compositions per experiment for batch process and 12 PD units x 5 studies =60 experiments of varying process variables for the semi-batch processes of acrylic polyols using the Chemspeed). Scientists can therefore explore a large number of composition and process variables in a short period of time, resulting in obtaining a large amount of data. This data can be characterized where structure-property relationships can be determined and those results can be stored in a database for use in the design of future experiments.

2.5. References

1. Pechmann, H. v.; Rohm, O. *Ber. Dtsch. Chem. Ges.* **1901**, 34, 427.
2. Bauer, W. Rohm & Haas, DE 571123, US 1829208, **1928**.
3. Scharf, E.; Fikentscher, H. IG Farenind, DE 615219, GB 387736, **1931**.
4. Fikentscher, H.; Heuck, C. IG Farenind, DE 654989, GB 358534, **1930**.
5. Yuki, H.; Hatada, K.; Ohta, K.; Okamoto, Y. *Appl. Polym. Symp.* **1975**, 26, 39.
6. Riddle, E. H. *Monomeric Acrlyic Ester*, Reinhold Publ., New York, **1954**.
7. Gaylord, N. G. *Methods of Organic Chemistry*, vol. XIV/1 Georg Thieme Verlag, Stuttgart, **1961**.
8. Moad, G.; Solomon, D. H. The Chemistry of Free Radical Polymerization, Pergamon, Oxford, **1995**.

9. Bamford, C. H. in *Comprehensive Polymer Science*, Eastmond, G. C.; Ledwidth, A.; Russo, S.; Sigwalt, P., eds., Pergamon, London, Vol. 3, 219, **1989**.

10. Odian, G. C. *Principles of Polymerization*, Wiley-Interscience, John Wiley & Sons, Hoboken, New Jersey, Fourth Edition. 189, 682, **2004**.

11. Boor, J. *Ziegler-Natta Catalysts and Polymerizations,* Academic Press: New York, **1979**.

12. *Coates, G. W. Chem. Rev.* **2000**, *100*(4), 1223–1252.

13. Gianotti, G.; Allegra, G.; Bassi, I. W.; Corradini, P.; Ganes, P. *Makromol. Chem.* **1962**, 58,242.

14. Gianotti, G.; Dall'Asta, G.; Mazzanti, G.; Pasquon, I.; Valvassori, A.; Zambelli, A. *J. Am. Chem. Soc.* **1961**, 83, 3343.

15. Kaminsky, W.; Laban, A. *Applied Catalysis A: General* **2001**, 222(1-2), 47-61.

16. Evans, M. G.; Polanyi, M. *Trans Faraday Soc.* **1936**, 32, 1340.

17. Bell, R. P. *Proc. Roy. Soc., Ser. A* **1947**, 154, 414.

18. Otsu, T. *J. Polym. Sci.; Part A. Polym. Chem.* **2000**, 38, 2121.

19. Otsu, T; Yoshida, M. *Makromol. Chem., Rapid Commun.* **1982**, 29, 127.

20. Otsu, T.; Matsumoto, A. *Adv. Polym. Sci.* **1998**, 136, 75.

21. Kukulj, D.; Davis, T. P.; Gilbert, R. G. *Macromolecules* **1998**, 31, 994.

22. Tobita, H.; Hamielec, A. E. *Makromol. Chem., Macromol. Symp.* **1988**, 20/21, 501.

23. Tobita, H.; Hamielec, A. E. *Macromolecules* **1989**, 22, 3098.

24. Mayo, F. R. *J. Amer. Chem. Soc.* **1943**, 65, 2324.

25. Nandi, U. S.; Palit, S. R. *Nature* **1960**, 185, 235-236.

26. Litvinenko, G. I.; Arest-Yakubovich, A. A. *Macromolecular Theory and Simulations* **1995**, 4(2), 347-355.

27. Norrish, R. G. W.; Smith, R. R. *Nature* **1942**, 150, 336.
28. Trommsdorff, E.; Köhle, H.; Lagally, P. *Makromol. Chem.* **1948**, 1, 69.
29. O'Neil, G. A.; Wisnudel, M. B.; Torkelson, J. M. *Macromolecules* **1996**, 29, 7477.
30. Gao, J.; Kornherr, A.; Zifferer, G. *Macromol. Chem. Phys.* **1996**, C36, 199.
31. Fikentscher, H.; Gerrens, H.; Schuller, H. *Angew. Chem.* **1960**, 72, 856.
32. Alexander, A. E.; Napper, D. H. *Prog. Polym. Sci.* **1971**, 145.
33. Charleux, B. *Macromolecules* **2000**, 33, 5358.
34. Dimonie, V. L.; Daniels, E. S.; Shaffer, O. L.; El-Aasser, M. S. *Emulsion Polymerization and Emulsion Polymers*, P. A. Lovell and M. S. El-Aasser, eds., Wiley, New York, **1997**, 567-587.
35. Cunningham, M. F.; Mahabadi, H. K.; Wright, H. M. *J. Polym. Sci.; Part A: Polym. Chem.* **2000**, 38, 345-351.
36. Arzamendi, G.; Asua, J. M. *J. Appl. Polym. Sci.* **1989**, 38, 2019-2036.
37. Galimberti, F.; Siani, A.; Morbidelli, M.; Storti, G. *Chem. Eng. Comm.* **1998**, 163, 69-95.
38. Buback, M.; Hesse, P.; Hutchinson, R. A.; Kasak, P.; Lacik, I.; Stach, M.; Utz, I. *Ind. Eng. Chem. Res.* **2008**, 47, 8197-8204.
39. Wang, W.; Hutchinson, R. A. *Macromol. React. Eng.* **2008**, 2, 199-214.
40. Li, D.; Grady, M. C.; Hutchinson, R. A. *Ind. Eng. Chem. Res.* **2005**, 44, 2506-2517.
41. Kiefer, H.; Traylor, T. G. *Tetrahedron Lett.*, **1966**, 6163-6168.
42. Walling, C. *Tetrahedron*, **1985**, 3887-3900.
43. Newcomb, M. *Tetrahedron*, **1993**, 1151-1176.
44. Cawse, J. N., Experimental Design for Combinatorial and High Throughput Materials Development; Wiley; New York, NY, **2003**.

45. Potyrailo, R., Amis, E. J., High Throughput Analysis: A Tool for Combinatorial Materials Science; Kluwer Acedamic/Plenum Publishers: New York, **2004**.

46. Hoogenboom, R.; Schubert, U. S. *J. Polym. Sci. Part. A: Polym. Chem.* **2004**, 41(16), 2425-2434.

47. Hoogenboom, R.; Meier, M. A. R.; Schubert, U. S. *Macromol. Rapid Commun.* **2003**, 24(1), 15-32.

48. Meier, M. A. R.; Hoogenboom, R.; Schubert, U. S. *Macromol. Rapid. Commun.* **2004**, 25(1), 21-33.

49. Schmatloch, S.; Bach, H.; van Benthem, R. A. T. M.; Schubert, U. S. *Macromol. Rapid. Commun.* **2004**, 25(1), 95-107.

50. Webster, D. C. *JCT Coatings Tech.* **2005**, 2, 24-29.

51. Webster, D. C.; Bennett, J.; Kuebler, S.; Kossuth, M. B.; Jonasdottir, S. *JCT Coatings Tech.* **2004**, 1(6), 34-39.

52. Nasrullah, M. J.; Webster, D. C. *Polym. Prepr.* **2008**, 47(1) 217–218.

53. http://www.chemspeed.com/

54. Kniep, C. S. *Macromol. Rapid Commun.* **2002**, 23, 643.

55. Willemse, R.X.E.; Staal, B.B.P.; van Herk, A.M.; Pierik, S.C.J.; Klumperman, B. *Macromolecules*, **2003**, 36 (26), 9797-9803.

56. Zavitsas, A. A. *J. Am. Chem. Soc.* **1972**, 94, 2779–2788.

57. Sanderson, R. T. *J. Am. Chem. Soc.* **1975**, 97, 1367.

58. Golden, D. M.; Benson, S. W. *Chem. Rev.* 1969, 69, 125.

59. Gray, P.; Herod, A. A.; Jones, A. *Chem. Rev.* **1971**, 71, 247.

60. Tedder, J. M. *Tetrahedron* **1982**, 38, 313.

61. de Gennes, P.-G. *J. Chem. Phys.* **1971,** 55**,** 572.

62. Leger, L; Hervet, H.; Rondelez, F. *Macromolecules* **1981,** 14, 1732.

63. Fox, T. G. *Bull. Am. Phys. Soc.* **1956**, 1, 123.

64. Matyjaszewski, K; Davis, T. P. *Handbook of Radical Polymerization*, Wiley-Interscience, **2002**, 340.

CHAPTER 3. COMBINATORIAL APPROACH TO STUDY THE EFFECTS OF ACRYLIC POLYOL LIBRARY COMPOSITIONS ON THE PROPERTIES OF CROSSLINKED SILOXANE-POLYURETHANE FOULING-RELEASE COATINGS

3.1. Introduction

Fouling-release coating technologies are currently under development in response to the need for a non-toxic coating alternative to toxic antifouling paints.[1-6] These coatings do not inhibit settlement of marine fouling organisms, but limit the ability of the fouling organisms to form an adhesive bond to the coating surface. Thus, low levels of shear are able to dislodge the organisms from the coating. Poly(dimethylsiloxane) (PDMS) elastomers are used most often in fouling-release coatings due to their low surface energy, high elastic modulus, and low glass transition temperature. However, PDMS elastomers are mechanically weak, easily damaged, and are challenging to adhere to marine corrosion primers.

We have been exploring the use of self-stratified crosslinked siloxane-polyurethane coating systems as an alternative to silicone elastomer fouling-release coatings.[7] Self-stratification is controlled by surface energy, phase separation, and the viscosity of the components of the coating formulation.[8-12] These siloxane-polyurethane coatings will stratify into a soft, rubbery top layer formed by the PDMS, while the polyurethane will form a tough lower layer. Isocyanate may also react with residual hydroxyl groups on the epoxy corrosion primer providing improved adhesion. Crosslinking helps to stabilize the system against rearrangement when the coating is immersed in water. A conceptual diagram is provided in Figure 3.1.

In this coating system there are a large number of variables which are

expected to play a role in the formation of the self-stratified morphology and impact the physical and mechanical properties.

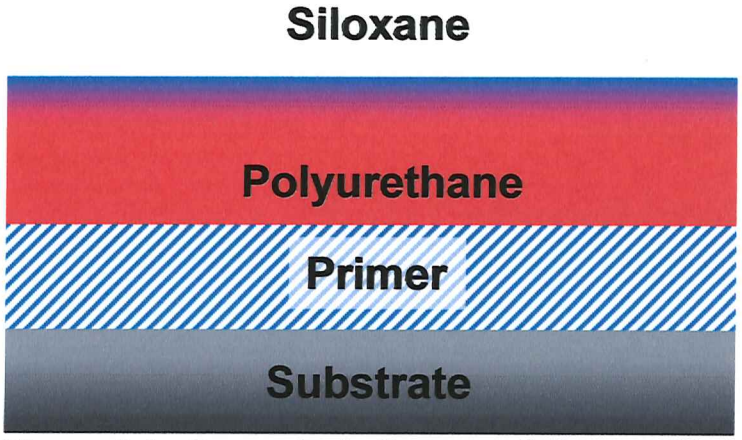

Figure 3.1. Conceptual diagram of the stratified siloxane-polyurethane coating system.

Thus, in order to efficiently explore a number of variables over a wide compositional range, we have used a combinatorial and high throughput approach to explore key variables. We have explored several formulation variables including the effect of solvent and crosslinker on the formation of stable self-stratified coatings,[7] and have synthesized libraries of 3-aminopropyl terminated PDMS, and poly(ε-caprolactone) (PCL)-PDMS-PCL triblock copolymers in order to explore the effects of PDMS molecular weight, PCL block length, and amount of PDMS polymer in siloxane-polyurethane coatings.[13,14] Researchers have also synthesized novel hydroxyalkyl carbamate terminated PDMS polymers and block copolymers and explored the effect of key variables on performance properties.[15,16]

In the previous experiments researchers had used a polycaprolactone triol as the organic polyol in the siloxane-polyurethane coating system. It is expected that the properties of the bulk polyurethane coating will have a major effect on the

fouling-release properties of the system, since in PDMS elastomer systems the bulk modulus has been found to have a significant impact on the release properties.[4,18-21]

Acrylic polyols have been favored for most aliphatic polyurethane systems because of their superior weathering, low cost, hydrolytic stability, and low isocyanate demand.[22] Since a wide range of compositions can be synthesized having varying hydroxyl functionality and glass transition temperature, acrylic polyols in the siloxane-polyurethane coating system synthesized by free-radical solution polymerization of acrylate monomers shown in Figure 3.2, can be used to vary the bulk properties of the coating.

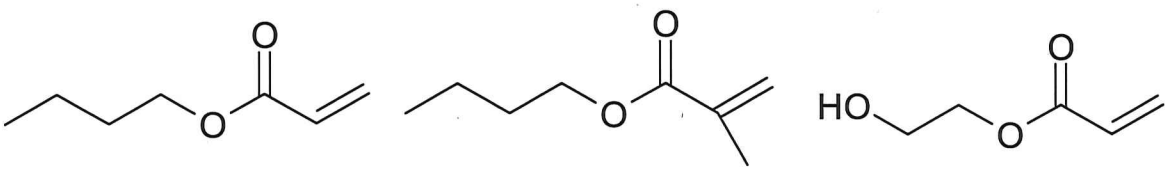

Butyl Acrylate
T_g = 219 K (-54°C)

Butyl Methacrylate
T_g = 293 K (20°C)

Hyroxyethyl Acrylate
T_g = 258 K (-15°C)

Figure 3.2. Monomers used in acrylic polyol synthesis, labeled by name and glass transition temperatures.

Thus, the objective of this research was to explore the effect of the bulk properties on the surface and fouling-release properties of the siloxane-polyurethane coating system. An acrylic polyol library of systematically varying composition was synthesized, characterized, and formulated into a siloxane-acrylic-polyurethane coating. The coatings were screened for key properties to determine if there are significant trends. Key laboratory screening properties were surface energy and pseudobarnacle pull-off adhesion.

To provide improved hydrolytic stability as well as the ability to control the bulk properties of the coatings a first library of acrylic polyols were synthesized and formulated into siloxane-polyurethane coatings. In those experiments, it was found that the fouling-release properties varied significantly as a function of acrylic composition. Coatings that were based on a low T_g polyol containing butyl acrylate and 20 percent hydroxyethyl acrylate formed siloxane-acrylic-polyurethane coatings having low bioadhesion with respect to *Ulva* spores.

Following the analysis of the data on the first library of experimental coatings, a second library was formulated focusing in detail on the compositional space of the first library; additional laboratory bioassays for characterization of the properties of the coatings were also implemented. Coatings from the second library were subjected to laboratory screening using two important marine fouling algae, a diatom *Navicula* and sporelings (young plants) of the green seaweed *Ulva*.[19, 23] Diatoms are unicellular algae that readily form yellow-brown colored biofilms, often referred to as 'slime', on illuminated submerged surfaces and are of importance from a fouling perspective because they adhere very strongly to fouling-release coatings.[24,25] The green seaweed *Ulva* comprises the most widespread species of alga that fouls man-made structures in the marine environment. Dispersal occurs through the settlement (attachment) of motile zoospores on surfaces, which germinate into sporelings (young plants) and ultimately grow into mature plants. The attachment strength of *Ulva* sporelings is low on fouling-release coatings[19] In addition, the coatings were also screened using several assays developed to challenge the coatings with marine bacteria.[20]

3.2. Experimental

3.2.1. Chemicals and reagents

Butyl methacrylate (BMA), n-butyl acrylate (BA), 2-hydroxyethyl acrylate (HEA), dibutyltin diacetate (DBTDA), 2,4-pentanedione, and methyl isobutyl ketone (MIBK) were obtained from Aldrich. DABCO K-15 was obtained from Air Products. Toluene was obtained from VWR and purified by a solvent purification system. The free radical initiator, 2-azobis (2-methylbutanenitrile) (Vazo 67) was obtained from DuPont. Aliphatic polyisocyanates based on hexamethylene diisocyanate trimer, Tolonate HDT and HDT 90 (90% solids in a blend of butyl acetate and aromatic hydrocarbon) were obtained from Rhodia. Polyurethane grade methyl n-amyl ketone (MAK) was supplied by Eastman Chemical. DC 3140 and T2 Silastic, products of Dow Corning Corporation, were received from Ellsworth Adhesives and used as silicone controls. DC 3140 and T2 Silastic were solvent reduced with MIBK and called Silicone A and Silicone B, respectively. 3-aminopropyl-terminated PDMS (M_n~10,000 g/mol) was synthesized and used as prepared.[13] A stock solution of 0.75 wt. % DABCO K-15 in MAK was used to prepare formulations. The polyurethane (PU) standard was composed of polycaprolactone and polyisocyanate and was used as a standard for the bioassays. All other reagents were used as received. The siloxane acrylic-polyurethane coatings had a final solids content of 60%.

3.2.2. Polymer synthesis

Synthesis library designs were done using Library Studio software (Symyx, Inc.). The software allows both statistical and full factorial experiment designs and

these designs are stored in a common database. In the studies, 6 X 4 arrays of experiments were designed. In order to provide a range of T_gs and crosslink densities, a library of acrylic polyols was designed using Library Studio based on BA, BMA, and HEA. A range of hydroxyl equivalent weights were obtained by adjusting the weight percent of HEA from 5% to 20% in the first library and 15% to 40% in the second library. The balance of the first acrylic polyol polymerization consisted of BA, BMA, plus four levels of HEA as shown in Table 3.1.

Table 3.1. First library design for the synthesis of acrylic polyols with HEA, BA, and BMA.

Array Position	HEA (%)	BA (%)	BMA (%)
A1	5	95	0
A2	5	76	19
A3	5	57	38
A4	5	38	57
A5	5	19	76
A6	5	0	95
B1	10	90	0
B2	10	72	18
B3	10	54	36
B4	10	36	54
B5	10	18	72
B6	10	0	90
C1	15	85	0
C2	15	68	17
C3	15	51	34
C4	15	34	51
C5	15	17	68
C6	15	0	85
D1	20	80	0
D2	20	64	16
D3	20	48	32
D4	20	32	48
D5	20	16	64
D6	20	0	80

In addition, a second acrylic polyol polymerization consisted of BA, BMA, plus six levels of HEA as shown in Table 3.2. The objective of the second acrylic polyol polymerization was to formulate siloxane acrylic-polyurethane coatings with higher hydroxy equivalent weights and thus, higher crosslink densities. This was done by narrowing the compositional space of the first library acrylic polyols experimental design.

Table 3.2. Second library design for the synthesis of acrylic polyols with HEA, BA, and BMA.

Array Position	HEA (%)	BA (%)	BMA (%)
A1	15.00	85.00	0.00
A2	20.00	80.00	0.00
A3	25.00	75.00	0.00
A4	30.00	70.00	0.00
A5	35.00	65.00	0.00
A6	40.00	60.00	0.00
B1	15.00	72.25	12.75
B2	20.00	68.00	12.00
B3	25.00	11.25	32.75
B4	30.00	10.50	59.50
B5	35.00	9.75	55.25
B6	40.00	9.00	51.00
C1	15.00	59.50	25.50
C2	20.00	56.00	24.00
C3	25.00	52.50	22.50
C4	30.00	49.00	21.00
C5	35.00	45.50	19.50
C6	40.00	42.00	18.00
D1	15.00	42.50	42.50
D2	20.00	40.00	40.00
D3	25.00	37.50	37.50
D4	30.00	35.00	35.00
D5	35.00	32.50	32.50
D6	40.00	30.00	30.00

All solution polymerizations were carried out in a Symyx batch reactor system.[27] The Symyx batch reactor system is comprised of a dual-arm liquid

dispensing robot housed inside a glove box under dry nitrogen. The robot dispenses liquids according to Library Studio designs. The three center wells in the synthesis platform holds arrays of reaction vials, and up to 288 simultaneous 1-mL reactions could be run in the batch mode with magnetic stirring and heating up to 120 °C. 8-mL vials in 6 X 4 arrays were used for the synthesis of the acrylic polyols. A stock solution of Vazo 67 (10%) in purified toluene was prepared for the synthesis experiments. Acrylate monomers, solvent and initiator were dispensed into 24 vials using a dual-arm liquid robotic pipette. Solutions were mixed with a magnetic stir bar and heated to 95 °C for 10 hours. The polymer library was synthesized in a single run to yield 24 acrylic polyols. Conversion was high (>97%) and the polyol solutions were used without additional purification.

Figure 3.3 depicts the 24 sample array template that was used to describe the first acrylic polyol synthesis library as well as the siloxane-polyurethane coating formulations made from the first acrylic polyol library.

Illustrated in Figure 3.4 is the 24 sample array template used to describe the second acrylic polyol synthesis (narrowed compositional space) as well as the siloxane-polyurethane coating formulations made from the acrylic polyols.

3.2.3. Polymer characterization

A TA Instruments Q1000 DSC with autosampler accessory was used for the T_g determinations. The samples were subjected to a heat-cool-heat cycle from -65 °C to +150 °C by ramping 20 °C per minute for both heating and cooling. The second heating cycle was used to characterize the samples. A Symyx Rapid GPC

with an evaporative light scattering detector (PL-ELS 1000) equipped with two PL-gel mixed-B columns (10 μm particle size) was used for molecular weight analysis.

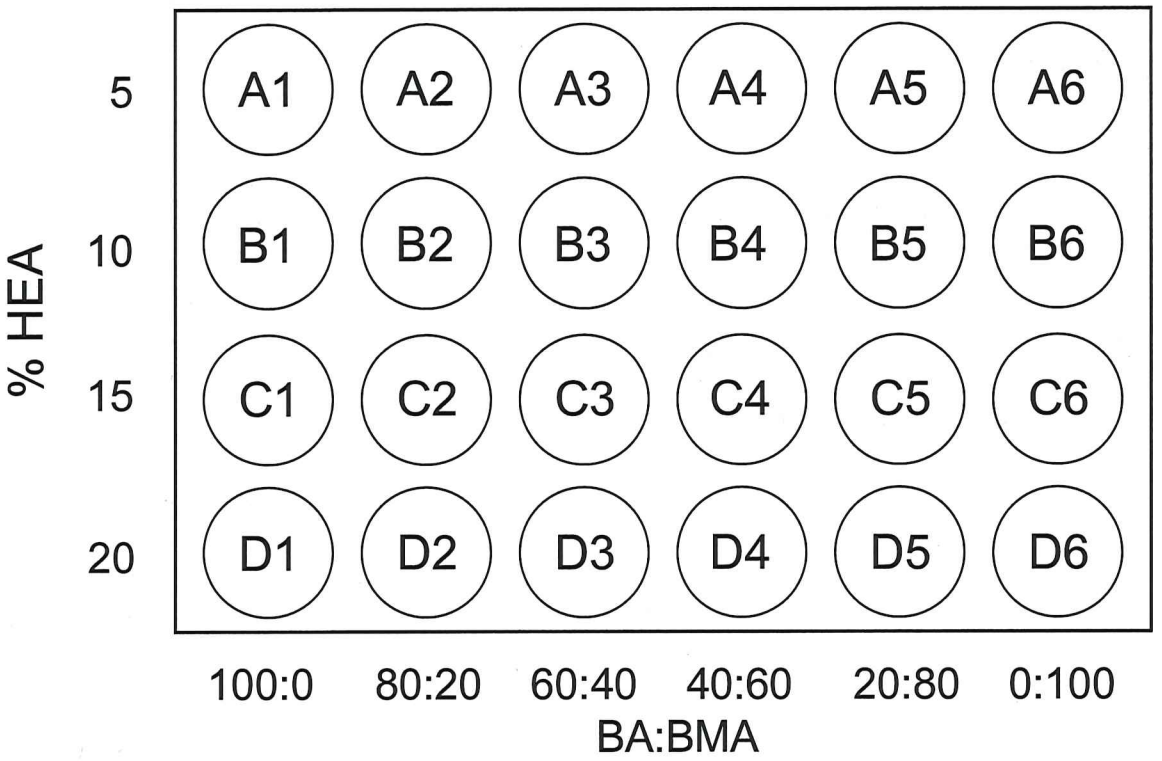

Figure 3.3. Experimental design for first combinatorial acrylic polyol library.

Solutions of 1 mg/mL sample in THF were prepared before the run; calibration was carried out with polystyrene standards and THF was used as the eluent at 45 °C at a flow rate of 2.0 mL/min. The molecular weight and PDI were determined with Epoch software (Symyx, Inc.).

3.2.4. Coatings formulation

Coating formulations were done according to Library Studio designs using a Symyx Coating Formulation System. Coating formulations are composed of the acrylic polyol library, catalysts DBTDA for the first library and DABCO K-15 for narrowed compositional space (second) library, 2,4-pentanedione, PDMS, and

HDT 90. Stock solutions of 30% PDMS in EEP, 1% DBTDA and 0.75% DABCO K-15 in MAK were prepared to form easily dispensed mixtures.

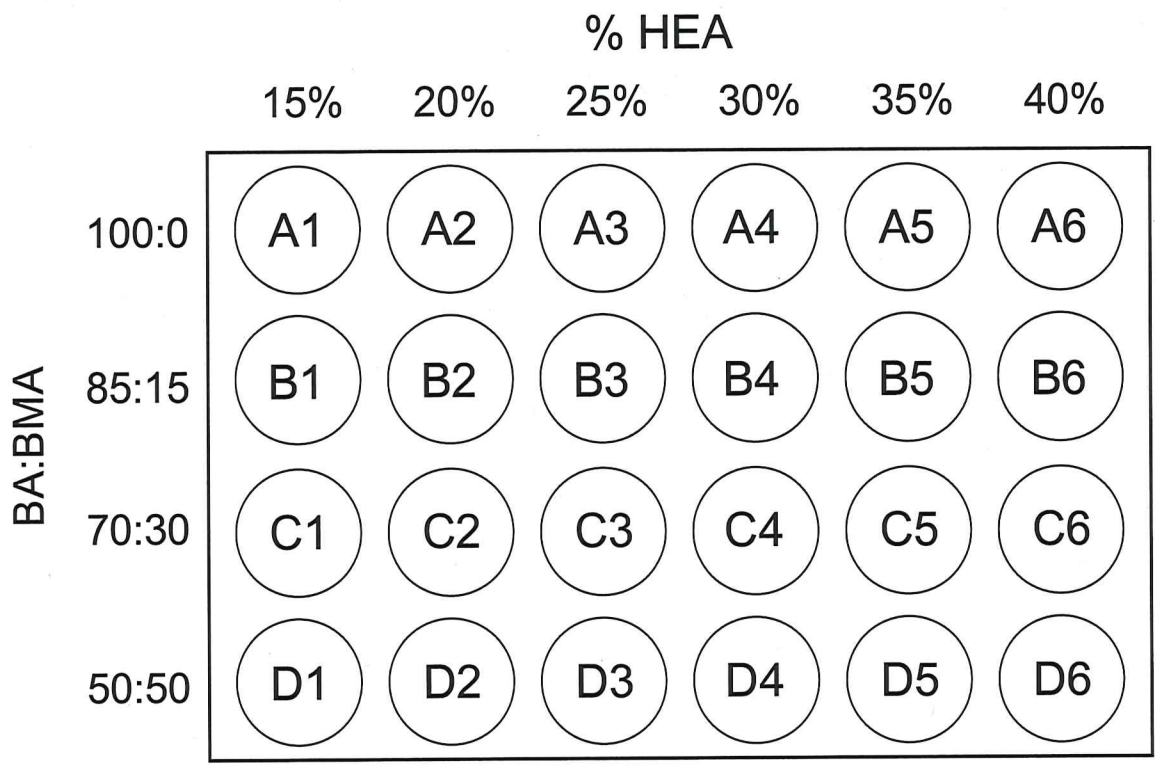

Figure 3.4. Experimental design for second combinatorial acrylic polyol library.

The ratio of isocyanate to hydroxyl functionality was kept at 1.1:1.0. The amount of catalyst, DBTDA was 0.001% by solids, DABCO K-15 was 0.18% by solids and the amount of 2,4-pentanedione was adjusted from 10% to 15% by solids. The automated coating formulation system manufactured by Symyx Discovery Tools, Inc. was used to prepare the formulations. First, the acrylic polyol library, stock solution of PDMS, and 2,4-pentanedione (non-reactive components) were placed into the holders of the formulation station and dispensed with the liquid handling robot using disposable pipettes to avoid cross

contamination. Coating formulations were prepared by adding 10% by weight PDMS into all formulations. After completion of dispensing all non-reactive components, the vials were capped and mixed with vortex for a few minutes. Catalyst (DBTDA or DABCO K-15) and HDT 90 (reactive components) were placed into the holders of the formulation station and dispensed with the liquid handling robot. After completion of dispensing of reactive components, the vials were capped again, and mixed with vortex until sufficient viscosity was obtained for coating application. For comparison, an acrylic-polyurethane library was prepared as above without the aminopropyl PDMS.

3.2.5. Coating application and curing

The Symyx Coating Application system was used to apply formulations to 4 x 8 inch aluminum and glass substrate panels.[27] The 4 X 6 formulation library was deposited onto 2 aluminum panels in an array format as seen in Figure 3.5.

The 24-element array of coatings "patches" of 100 µL/ sample were deposited on the panels using disposable pipettes to prevent cross contamination, then a robotic doctor blade spread the coating at a wet film thickness of 200 μm. The automated doctor blade was washed with toluene under sonication three times after each application and dried with an air knife. After completion of deposition of all the coatings, the panels were removed from the coating application station, placed into an enclosed drying cabinet with ventilation, and left overnight to cure at ambient temperature. Coatings were cured at 100 °C for one hour the following day. For the barnacle reattachment assay, 1 mL/ sample of the 24-element array were deposited using a pipette into modified 4"X8" epoxy primed

aluminum panels. Coatings were cured at 100 °C for one hour. For the bacterial assays, 100 µL/ samples of the formulations were deposited by pipette into 24-well microtiter plates modified with primed aluminum bottom liners.

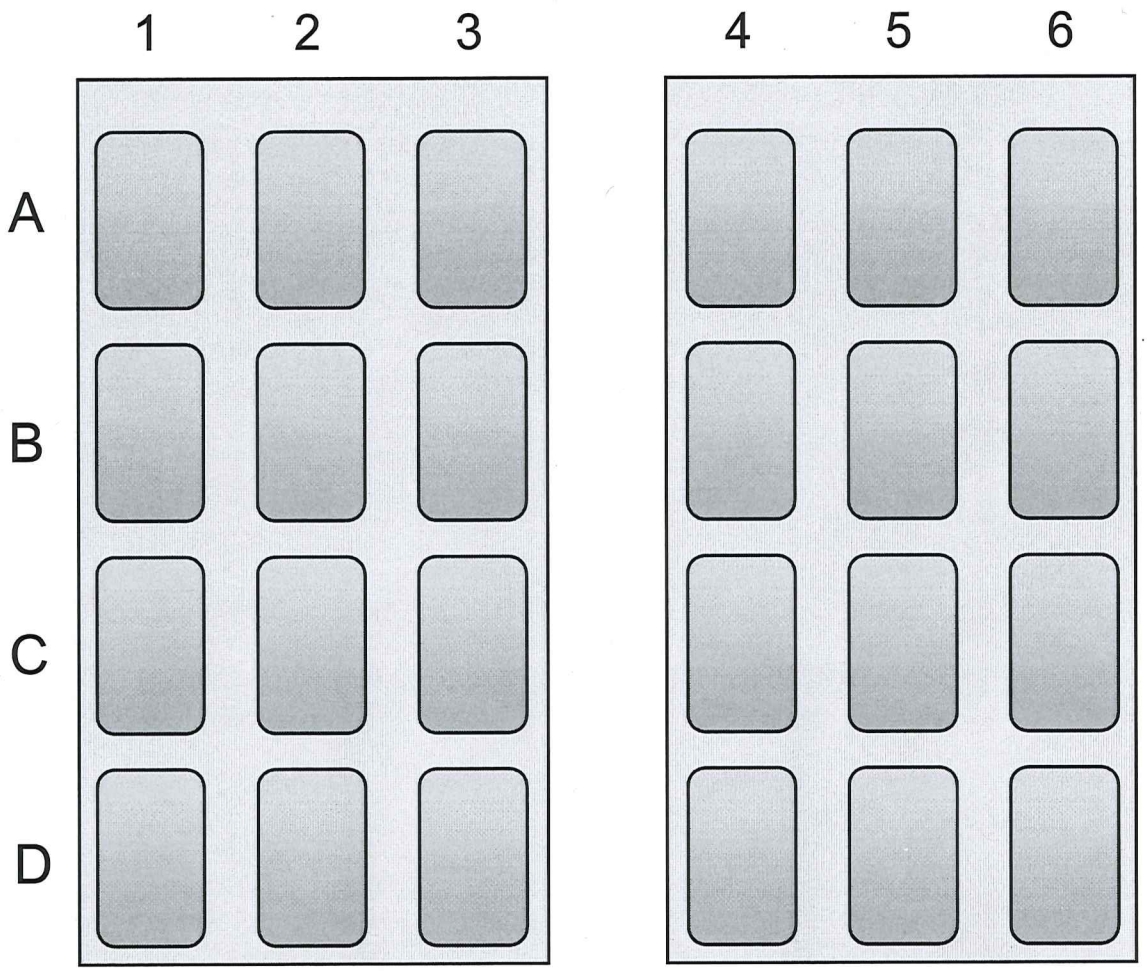

Figure 3.5. Panel layout for siloxane-polyurethane coating arrays.

3.2.6. Coating characterization

A Symyx parallel DMTA was used for determination of the viscoelastic properties of the coating libraries.[29] The samples were subjected to heating from -110 °C to +100 °C with a heating rate of 1 °C per minute and a frequency of 10

Hz.. T_g was determined from the peak of the tan delta curve. A Symyx Coating Surface Energy system was used for surface energy analysis. The surface energy system measures and averages contact angles of various liquids and calculates the surface energy. The system receives two 4 X 8 inch coating array panels. The images of three droplets of each test liquid are taken by a CCD camera, and the contact angles are determined using automated image analysis. Water and methylene iodide (MI) are used as test liquids, and the surface energies are calculated using the Owens-Wendt method.[31]

The Symyx pull-off adhesion system was used for the pseudo-barnacle pull-off adhesion analysis.[32] The adhesion system can be used to either determine the adhesive strength of a coating on the substrate or the adhesive strength of an epoxy to the coating surface (pseudo-barnacle). The instrument can receive two 4 X 8 inch coating array panels. First, the two array panels were placed onto the holders of the adhesive application system by applying a vacuum underneath the panels. Then, a plastic template was placed on top of the coatings using pins on the substrate holder for alignment. The plastic sheets have three 7 mm diameter holes over each coating on the array panel. Then Loctite Hysol® Epoxy 1C-LV glue was spread on the coatings through the custom made plastic sheets, resulting in the placement of three 7-mm spots of adhesive on each coating. The plastic sheet was removed and the panels were removed from the adhesion preparation station and placed into clamping jigs. After the panels were clamped, three aluminum studs per coating sample were placed into the clamping jig on top of the applied glue. Weighted foam blocks were placed on top of the studs and the epoxy glue

was cured overnight. The next day, the clamped panels with the holders still attached to them were placed into the holders of the automated adhesion system. A pull-off head removes each test stud and the maximum force at failure is recorded. The three values are then averaged.

Atomic Force Microscopy (AFM) studies were performed on a Dimension 3100® microscope with Nanoscope IIIa controller (Digital Instruments, Inc., California). Experiments were operated under tapping mode in air at ambient condition using silicon probes with spring constant 0.1-0.4 N/m and resonant frequency 17-24 kHz. The set point ratio was 0.9.

3.2.7. Evaluation with the marine microalgae *Navicula incerta*

Algal analysis was carried out after an overnight pre-equilibration in artificial sea water. For the assessment of biofilm growth, algae were diluted to an OD of 0.03 at 660 nm in ASW supplemented with nutrients. 1 ml was added to each well of the plate and allowed to incubate statically for 48 hours. Algal biofilm growth was determined by fluorescence measurement of DMSO extracts. Biofilm growth was reported as fluorescence intensity (relative fluorescence units). Water jet adhesion was carried out after 2 hrs of algal cell growth. The first column of each plate was not treated and served as the measure of cell growth before water jetting. The second and third column of each coating was jetted for 10 seconds at a pressure of 10 psi (~69 kPa). Each data point was the mean value of four replicate wells. Algal cell attachment was reported as the percent removal for the pressure indicated above.

Biological screening at the University of Birmingham, U.K. involving *Navicula incerta* was also completed. For the *Navicula incerta* study microtiter plates containing the siloxane acrylic-polyurethane coatings were leached in recirculating distilled water tanks fitted with a carbon filter for a total of 26 weeks and placed in sea water to equilibrate two hours before the start of the experiment. Three replicate microtiter plates were incubated with a culture of *Navicula incerta* in trays for three hours in the light at ~20°C.[24-25] After gentle washing, the panels with adhered cells were cultured in illuminated tanks of enriched seawater. After three days the panels, which were covered by cells, were subjected to an impact pressure of 34 kPa and 172 kPa from a water jet. Percentage removal was estimated visually.

3.2.8. Evaluation with the marine algae *Ulva linza* sporelings leachate toxicity, growth and removal

Biological screening involving *Ulva linza* was completed at the University of Birmingham, U.K. For the *Ulva* sporelings study microtiter plates were leached in a recirculating distilled water tank fitted with a carbon filter for a total of eight weeks and placed in seawater to equilibrate two hours before the start of the experiment. Three replicate microtiter plates were incubated in trays with a suspension of *Ulva* zoospores for three hours in the dark.[19,23] After washing to remove unattached zoospores, the panels with settled spores were cultured in enriched sea water for 7 days. After 7 days, the settled spores had germinated and the surface of the panels was covered with young plants. The panels were

subjected to impact pressures of 93 kPa and 151 kPa from a water jet[25], percentage removal was estimated visually.

3.2.9. Evaluation with the Marine Bacterium *Cellulophaga lytica*

Bacterial analysis was carried out after 28 days of water immersion. Leachate toxicity was assessed by introducing the bacterium into overnight extracts (artificial sea water with nutrients (ASW)) of each coating and evaluating growth after 24 hours via a crystal violet colorimetric assay. Growth in coating leachates was reported as an absorbance ratio (600 nm) *C. lytica* biofilm retention and retraction analysis was assessed by a crystal violet colorimetric assay. A 5% suspension of *C. lytica* in ASW + nutrients (~107 cells.ml^{-1}) was prepared and 1ml was added to each well of the coating plate. Plates were incubated statically at 28 °C for 24 hours to facilitate bacterial attachment and colonization. Plates were rinsed three times with DI water and stained with crystal violet. Images were taken after staining, and then the crystal violet was extracted in 33% acetic acid and the resulting eluates were measured for absorbance at 600nm. Biofilm retention was reported as the mean absorbance value of three replicate samples. Biofilm retraction was assessed by determining percent coverage calculations from digital images taken of each coating plate using an automated software tool. Biofilm retraction was reported as the mean percent coverage value of three replicate samples. Water jet adhesion was carried out after 24 hrs of bacterial biofilm growth. The first column of each plate was not treated and served as the measure of biofilm growth before water jetting. The second and third column of each coating was jetted for 5 seconds at a pressure of 30 psi. Each data point

was the mean value of four replicate wells. Biofilm adhesion was reported as the percent removal for the pressure indicated above.

3.2.10. Evaluation with the marine fouling barnacle *Amphibalanus amphitrite.*

Adult barnacles were allowed to attach to sample coatings surfaces for two weeks. Coatings were analyzed after 2 weeks of water immersion and daily feeding of the barnacles with brine shrimp. A hand held digital force gauge, mounted to an automated stage, was used to measure the peak force of release for each barnacle using the protocols described in ASTM D5618-94. Adhesion strength in shear was calculated by dividing the measured force required to remove the barnacle by the basal area and reported in megapascals (MPa). Each data point is the mean value of nine individual barnacle measurements.

3.2.11. Evaluation with the marine bacterium *Halomonas pacifica*

Bacterial analysis was carried out after 28 days of water immersion. A 10% suspension of *H. pacifica* in ASW + nutrients (~108 cells.ml^{-1}) was prepared and 1ml was added to each well of the coating plate. Plates were incubated statically at 28 °C for 24 hours to facilitate bacterial attachment and colonization. Water jet adhesion was carried out after 24 hrs of bacterial biofilm growth. The first column of each plate was not treated and served as the measure of biofilm growth before water jetting. The second and third column of each coating was jetted for 5 seconds at a pressure of 30 psi. Each data point was the mean value of four replicate wells. Biofilm adhesion was reported as the percent removal for each pressure indicated above.

3.3. Results and Discussion

Previous work on the exploration of crosslinked siloxane-polyurethane coatings showed that tough and durable coatings having low surface energy could be prepared and that the low surface energy could be maintained after water immersion, which was attributed to crosslinking.[7,13-17] The coating system is based on an organofunctional PDMS, a polyisocyanate crosslinker, and an organic polyol. A solvent blend, cure catalyst, and pot life extender also are used in formulating the coating system. Acrylic polyols are commonly used in a number of coating applications and are typically crosslinked with either a polyisocyanate or an amino resin. Hydroxy- group functionality is provided by a monomer such as hydroxyethyl acrylate, hydroxyethyl methacrylate or the corresponding hydroxypropyl acrylate or methacrylate. Typically, the hydroxyl monomer is copolymerized with two additional monomers and the composition is optimized for hydroxyl-group content and glass transition temperature.

To explore the effect of acrylic polyol composition on the physical, mechanical, and performance properties of the self-stratifying siloxane-polyurethane coatings, a combinatorial library was prepared using three monomers to vary the acrylic polyol composition, HEA, BA, and BMA. There were 24 different acrylic polyol compositions for the first library synthesized as described in Table 3.1 and illustrated in Figure 3.3. HEA was varied from 5 to 20 percent to provide a range of hydroxyl content and crosslink density in the final coating and to provide a range of hydroxyl equivalent weight from 581 g/mol to 2324 g/mol, respectively. The T_g was adjusted over a wide range by using a

combination of BA and BMA. All of the polyols were synthesized in a single experiment using an automated batch synthesis system.

The RGPC molecular weight results for the first acrylic polyol library can be seen in Figure 3.6. A general trend from the results shows a decrease in molecular weight as the ratio of BA decreases and BMA increases. This may be due to BA terminating predominately by combination, whereas BMA terminates predominately by disproportionation.[32] The termination reactions of the acrylic polyols play a large factor in the Mw evident by the copolymers comprised of BA and HEA having Mw of 110-125 kDa. As the acrylic polyols composition changes to a ratio consisting of BMA and HEA the Mw shows a decrease of 100kDa to 20-30 kDa. Overall, the amount of HEA in the acrylic polyols has a small effect on the overall molecular weight, however there is a slight increase in MW (~10K/ BA:BMA composition) as the HEA is increased, which seems to be a common trend throughout the acrylic polyol library.

The RGPC molecular weight results for the second acrylic polyol library are depicted in Figure 3.7. A few molecular weight trends are observed. The initial trend is the molecular weights of the acrylic polyols consisting of 100:0 (BA:BMA) and 20% HEA and 15% HEA have about the same values in Figure 3.6 and Figure 3.7. This gives credibility to those values since there is good correlation between the two acrylic polyol studies. It should be mentioned that at 25% HEA as well as higher amounts of HEA that a gelled product was observed. This is most likely due to autoacceleration (Trommsdorff effect) where a localized increase in

viscosity slowed the termination reaction resulting in very high Mw, as well as diacrylate in the HEA and grafting on the acrylate backbone.

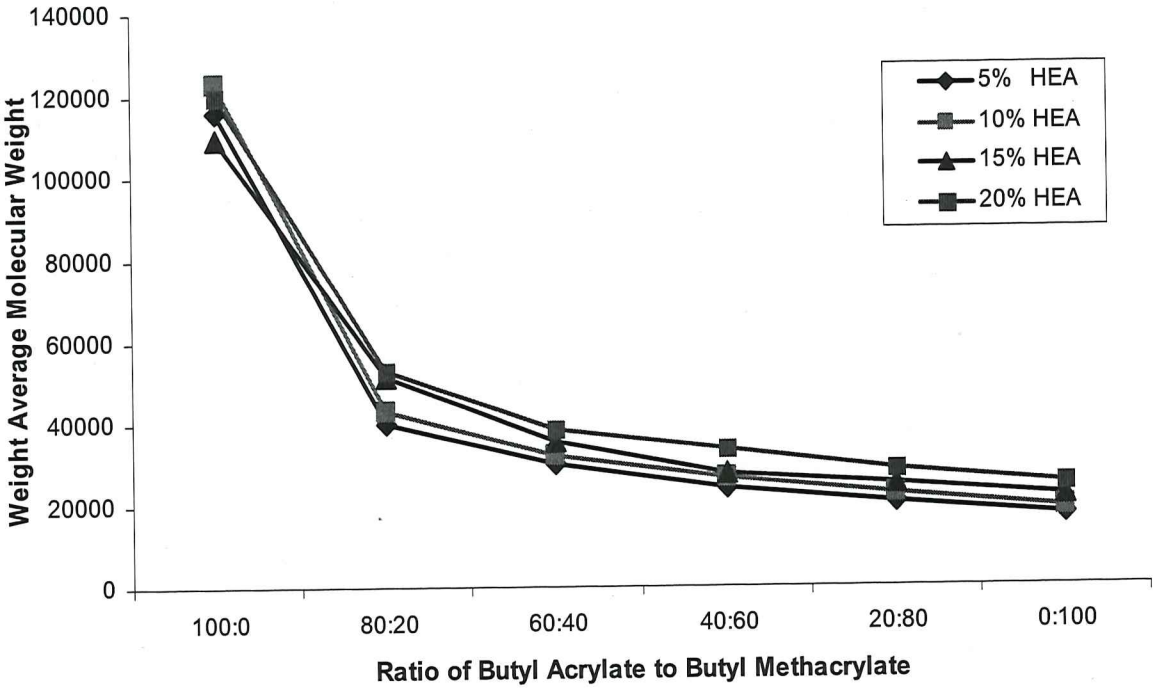

Figure 3.6. Weight average molecular weight of first acrylic polyol library by Rapid-GPC.

However, because it formed a gel, only the soluble portion of the polyol was actually characterized. This observation is seen in the significant drop in Mw for the 100:0 (BA:BMA) at 25% HEA which is probably due to the increase in hydrogen bonding with the increase of HEA content creating a gel. So the value that is present is actually the soluble portion of the acrylic polyol resulting in a lower Mw.

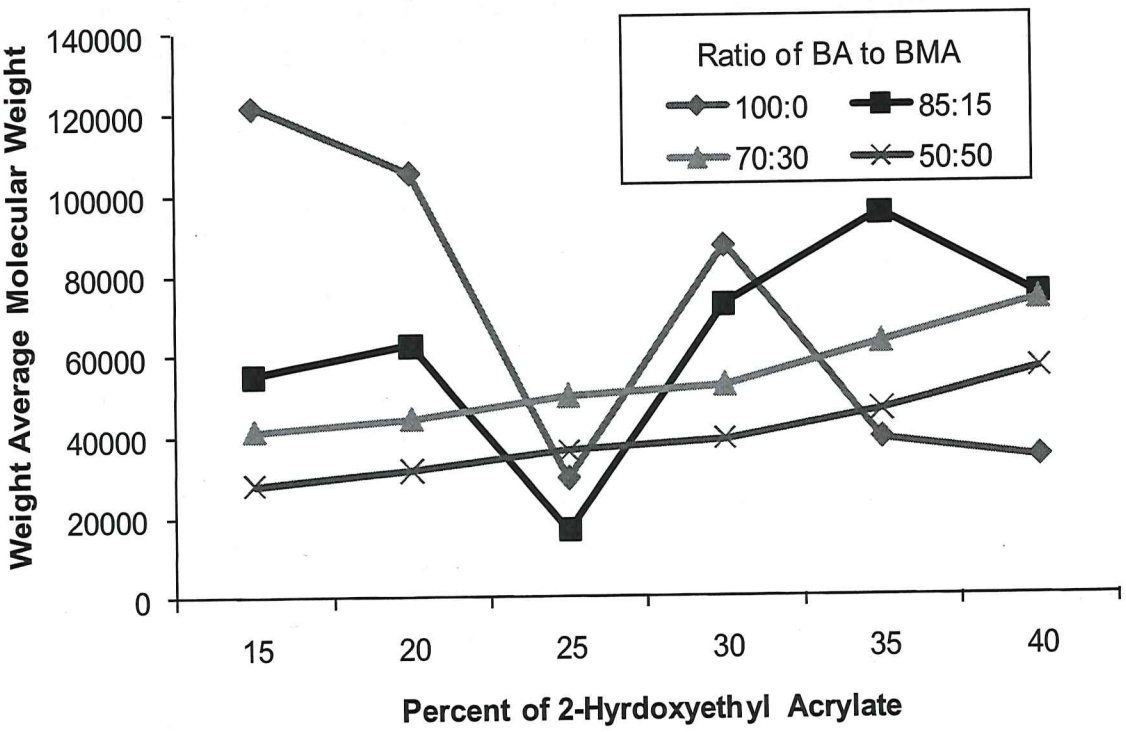

Figure 3.7. Weight average molecular weight of second acrylic polyol library by Rapid-GPC.

It appears that at 30% HEA and 100:0 (BA:BMA), there is an increase in Mw again, this may be due to more of the acrylic polyols high Mw gel being soluble resulting in a value with higher Mw. However, as the HEA was increased to 35% and 40%, the Mw values decreased once again, which is consistent with the possible Trommsdorff effect.

Another trend observed in Figure 3.7 was the linear increase in Mw with an increase in HEA content for the acrylic polyols consisting of 70:30 and 50:50 (BA:BMA). At these ratios of BA to BMA, it should be mentioned that it was observed that these acrylic polyols did not form a gelled product. So it seems that the Trommsdorff effect seen with the higher BA content acrylic polyols did not have the same affect on the polyols with somewhat higher amounts of BMA.

Overall, there was good Mw correlation with the acrylic polyols consisting of 15% and 20% HEA and 100:0 (BA:BMA) between the first and second acrylic polyol libraries. Also, due to potential autoacceleration, the acrylic polyols consisting of higher BA content formed gelled products that made reliable Mw characterization difficult due to analyzing only the soluble portion of the acrylic polyol.

In Figure 3.8, DSC measurements were completed and the glass transition temperatures of the first acrylic polyols library (a) comprised of HEA, BA, and BMA and the acrylic-polyurethane coatings (b) from the experimental acrylic polyols are illustrated. In Figure 3.8(a), a general trend is seen as determined by DSC that, as the ratio of butyl acrylate to butyl methacrylate is changed, the T_g increases, due to butyl methacrylate homopolymer having a much higher T_g than butyl acrylate homopolymer, 20°C to -54°C, respectively a trend of increasing T_g is seen with increasing HEA content in the polyols.

However, at a ratio of 0:100, BA:BMA, there is a convergence of T_g at approximately 10°C, regardless of the level of HEA. Thus, in this library, acrylic polyols having a range of glass transition temperatures from -48 to 10°C were successfully synthesized.

The acrylic polyols were then formulated into polyurethane coatings using HDT as the crosslinker and the experimental coatings were tested to find the glass transition temperature. The glass transition temperatures of the acrylic-polyurethanes, illustrated in Figure 3.8(b), are generally higher than that of the acrylic polyols in Figure 3.8(a).

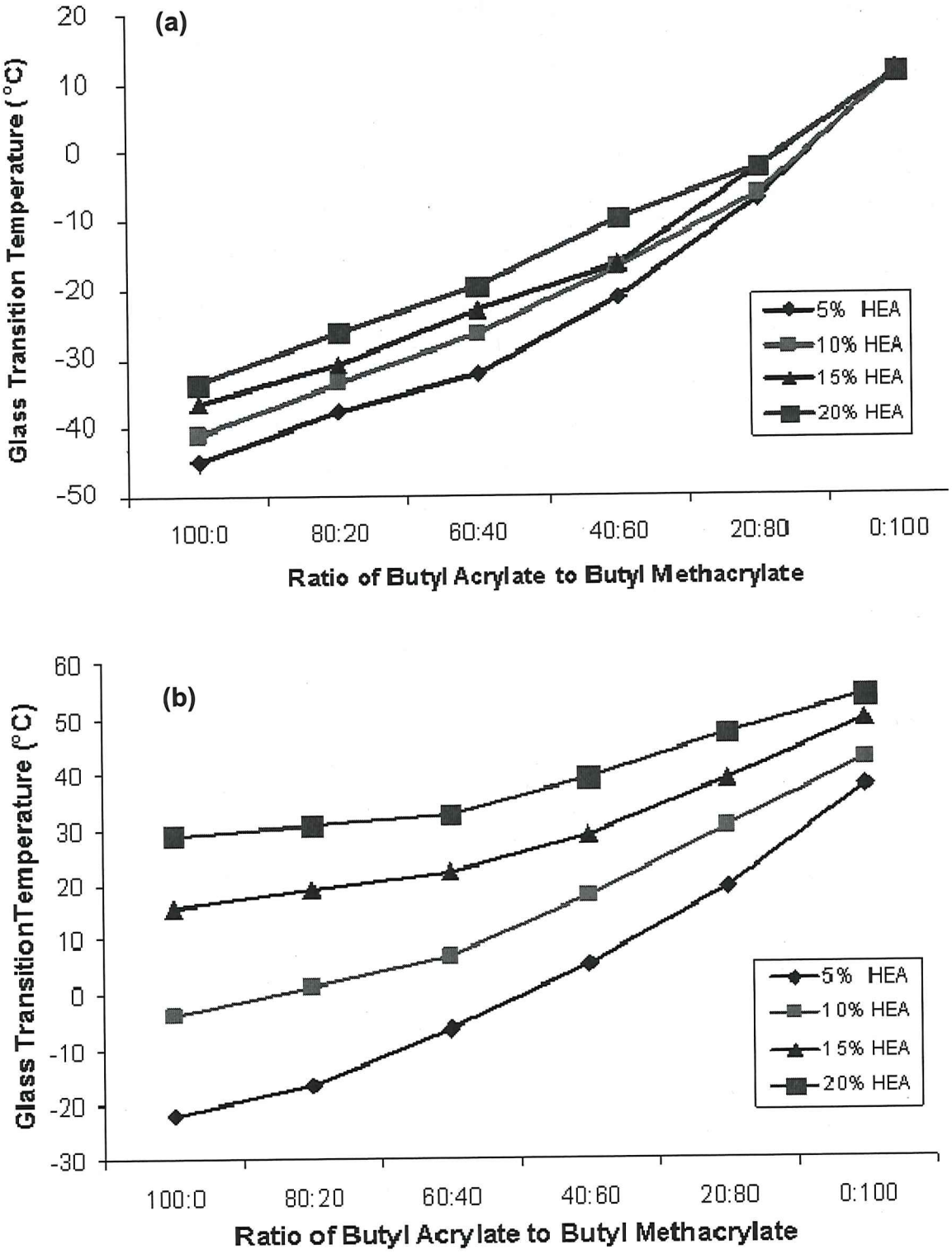

Figure 3.8. DSC glass transition temperatures of first (a) acrylic polyols (b) acrylic-polyurethane coatings library.

A wide range of T_gs are seen both from the increase in HEA as well as due to the BA:BMA ratio. The increase in T_g from increasing HEA content is higher for the coatings than for the polyols since higher levels of isocyanate are used for polyols containing higher HEA content. This leads to increased crosslink density and increased hydrogen bonding. Another trend seen is when BMA (from the acrylic polyol) is increased in the acrylic-polyurethane there is a tighter grouping of T_gs with addition of HEA content from the acrylic polyol. For example, the range of T_gs for the 100:0 (BA:BMA) was 30°C to -22°C a difference of 52°, in comparison the range for 0:100 (BA:BMA) was 45°C to 35°C a difference of only 10°. Overall, the increase in T_gs for the acrylic-polyurethane coatings would be consistent with the same respective examples of the corresponding acrylic polyol T_gs seen in Figure 3.8(a).

In order to better understand the surface properties of the coatings system water contact angle measurements were completed and shown in Figure 3.9. Figure 3.9 illustrates the initial WCA for the acrylic-polyurethane coating system. The WCA data from the acrylic-polyurethane coatings show that the polyurethane coatings are all hydrophilic having water contact angles less than 90°. It is known that polyurethane surfaces are hydrophilic in nature, so these values are consistent with previous studies.

The acrylic-polyurethane coatings were formulated with the incorporation of 10% 3-aminopropyl-terminated PDMS (Mn ~ 10,000 g/mol) to form the siloxane acrylic-polyurethane coatings.

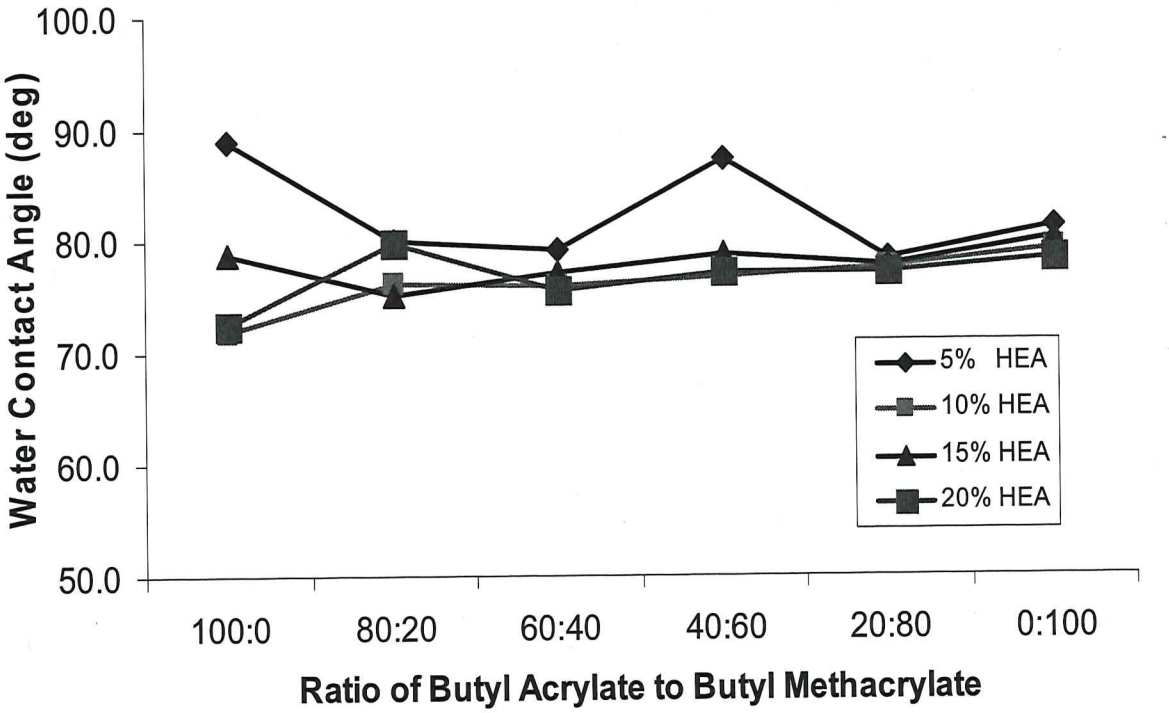

Figure 3.9. Water contact angle of first acrylic-polyurethane coatings library.

The siloxane acrylic-polyurethane coatings were then characterized by water contact angle measurements both before water immersion and after 14 days water immersion, as well as, methylene iodide (MICA), and surface energy (SE) and are illustrated in Figure 3.10. The water contact angle data for the experimental coatings depicted in Figure 3.10(a) indicates that the coatings are all hydrophobic since the water contact angles vary between 94° to 100°. This is likely due to the self-stratification of the low surface energy PDMS migrating to the surface of the coatings.[8-12] However, a general trend is observed with the experimental coatings when the amount of BMA is increased there is a slight decrease in the WCA. Even though there is a decrease in WCA, the incorporation

of 10% PDMS is sufficient to convert the hydrophilic polyurethane coatings into hydrophobic coatings.

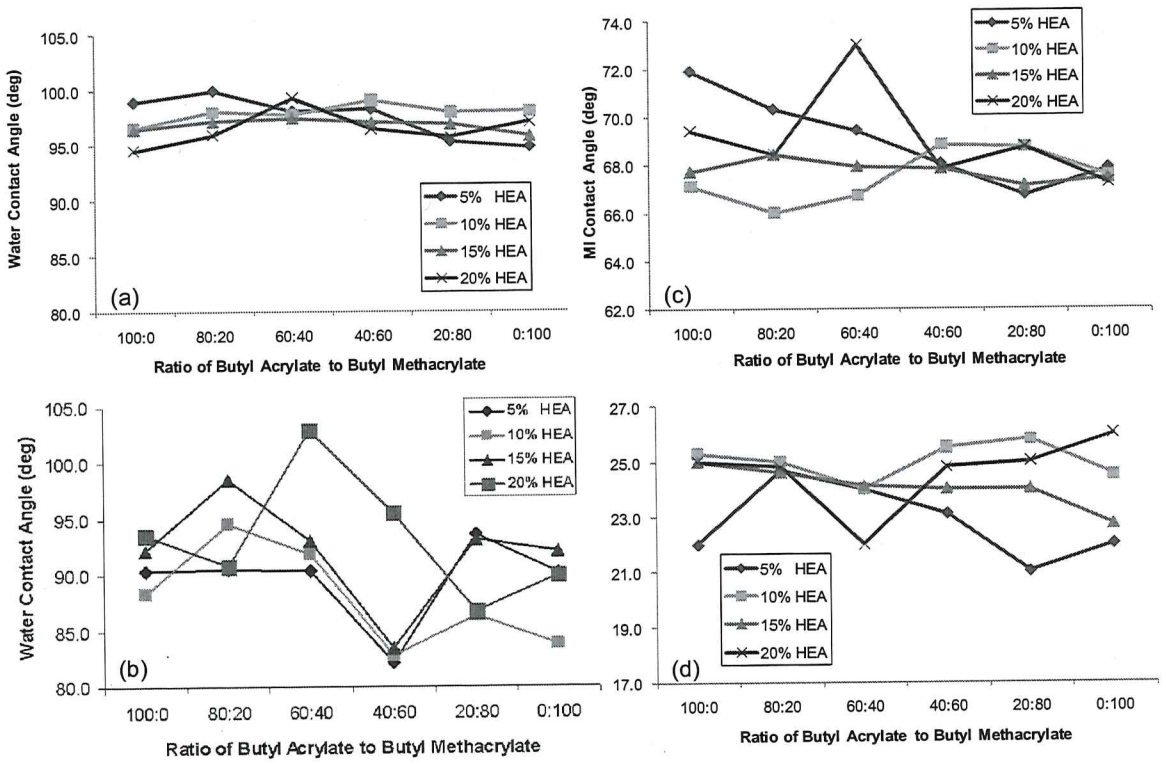

Figure 3.10. Results from first siloxane acrylic-polyurethane library of (a) water contact angle (b) water contact angle after 14 days water immersion (c) methylene iodide contact angle and (d) surface energy.

Measuring the water contact angle after 14 days water immersion was done since the final application for these experimental coatings are in a marine environment. Figure 3.9(b) depicts the water contact angle data after 14 days of water immersion. While there is some change in water contact angle, many of the coatings still show evidence of hydrophobicity. Thus, the incorporation of 10% PDMS is sufficient to generate hydrophobic acrylic-polyurethane coatings that have a stable surface chemistry after water immersion. The MICA is depicted in

Figure 3.10(c) for the first library of siloxane acrylic-polyurethane coatings. Previous researchers have reported that the MICA values for PDMS is ~70° [34] and polyurethane (PU) is ~67°[35]. Therefore; the majority of the experimental coatings are in the same range of the reported PDMS MICA with the exception of the coatings formulated with the acrylic polyols consisting 10% HEA, which had a MI contact angle of ~66-67° equivalents to PU-like surfaces. It was also observed that the coatings formulated with the acrylic polyols consisting of 20:80 (BA:BMA) at 5% and 15% HEA showed similar MICA to PU-like surfaces. A general trend that is seen with the MICA is with the increase in BMA content in the acrylic polyols formulated in the experimental coatings there is a decrease in MICA, with values similar to PU. The surface energy of the experimental coatings can be seen in Figure 3.10(d). Previous literature has reported that PDMS has a surface energy of ~20 mN/m[34] and PU was reported to have a surface energy of 32.4 mN/m[35]. In general, the experimental coatings exhibit a surface comparable to PDMS more so than PU, with values ranging from 21 mN/m to 26 mN/m. When comparing the MICA results with the SE results it is observed that even though several experimental coatings show PU-like surfaces using MI, these same coatings show to be more PDMS-like overall for the SE. Also, comparing the results of the WCA for the experimental coatings which showed all were hydrophobic (PDMS enriched surface) with the MICA showing that some of the experimental coatings were exhibiting the surface to be PU-like, a reason for this may be due to the amount of PDMS at the surface in comparison to the amount of the acrylic-polyurethane at the surface. This was observed in the same respective experimental coatings

WCAs in Figure 3.10(a), where there was a slight decrease, which may suggest that there is some amount of PU at the surface as well as PDMS, but the difference is small that it is difficult to distinguish with the surface energy results. Overall, siloxane acrylic-polyurethane coatings were formulated and successful in creating a surface that was hydrophobic and mostly stable after water immersion and most experimental coatings exhibited surface energy properties similar to PDMS.

For the second siloxane acrylic-polyurethane coatings library, the water contact angle data, depicted in Figure 3.11(a), indicates that the coatings are all hydrophobic since there is no significant difference in the water contact angles, with angles varying between 100° to 110°. Figure 3.11(b) illustrates the methylene iodide contact angle of the experimental coatings. The methylene iodide angles for the siloxane-acrylic-urethane coatings are similar for all coatings at 15-25 percent HEA and then begin to increase with the addition of HEA. As stated before, literature MICA values for PDMS have shown to be ~70°[34], while MICA values for PU are ~67°[35]. Most experimental coatings show to have MICA values similar to PDMS. However, with the increase in HEA there were significant changes in MICA values. This is most likely due to the strong effects of the polyurethane system with those respective compositions and possible surface effects from microdomains during the self-stratification mechanism of film formation.

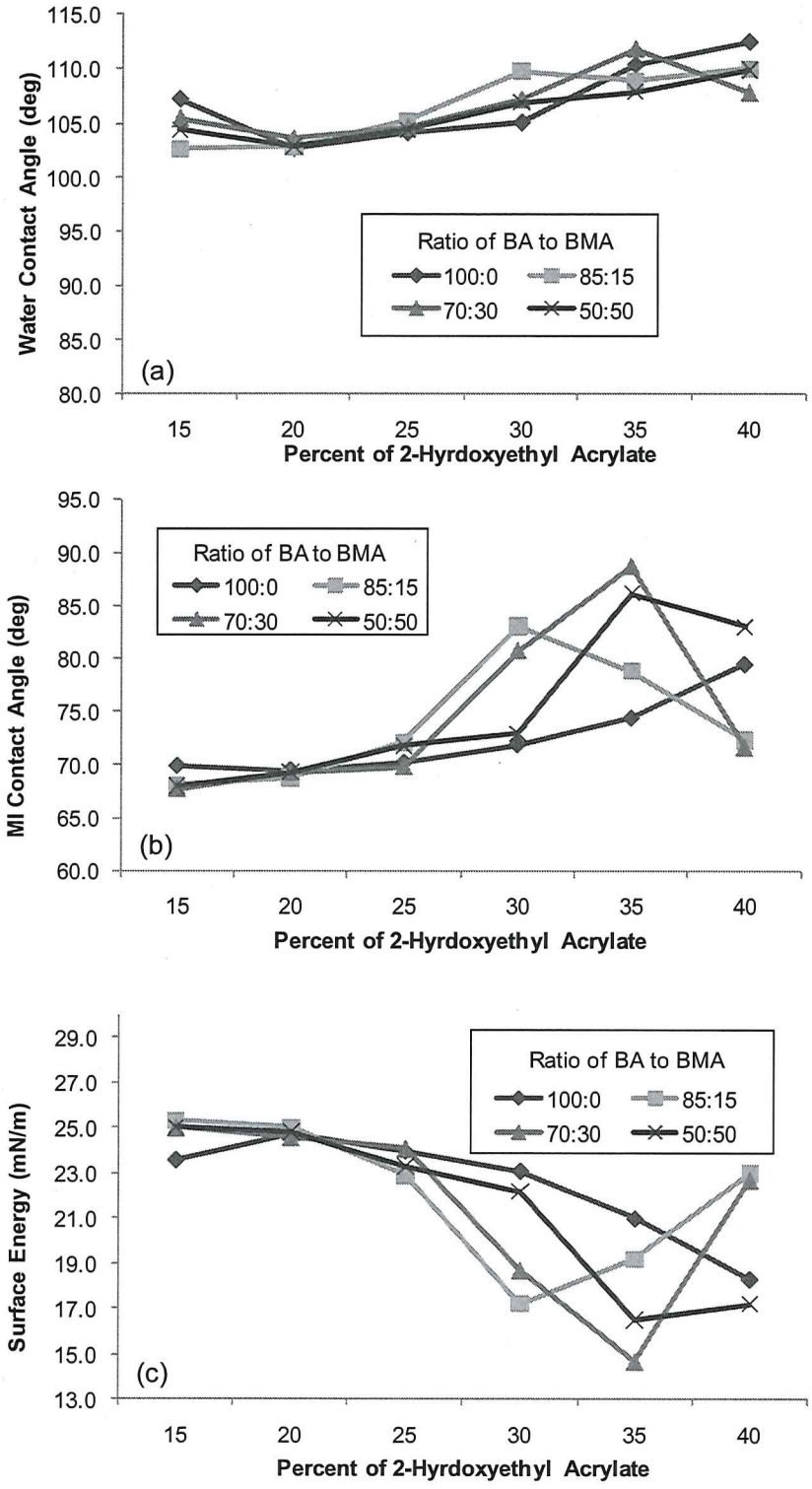

Figure 3.11. Results from second library of siloxane-polyurethane coatings (a) water contact angle, (b) methylene iodide contact angle and (c) surface energy.

Likewise, in Figure 3.11(c) the surface energy values are similar to literature values of PDMS for low levels of HEA and then surface energy values begin to decrease with the addition of higher levels of HEA, ranging from 17 to 15 mN/m, similar to what would be observed with superhyrophobic surfaces (i.e.-PTFE). However, it is shown that the SE values for the experimental coatings consisting of 85:15 and 70:30 (BA:BMA) and 30% and 35% HEA an increase back to similar SE values of 23 mN/m. Once again, the decrease in SE is likely due to surface effects, such as microdomains leading to a change in surface roughness. Another possible explanation for the decrease in SE with the increase in HEA content was the use of Dust-off®, which uses 1,1-difluoroethane, when cleaning off the respective coating surfaces (30-35% HEA coatings) after curing. 1,1-difluoroethane has a SE value of 15.3 mN/m.[36] This would also explain the slight increase in the WCA for those coatings containing 30-35% HEA. Overall, the second experimental coatings library showed that all were hydrophobic and most showed MICA and SE comparable to PDMS values.

Figure 3.12 illustrates the parallel DMTA (pDMTA) results for the first siloxane acrylic-polyurethane coatings system. The T_gs of the first siloxane acrylic-polyurethane coatings system follows a similar T_g trends from both the first acrylic polyol and first acrylic-polyurethane coatings system seen in Figure 3.8(a) and (b), respectively. The T_gs of the first experimental coatings increase with the addition of BMA and HEA in the coatings. Taking a closer look, the first acrylic-polyurethane coatings T_gs are almost exactly the same as the first siloxane acrylic-

polyurethane coatings. This trend indicates that the 10% load of PDMS in the coating is likely at the surface due to the self-stratification mechanism and the incompatibly with the system, however, the pDMTA doesn't go low enough to see the T_g of PDMS. This observation would indicate that the PDMS doesn't have any major effect on the overall T_gs of the first experimental coatings; rather the bulk of the coatings system (acrylic-polyurethane) plays the largest effect on the coatings systems T_gs.

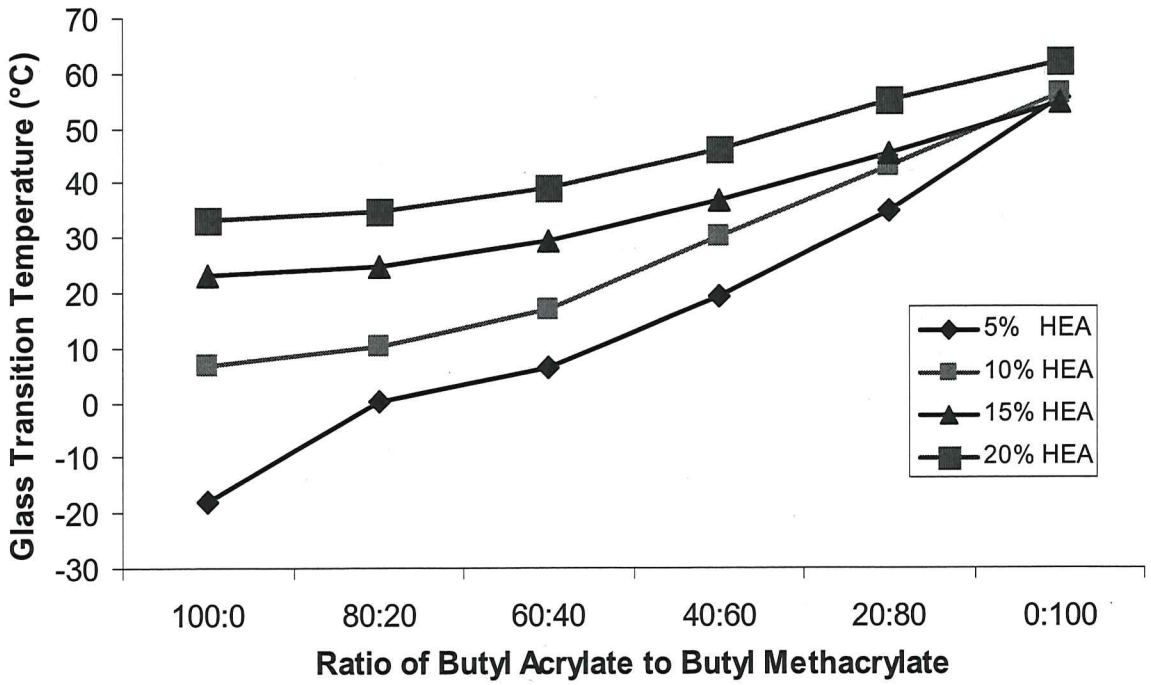

Figure 3.12. pDMTA glass transition temperatures of the first siloxane acrylic-polyurethane coatings library.

Figure 3.13 illustrates the parallel DMTA results showing the T_gs of the second siloxane acrylic-polyurethane coatings library. The experimental coatings follow a trend were the T_gs of the experimental coatings increases systematically

with increasing the amount of BMA and HEA in the coatings similar to the first coatings library in Figure 3.12. The largest effect comes from the amount of the crosslinking monomer, HEA, resulting in higher crosslink densities for the experimental coatings and thus, higher T_gs.

Pseudobarnacle adhesion is a measure of the adhesion strength for an epoxy attached to the surface of the coating. Pseudobarnacle adhesion results for the first siloxane acrylic-polyurethane coatings are illustrated in Figure 3.14. The force at release for the experimental coatings shows that for many of the coatings the release force was very low in comparison to the silicone control (20N).

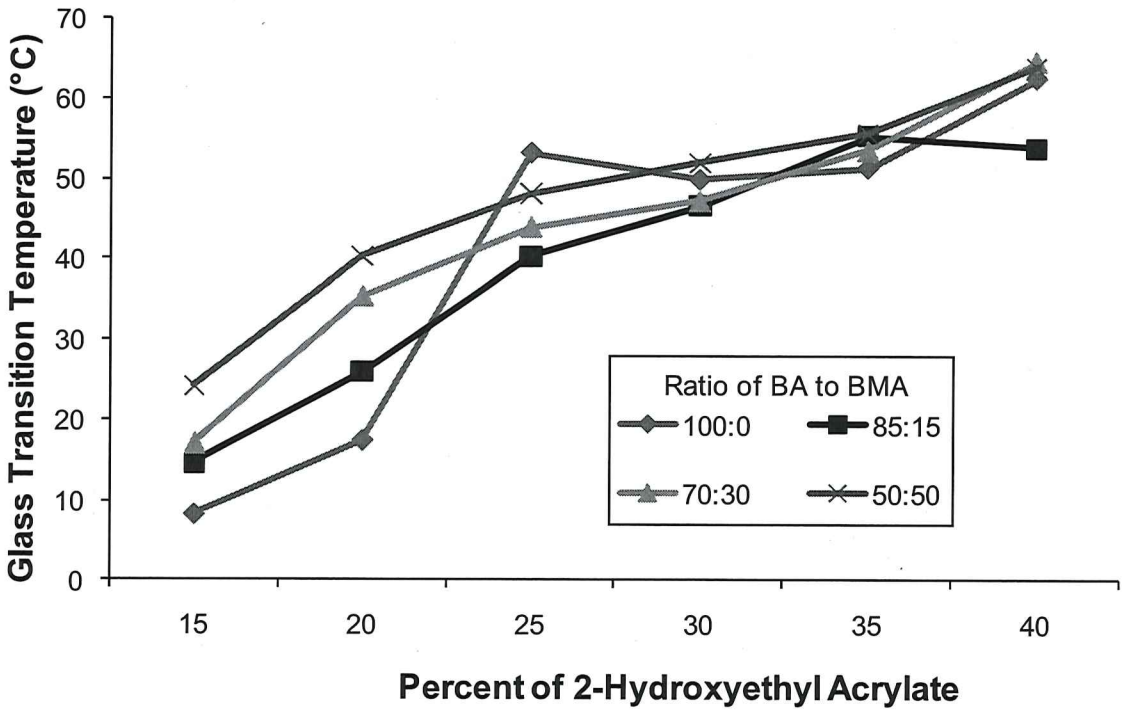

Figure 3.13. pDMTA glass transition temperatures of the second siloxane acrylic-polyurethane coatings library.

A general observation was the force at release was lowest for the experimental coatings consisting of HEA at 15% and 20%, with force values ranging from 8N to 12N. The coatings consisting of 5% HEA start out with lower force at release values until the composition of BA:BMA reaches 40:60, at this point the force at release increases dramatically to a value of 45N and continues to increase slightly at the final composition of 0:100 (BA:BMA). The increase in adhesion may be due to coatings surface behaving more PU-like, although the SE results would not indicate this phenomenon. Similar results were obtained with the coatings comprised of the 10% HEA, but the increase was not as drastic as the 5% HEA experimental coatings with a value of 30N.

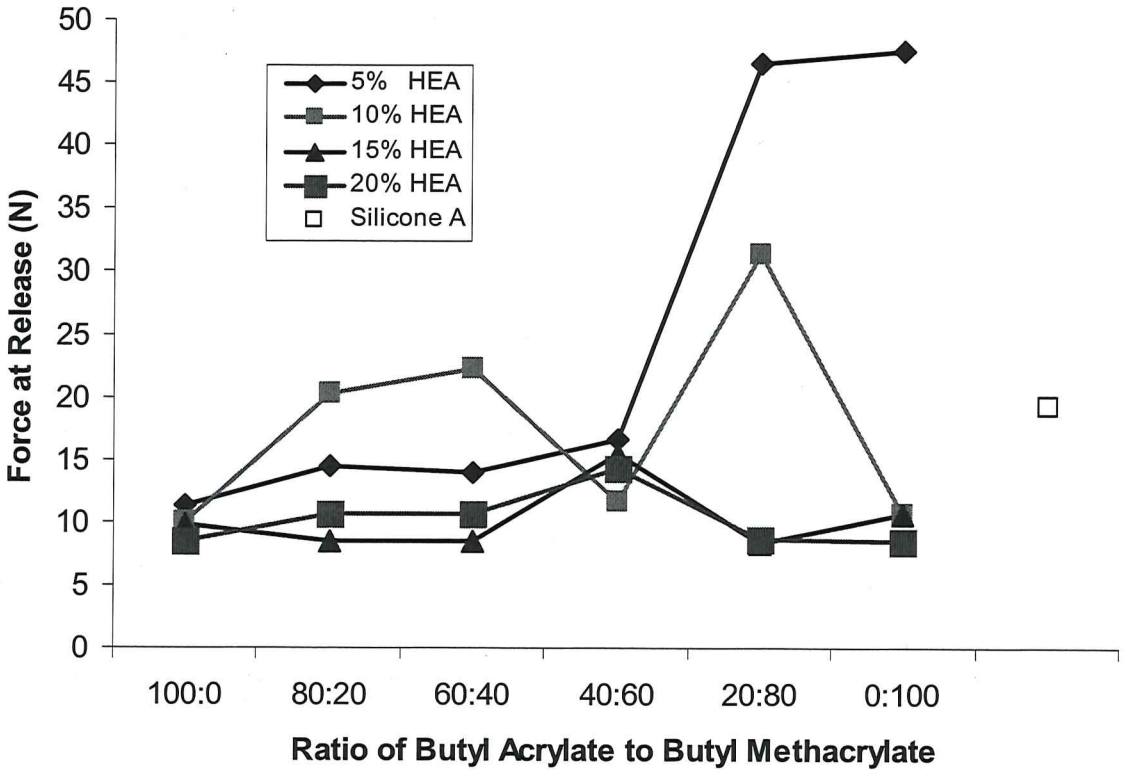

Figure 3.14. Pseudo barnacle pull-off adhesion of first siloxane acrylic-polyurethane coatings library. Standard silicone A is shown.

However, at 0:100 (BABMA) the force decreased to 10N, similarly the SE results would not indicate that the surface is behaving like PU, so it may be due to a structure-property relationship were the increase in BMA causes the bulk of the coating to have more of an effect on the overall adhesion.

PB results for the second library of siloxane-acrylic-polyurethane coatings are illustrated in Figure 3.15. The data shows that for all of the coatings, the release force is very low, lower than that of the control Silicone A. Comparing the overlapping compositional (15% and 20% HEA, 100:0 (BA:BMA)) force at release results from the first and second experimental libraries show similar trends, which demonstrates good reproducibility by the two siloxane acrylic-polyurethane studies.

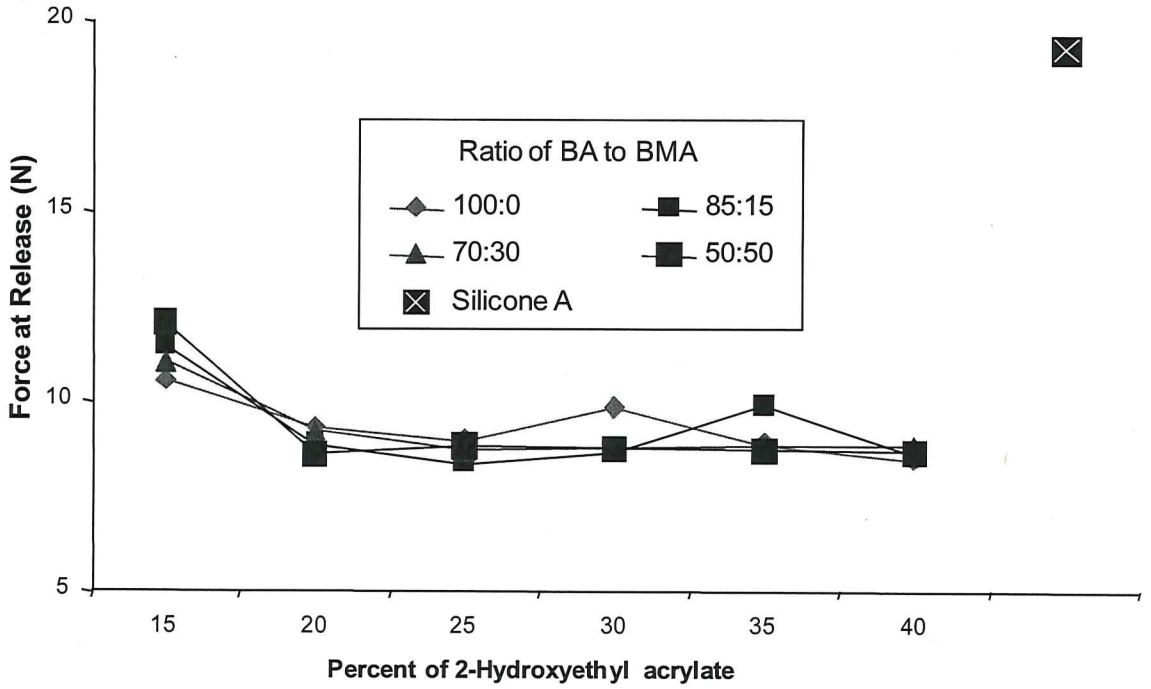

Figure 3.15. Pseudo barnacle pull-off adhesion of second siloxane acrylic-polyurethane coatings library. Standard silicone A is shown.

Overall, the second library of experimental coatings show to have good release properties and performed better than the first experimental library, as well as, the silicone control.

AFM characterization was done using tapping mode over a 10 x 10 μm area on the second library of the siloxane-polyurethane coating surfaces. The only variable that was changed in the formulation of the siloxane-polyurethane coatings was the acrylic polyol composition, the amount of PDMS, isocyanate, catalyst, and solvents were kept constant throughout the library. The AFM results of the second library siloxane-polyurethane coatings are listed in Table 3.3 and shown in Figure 3.16. As the amount of HEA in the acrylic polyol increases, the surface topography becomes more complex, with the formation of dimples or depressions of increasing size.

All coatings made from the acrylic polyols with 15% HEA generated smooth or lamellae surfaces. As illustrated in Figure 3.16, the surface phase separation began with the incorporation of 20% HEA into the acrylic polyol. Surface feature size ranged from 10 nm to 200 nm. It was observed in row A (100:0, BA:BMA) that with the increase in HEA there was an increase in the domain size from 10 nm to 200 nm. However, an interesting trend observed was with the increase in BMA content the domains didn't show up until the 25% HEA compositions, and similar to row A, the increase in HEA showed an increase in the domain size. Row D (50:50, BA:BMA) showed the smallest domains overall with sizes ranging from 25-50 nm; at 35% and 40% HEA there was dimple formation.

Table 3.3. AFM analysis of second library of the siloxane-polyurethane coating surfaces

Coating Position	Surface Appearance	Feature Size (nm)
A1	smooth	--
A2	small dimples	30
A3	small dimples	10
A4	small dimples	40
A5	large dimples	75
A6	large dimples	200
B1	lamellae	--
B2	mix	20 domain, 5 dimples
B3	dimples	35
B4	dimples	70
B5	dimples (lamellae inside dimples)	150
B6	dimples	150
C1	lamellae	--
C2	lamellae	--
C3	dimples	25
C4	dimples	40
C5	dimples	100
C6	dimples (lamellae inside dimples)	80
D1	lamellae	--
D2	lamellae	--
D3	mix	25
D4	dimples	20
D5	dimples	50
D6	dimples	70

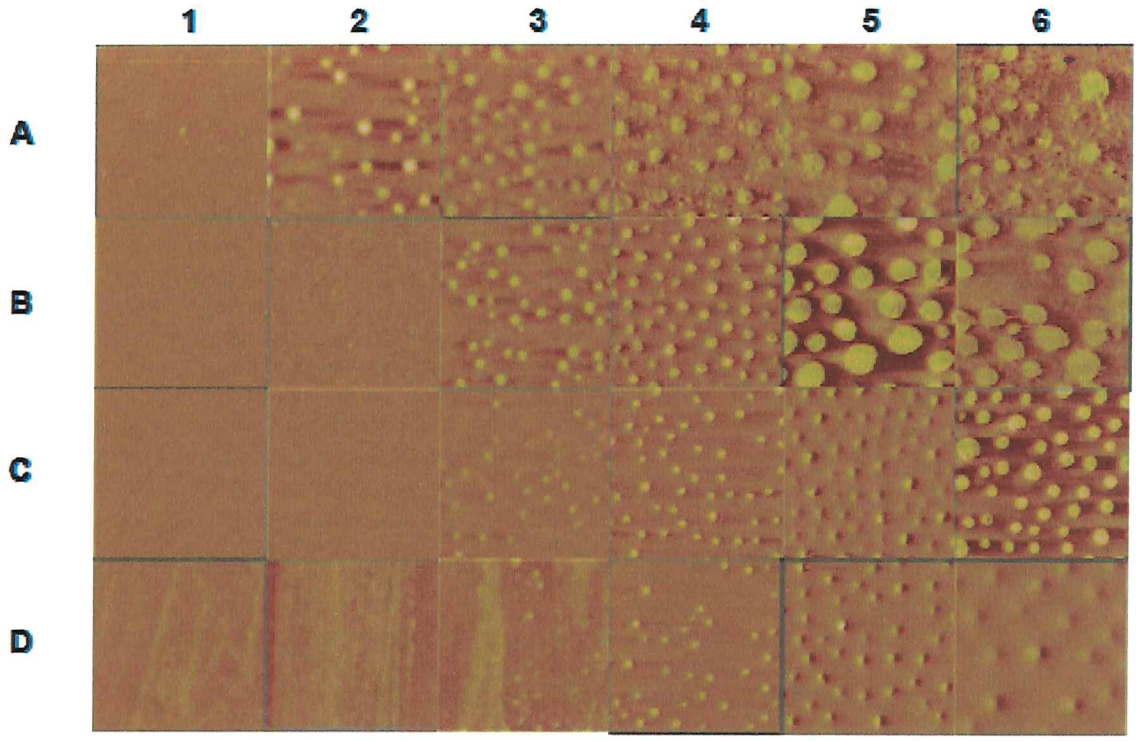

Figure 3.16. AFM phase images of second library of the siloxane-polyurethane coating surfaces. Scan size is 10 x 10 μm.

The observed domains from the second siloxane acrylic-polyurethane coatings library could also explain the SE results illustrated in Figure 3.12 with the increase in surface roughness, however, with an increase in surface roughness an increase in SE would be expected instead of a decrease shown in the experimental coatings SE results.

For biofouling assays, the siloxane-acrylic-polyurethane library array was coated onto 4" X 8" panels coated with an epoxy primer, illustrated in Figure 3.17. To provide space for standard samples on each panel, a full library set required three panels, the first column of each panel were the standard patches, consisting of two patches of Silicone A and two patches of Silicone B for a total of four standard patches per panel.

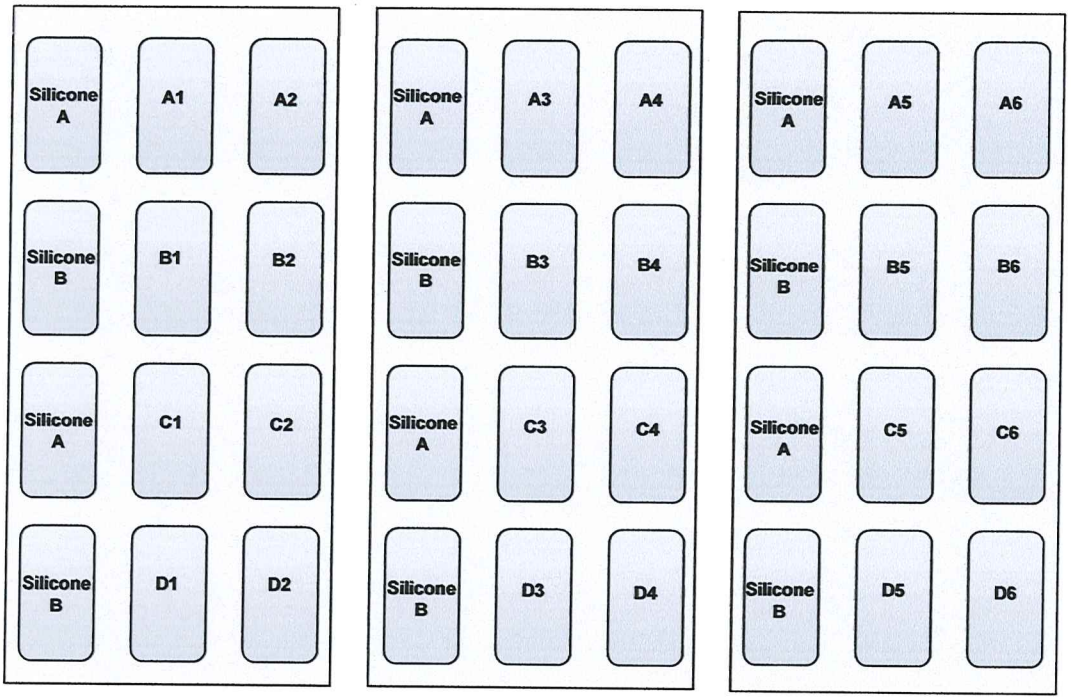

Figure 3.17. Panel layout of silicone controls and experimental coatings for biofouling experiments.

Figure 3.18 shows that a brown biofilm of *Navicula incerta* had grown evenly and uniformly over the entire surface of the experimental array panels before the water jet washing at a pressure of 34 kPa. After the water jet washing a general observation is seen where several of the experimental coatings show visible biofilm removal from the coatings surface where the water jet moved down the panel. Percent removal of *Navicula incerta* at 34 kPa provided the most discrimination and is plotted as a function of the composition of the coatings in Figure 3.19. When compared to standard silicones, Silicone A and Silicone B, many of the formulations were shown to have release properties better or comparable to the standard silicones through and including 40:60 (BA:BMA) at all levels of HEA. The removal increased as the ratio of BA to BMA increased

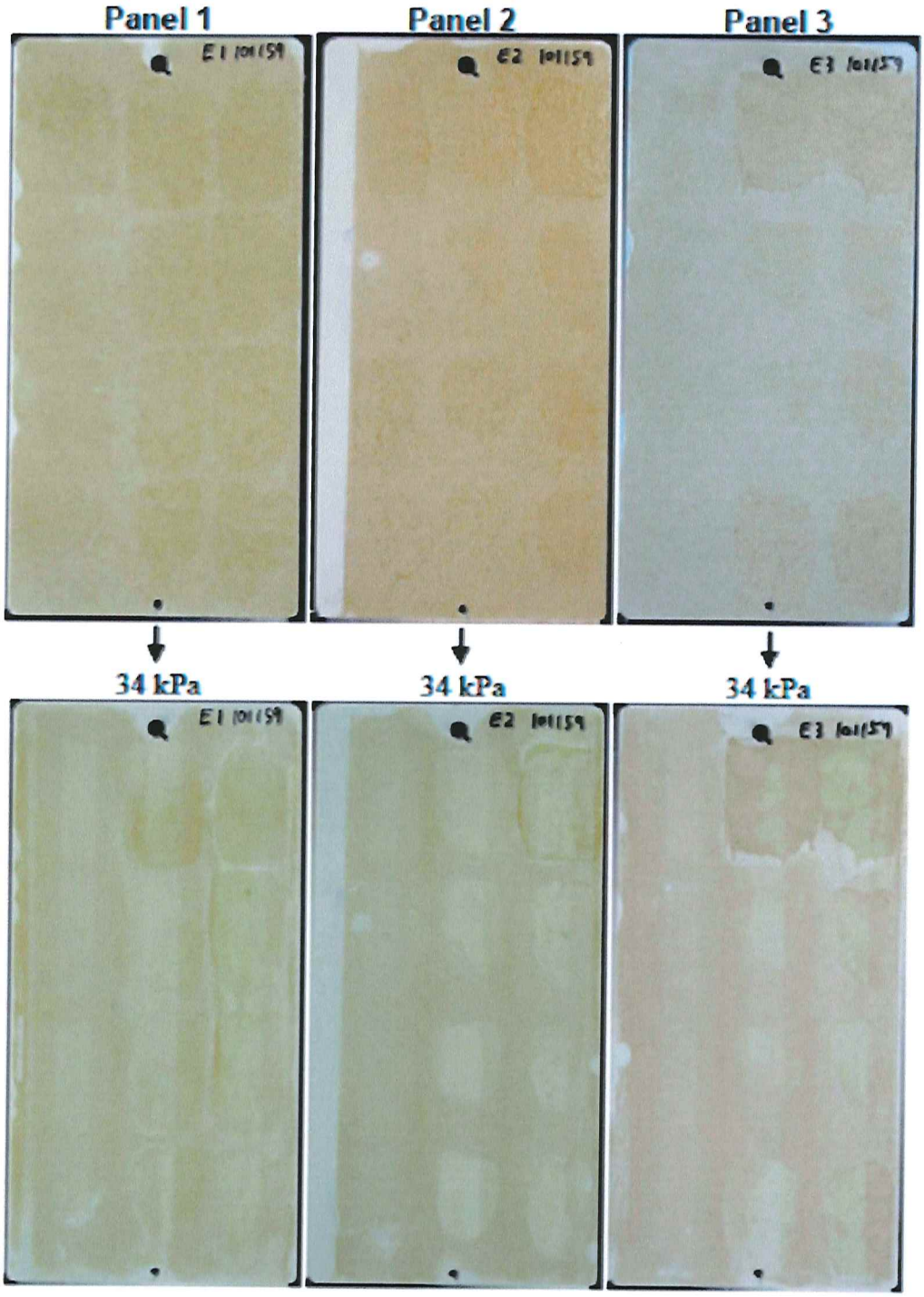

Figure 3.18. *N. incerta* assay panels 1, 2, and 3 from first experimental coatings library before and after being sprayed at 34 kPa impact pressure with a water jet.

regardless of the amount of 2-hydroxyethyl acrylate to a ratio of 60:40 BA:BMA, at which point the percent removal deceases.

The formulation that performed the best was 60:40 BA:BMA with 20% HEA, which had 50% removal. Studies have shown that *Navicula* tend to adhere strongly to silicone based coatings and are readily removed from more polar surfaces such as polyurethane,[23] which is evident from the data for the standard silicones shown in Figure 3.19. An interesting observation was seen when comparing the MICA and SE for the experimental coatings with the *N. incerta* removal results. The coatings that show similar values to PDMS have the highest removal, which is not expected due to previous studies that show *N. incerta* attaches strongly to PDMS-type coatings.[23]

Overall, the results of the removal at 34 kPa from the first siloxane acrylic-polyurethane coatings are encouraging since many of these coatings have better release than the silicone standards.

Percent removal of *N. incerta* at a water jet pressure is 69 kPa for ten seconds for the second library of experimental siloxane acrylic-polyurethane coatings were plotted in Figure 3.20. The water jet results for the second library of the siloxane-polyurethane coatings show better removal than the silicone control for most of the coatings. As mentioned above, *N.* incerta shows good removal from polyurethanes, but adheres strongly to silicone containing surfaces, which is evident in Figure 3.19, with the control polyurethane having the highest removal in comparison to the removal of the silicone A control.

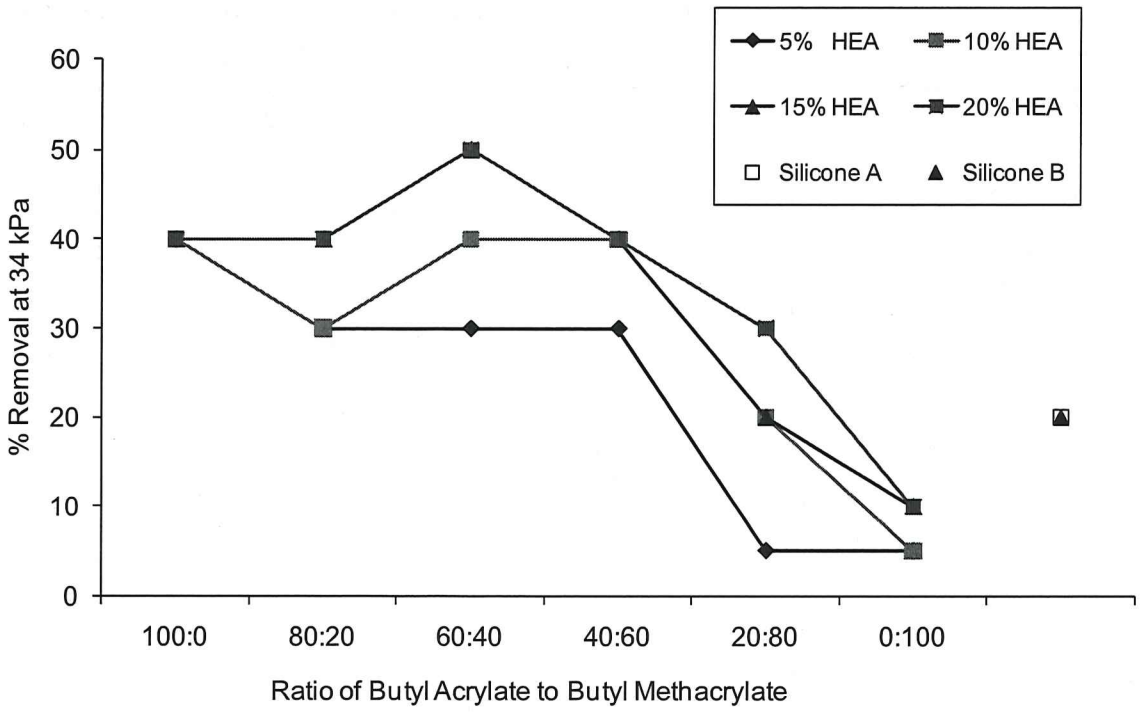

Figure 3.19. Percent *Navicula* biofilm removal from first experimental coatings library at 34 kPa.

A general trend observed in Figure 3.20, was the increase in removal with the increase in the percent HEA until 35% HEA, at this point there was a slight decrease in removal for the experimental coatings comprised of 100:0 and 70:30 (BA:BMA) and a larger decrease for the coatings composition of 85:15 and 50:50 (BA:BMA). This seems to correlate with the SE results from Figure 3.12, where there was a decrease in SE for the 35% and 40% HEA experimental coatings and also the AFM results that showed larger microdomains with the larger percentages of HEA. The increase in surface roughness and the low SE values could likely lead to higher adhesion for the PDMS-like surfaces of the experimental coatings.

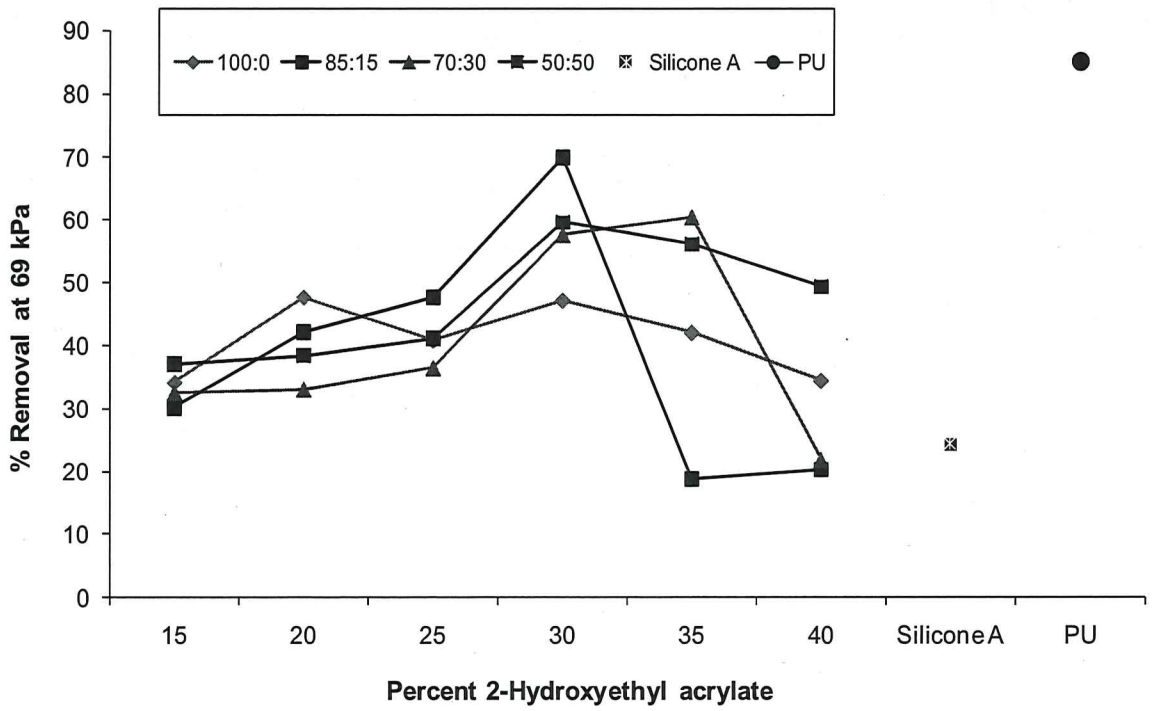

Figure 3.20. Removal of *Navicula incerta* by 69 kPa water jet pressure for the second experimental coatings library including silicone A control, and polyurethane control. The legend illustrates the ratio of BA:BMA for the experimental coatings.

The fouling-release study using *Ulva* sporelings (young plants) used the same coatings deposition array scheme that was used for the *Navicula* assay, illustrated in Figure 3.21. For the *Ulva* assay, the siloxane-acrylic-polyurethane library array was coated onto 4" X 8" panels coated with an epoxy primer. Standard Silicone A and B were used as controls. Figure 3.21 depicts that young plants of *Ulva* covered the whole panel before water jetting. Some areas were denser due to higher settlement of spores on those areas. The removal of *Ulva* sporelings from the coatings at 93 kPa water jet was non-uniform, and on some coatings, areas of coatings devoid of algae are clearly visible. The results from

the different water jet impact pressures indicate a trend in the fouling-release properties of the coatings as a function of composition.

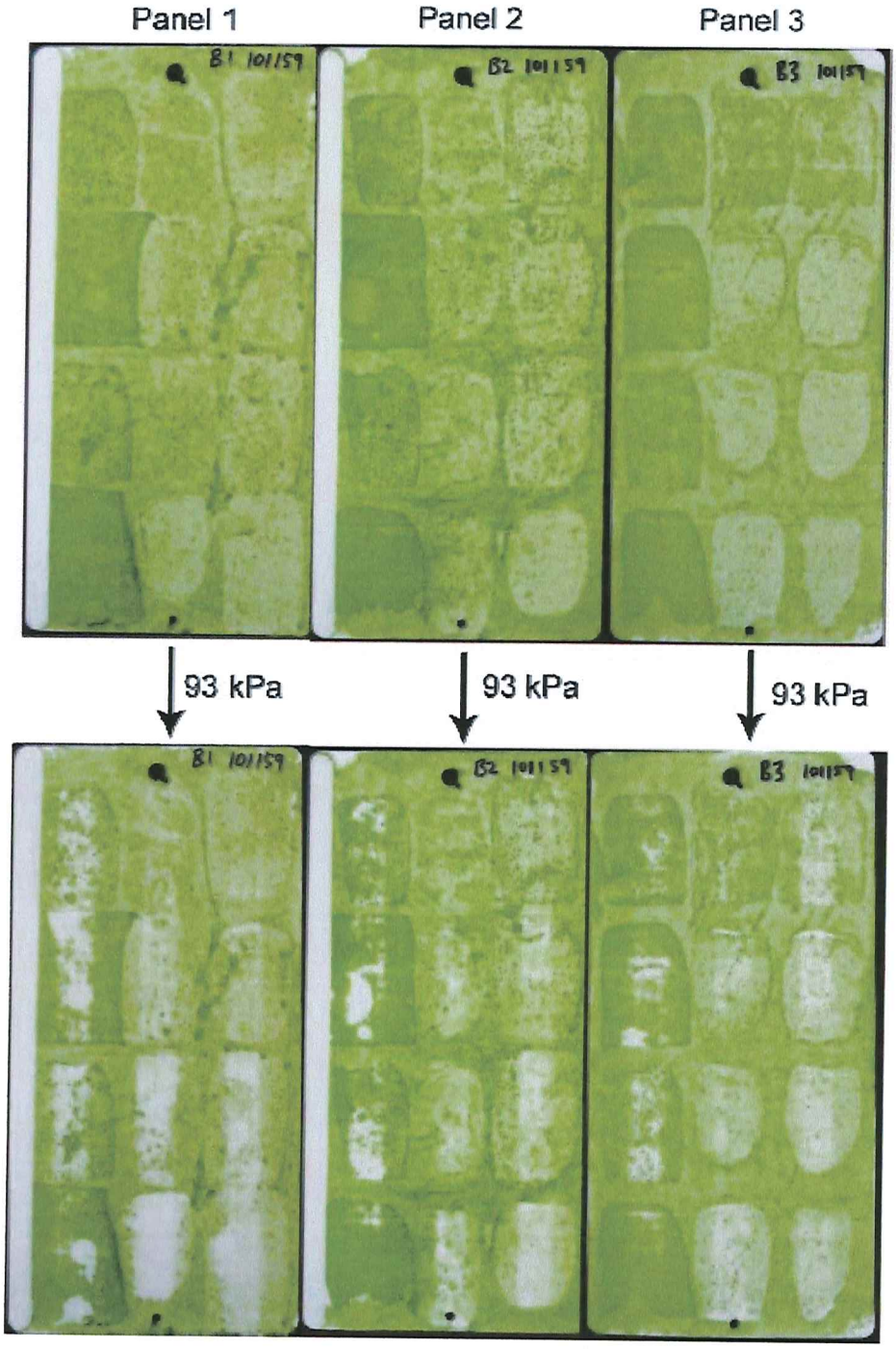

Figure 3.21. *Ulva* assay panels from first experimental coatings shown before and after being water jetted at 93 kPa.

Figure 3.22 illustrates that the removal of the *Ulva* biomass at an impact pressure of 93 kPa. The percent removal of the biomass decreases as the ratio of BA decreases and BMA increases. There is also an influence of biomass removal with regards to the percentage of HEA in the composition, which shows that as the amount of HEA in the bulk of the polyurethane increases, the greater the percent biomass removal. The formulation that performed the best had a composition of 100:0 BA:BMA and 20% HEA. Studies of the release behavior of silicone elastomer fouling-release coatings have indicated that release of fouling organisms is better for lower modulus coatings.[19-21] For the siloxane-acrylic-polyurethane system, as the ratio of BA:BMA increases, the T_g of the coating decreases (and, hence, the modulus) and the removal of *Ulva* sporelings increases, consistent with these prior observations. However, in these siloxane-acrylic-polyurethane coatings, an increase in the release of *Ulva* sporelings is seen with the increase in the HEA content of the acrylic polyols. As the HEA content increases, the coating T_g and modulus increases as a result of the higher crosslink density. Thus, these results are in striking contrast to previous findings based on silicone elastomer coatings systems and this effect was explored further with the second experimental coatings library.

The second library of siloxane acrylic-polyurethane coatings were also tested using *Ulva* sporelings. Several of the coatings did not cure properly, thus, some data points are missing.

Removal of the *Ulva* sporelings using the water jet at 132 kPa is shown in Figure 3.23. The coating formulations based on acrylic composition of 85:15,

70:30, and 50:50, butyl acrylate to butyl methacrylate ratio and regardless of percent HEA content, showed removal of the biomass similar to the silicone controls, with values under 20% removal.

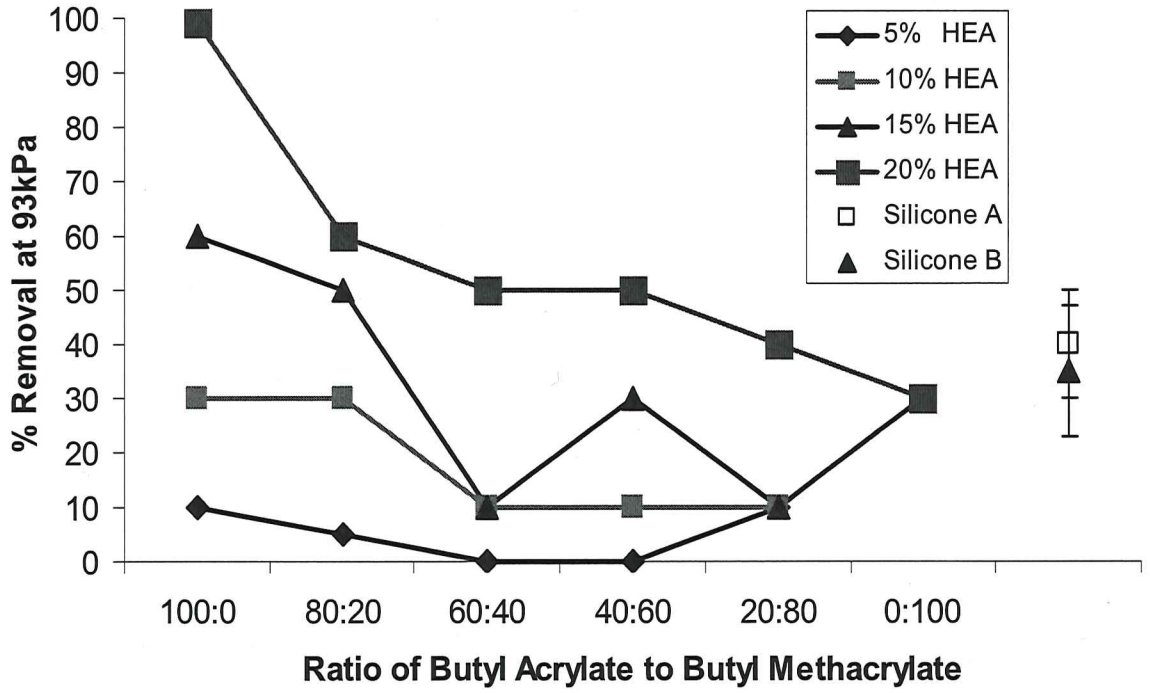

Figure 3.22. Percent removal of *Ulva* sporelings from first library of experimental coatings, and silicone controls at 93 kPa.

However, the coating based on the acrylic composed of 100% butyl acrylate had significantly higher removal, with the highest removal near 90 %, an amount of removal notably higher than the silicone controls. This high biomass percent removal is consistent with our earlier observations depicted in Figure 3.22 of experimental coatings with similar composition.

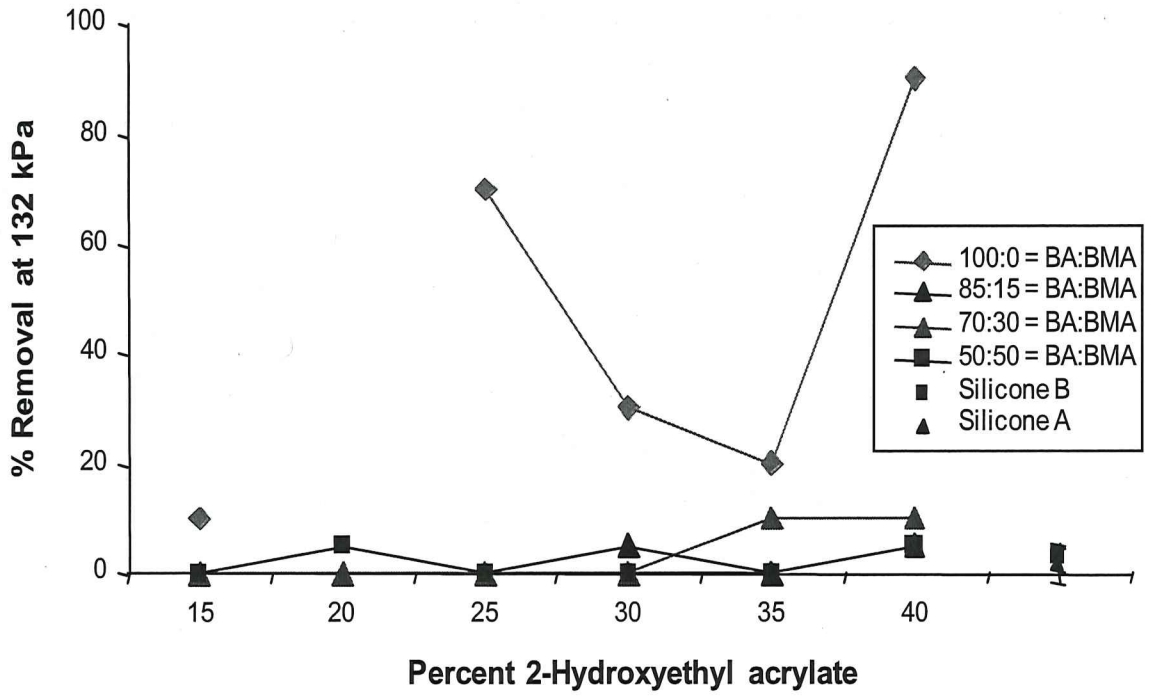

Figure 3.23. Percent removal of *Ulva* sporelings for second library of experimental coatings and silicone A and B controls at 132 kPa.

It should be noted that based on the previous performance properties results from the second siloxane acrylic-polyurethane library the remaining bioassays were only performed on the second experimental coatings library and not on the first siloxane acrylic-polyurethane library.

In the barnacle reattachment assay, adult barnacles were pushed off of silicone elastomer coatings and reattached to siloxane-acrylic-polyurethane coatings for two weeks. The reattached barnacles were then pushed off in shear with a digital force gauge to measure adhesion strength (MPa). The reattached barnacle adhesion strength is illustrated in Figure 3.24. The graph depicts a trend where barnacle adhesion increases with the increase in the siloxane-polyurethane coatings glass transition temperature.

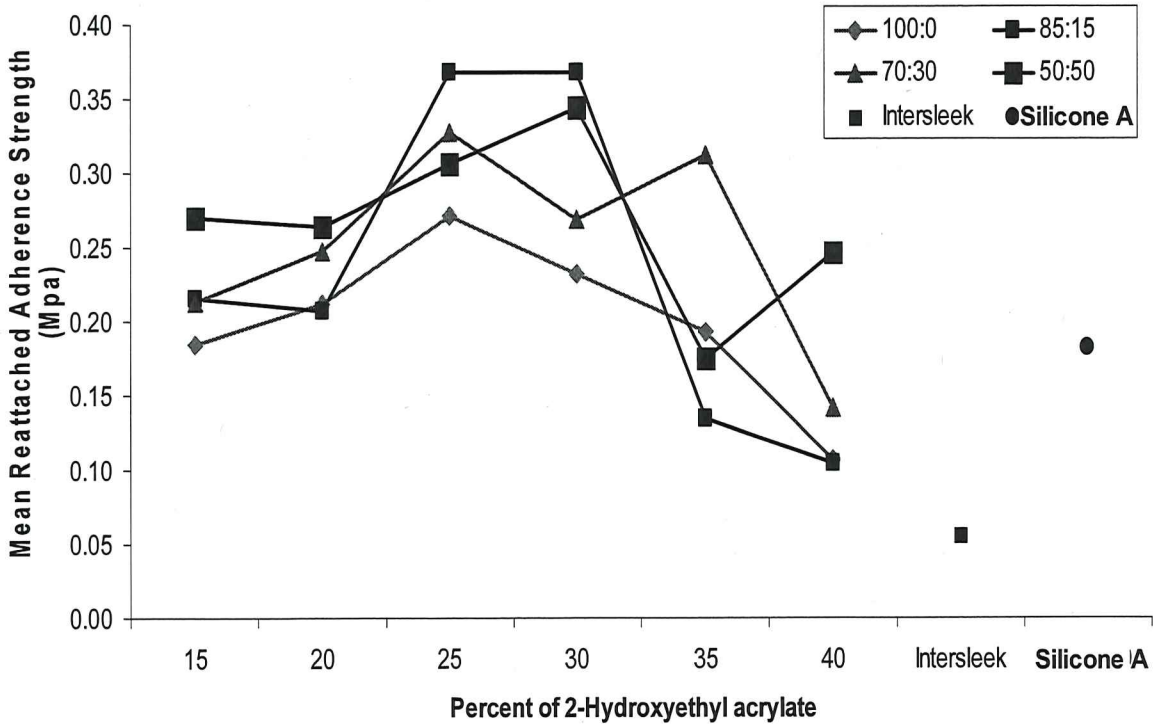

Figure 3.24. Barnacle reattachment strength for second library of experimental coatings, silicone A, and commercial fouling-release coating (Intersleek). The legend illustrates the ratio of BA:BMA for the experimental coatings.

These results are consistent with one of the properties needed for formulating fouling-release coatings (low T_g coating). However, it is evident in Figure 3.24 that the adhesion then decreases as the second library of siloxane acrylic-polyurethane coatings modulus increases, which is not expected since one of the properties for formulating a successful fouling-release coating is that the coating has a low modulus. The commercial coating, Intersleek, performed better than the experimental coatings, however, several coatings performed as well or better than the silicon standard, and were close to the adhesion of Intersleek.

Leachate toxicity was assessed by evaluating *C. lytica* growth after 24 hours via a crystal violet colorimetric assay of each experimental coating. Growth in experimental coating leachates was reported as an absorbance ratio (600 nm) to a growth control and the results are illustrated in Figure 3.25. As depicted in the *C. lytica* leachate toxicity results for the experimental coatings there was no significant leachate toxicity observed for any of the coatings.

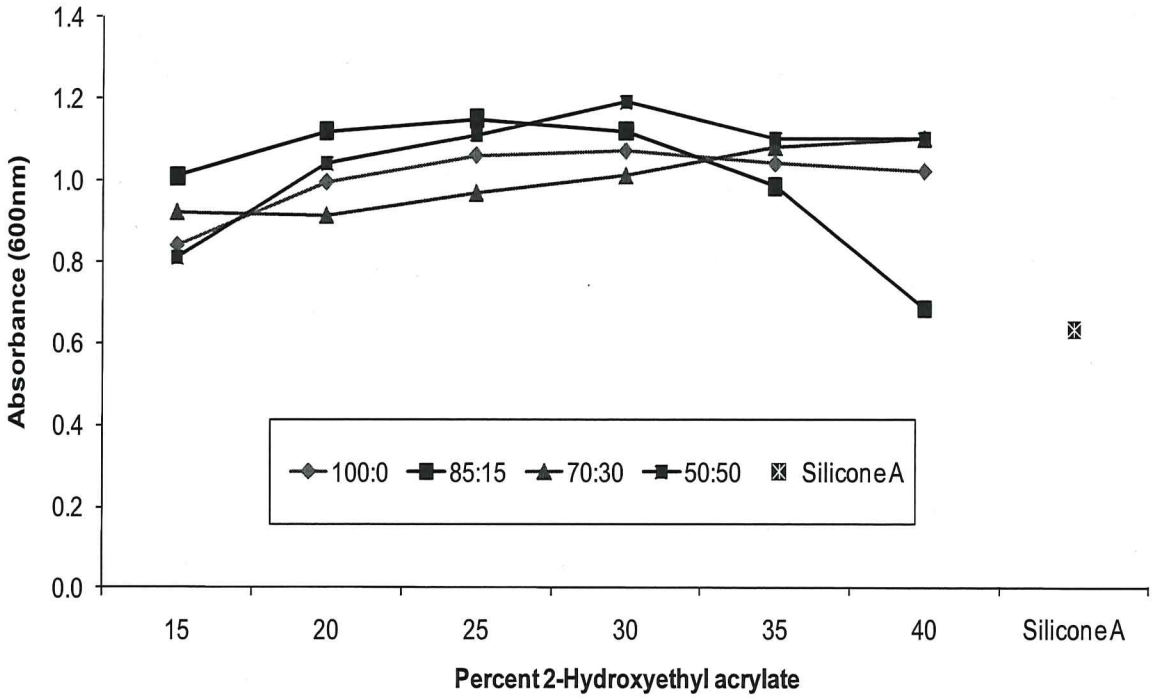

Figure 3.25. *C. lytica* leachate toxicity on second library of experimental coatings and standard silicone A. The legend illustrates the ratio of BA:BMA for the experimental coatings.

C. lytica biofilm retention analysis was assessed by a crystal violet colorimetric assay and the results are illustrated in Figure 3.26. For the assay a 5% suspension of *C. lytica* in artificial sea water was prepared and 1ml was added to each well of the experimental coating plates. The plates were then incubated statically at 28°C for 18 hours to facilitate bacterial attachment and colonization.

Plates were rinsed three times with DI water and stained with crystal violet. Images were taken after staining and then the crystal violet was extracted in 33% acetic acid and the resulting eluates were measured for absorbance at 600nm.

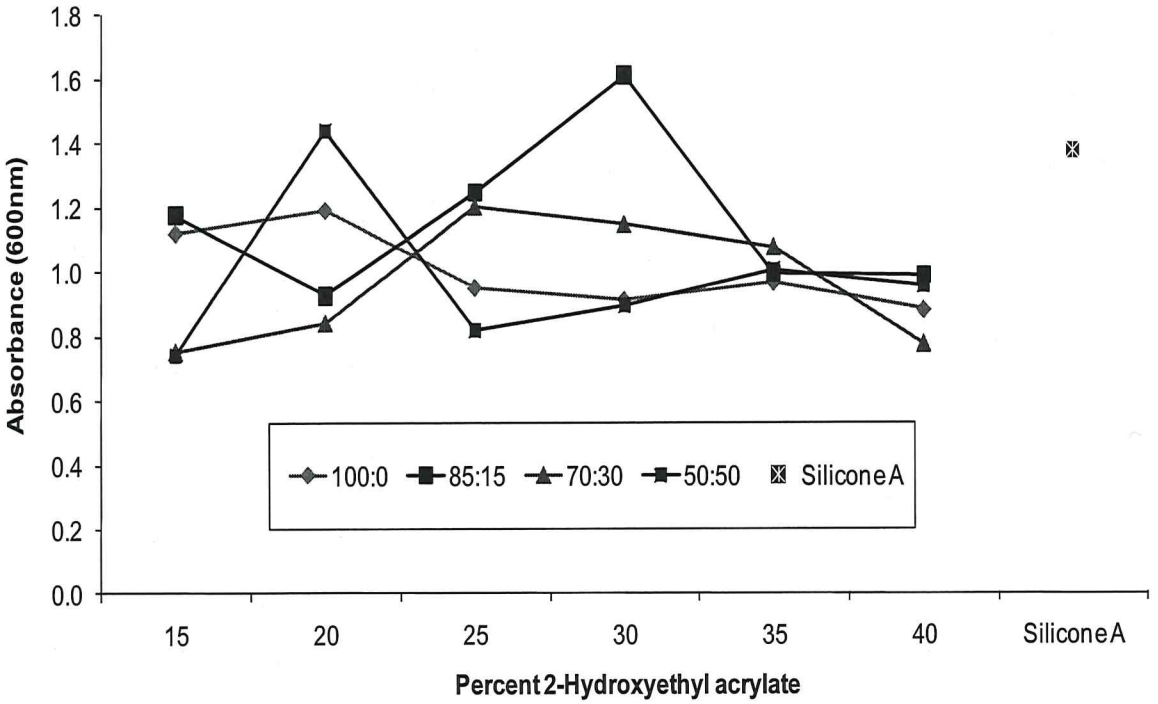

Figure 3.26. *C. lytica* biofilm growth and retention on second library of experimental coatings and silicone A. The legend illustrates the ratio of BA:BMA for the experimental coatings.

Biofilm retention was reported as the mean absorbance value of three replicate samples. The results show that there was no significant difference in biofilm retention for most of the experimental coatings. In terms of the fouling process this is significant because it shows that the bacteria actually avoids, or deters settlement on the surface of the experimental coatings, for microfoulers that require bacteria cues this may stall or even stop the microfouling stage of the process and thus impeding continuation of the biofouling process on the

experimental coatings surface. Experimental coatings composed of 20% HEA and 50:50 (BA:BMA) and 30% HEA and 85:15 (BA:BMA) showed the largest amount of biofilm retention. Overall, the majority of the experimental coatings showed lower biofilm retention than the silicone control.

The *C. lytica* bacterial biofilm percent surface coverage from the biofilm retraction assay is depicted in Figure 3.27. Biofilm retraction was assessed by determining percent coverage calculations from digital images taken of each coating plate using an automated software tool. Biofilm retraction was reported as the mean percent coverage value of three replicate samples. The biofilm retraction assay is an important study because it illustrates which experimental coatings surfaces the biofilm wets or spreads over, or which surfaces the biofilm has difficulty wetting (spreading across the surface). Indicated in Figure 3.27 the experimental coatings based on acrylics containing both butyl acrylate and butyl methacrylate show similar trends were the percent surface coverage is very low at the lower T_g coatings and begins to increase as modulus increases. At 15% HEA for the experimental coatings with BA and BMA the percent coverage ranged from 8-10%, as the HEA amount was increased to 20%, similar coatings continued to have low coverage ranging from 15-50%. At 30% HEA, both the experimental coatings with 85:15 and 70:30 (BA:BMA) had surface coverage of 100%, but as the HEA amount was increased to 35% and 40% there was a significant decrease again ranging from 5-10%. This general trend follows one of the key properties for fouling-release coatings were low modulus coatings perform better and the experimental coatings biofilm retraction correlates well with this observation.

However, the highest T_g and modulus coatings show low surface coverage again, which would suggest that perhaps the microdomains on the surface of the experimental coatings contribute to the low surface coverage.

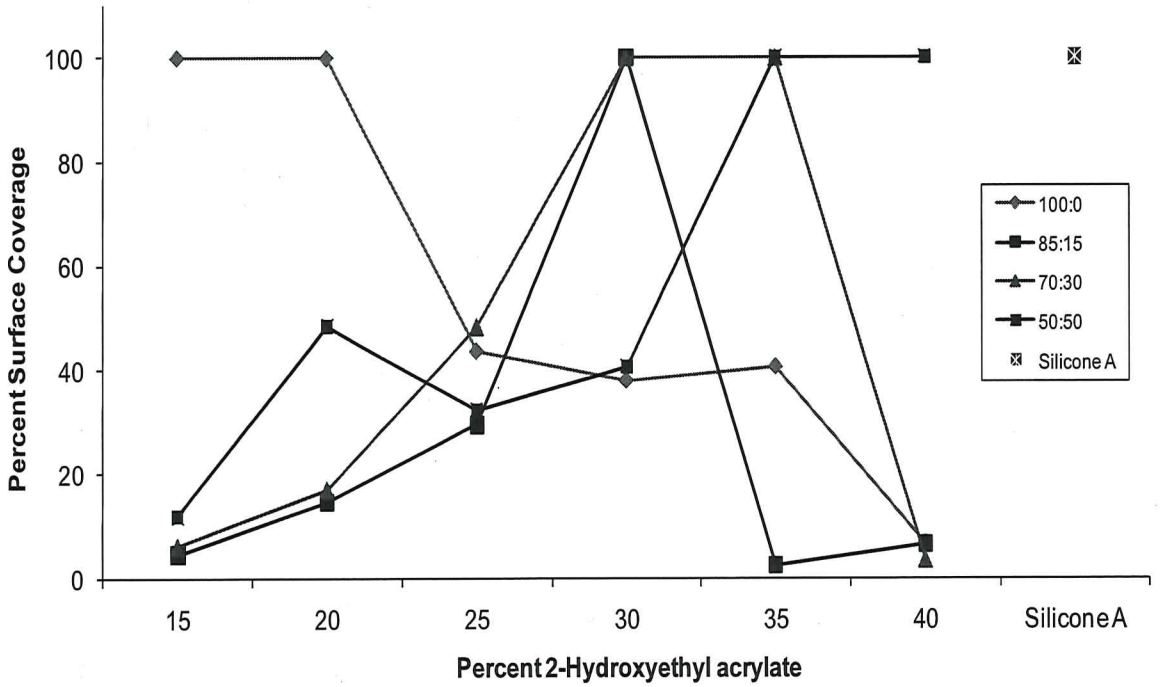

Figure 3.27. *C. lytica* percent surface coverage from biofilm retraction on second library of experimental coatings and silicone A. The legend illustrates the ratio of BA:BMA for the experimental coatings.

For the coatings based solely on butyl acrylate, surface coverage decreases systematically as the T_g and modulus increases. Overall, the majority of the experimental coatings showed lower percent surface coverage then the silicone control, which had complete bacterial biofilm surface coverage.

Settled *C. lytica* biofilms were subjected to water jet to determine the adhesion strength. Water jet pressure was 200 kPa for five seconds. Water jet data for *C. lytica* is depicted in Figure 3.28. The water jet results show that all of the siloxane acrylic-polyurethane coatings performed as well or had better removal

than the silicone control coatings, with some of the experimental coatings comparing to the biofilm removal from the polyurethane control. The percent removal ranged from 60% to almost 90% removal, while the silicone standards had a range of removal from 60% to about 65%.

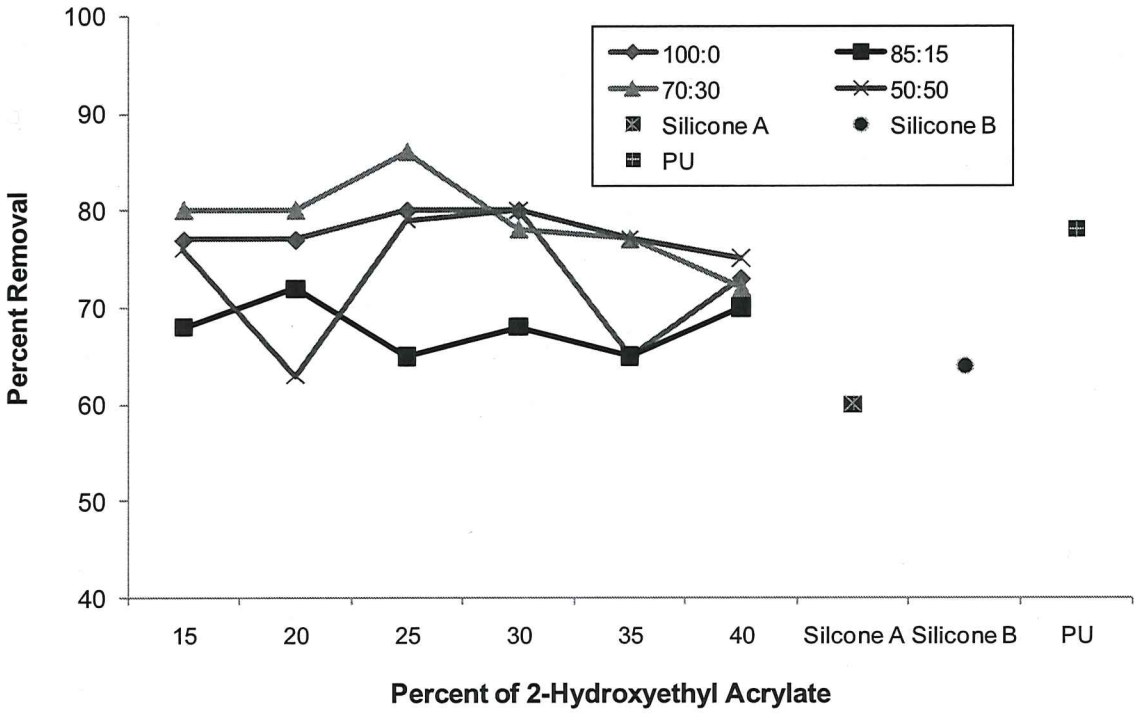

Figure 3.28. Removal of *C. lytica* biofilm by water jet (200 kPa) for second library of experimental coatings, silicone controls, and polyurethane control. The legend illustrates the ratio of BA:BMA for the experimental coatings.

A general trend observed from the percent removal results for the experimental coatings was the slight decrease in percent removal with the increase in HEA content, which correlates with the increase in the experimental coatings modulus seen in prior bioassays. Overall, the experimental coatings performed, on average, better than the silicone standards and several

experimental coatings had removal percentages comparable to the polyurethane control.

H. pacifica biofilms were grown on the surface of the coatings and then subjected to a water jet to determine their adhesion strength. Water jet pressure was 172 kPa for five seconds and the results of the assay are illustrated in Figure 3.29. It is known in the scientific community that *H. pacifica* adheres strongly to PDMS and weekly to polyurethanes.[23,25] According to the percent removal data from the study, the experimental coatings performed more polyurethane-like than

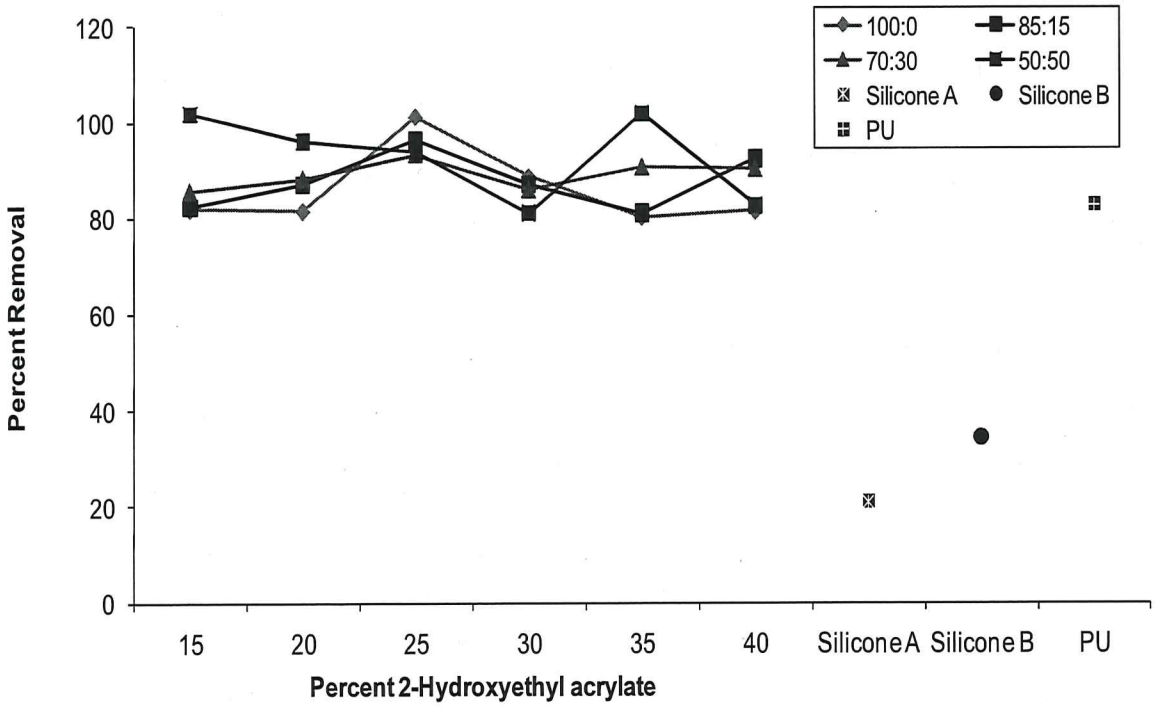

Figure 3.29. Removal of *H. pacifica* biofilms by water jet for experimental coatings, silicone controls, and polyurethane control. The legend illustrates the ratio of BA:BMA for the experimental coatings.

a siloxane-polyurethane due to the excellent biofilm removal which was better than the control polyurethane. However, the SE results would indicate that all coatings

surfaces were PDMS-like rather than PU-like. Overall, the water jet data in Figure 3.29 shows that all siloxane acrylic-polyurethane coatings have good removal and perform better than the silicone standards and comparable to the polyurethane control.

3.4. Conclusions

Two siloxane acrylic-polyurethane coatings studies were formulated and tested for mechanical and physical properties using combinatorial and high-throughput methods. The glass transitions of the acrylic polyol, acrylic-polyurethane and siloxane-acrylic-polyurethane coatings followed similar trends. The T_g data also showed that the bulk properties of the coatings varied independently of the surface properties. The contact angle data showed evidence that the first library of acrylic-polyurethane coatings went from a hydrophilic surface to a hydrophobic surface when the PDMS was incorporated into the polyurethane formulation; the silicone covered the surface of the coating indicated by an increase in water contact angles from 70° to 80° for the polyurethane to 95° to 100° for the experimental coatings. WCA for the second experimental coatings library showed a range from 102° to 111°. After water immersion the majority of the coatings kept their hydrophobic nature. Increasing the BA and the HEA in the acrylic polyol improved the release properties of the coatings for both cells of the diatom *Navicula* and sporelings of the green microalgae *Ulva*. There are many similarities between several of the bioassays when comparing the trends that the siloxane acrylic-polyurethane coatings showed. The trends observed were that adhesion increased with an increase in modulus, and then adhesion decreased at

the highest modulus coatings. Studies of the release behavior of silicone elastomer fouling-release coatings have indicated that release of fouling organisms is better for lower modulus coatings.[18-21] As the HEA content increases, the coating T_g and modulus increases as a result of the higher crosslink density. These results are in contrast to previous findings based on silicone elastomer coatings systems and indicate that the siloxane acrylic-polyurethane system is very different with respect to typical fouling-release and network properties.

3.5. References

1. Callow, M. E.; Callow J. E. *Biologist* **2002**, 49 (1), 4-10.
2. Champ, M. A. The Science of the Total Environment **2000**, 258, 21.
3. Brady, R. F. *Progress in Organic Coatings* **1999**, 35 (1-4), 31-35.
4. Brady, R. F.; Jr., Singer I.L. *Biofouling* **2000**, 15 (1-3), 73-81.
5. Yebra, D. M.; Kiil S.; Dam-Johansen, K. *Progress in Organic Coatings* **2004**, 50 (2), 75-104.
6. Candries, M.; Atlar, M.; Anderson, C. D. Conference Proceedings ENSUS **2000**, 88-95.
7. Majumdar, P.; Ekin, A.; Webster, D. C. ACS Symposium Series **2007**, 957, 61-75.
8. Verkholantsev, V.; Flavian, M. *Progress in Organic Coatings* **1996**, 29 (1-4), 239-246.
9. Vink, P.; Bots, T.L. *Progress in Organic Coatings* **1996**, 28 (3). 173-181.

10. Benjamin, S.; Carr, C.; Walbridge D. J. *Progress in Organic Coatings* **1996**, 28 (3), 197-207.

11. Carr, C.; Wallstoem, E. *Progress in Organic Coatings* **1996**, 28 (3), 161-171.

12. Walbridge, D. J. *Progress in Organic Coatings* **1996**, 28 (3), 155-159.

13. Ekin, A.; Webster, D. C. *Journal of Polymer Science, Part A: Polymer Chemistry* **2006**, 44 (16), 4880-4894.

14. Ekin, A.; Webster, D. C. *J. Combinatorial Chem.* **2007**, 9 (1), 178-188.

15. Ekin, A.; Webster D. C.; Daniels, J.; Stafslien, S. J.; Casse, F.; Callow J. A.; Callow M.E. *J. Coatings Tech. & Res.* **2007**, 4(4), 435-451.

16. Ekin, A.; Webster, D. C. *Macromolecules* **2006**, 39, 8659-8668.

17. Brady R.F. *Progress in Organic Coatings* **2001**, 43 (1-3), 188-192.

18. Chaudhury, M. K.; Finlay, J. A.; Chung, J. Y.; Callow, M. E.; Callow, J. A. *Biofouling* **2005**, 21 (1), 41-48.

19. Kohl, J. G.; Singer, I. L. *Progress in Organic Coatings* **1999**, 36 (1-2), 15-20.

20. Singer, I. L.; Kohl, J. G.; Patterson, M. *Biofouling* **2000**, 16 (2-4), 301-309.

21. Wicks, Z. W.; Jones, F.N.; Pappas, S. P. Organic Coatings: Science and Technology, 2nd Edition. NY: Wiley; **1999**.

22. Cassé, F.; Ribeiro, E.; Ekin, A.; Webster, D. C.; Callow, J. A.; Callow, M. E. *Biofouling* **2007**, 23 (3/4), 179-192.

23. Holland, R.; Dugdale, T. M.; Wetherbee, R.; Brennan, A. B.; Finlay, J. A.; Callow, J. A.; Callow, M. E. *Biofouling* **2004**, 20 (6), 323-329.

24. Cassé, F.; Stafslien, S. J.; Bahr, J. A.; Daniels, J.; Finlay, J. A.; Callow, J. A.; Callow, M. E. *Biofouling* **2007**, 23 (2), 121-130.

25. Stafslien, S. J.; Daniels, J.; Mayo, B,; Christianson, D.; Chisholm, B.; Ekin, A.; Webster, D. C.; Swain, G. *Biofouling* **2007**, 23(1/2), 45-54.

26. Webster, D. C.; Bennett, J.; Kuebler, S.; Kossuth, M.B.; Jonasdottir, S. *J. Coatings Tech. & Res.* **2004**, 1 (6), 34-39.

27. Kossuth, M. B.; Hajduk, D. A.; Freitag, C.; Varni, J. *Macromolecular Rapid Communications* **2004**, 25 (1), 243-248.

28. Owens, D. K.; Wendt, R.C. *Journal of Applied Polymer Science* **1969**, 13 (8), 1741-7.

29. Chisholm, B. J.; Webster, D. C.; Bennett, J. W.; Berry, M.; Christianson D. A.; Kim, J.; Mayo, B.; Gubbins, N. J. *Rev. Sci. Instr.* **2007**, 78, 072213.

30. Willemse, R. X. E.; Staal, B. B. P.; van Herk, A. M.; Pierik, S. C. J.; Klumperman, B. *Macromolecules* **2003**, 36 (26), 9797-9803.

31. Statz, A.; Finlay, J.; Dalsin, J.; Callow, M. E.; Callow, J. A.; Messersmith, P.B. *Biofouling* **2006**, 22, 391-399.

32. Bullock, S.; Johnston, E. E.; Willson, T.; Gatenholm, P.; Wynne, K. J. *Journal of Colloid and Interface Science* **1999**, 210 (1), 18-36.

33. Pike, J. K.; Ho, T.; Wynne, K. J. *Chemistry of Materials* **1996**, 8 (4), 856-60.

34. van Oss, C. J.; Good, R. J.; Busscher, H. J. *J. Disp. Sci. Tech.* **1990**, 11, 75.

35. Vargo, T. G.; Hook, D. J.; Gardella, D. J. Jr.; Eberhardt, M. A.; Meyer, A. E.; Baier, R. E. *J. Polym. Sci., Part A: Polym. Chem.* **1991**, 29, 535-545.

36. Zhao, G.; Bi, S.; Wu, J.; Liu, Z. *J. Chem. Eng. Data* **2010**, Publication Date (Web): March 25, 2010.

CHAPTER 4. NOVEL AMPHIPHILIC ACRYLIC-POLYURETHANE COATINGS FOR UNDERWATER MARINE APPLICATIONS

4.1. Introduction

Underwater structures and ships' hulls in particular have a tendency to rapidly accumulate organisms that may range from microscopic bacteria, algae spores, and eukaryotes such as diatoms to large larvae of invertebrates. Whether these biofoulers adhere strongly to hydrophilic or hydrophobic polymer surfaces has become a relevant question in the area of antifouling and fouling-release surfaces. It is a challenging task to produce marine coatings without resorting to toxic biocides which have been shown to have adverse affects on marine ecosystems by leaching certain metals that bioaccumulate.[1] Hence, a more environmentally friendly approach is to use nontoxic coatings that can resist biofouling or minimize the adhesion strength of the biofoulers that settle on the marine surfaces.[2-3] Studies have shown that marine organisms attach to surfaces by a primary mechanism that involves wetting of the surface by the secretion of protein or glycoprotein adhesives,[4-8] followed by crosslinking corresponding to an increase in adhesion strength. Wetting of the surface is controlled by molecular interactions of the adhesive matrix with the surface, quantified by surface energy.[9-10] In general, low-energy surfaces are difficult to wet.[9] Several studies have used low surface energy poly(dimethyl siloxane) (PDMS) elastomers in fouling-release marine coatings, where fouling organisms adhere weakly and under suitable hydrodynamic conditions or by water jet cleaning "release" from the coating.[11-14] However, due to the amphiphilic nature of the adhesives produced by biofoulers, these types of coatings are not always effective in preventing adsorption of marine

organism. While some species, such as *Ulva*, are easily removed from hydrophobic surfaces,[15-16] others, such as diatoms show strong adhesion to hydrophobic surfaces.[17-18] Thus, it appears that a single substrate chemistry cannot be utilized single-handedly in designing multipurpose marine coatings for all forms of biofouling, including *Ulva* and diatoms.[19] To end this, several research groups designed amphiphilic coatings comprising of poly(ethylene glycol) (PEG) and a hydrophobic moiety such as PDMS or fluorinated chemistries in order to minimize adhesion of numerous marine organisms. These amphiphilic polymer coatings were designed to prevent biofouling by providing a surface with a compositional,[20-22] topological,[23-25] and morphological complexity,[10, 15, 26-28] which either reduces settlement of the motile spores or larvae or makes energetically unfavorable the hydrophobic or the hydrophilic interactions between the organisms' adhesives and the coating substrate.

We are interested in the design of new marine coatings systems composed of crosslinked polyurethane modified with an amphiphilic PDMS/ poly(ethylene glycol) (PEG) based triblock copolymer to provide coatings having low surface energy, durability, hydrolytic stability, and amphiphilic compositional complexities to discourage favorable interactions with particular marine organism adhesives.

Figure 4.1 shows the general chemical structures of the amphiphilic triblock copolymers synthesized via Michael Addition reactions. In general, the PEG functionalized methacrylate reacts with an amine terminated siloxane via nucleophilic addition at the primary amine site of the siloxane and the unsaturated carbonyl of the methacrylate. Thus, the resulting triblock copolymer contains a

secondary amine linker between each block; used as a crosslinking site when formulated into the polyurethane coatings.

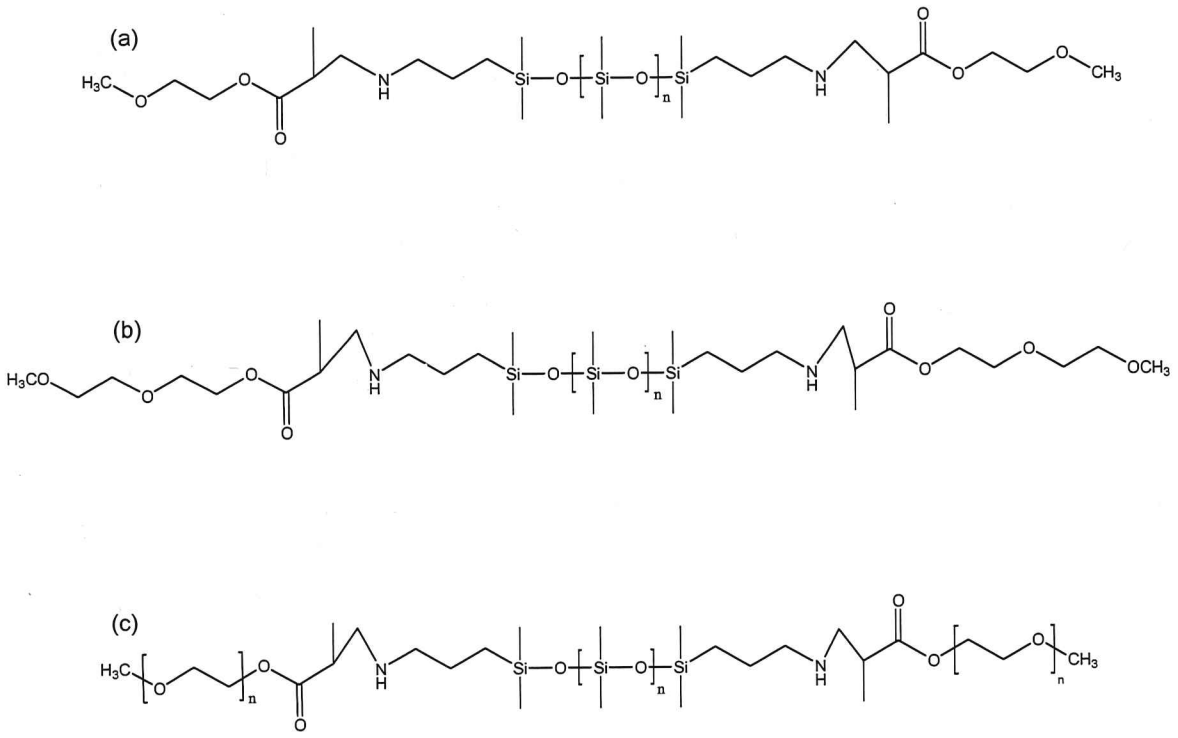

Figure 4.1. General structures of the amphiphilic triblock copolymers comprised of a middle block of PDMS and side blocks of PEG-based monomers (a) mono(ethylene glycol) methyl ether methacrylate, (b) di(ethylene glycol) methyl ether methacrylate and (c) oligo(ethylene glycol) methyl ether methacrylate with M_n of 300 or 475.

Crosslinked siloxane-polyurethane coatings exhibited a self-stratifying mechanism via various driving forces (molecular weight, surface energy, type of solvent, etc.) during film formation.[29] A key driving force in the siloxane-polyurethane self-stratification was the low surface energy of the siloxane phase separating into a low surface energy, low modulus PDMS top layer, and a tough, durable polyurethane lower layer.[30-35] Thus, it is expected that when the amphiphilic triblock copolymers are incorporated into acrylic-polyurethane coatings

a similar self-stratifying mechanism will be observed since the amphiphilic triblock component consists of chemically bonded PDMS blocks. The amount of amphiphilic copolymer was based on a 10% load of siloxane by weight per experimental coating. Therefore, 24 experimental coatings were designed to explore the effects on the addition of PEG blocks to siloxane backbone, PEG block length, and siloxane molecular weight on the coatings fouling-release properties using a combinatorial workflow consisting of automated characterization systems.[36-37]

Figure 4.2 illustrates a schematic of the self-stratified coating surface before and after an external force is applied to the surface. With the idea that the biofoulers have weak adhesion to the surface, the surface is cleaned easily by the application of an external force resulting in the removal the marine biofoulers.

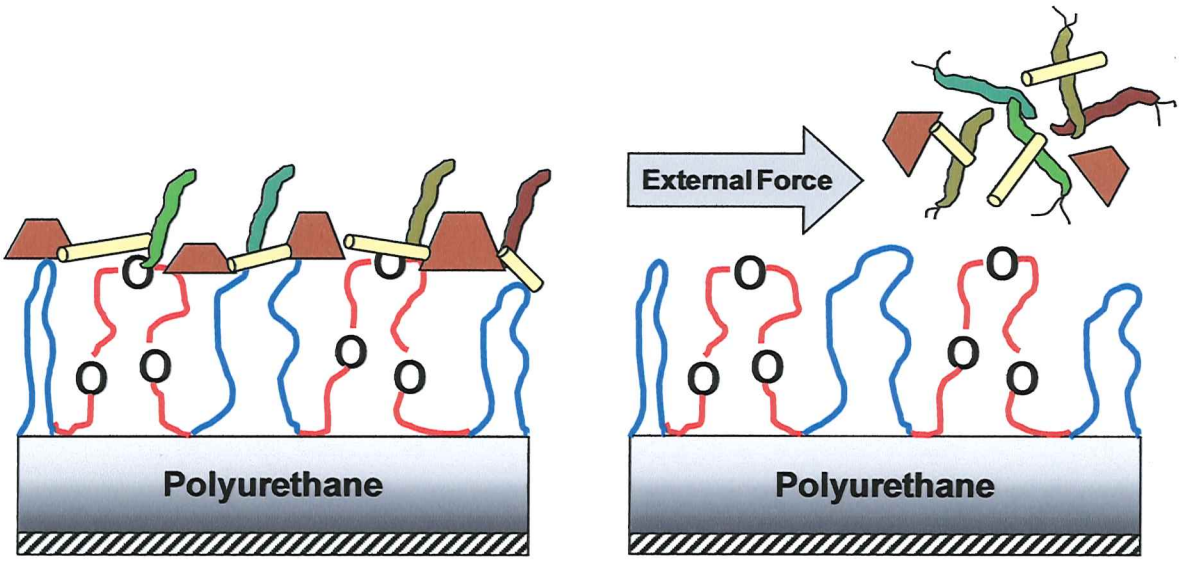

Figure 4.2. Schematic representing the proposed self-stratifying amphiphilic coating surface covered with marine organisms before (left) and after an external force (i.e.-hydrodynamic shear) is applied to coating surface (right). PDMS and PEG blocks represented by the solid domains and domains with oxygen, respectively.

The final amphiphilic copolymers were characterized and formulated into a crosslinked polyurethane coatings system. These coatings were screened for their initial surface properties, pseudo-barnacle adhesion properties, and evaluated against several marine bacteria (*H. pacifica, C. lytica*), barnacle reattachment (*A. amphitrite)*, diatom *N. incerta* bioassays, and *Ulva* sporelings.

4.2. Experimental

4.2.1. Chemicals and reagents

Dibutyltin diacetate (DBTDAc), 2,4-pentanedione, and methyl isobutyl ketone (MIBK), mono(ethylene glycol) methyl ether methacrylate (MEOMA), di(ethylene glycol) methyl ether methacrylate (MEO_2MA), oligo(ethylene glycol) methyl ether methacrylate (MW=300) ($OEGEMA_{300}$), oligo(ethylene glycol) methyl ether methacrylate (MW=475) ($OEGEMA_{475}$), n-butyl acrylate (BA), and 2-hydroxyethyl acrylate (HEA) were obtained from Aldrich. Toluene was obtained from VWR and purified by a solvent purification system. The free radical initiator, 2-azobis (2-methylbutanenitrile) (Vazo 67) was obtained from DuPont. IDT (Tolonate IDT 70B, 70% in butyl acetate) isocyanate was received from Rhodia. IDT is a triisocyanurate resin of isophorone diisocyanate. Polyurethane grade methyl n-amyl ketone (MAK) was supplied by Eastman Chemical. Intersleek 425®, 700®, 900®, and 970® were obtained from International Paint Ltd and used as a fouling-release control. DC 3140 and T2 Silastic were received from Ellsworth Adhesives. DC 3140 and T2 Silastic were solvent reduced with MIBK and used as silicone controls. Bis(3-aminopropyl)tetramethyldisiloxane (BAPTMDS) and D_4 were purchased from Gelest Inc. 3-aminopropyl-terminated PDMS (M_n ~ 3800,

7000, 11,000, 19000, and 30000 g/mol) were synthesized as previously reported and used as prepared.[11] An acrylic polyol composed of 80% butyl acrylate and 20% 2- hydroxyethyl acrylate was prepared by solution polymerization.[29] Amphiphilic polyurethane coatings had a final solids content of ~75%.

4.2.2. Amphiphilic copolymer synthesis

The typical protocol for the amphiphilic copolymer synthesis was as follows. A simple Michael Addition reaction[38-39] was carried out using calculated amounts of PDMS and PEG-based monomers based on a reaction ratio of 2:1 (PEG:PDMS). The reagents were dispensed into 20 mL glass vials, capped, heated to 90°, and stirred via magnetic stirring overnight. Figure 4.3 describes the 6x4 array design for the synthesis of the amphiphilic copolymer, the type of PEG used, the type of siloxane/molecular weight of APT-PDMS used, and the array position are summarized. In the library, the siloxane molecular weight was increased from left to right from column 1 to column 6 in Figure 4.3., starting with BAPTMDS to 30000 Mn PDMS, respectively. Row A consists of the mono(ethylene glycol) methyl ether methacrylate, Row B consists of the di(ethylene glycol) methyl ether methacrylate, Row C consists of the oligo(ethylene glycol) methyl ether methacrylate (Mn=300), and Row D consists of oligo(ethylene glycol) methyl ether methacrylate (Mn=475).

The 6x4 array format is used throughout the rest of the coating formulations and the results of the coatings physical and performance properties. The amphiphilic product was characterized by ^{1}H NMR (400 MHz, $CDCl_3$) to confirm the completion of the reaction.

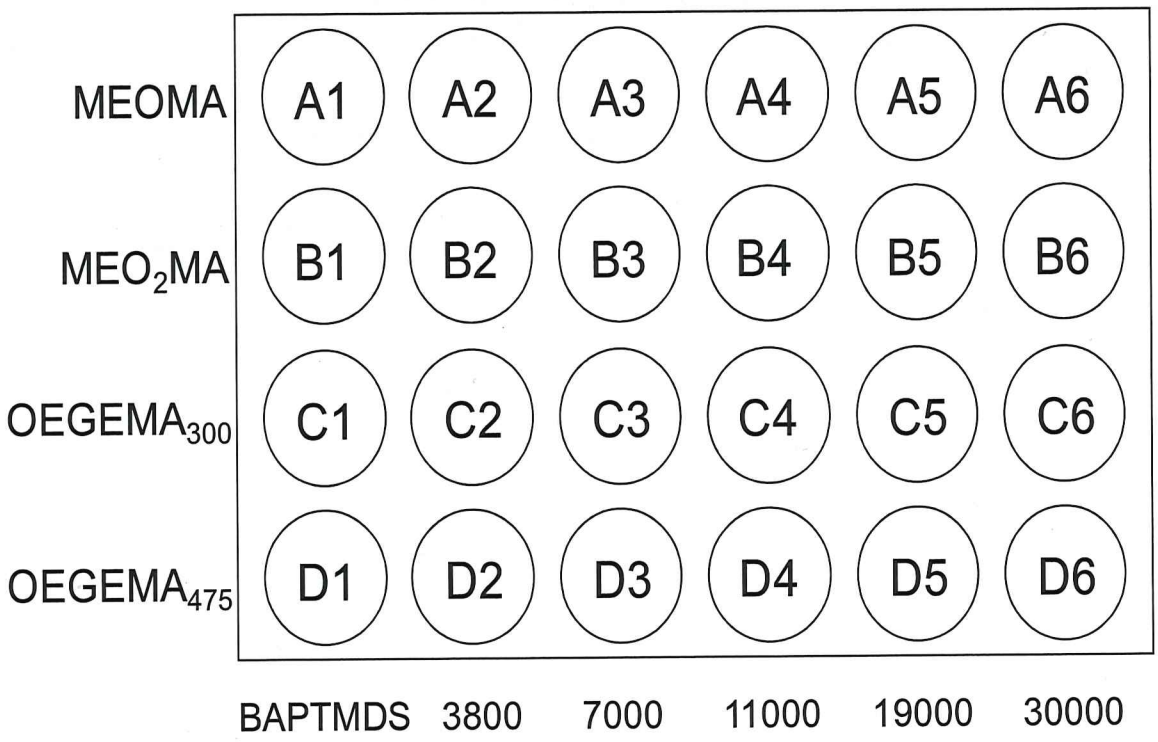

Figure 4.3. Design for the synthesis of amphiphilic copolymers including the type of PEG-based monomer, siloxane/molecular weight of PDMS used, and the array positions

4.2.3. Amphiphilic copolymer characterization

A Symyx Rapid GPC with an evaporative light scattering detector (PL-ELS 1000) equipped with two PLgel mixed-B columns (10 μm particle size) was used for PDMS molecular weight analysis. Solutions of 1 mg/mL sample in THF were prepared before the run; calibration was carried out with polystyrene standards and THF was used as the eluent at 45 °C at a flow rate of 2.0 mL/min. The molecular weight and PDI were determined with Epoch software (Symyx, Inc.). Amine-terminated PDMS oligomers were reacted with acetic acid prior to analysis to prevent their adsorption on the GPC column. ^{1}H Nuclear Magnetic Resonance

(NMR) spectroscopy measurements were done using a Varian Unity/Inova-400NB (400-MHz) NMR spectrometer coupled with an autosampler accessory. The sample concentration was 25 mg/ml and $CDCl_3$ was used as the solvent. Data acquisition was done using 16 scans with a 0.3 s delay time.

4.2.4. Amphiphilic acrylic-polyurethane coatings formulation

Table 4.1 lists the components and their amounts for the amphiphilic acrylic-urethane coating formulations. The dispensing of all components for the coating formulations was done using an Eppendorf repeat pipette. The ratio of isocyanate to other functional groups (amine or hydroxyl) was kept at 1.1:1.0. The amount of catalyst DBTDAc was 0.075% on solids, and the amount of pentanedione varied from 10-15% based on solids and reactivity of the specific coating sample. All coatings were prepared by adding 10% by weight siloxane polymer based on the amphiphilic copolymer from Table 4.1 into the formulation. The amphiphilic acrylic-urethane coatings were prepared by first adding the non-reactive compounds into a glass 4 oz. jar. The non-reactive components consisted of the acrylic polyol (50% solids in toluene), pentanedione, and the amphiphilic copolymer (100% solids). The non-reactive components were stirred by magnetic stirring for 30 minutes at room temperature. The reactive components (isocyanate, 70% solids and DBTDAc) were added to the 4 oz. jar to complete the formulation and stirred for 30 minutes. An additional hour was

Table 4.1. Coating components and amounts for formulation of amphiphilic acrylic-polyurethane coatings.

Array Position	Amphiphilic Copolymer (ml)	Acrylic Polyol (ml)	Isocyanate (ml)	Pentanedione (ml)	DBTDAc (ml)
A1	4.905	0.990	6.469	0.549	0.644
A2	5.553	6.680	3.024	0.549	0.644
A3	6.941	7.324	3.107	0.585	0.644
A4	7.083	6.943	2.865	0.549	0.601
A5	4.905	7.467	3.019	0.585	0.644
A6	5.553	7.502	2.999	0.585	0.644
B1	6.941	0.990	6.469	0.549	0.644
B2	7.083	6.680	3.024	0.549	0.601
B3	4.905	6.687	2.913	0.585	0.644
B4	5.553	6.943	2.865	0.549	0.644
B5	6.941	7.467	3.019	0.585	0.644
B6	7.083	7.502	2.999	0.585	0.601
C1	4.905	0.990	6.469	0.549	0.644
C2	5.553	6.680	3.024	0.549	0.644
C3	6.941	6.687	2.913	0.585	0.644
C4	7.083	6.943	2.865	0.549	0.601
C5	4.905	7.000	2.830	0.585	0.644
C6	5.553	7.502	2.999	0.585	0.644
D1	6.941	0.994	6.469	0.512	0.644
D2	7.083	6.235	3.024	0.512	0.601
D3	4.905	6.687	2.913	0.512	0.644
D4	5.553	6.943	2.865	0.512	0.644
D5	6.941	7.000	2.830	0.512	0.644
D6	7.083	7.033	2.812	0.512	0.601

allowed for an adequate viscosity for drawdowns. The coatings were drawdown on full panels (one coating per panel) with a wet film thickness of 8mils.

4.2.5. Amphiphilic coating deposition

The coating formulations were drawndown on standard 4"x8" aluminum panels (4"x8", Q-panel, 0.6 mm thickness, type A: alloy 3003 H14) and aluminum panels with Intersleek epoxy primed surface at a wet thickness of 8 mils. The formulations were also dispensed on stamped primed aluminum panels, and 24-well microtiter plates for further characterization. After completion of the application of all the coatings, the panels were allowed to ambient cure overnight in dust free drying racks. After the overnight cure, the panels were placed in ovens at 80 °C for one hour, after compete cure they were placed back into the drying racks until needed for further testing and characterization.

4.2.6. Amphiphilic coating characterization

The Symyx surface energy system measures and averages contact angles of various liquids and calculate the surface energy. The system receives a 4"x8" coated panel. The images of three droplets of each test liquid are taken by a CCD camera, and the static contact angles are determined using automated image analysis. Water and methylene iodide (MI) are used as test liquids, and the surface energies are calculated using the Owens-Wendt method.[40] Dynamic contact angles with water and MI were measured with the same automated surface energy measurement unit. Advancing contact angle was measured by dispensing additional liquid over a droplet of liquid placed on the surface. Receding contact angle was measured during the withdrawing of the liquid.

Liquids were dispensed and aspirated at a rate of 0.2 µl/sec. Since the coatings final application is for a marine environment both static and dynamic water contact angle and surface energy was measured before and after 30 days water immersion to test the overall surface stability of the coatings.

The Symyx pull-off adhesion system was used for the pseudo-barnacle pull-off adhesion analysis.[41] The adhesion system can be used to either determine the adhesive strength of a coating on the substrate or the adhesive strength of an epoxy to the coating surface (pseudo-barnacle). The instrument can receive two 4X8 inch coating array panels. First, the two array panels were placed onto the holders of the adhesive application system by applying a vacuum underneath the panels. Then, a plastic template was placed on top of the coatings using pins on the substrate holder for alignment. The plastic sheets have three 7 mm diameter holes over each coating on the array panel. Then Loctite Hysol® Epoxy 1C-LV glue was spread on the coatings through the custom made plastic sheets, resulting in the placement of three 7-mm spots of adhesive on each coating. The plastic sheet was removed and the panels were removed from the adhesion preparation station and placed into clamping jigs. After the panels were clamped, three aluminum studs per coating sample were placed into the clamping jig on top of the applied glue. Weighted foam blocks were placed on top of the studs and the epoxy glue was cured overnight. The next day, the clamped panels with the holders still attached to them were placed into the holders of the automated adhesion system. A pull-off head removes each test stud and the maximum force at failure is recorded and saved in a database. The three values are then averaged.

4.2.7. Evaluation with the marine bacterium *Cellulophaga lytica*

Bacterial analysis was carried out after 14 and 28 days of water immersion. Leachate toxicity was assessed by introducing the bacterium into overnight extracts (artificial sea water with nutrients (ASW)) of each coating and evaluating growth after 24 hours via a crystal violet colorimetric assay. Growth in coating leachates was reported as an absorbance ratio (600 nm) to a growth control.

A series of negative growth controls (medium + bacteria + triclosan) was also included in the analysis. [TC15= triclosan 15 μg, TC6= 6 μg, and TC3= 3 μg.] *C. lytica* biofilm retention and retraction analysis was assessed by a crystal violet colorimetric assay. A 5% suspension of *C. lytica* in ASW + nutrients (~107 cells.ml^{-1}) was prepared and 1ml was added to each well of the coating plate. Plates were incubated statically at 28 °C for 24 hours to facilitate bacterial attachment and colonization. Plates were rinsed three times with DI water and stained with crystal violet. Images were taken after staining, and then the crystal violet was extracted in 33% acetic acid and the resulting eluates were measured for absorbance at 600nm. Biofilm retention was reported as the mean absorbance value of three replicate samples. Biofilm retraction was assessed by determining percent coverage calculations from digital images taken of each coating plate using an automated software tool. Biofilm retraction was reported as the mean percent coverage value of three replicate samples.

4.2.8 Evaluation with the marine bacterium *Halomonas pacifica*

Bacterial analysis was carried out after 14 and 28 days of water immersion. Leachate toxicity was assessed by introducing bacterium into overnight extracts

(artificial sea water with nutrients) of each coating and evaluating growth after 24 hours via a crystal violet colorimetric assay. Growth in coating leachates was reported as an absorbance ratio (600 nm) to a growth control. A negative growth control (medium + bacteria + triclosan) was also included in the analysis. *H. pacifica* biofilm retention analysis was assessed by a crystal violet colorimetric assay. A 10% suspension of *H. pacifica* in ASW + nutrients (~108 cells.ml^{-1}) was prepared and 1ml was added to each well of the coating plate. Plates were incubated statically at 28 °C for 24 hours to facilitate bacterial attachment and colonization. Plates were rinsed three times with DI water and stained with crystal violet. Images were taken after staining, and then the crystal violet was extracted in 33% acetic acid and the resulting eluates were measured for absorbance at 600nm. Biofilm retention was reported as the average crystal violet absorbance value of three replicate samples. Water jet adhesion was carried out after 24 hrs of bacterial biofilm growth. The first column of each plate was not treated and served as the measure of biofilm growth before water jetting. The second and third column of each coating was jetted for 5 seconds at a pressure of 15 psi and 25 psi, respectively. Biofilm adhesion was reported as the percent removal for each pressure indicated above.

4.2.9. Evaluation with the marine microalgae *Navicula incerta*

Algal analysis was carried out after an overnight pre-equilibration in artificial sea water. Leachate toxicity was assessed by introducing algae into overnight extracts (artificial sea water with nutrients) of each polymer and evaluating growth after 48 hours via fluorescence of chlorophyll. Growth in polymer leachates was

reported as a fluorescence ratio to a growth control. A series of negative growth controls (medium + bacteria + triclosan) was also included in the analysis. For the assessment of biofilm growth, algae were diluted to an OD of 0.03 at 660 nm in ASW supplemented with nutrients. 1 ml was added to each well of the plate and allowed to incubate statically for 48 hours. Algal biofilm growth was determined by fluorescence measurement of DMSO extracts. Biofilm growth was reported as fluorescence intensity (relative fluorescence units). Water jet adhesion was carried out after 24 hrs of algal cell growth. The first column of each plate was not treated and served as the measure of cell growth before water jetting. The second and third column of each coating was jetted for 5 seconds at a pressure of 15 psi and 25 psi, respectively. Algal cell attachment was reported as the percent removal for each pressure indicated above.

Biological screening at the University of Birmingham, U.K. involving *Navicula incerta* was also completed. For the *Navicula incerta* study microtiter plates containing the amphiphilic acrylic-urethane coatings were leached in recirculating distilled water tanks fitted with a carbon filter for a total of 26 weeks and placed in sea water to equilibrate two hours before the start of the experiment. Three replicate microtiter plates were incubated with a culture of *Navicula incerta* in trays for three hours in the light at ~20°C.[17,42-43] After gentle washing, the panels with adhered cells were cultured in illuminated tanks of enriched seawater. After three days the panels, which were covered by cells, were subjected to an impact pressure of 34 kPa from a water jet. Percentage removal was estimated visually.

4.2.10. Evaluation with the marine fouling barnacle *Amphibalanus amphitrite.*

Adult barnacles were allowed to attach to sample coatings surfaces for two weeks. Coatings were analyzed after 2 weeks of water immersion and daily feeding of the barnacles with brine shrimp. A hand held digital force gauge, mounted to an automated stage, was used to measure the peak force of release for each barnacle using the protocols described in ASTM D5618-94. Adhesion strength in shear was calculated by dividing the measured force required to remove the barnacle by the basal area and reported in megapascals (MPa). Each data point is the mean value of nine individual barnacle measurements.

4.2.11. Evaluation with the marine algae *Ulva linza* sporelings leachate toxicity, growth and removal.

Biological screening involving *Ulva linza* was completed at the University of Birmingham, U.K. For the *Ulva* sporelings study microtiter plates were leached in a recirculating distilled water tank fitted with a carbon filter for a total of eight weeks and placed in seawater to equilibrate two hours before the start of the experiment. Three replicate microtiter plates were incubated in trays with a suspension of *Ulva* zoospores for three hours in the dark.[16,43-44] After washing to remove unattached zoospores, the panels with settled spores were cultured in enriched sea water for 7 days. After 7 days, the settled spores had germinated and the surface of the panels was covered with young plants. The panels were subjected to impact pressures of 18 kPa , 67 kPa, 111 kPa, and 152 kPa from a water jet[41], percentage removal was estimated visually.

After leaching the coatings in distilled water for 48 h, 1 ml of artificial seawater was added to one row of each coating (6 replicates) and plates were gently shaken (60 movements/min) for 18 h. One ml of each leachate was then deposited in a well of untreated Costar® 24-well plates. To each well, 1 ml *Ulva* spore solution adjusted to 5 x 10^5 spores ml^{-1} in double strength enriched seawater medium was added. The plates were incubated for 2 h in darkness at room temperature before being transferred to an illuminated incubator at 18°C with a 16:8 light: dark cycle (photon flux density 44 $\mu mol.m^{-2}.s^{-1}$). After 7 days growth, the seawater medium was removed from the wells and the chlorophyll extracted from the attached biomass. The mean (6 replicates) percentage inhibition compared to a seawater control was calculated. Chlorophyll was determined in a Tecan plate reader.

4.3. Results and Discussion

The aim of this study was to investigate the effects of the addition of PEG blocks to siloxane backbone, PEG block length, and siloxane molecular weight on the fouling-release properties of crosslinked amphiphilic acrylic-polyurethane coatings. Since there were many variables, combinatorial high-throughput experimentation was used to explore the effects of these variables on the properties of the amphiphilic acrylic-polyurethane coatings. The experiment started with the design of the amphiphilic polyols and subsequent synthesis of the polymers.

The synthesis of the amphiphilic triblock copolymers, described in scheme 4.1, consisted of the reaction of the PEG functionalized methacrylates with the

amine terminated siloxanes via nucleophilic addition using the Michael Addition reaction. Since the primary amine is a good nucleophile it easily adds to the alpha, beta unsaturated carbonyl of the methacrylate under mild conditions. The resulting triblock copolymer has both the hydrophobic properties of the PDMS and the hydrophilic properties of the PEG-based methacrylates providing a chemically bonded triblock copolymer that has unique amphiphilic characteristics. The synthesis library of experiments was designed for a total of 24 PEG-siloxane triblock copolymers.

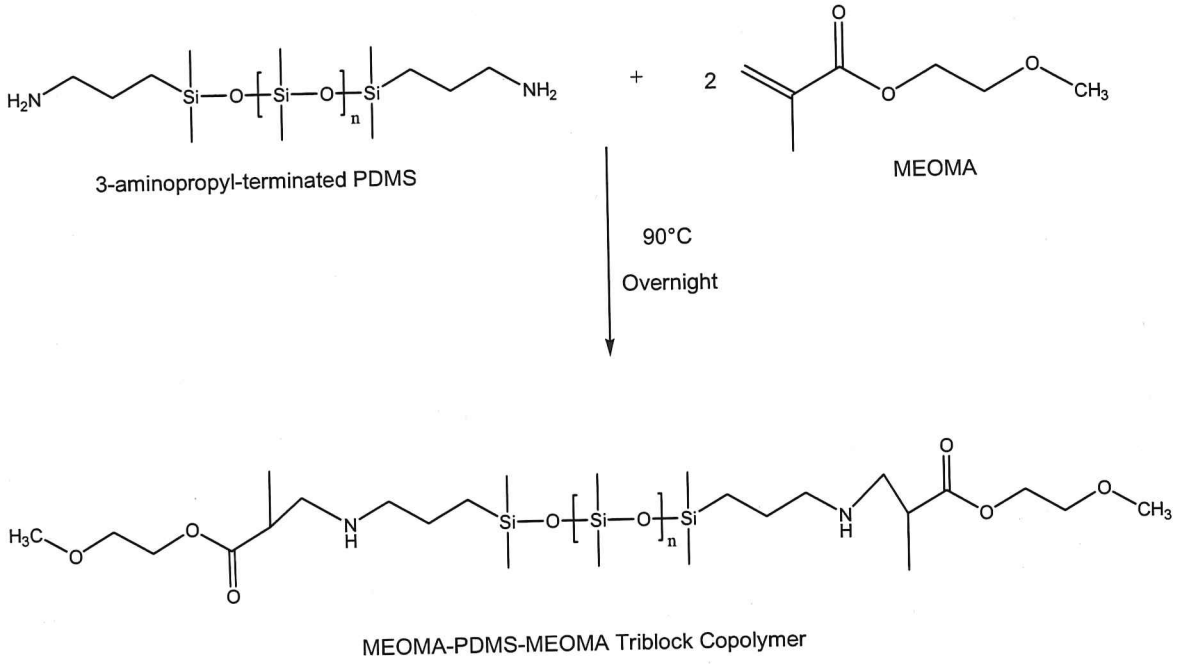

Scheme 4.1. Example reaction scheme for the synthesis of MEOMA-PDMS-MEOMA triblock copolymer via Michael Addition reaction with PDMS and MEOMA as starting materials.

Following the Michael Addition reactions illustrated in scheme 4.1, the triblock copolymers were characterized by ^{1}H NMR to verify completion of the reaction and were then incorporated into coatings formulations. As previously

described, the amphiphilic triblock copolymers were incorporated into acrylic-polyurethane coatings based on a 10% load of siloxane by weight per experimental coating depicted in Table 4.1. The resulting 24 unique amphiphilic acrylic-polyurethane experimental coatings were then applied to substrates and were characterized after ambient curing overnight and heat curing at 80°C for one hour.

The experimental coatings that were prepared were screened for their surface energy using contact angle measurements, dynamic water contact angle, and pseudo-barnacle adhesion, as well as biological screening including *C. lytica*, *H. pacifica*, *N. incerta*, *Ulva linza*, and *A. amphitrite* to check their performance with marine organisms to help understand these systems better and make a correlation between analytical techniques and biological screening. Water contact angle, dynamic water contact angle and pseudo-barnacle were done initially and after 30 days of water immersion. The tests were done after 30 days of water immersion as initial screen of stability after immersion in water since the ultimate use of these coatings is for underwater marine applications.

Initial static water contact angle (a), methylene iodide contact angle (b), and surface energy (c) results of all 24 amphiphilic acrylic-urethane coatings can be seen in Figure 4.4. First, it can be seen that most of the coatings are hydrophobic (water contact angle >90°).

Also, it can be seen that the water contact angle increases with an increase in the PDMS molecular weight. The coatings with BAPTMDS show the lowest water contact angle from ~72° (C1) to ~84° (A1, B1, D1), since these coatings have the

lowest amount of siloxane it is expected. The addition of the PEG blocks does not have a significant effect on the water contact angle of the coatings, with the exception of the coatings formulated with BAPTMDS, where the hydrophilic WCA properties may out weight the hydrophobic property. Coatings A1, B1, and D1 actually have similar WCAs of acrylic-polyurethane (PU) which was found to be ~80-85° from previous research on acrylic-polyurethane coatings. Interestingly, the WCA for PEG is ~63°[45] which is comparable to C1 more so than the other coatings. So, it appears that the surface of coatings A1, B1 and D1 are polyurethane-like having WCA comparable to PU and coating C1 appears to have more PEG at the surface providing a lower WCA near the reported PEG WCA value.

The same general trend can be seen in the methylene iodide contact angles as well. The coatings formulated with PDMS, regardless of molecular weight seem to average ~80-85° MI contact angle (MICA). However, the coatings with BAPTMDS have lower MICA, ~ 65° for A1, B1 and D1, and with C1 showing MICA of ~45°. Previous researchers have reported that the MICA values for PDMS is ~70° [46], MICA for PEG is ~46° [47], and PU is ~67°. Therefore; the majority of the experimental coatings are in the same range of the reported PDMS MICA with the exception of C1, which had a MI contact angle of ~45°equivalent to PEG and A1, B1, and D1 continue to have comparable results to a PU-like surface. When comparing the initial WCA and MI contact angle with the initial surface energy an inverse trend can be seen were the surface energy decreases with the increase in siloxane molecular weight.

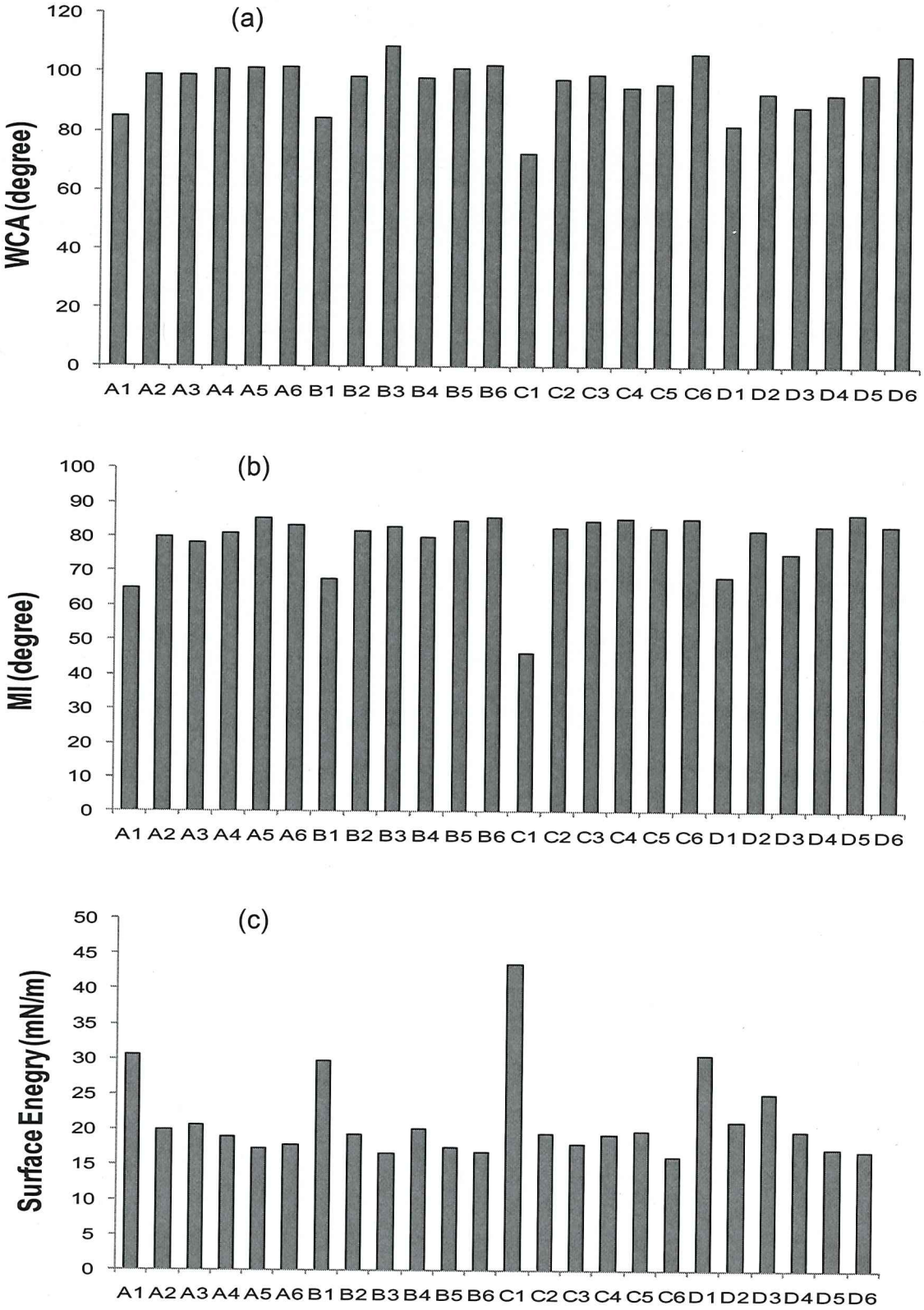

Figure 4.4. Initial (a) water contact angle, (b) methylene iodide contact angle and (c) surface energy results of 24 experimental coatings.

This surface energy trend can be easily observed when comparing the coatings formulated with the higher molecular weight PDMS with the coatings using BAPTMDS. Previous literature has reported that PEG has a surface energy of ~43 mN/m[47] and PU was reported to have a surface energy of 32.4 mN/m[48]. There is good correlation when comparing the reported values of PEG and PU to the experimental values obtained for coatings A1-D1 in this study. Coating C1 had a surface energy value of 44 mN/m and A1, B1, and D1 had values in the range between 31-33 mN/m, very similar to the reported literature values.

Initial dynamic water contact angle for the 24 experimental coatings is illustrated in Figure 4.5. Dynamic water contact angle is a general indicator of surface chemical and morphological stability and is known to be attributed to one of several effects such as surface roughness, chemical heterogeneity, surface deformation, surface configuration change, adsorption/desorption mechanisms, or some combination of these effects. In general, the dynamic water contact angle can be used as an indication of the degree of surface instability resulting from wetting of the surface. From the data in Figure 4.5, a very general trend of decreasing water contact angle over time can be seen for all experimental coatings. Similar to the static WCA results from Figure 4.4, most coatings are hydrophobic at the beginning of the test, the exception being those coatings formulated with BAPTMDS, which indicates that PEG or PU are at the surface. All 24 experimental coatings show surface stability for the first 60 minutes of the test, demonstrated by very little change in the WCA. However, after 60 minutes the WCA for the coatings decrease, possibly due to the hydrophilic block migrating to

the surface. Most of the coatings formulated with PDMS of varying molecular weights (represented by 3800, 7000, 19000, and 30000 in the legend, Figure 4.4) stay hydrophobic throughout the test with the exception of coating formulation in graph (b), PDMS molecular weight of 3800, which dips below the hydrophobic WCA (90°) at 110 minutes. An interesting trend in all of the coatings is the slight increase in WCA towards the end of the test. Indicating another possible surface rearrangement where the hydrophobic (PDMS) block is returning to the surface.

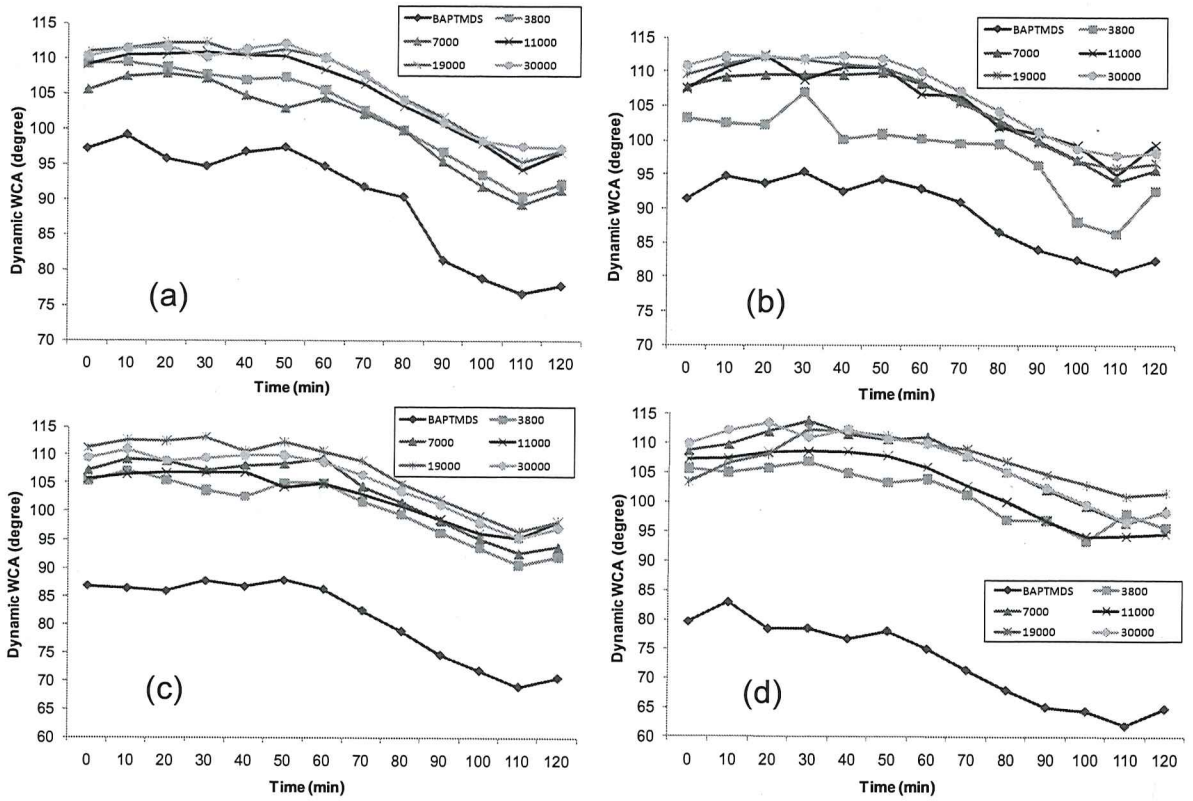

Figure 4.5. Initial dynamic water contact angle (DWCA) on amphiphilic acrylic-polyurethane coatings. The legend corresponds to the siloxane-type or MW of PDMS in each coating consisting of a) MEOMA, b) MEO_2MA, c) $OEGEMA_{300}$, and d) $OEGEMA_{475}$.

In order to look at additional surface properties initial AFM images of all 24 coatings were taken by tapping mode in air. All 24 AFM images are shown in

Figure 4.6. A general behavior of microscale ripple-type tracks on the surface is observed for all coatings with the exception of coatings A4, A5, and C2. The formations of the ripple-type tracks on the coatings surface are from the hydrophilic and hydrophobic components physical self-organization by interfacial tension between the coating-air surfaces. Coating formulations A4 and A5 show microdomains which are the result of microphase separation between the PDMS and the PEG blocks.[60]

.

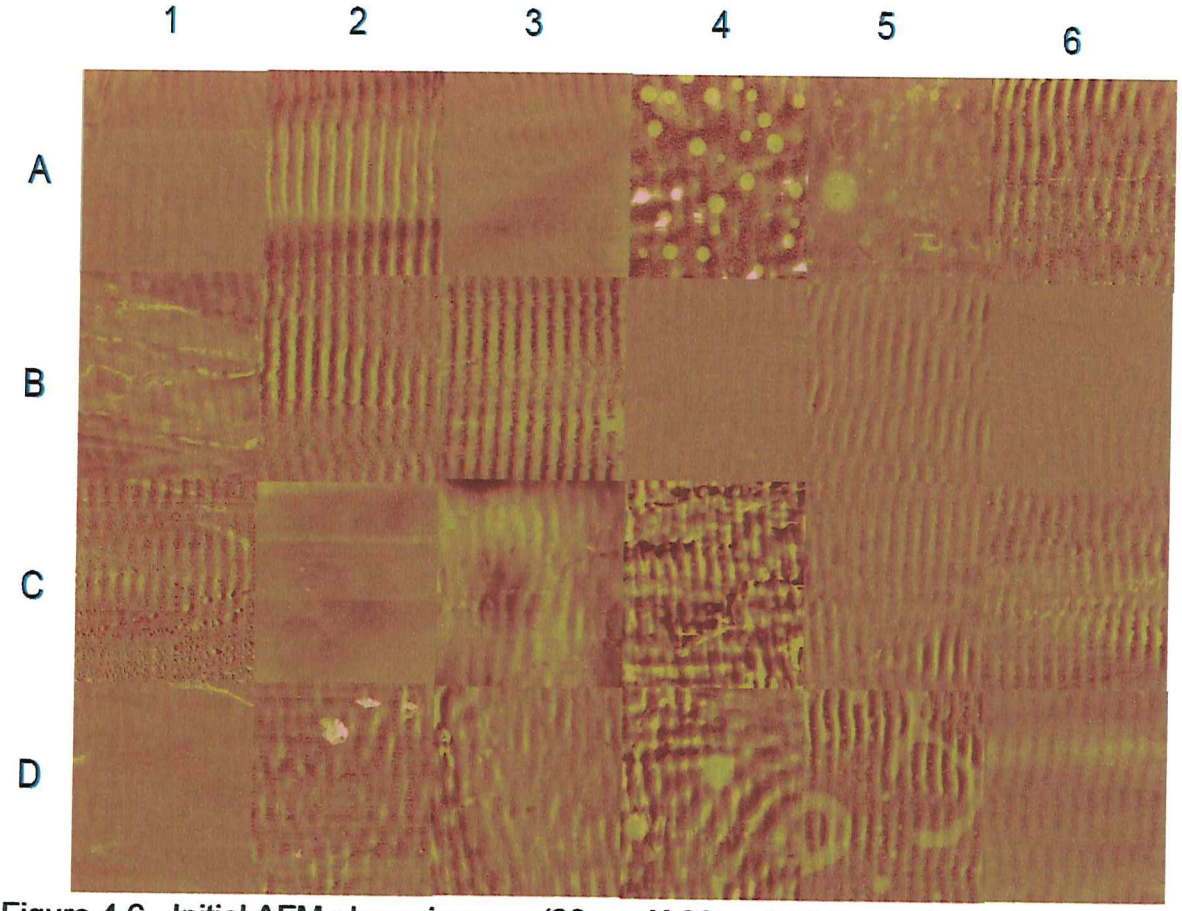

Figure 4.6. Initial AFM phase images (20 μm X 20 μm) of the surfaces from the 24 experimental coatings.

It was found that as the molecular weight of the PDMS segment increased the domains became more obvious on the coatings surface. However, as the molecular weight of the PEG segment increased the extent of phase separation decreased. This correlates with the results seen from the AFM images in Figure 4.6. It should be know that the Coating C2 formed a smooth coating with depressions which were imperfections in the coatings surface and not microdomains.

The automated pull-off adhesion system was used to determine the pseudo-barnacle adhesion of the 24 experimental coatings. This test measures the force required to remove an epoxy adhesive from the surface of the coating, and may be indicative of how strongly a barnacle would adhere to the coating. The initial pseudo-barnacle adhesion results as a function of the hydrophobic (siloxane) components and the hydrophilic (ethylene glycol) components can be seen in Figure 4.7. A range of force at release values are observed over all experimental coatings from 19 N to 65 N. As recalled from Chapter 3, the force at release for the silicone control was ~20 N. Several coatings have initial force values at or better then the control, however, the majority of the coatings showed relatively higher values when compared to the silicone control. No strong trends are present from the results, but coatings formulated with MEO_2MA and $OEGEMSA_{475}$ seem to mimic the force at release trend from each other. It's interesting to look at the difference in adhesion strength when comparing coatings formulated with $OEGEMA_{300}$ and $OEGEMA_{475}$, with the difference of only four PEG repeat units between them, there is a remarkable initial drop in adhesion with

$OEGEMA_{475}$. Starting with the first formulation using BAPTMDS, there is a difference of 30 N between the two oligomeric PEG based copolymers ($OEGEMA_{475}$ =35N, $OEGEMA_{300}$=65N), as PDMS is incorporated into the formulation there is a steady increase in adhesion for both, however, with PDMS (MW=11000) adhesion flips, now with $OEGEMA_{300}$ being lower (30 N) compared to $OEGEMA_{475}$ (45 N). This observation again switches for high molecular weight PDMS (19000 and 30000) and once again $OEGEMA_{475}$ has lower adhesion. A key observation is that the adhesion is lowest for coatings formulated with MEOMA and PDMS with molecular weight of 7000 and 30000. This is due to the lower PEG block length formulated into the amphiphilic coating where the amphiphilic coating is dominated by PDMS migrating to the air interface (the coating surface) resulting in lower adhesion.

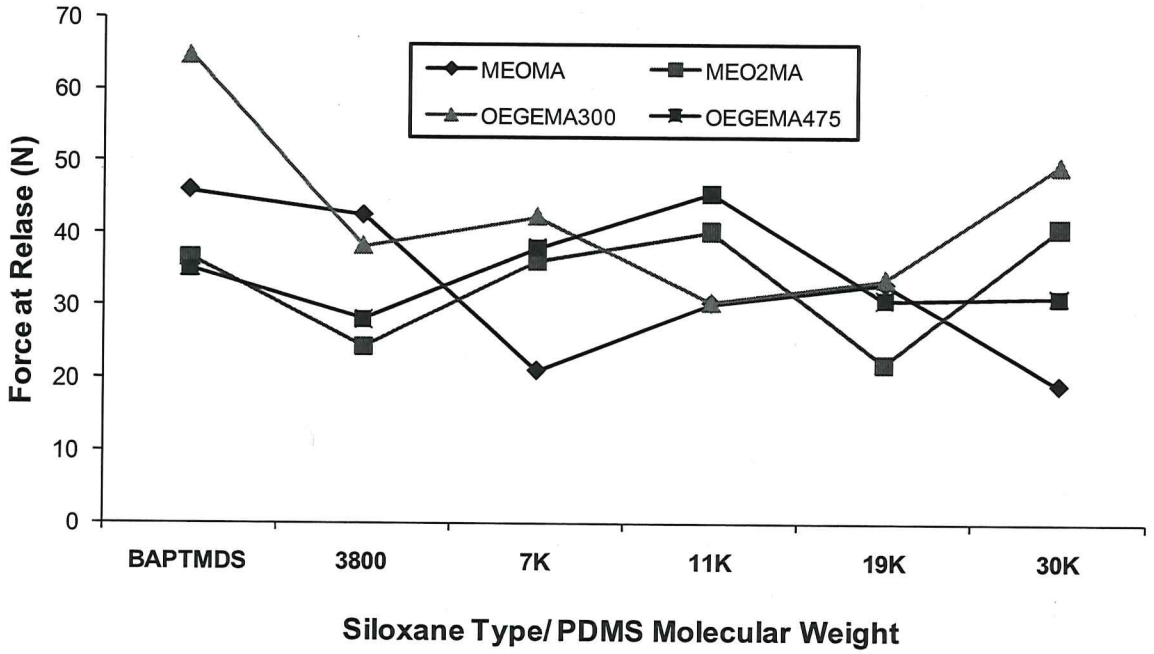

Figure 4.7. Initial pseudo-barnacle pull-off adhesion of amphiphilic acrylic-polyurethane coatings.

To assess the stability of the coatings, the surface properties were measured after 30 days of water immersion. Since the coatings are intended for underwater marine applications, the evaluation of the properties after water immersion will be more relevant to the final application of the coating.

(*Differences between the initial and 30 day WCA, MICA, and surface energy results for the experimental coatings are in Figure 4.9 and are explained after the analysis of the 30 day water immersion results*).

Figure 4.8 illustrates the water contact angle (a), methylene iodide contact angle (b), and surface energy (c) results from the 24 experimental coatings after 30 days water immersion. There is an overall trend that is observed in the WCA of the experimental coatings that shows the majority of the coatings are hydrophobic evident by WCA ≥100°. This observation is consistent with PDMS covering the entire surface of the coating due to its lower surface energy compared to the other organic components of the coating formulation. However, the coatings formulated with the triblock containing BAPTMDS and PDMS of 3800 molecular weight (A1, B1, C1, and D1) show lower WCAs. Coatings A1 and B1 are still hydrophobic with WCAs of ~93°, showing that even with BAPTMDS the coatings behave similar to the experimental coatings with higher molecular weight PDMS with the same PEG-based segments in the triblock. Coating C1 and D1 were observed to be hydrophilic with a WCA of 83° and 78°, respectively. This observation is consistent with the coatings surface behaving PU-like or PEG-like rather than PDMS-like, which is likely caused by the surface rearrangement of the higher molecular weight hydrophilic PEG-based block in the triblock of the copolymer.

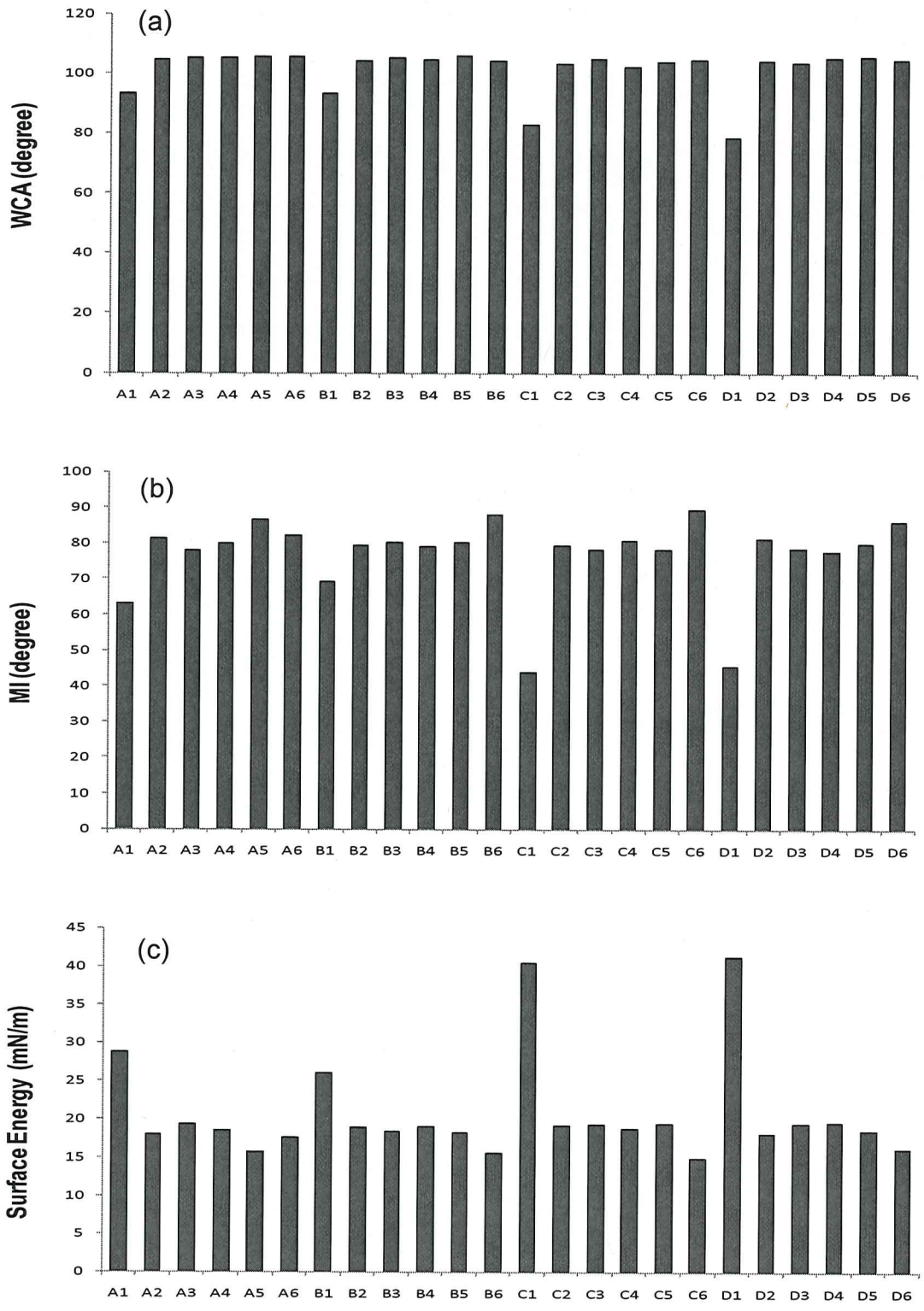

Figure 4.8. 30 day water immersion for (a) water contact angle, (b) methylene iodide contact angle and (c) surface energy results of 24 experimental coatings.

The Methylene iodide contact angle results for the experimental coatings show a similar contact angle trend that was seen with the WCA results. The majority of the coatings show MICA above 70°, consistent with reported MICA values for PDMS covering the coatings surface. Both coatings A1 and B1 had MICA values similar to the reported value for PU which is 65-67°. The MICA results for coatings C1 and D1 were 44° and are 45°, respectively and are similar to the reported literature value of PEG, which is ~46°. The surface energy results for the experimental coatings correlate nicely with the previous observed WCA and MICA results. Once again, the majority of the coatings showed surface energies comparable to PDMS with reported experimental values ≤20 mN/m, similar to the reported literature value of PDMS. Both coatings A1 and B1 had surface energy values similar to the reported value for PU which is 32 mN/m. Coating A1 had a value of 28 mN/m and B1 was 27 mN/m. The surface energy results for coatings C1 and D1 were 41 mN/m and 42 mN/m, respectively and show a similar reported literature value to PEG, which is 43 mN/m. Overall, Figure 4.8 showed trends that the surface of the experimental coatings are behaving either as PDMS-like, PU-like, or PEG-like based on the reported experimental values compared to literature values of PDMS, PU, and PEG of the respective surface property tests.

Differences from Figure 4.4 (initial measurements of same properties) and Figure 4.8 were observed and are illustrated in Figure 4.9. The water contact angles for almost all coatings increased after the 30 days water immersion. Row A (formulated with MEOMA) showed an average of +5.6°, Row B (formulated with MEO_2MA) showed an average of +3.6°, Row C (formulated with $OEGEMA_{300}$)

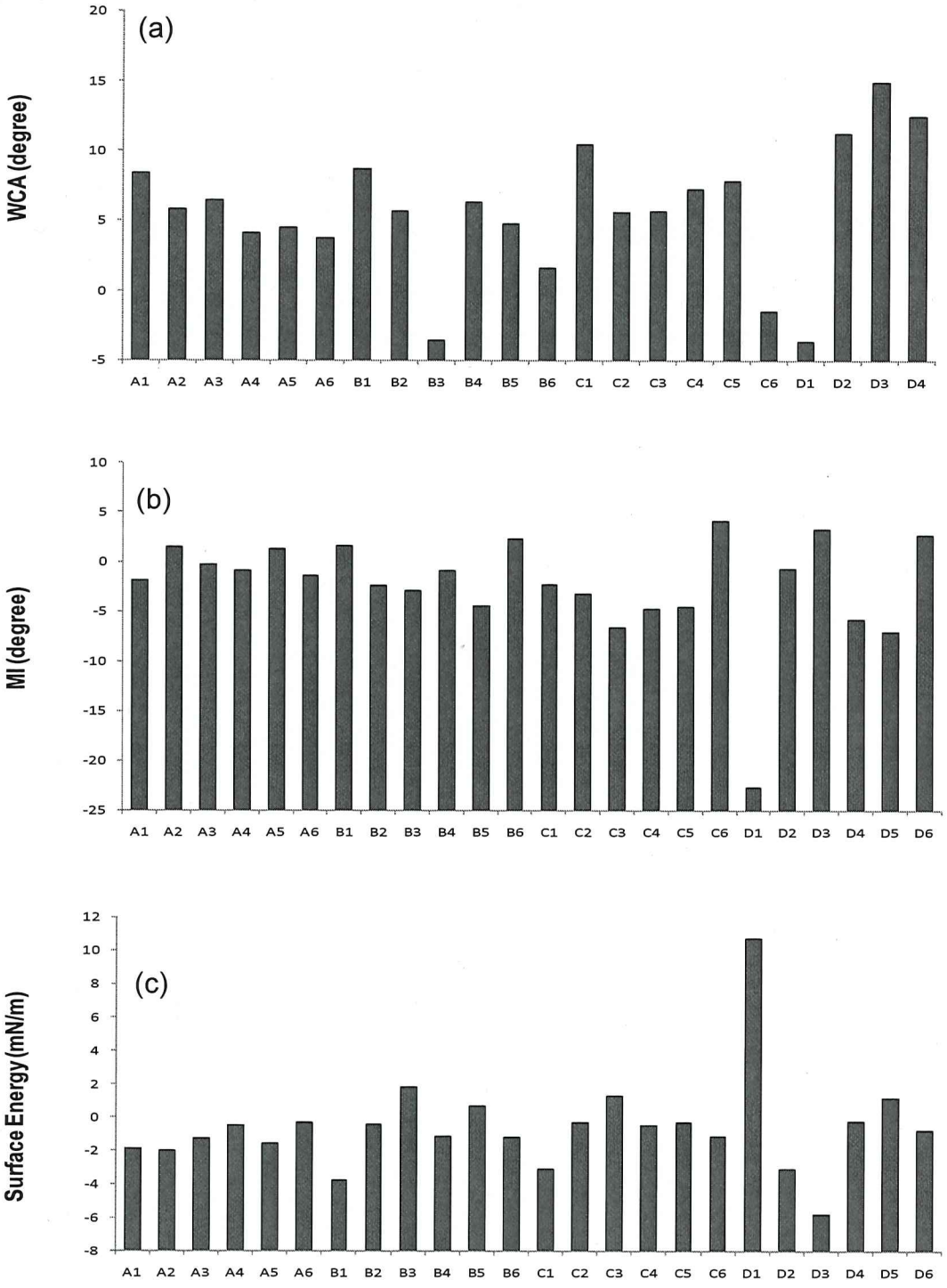

Figure 4.9. Difference in initial to 30 day water immersion results for (a) water contact angle, (b) methylene iodide contact angle and (c) surface energy results of 24 experimental coatings.

showed an average of +6.2°, and Row D (formulated with $OEGEMA_{475}$) showed an average of +6.5°, a significant increase compared to the initial WCA from Figure 4.4. Coatings B3, C6, D1 and D6 were the only coatings that showed a decrease in WCA after the water immersion, -4.1°, -1.3°, -4.5°, and -1.4° respectively. However, it is important to point out that the coatings in Row C and Row D also had the largest increase for the coatings in those respective rows, especially coatings C1, D2, D3, and D4, which all had average increases over 10°. This large increase in WCA for those coatings suggests significant surface rearrangement; this observation is interesting since those coatings are formulated with the largest hydrophilic blocks and consequently should have lower WCA's. The methylene iodide contact angle results for the coatings after 30 days water immersion showed a slight increase overall, but nothing significant with an average of +1.6° for all coatings. It shows the same trends seen in Figure 4.4 (b) where the coatings formulated with PDMS, regardless of molecular weight seem to average ~80-90° MI contact angle, the highest molecular weight PDMS showing the highest MI contact angles. Coatings formulated with BAPTMDS, especially D1, showed the lowest MI contact angles similar to the values seen in Figure 4.4 (b) due to the low amount of siloxane and the higher amount of PEG segments. Coating formulation D1, showed a decrease of 28° indicating a surface rearrangement where the hydrophilic component dominates the surface, which is opposite of what was observed in the initial values seen in Figure 4.4 (b). This correlates with the 30 day water immersion WCA data, which showed a decrease value compared to the initial WCA value observed. The surface energy data after

30 days water immersion illustrated in Figure 4.8(c) shows a trend that can be seen were the surface energy decreases with the increase in siloxane molecular weight, similar to the initial values reported in Figure 4.4(c). This surface energy trend can, once again, be easily observed when comparing the coatings formulated with the higher molecular weight PDMS with the coatings using BAPTMDS. As seen with the WCA and the MI contact angle data for coating D1 where there is a dramatic change in the surface properties, a similar trend is seen with the surface energy, with an increase of 11 mN/m after the 30 days water immersion. This further confirms that a surface rearrangement on coating D1 happened after the water immersion.

Dynamic water contact angle for the 24 experimental coatings after 30 days water immersion is illustrated in Figure 4.10. From the data, a very general trend, similar to the initial DWCA (Figure 4.5) is the decreasing water contact angle over time can be seen for all experimental coatings. Similar to the 30 day water immersion static WCA results from Figure 4.8, most coatings are hydrophobic at the beginning of the test, the exception being those coatings formulated with BAPTMDS. The major difference between the initial and the 30 day water immersion results can be seen with the coatings formulated with the highest molecular weight PEG (d) and the second lowest MW PEG formulation (b). An average decrease of ~10° for those coatings is a result of the PEG component migrating to the surface and lowering the water contact angle at time=0. An interesting observation that can be seen is the larger separation of values when compared to the initial DWCA data. In Figure 4.5, the coatings formulated with

PDMS have a very tight grouping (PDMS formulated coatings) over the course of the test, after the 30 days of water immersion that grouping spreads out confirming that the hydrophilic component has begun to dominate the surface properties of the coatings depending on the molecular weight of the PDMS used in the formulation.

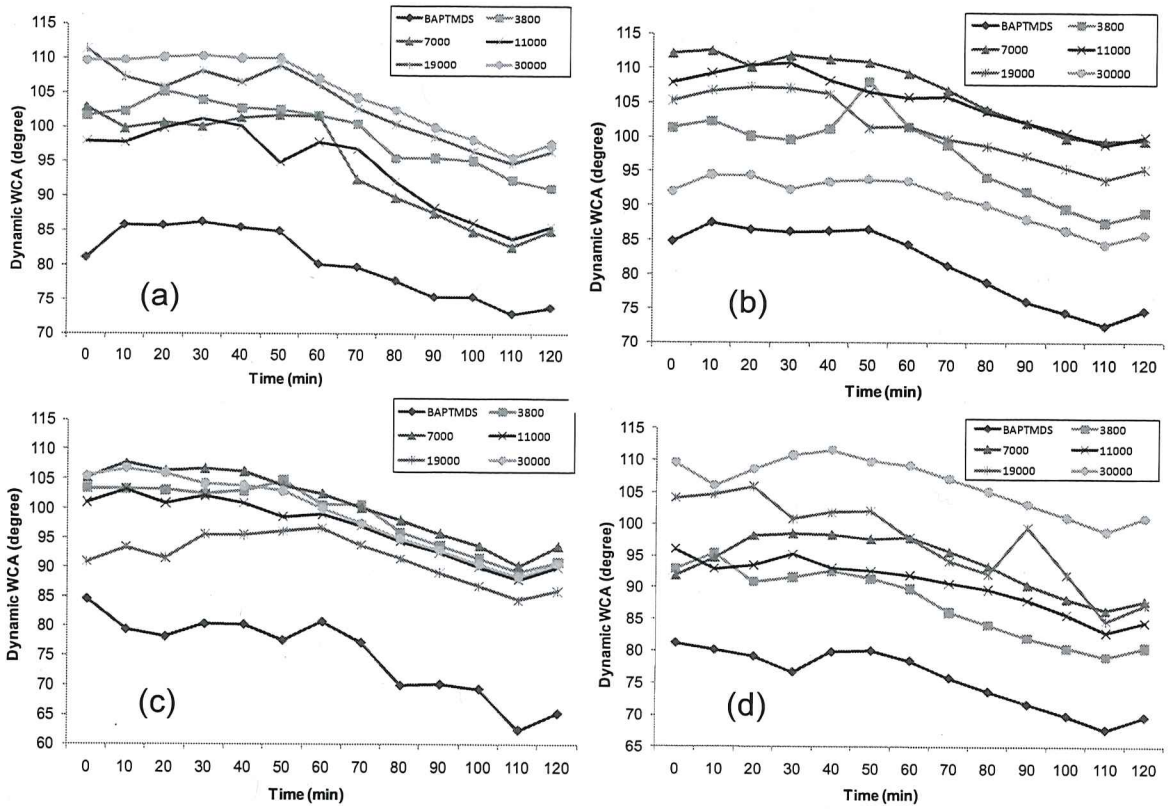

Figure 4.10. DWCA after 30 days water immersion on amphiphilic acrylic-polyurethane coatings. The legend corresponds to the siloxane-type or MW of PDMS in each coating consisting of a) MEOMA, b) MEO_2MA, c) $OEGEMA_{300}$, and d) $OEGEMA_{475}$.

However, with the incorporation of the PDMS, the coatings are still hydrophobic in nature (exception- BAPTMDS formulated coatings). Overall, the coatings still show relatively stable surfaces after 30 days water immersion. Row A had an average WCA difference from time=0 to 120 minutes of 12.5°, Row B

had an average WCA difference from 0 to 120 minutes of 9.9°, Row C had an average WCA difference from 0 to 120 minutes of 12.4°, and Row D had an average WCA difference from 0 to 120 minutes of 10.9°. To summarize, the only clear trends are the decrease of contact angle for all coatings over the course of the dynamic water contact angle test, and the coatings formulated with higher molecular weight PDMS showed coatings that remained hydrophobic in nature during the entire test.

In order to look at additional surface properties, AFM images of all coatings were taken 30 days water immersion by tapping mode in air (coating C1 surface was damaged, thus was unable to allow for an adequate scan) . The AFM images of the experimental coatings are shown in Figure 4.11. After the 30 days water immersion a key observation is the ripple-type tracks on the coatings surface are clearly evident for the majority of the coatings similar to what was seen previously in the initial AFM images in Figure 4.6. Coating A4 still shows evidence of domain formation; however, A5 does not have domains after the water immersion. This may be due to the surface rearranging to the most thermodynamically favorable configuration. The surface of coating C2 changed from an initial smooth coating to showing the ripple-type tracks after the 30 days water immersion, giving evidence of surface rearrangement of the amphiphilic copolymer self-organizing along the coating surface-air interface. Overall, the majority of the experimental coatings retained their relatively smooth surfaces with the exception of C1 which was damaged and A4 which continued to show domain formation after the water immersion.

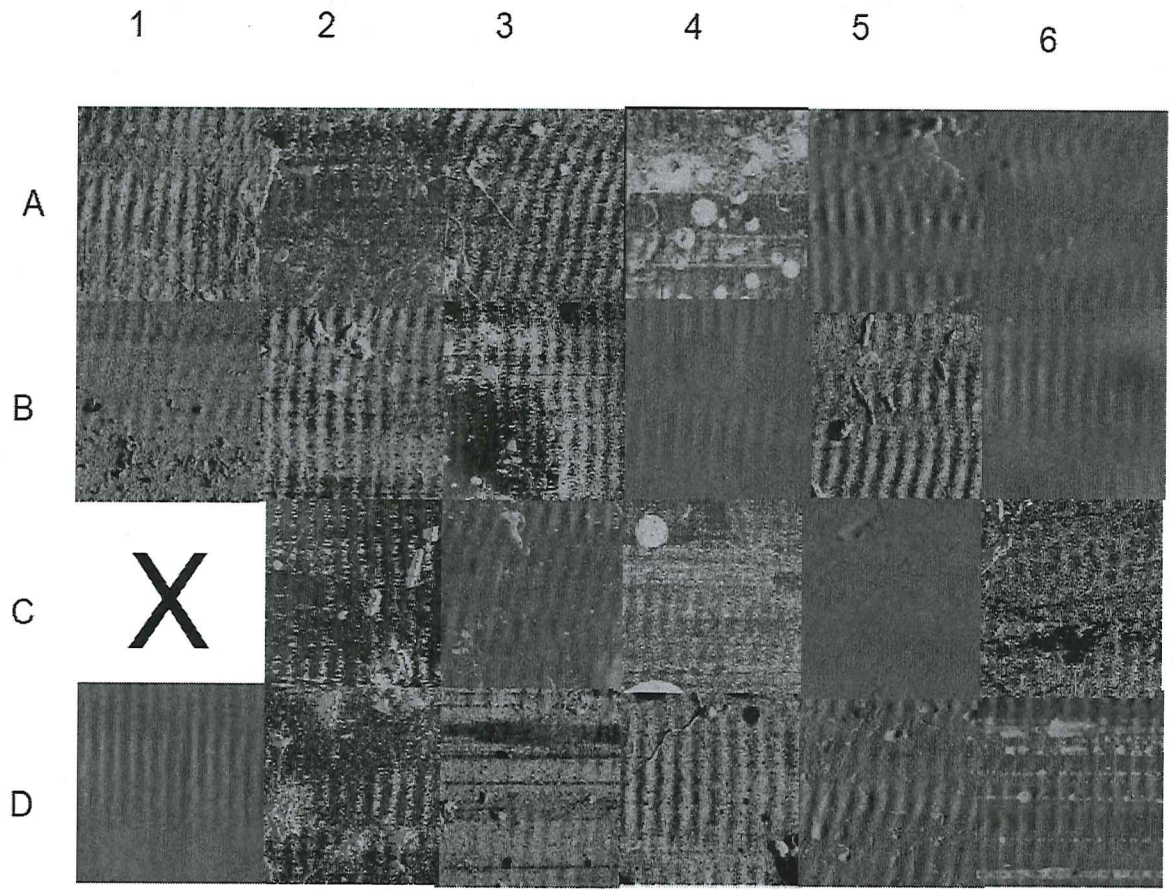

Figure 4.11. AFM phase images (20 μm X 20 μm) of the surfaces from the 24 experimental coatings after 30 days water immersion.

The automated pull-off adhesion system was used to determine the pseudo-barnacle adhesion of the 24 experimental coatings after the coatings were subjected to 30 days water immersion. The pseudo-barnacle adhesion of the 24 coatings after 30 days water immersion results as a function of the hydrophobic (siloxane) components and the hydrophilic (ethylene glycol-based) monomer components can be seen in Figure 4.12. A range of force at release values are observed over all experimental coatings from 14 N to 40 N, significantly lower than the initial results seen in Figure 4.7 which ranged from 19 N to 65 N. In Chapter 3, the silicone control had a force at release of ~20 N, several coatings have initial

force at release values at or better then the silicone control, however, unlike the initial pseudo-barnacle measurements, the majority of the coatings showed much lower pull-off force values (compared to initial) with an overall average drop of 27.1%. A key trend that is observed is the low pull-off force for the coatings formulated with 7000 and 11000 MW PDMS. Those coatings showed a grouping with a 67.6% lower adhesion force than the initial values. The coatings formulated with 3800 and 19000 MW PDMS were nearly identical in both the initial and 30 days water immersion values. This observation correlates with the surface energy results which showed those experimental coatings showed very little change

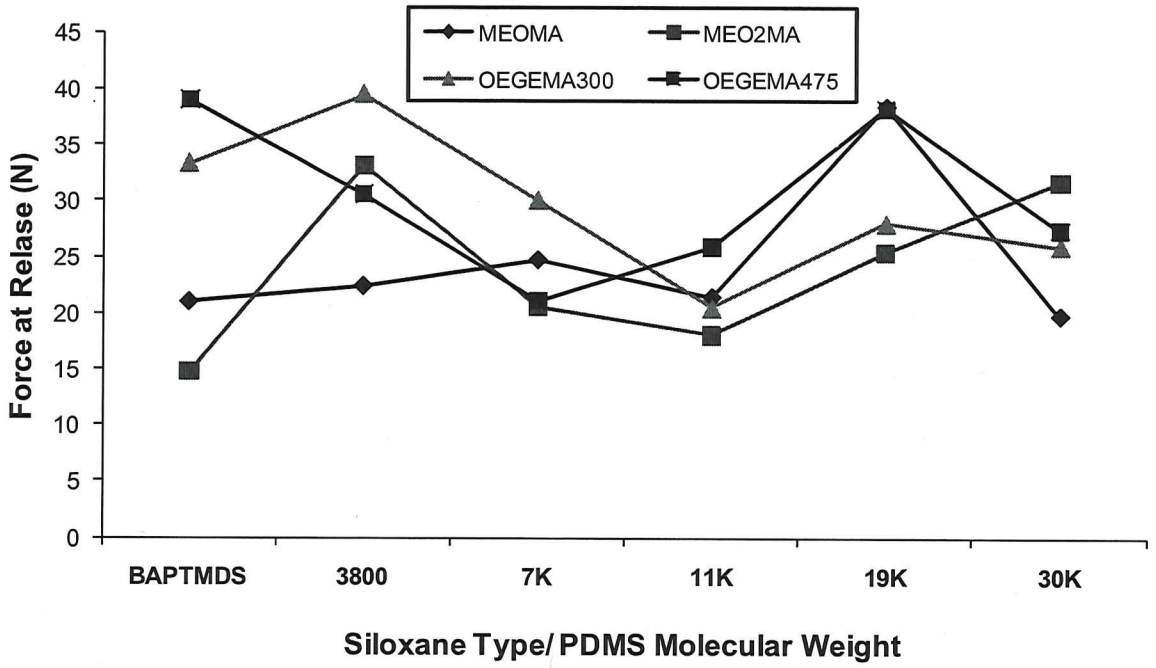

Figure 4.12. Pseudo-barnacle pull-off adhesion of amphiphilic acrylic-polyurethane coatings after 30 days water immersion.

overall in their respective values. Since the several of these coatings showed surface energy values similar to PDMS subsequently the pull-off force were

relatively close to the force at release for PDMS. The low value for the coating with BAPTMDS/MEOMA is due to coating failure at the substrate/coating interface and should not be considered as the lowest force at release coating. Overall, the coatings showed a slight decrease in PB adhesion after the 30 day water immersion which is consistent with the SE results from the 30 day water immersion as well. This is likely due to surface rearrangement of the amphiphilic triblock copolymer to the most thermodynamically favorable position.

Bacterial biofilm assays using marine bacteria are used as a screening tool to further characterize the coatings. *C. lytica* biofilm retention analysis, illustrated in Figure 4.13, was assessed by a crystal violet colorimetric assay. A 5% suspension of *C. lytica* in ASW + nutrients (~10^7 cells.ml^{-1}) was prepared and 1ml was added to each well of the coating plate. Plates were incubated statically at 28°C for 24 hours to facilitate bacterial attachment and colonization. Plates were rinsed three times with DI water and stained with crystal violet. Images were taken after staining, and then the crystal violet was extracted in 33% acetic acid and the resulting eluates were measured for absorbance at 600nm. Biofilm retention was reported as the mean absorbance value of three replicate samples. In Figure 4.13, all coatings were determined to retain less of the *C. lytica* biofilm, which was better or comparable to the commercial fouling-release coatings. In terms of the fouling process this is significant because it shows that the biofilm actually avoids, or deters, settlement on the surface of the experimental coatings, theoretically stalling or even stopping the microfouling stage of the process and

thus impeding continuation of the biofouling process on the experimental coatings surface.

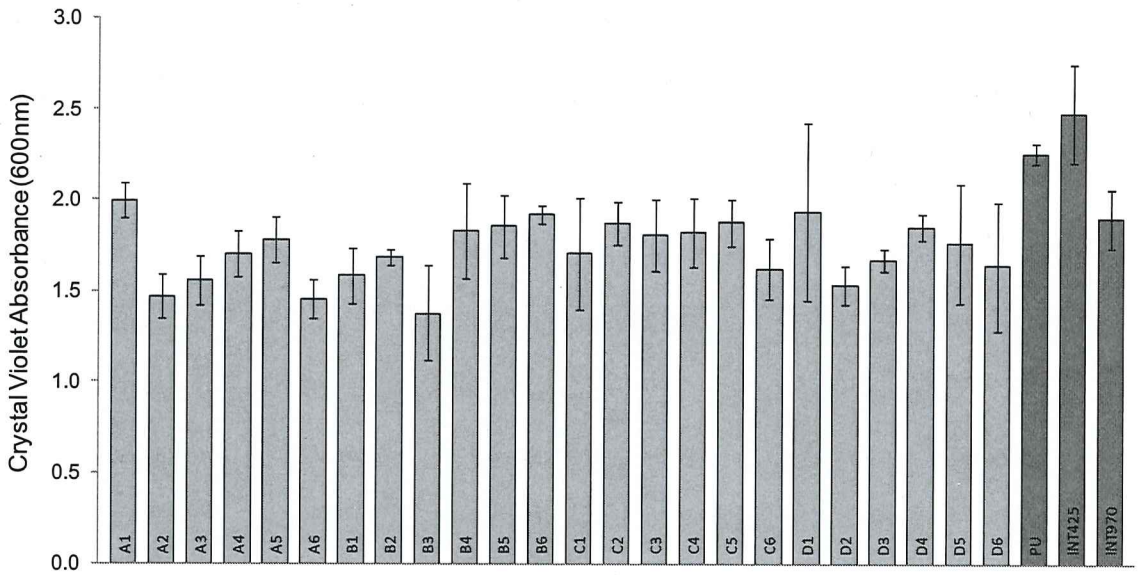

Figure 4.13. *C. lytica* biofilm retention after forty two days preleach of amphiphilic acrylic-polyurethane coatings, polyurethane control, and commercial fouling-release. Error bars represent one standard deviation of the mean.

Water jet adhesion of the *C. lytica* biofilm was carried out after 24 hrs of bacterial biofilm growth. Each coating was jetted for 5 seconds at a pressure of 10 psi and then a new set of each coating was jetted at a pressure of and 20 psi and biofilm adhesion is represented by percent removal. In Figure 4.14, *C. lytica* cell percent removal for the coatings treated with a water jet pressure of 10 psi and 20 psi are shown. The results of the water jet of 10 psi on the *C. lytica* biofilm percent removal showed that all coatings performed better than the polyurethane control and the commercial fouling-release coatings. On average, the experimental coatings had 59.7% biofilm removal at 10 psi, compared to the commercial fouling-

release coatings, Intersleek 425 and 970, which had 15% and 45% removal, respectively.

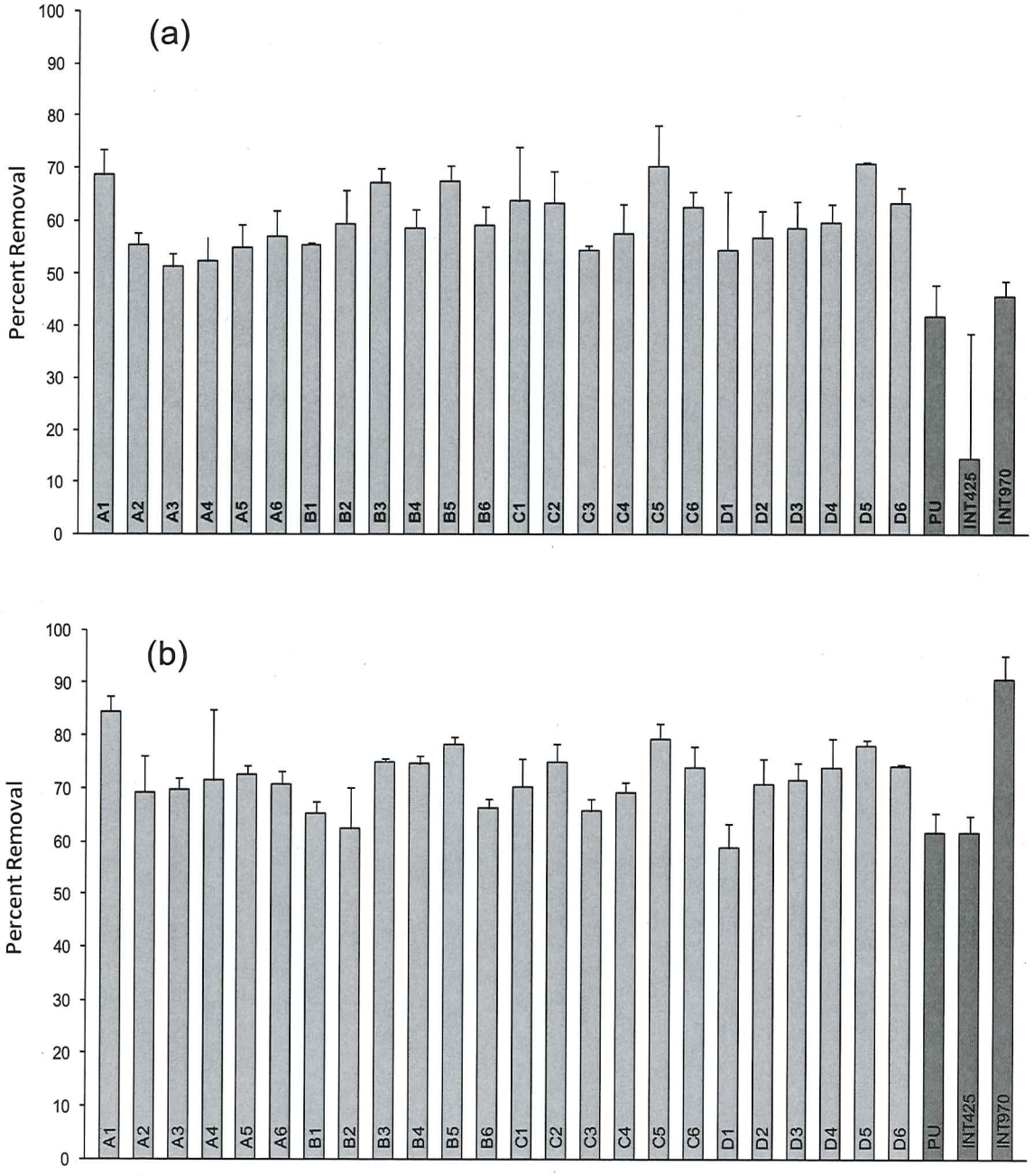

Figure 4.14. *C. lytica* cell adhesion after four weeks preleach of amphiphilic acrylic-polyurethane coatings, polyurethane control, and commercial fouling-release coatings using water jet at (a) 10 psi, and (b) 20 psi. Error bars represent one standard deviation of the mean.

The coatings with the highest percent removal were A1, B3, B5, C5, and D5 with removal all above 65%. With the exception of A1 (SE value similar to PU), all of these coatings had surface energy values comparable to PDMS. There is a slight trend that is observed where there is an increase in percent removal with an increase in the hydrophilic component regardless of the molecular weight of the PDMS in the coatings. When comparing the PU control, coatings A1 and B1 both showed SE similar to PU, however, the removal of these coatings were higher than the PU control which shows that even though the coatings SE represents values similar to PU the surfaces of the experimental coatings behave more like PDMS. In general, the SE of the experimental coatings numbered 2-6 had values resembling PDMS, even though their composition included a hydrophilic component. Overall, all experimental coatings performed better than the controls, regardless of their SE and coating composition.

When the water jet pressure is increased to 20 psi the trend remains with the only difference being there is an average of ~10% increased removal of the biofilm on the coatings. However, there was a large percent removal increase for the commercial fouling-release coatings. Intersleek 425 increased from 15% (10 psi) to 60% (20 psi) and Intersleek 970 increased from 45% (10 psi) to 90% (20 psi). All of the coatings outperformed the polyurethane control and Intersleek 425, but Intersleek 970 percent removal was better than all of the coatings, with A1 performing the best with 85% removal. Coating B1 had removal similar to the PU control which correlates the SE of B1 which was comparable to PU; this observation was not seen until the water pressure was increased to 20 psi

however. Coating D1 had the least percent removal (59%) with the increase in water pressure, the SE of D1 was comparable to PEG which could have some effect on the removal of the biofilm, however, coating C1 had a similar SE and the removal was better than both the PU control as well as the commercial fouling-release coating, Intersleek 425. Overall, the experimental coatings percent removal of the *C. lytica* biofilm performed better than the PU control and Intersleek 425.

Biofilm retention analysis using marine bacteria, *H. pacifica* is shown in Figure 4.15. A key trend observed is the average increase in biofilm retention with the increase in the hydrophilic component for all formulations, exceptions being coatings A1 and D1, which showed the highest retention of all the coatings. The

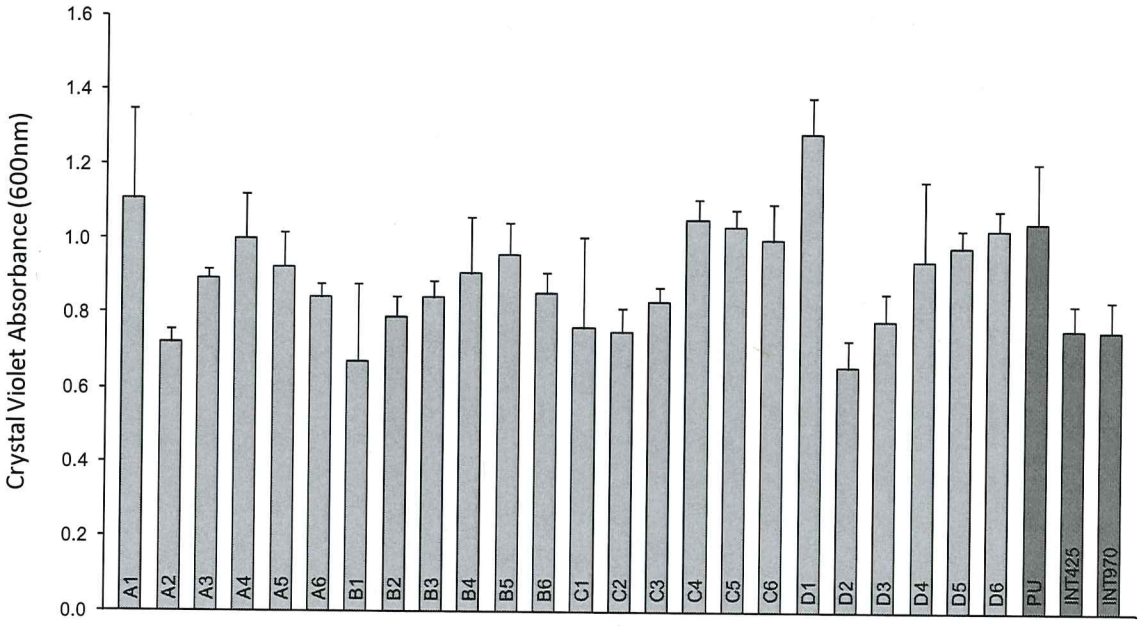

Figure 4.15. *H. pacifica* biofilm retention after forty two days preleach of amphiphilic acrylic-polyurethane coatings, polyurethane control, and commercial fouling-release. Error bars represent one standard deviation of the mean.

commercial fouling-release coatings showed a lower retention than most of the coatings except coatings A2, B1, C2, and D2, which are the coatings, formulated with lower molecular weight PDMS and smaller hydrophilic blocks.

Water jet adhesion of the *H. pacifica* biofilm was carried out after 24 hrs of bacterial biofilm growth. Each coating was jetted for 5 seconds at a pressure of 15 psi and then a new set of each coating was jetted at a pressure of 25 psi and biofilm adhesion is represented by percent removal. In Figure 4.16, *H. pacifica* cell percent removal for the coatings treated with a water jet pressure of 15 psi and 25 psi are shown. As previously reported in Chapter 3, *H. pacifica* had been known to adhere poorly to polyurethane. In Figure 4.16 the 15 psi water pressure percent removal values for the experimental coatings show that several coatings performed comparable or better than the commercial fouling-release coatings which had removal of 15% (Intersleek 425) and 25% (Intersleek 970), however, only coating B1 performed better than the polyurethane control (35% removal) with a 50% removal, this is likely due to coating B1 behaving as a PU correlating to the SE value of coating B1 being comparable to the SE literature value of PU.

A general trend that is observed from the 15 psi percent removal values is that if the coatings are separated into their respective groups (i.e.- A, B,C, and D) there is a increase in removal as the hydrophilic component is increased in the formulation, than once the coating formulations reach the oligomeric hydrophilic component the values decrease. There are a few experimental coatings that are exceptions, but overall that is the general trend. When the water jet pressure is

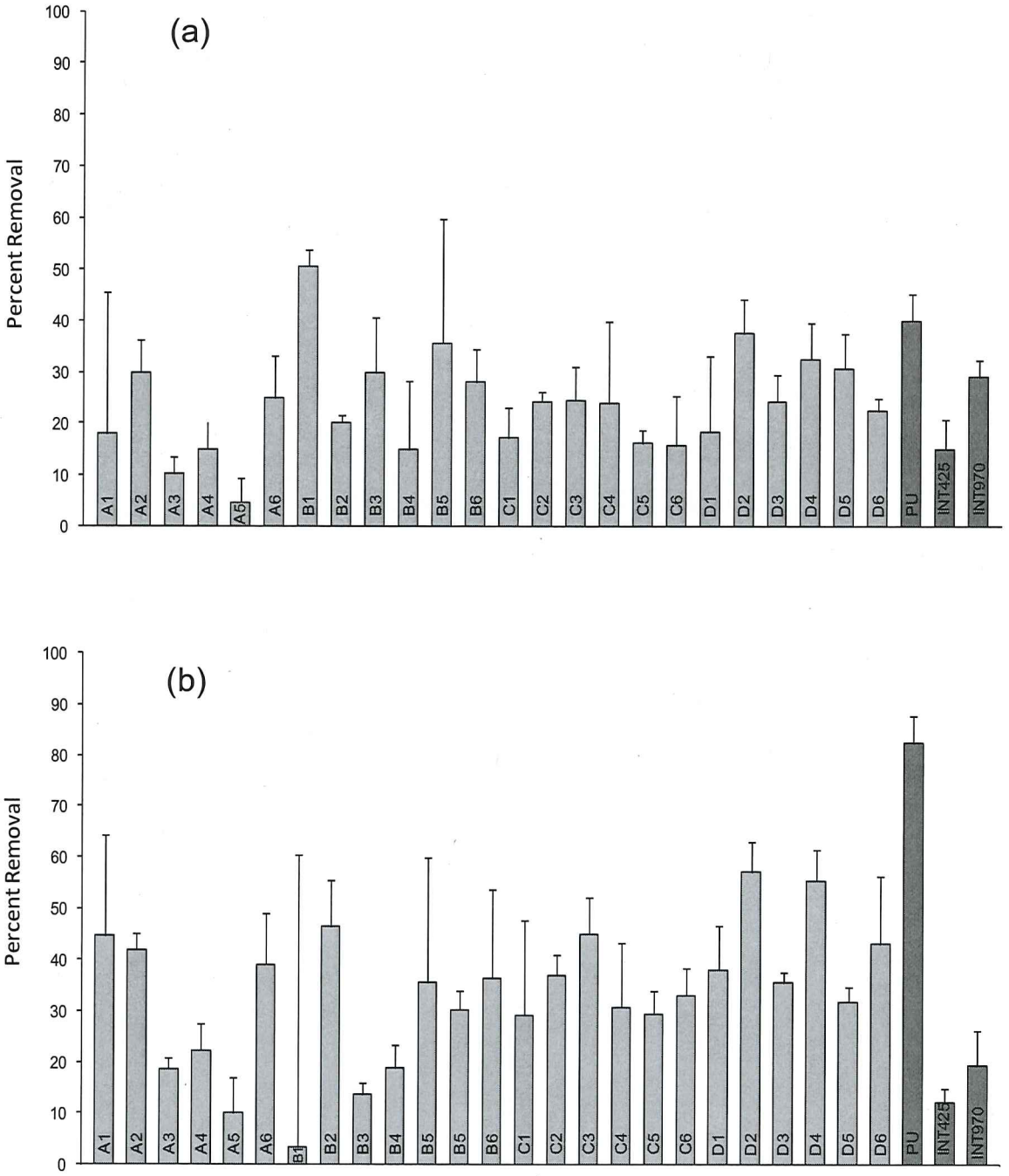

Figure 4.16. *H. pacifica* cell adhesion after forty two days preleach of amphiphilic acrylic-polyurethane coatings, polyurethane control, and commercial fouling-release coatings using water jet at (a) 15 psi and (b) 25 psi. Error bars represent one standard deviation of the mean.

increased to 25 psi the general trend that is seen with the 10 psi values still hold, the only difference is the increase in percent removal, which would be expected with a higher pressure. One interesting observation is the large percent removal with the polyurethane control, which agrees with previous reports of *H. pacifica* adhering poorly to polyurethane. Another observation made from the values from the 25 psi graph is that the commercial fouling-release coatings percent removal didn't change with the increase in water jet pressure; they stayed at 15% removal for Intersleek 425 and 25% removal for Intersleek 970. Overall, the coatings performed better or comparable to the commercial fouling-release coatings at both 10 psi and 25 psi water jet pressure, the best performers being the coatings formulated with the oligomeric hydrophilic components. With the exception of experimental coating B1, it seems that the SE of the coatings didn't have a large affect on the outcome of the percent removal of the biofilm since no real trend was seen comparing SE and removal of the biofilm.

Figure 4.17 illustrates the initial cell attachment of *N. incerta* algae was assessed before water jet adhesion analysis. Algae were diluted to an OD of 0.03 at 660 nm in artificial sea water (ASW) supplemented with nutrients. 1 ml was added to each well of the plate and allowed to incubate statically for 2 hours (cell attachment). Algal cell attachment was measured by fluorescence measurement of DMSO extracts. Attachment was reported as fluorescence intensity (relative fluorescence units). The coatings that showed better inhibition to cell attachment were A2, B6 and C1 when compared to the polyurethane control and commercial fouling-release coating standard Intersleek 970. All coatings inhibited cell

attachment better than the commercial fouling-release coating standard Intersleek 425.

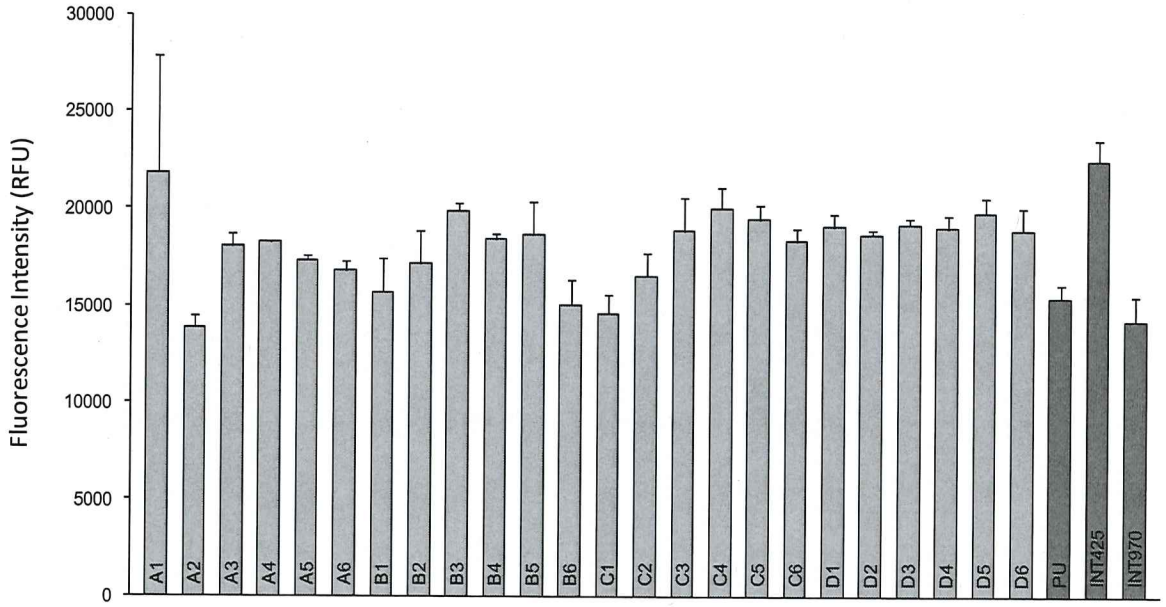

Figure 4.17. *N. incerta* initial cell attachment after forty two days preleach of amphiphilic acrylic-polyurethane coatings, polyurethane control, and commercial fouling-release. Error bars represent one standard deviation of the mean.

Water jet adhesion was carried out after 2hrs of initial cell attachment. The coatings were jetted for 10 seconds at a pressure of 10 psi and then a new set of each coating was jetted at a pressure of 20 psi. Algal adhesion was reported as the percent removal for each pressure indicated above. Figure 4.18 illustrates *N. incerta* cell adhesion after forty two days preleach of the amphiphilic acrylic-urethane coatings, polyurethane control, and commercial fouling-release coatings using water jet at (a) 10 psi and (b) 20 psi. Previous studies have shown that *N. incerta* attaches very well to PDMS and releases from polyurethane coatings. In Figure 4.16 (a), all of the coatings had better or comparable removal to the

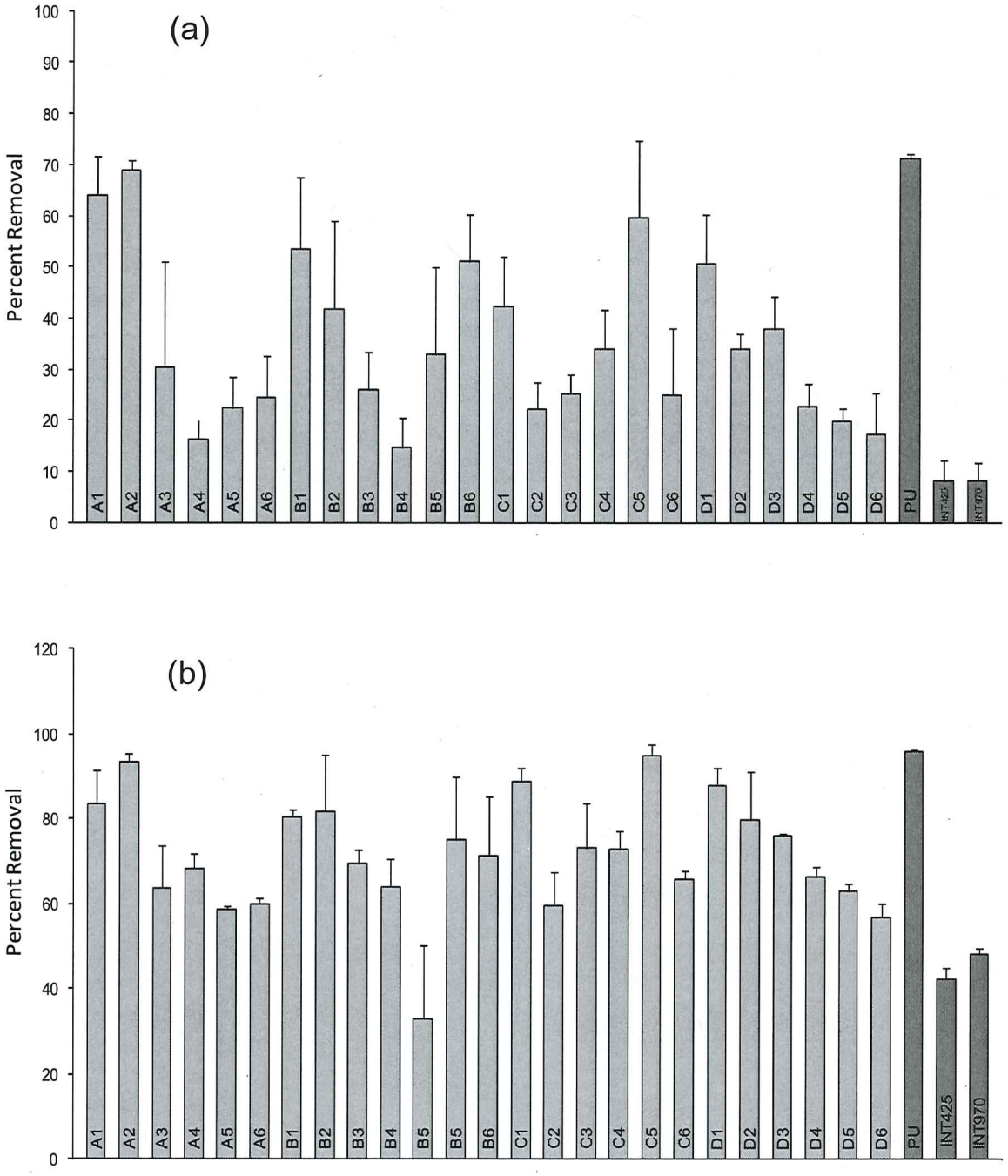

Figure 4.18. *N. incerta* cell adhesion after forty two days preleach of amphiphilic acrylic-polyurethane coatings, polyurethane control, and commercial fouling-release coatings using water jet at (a) 10 psi and (b) 20 psi. Error bars represent one standard deviation of the mean.

commercial fouling-release coatings; the polyurethane control performed the best at 10 psi water jet pressure with a removal of 75%. Experimental coatings, A1, A2 B1, B6, C5, and D1 performed better than the other coatings with removal all over 50%. Coating A2 preformed the best of all the coatings with cell removal of 70%.

A key trend that is observed is the decrease in removal as the higher molecular weight PDMS is formulated into the coatings which correlates with the reported SE values of those experimental coatings. Coatings labeled with a 2, 3, 4, 5, or 6 have PDMS. There are exceptions such as A2, B6, and C5, which all have PDMS incorporated into the formulation and show higher removal. These coatings however, had lower initial cell attachment, as illustrated in Figure 4.17, which would result in an observed removal percentage slightly higher. When the pressure was increased to 20 psi, as depicted in Figure 4.18 (b), the same trend is seen from the 10 psi graph only with an increased removal from all the coatings, especially those formulated with PDMS. Once again, all of the coatings statistically show removal better than commercial fouling-release coatings. The polyurethane control has the best removal of almost 100%, coatings A2 and C5 are comparable with removal of 96% and 98%, respectively. An interesting trend seen from the 20 psi water jet pressure is the coatings formulated with $OEGEMA_{475}$ (group D) show an almost linear decrease with increased molecular weight PDMS, this is in agreement with previous studies showing *N. incerta* attaches well to PDMS coatings. Overall, the experimental coatings performed better than the commercial fouling-release coatings and several coatings were

comparable to the polyurethane control even when the SE of the experimental coatings were comparable to PDMS.

Growth and release measurements of *Ulva* sporelings from the experimental coatings were conducted at the University of Birmingham, UK. The control coatings for the test were Intersleek 700 (IS 700) and Intersleek 900 (IS 900), Dow Corning Silastic-T2 (T2) and polyurethane (PU). Coatings were applied to 24-well microtiter plates (one coating per plate). The sample coatings were pre-leached at NDSU for 14 days. All 24-well plates were equilibrated in artificial seawater for 2 h in Birmingham, after leachate collection, before the start of the *Ulva* experiment. The *Ulva* spore inoculum was adjusted to 0.05 OD at absorbance 660 nm (5×10^5 spores ml^{-1}). Spores settled on the plates were grown for 8 days inside an illuminated incubator at 18°C with a 16:8 light: dark cycle (photon flux density 44 $\mu mol \cdot m^{-2} \cdot s^{-1}$) with renewal of nutrients every 48 hours. After 8 days growth, the plates were sprayed at 18 kPa, 67 kPa, 111 kPa, and 152 kPa impact pressure with the water spin-jet.

Leachate toxicity was performed on the coatings prior to the *Ulva* sporelings release measurements. After leaching the coatings in distilled water for 48 h, 1 ml of artificial seawater was added to one row of each coating (6 replicates) and plates were gently shaken (60 movements/min) for 18 h. One ml of each leachate was then deposited in a well of untreated Costar® 24-well plates. To each well, 1 ml *Ulva* spore solution adjusted to 5×10^5 spores ml^{-1} in double strength enriched seawater medium was added. The plates were incubated for 2 h in darkness at room temperature before being transferred to an illuminated

incubator at 18°C with a 16:8 light: dark cycle (photon flux density 44 $\mu mol \cdot m^{-2} \cdot s^{-1}$). After 7 days growth, the seawater medium was removed from the wells and the chlorophyll extracted from the attached biomass. The mean (6 replicates) percentage inhibition compared to a seawater control was calculated. The results of the leachate toxicity assay are depicted in Figure 4.19 in terms of sporeling inhibition. Results presented in Figure 4.19 show that there was some inhibition of the growth of *Ulva* sporelings when cultured in leachate from a number of the coatings. Leachates from coating D2 showed the greatest inhibition of growth at 70%, and 44% inhibition was seen for leachate from coating A4. Coatings A2, A3, A5, A6, C2, C4 and D1 all have 30 - 40% inhibition. Despite this, biomass on most of the coatings was statistically similar (Figure 4.20). A trend is seen with the experimental coatings consisting of MEOMA (the "A's"), where there is a linear increase in percent inhibition with an increase in the molecular weight of PDMS until the higher MW PDMS is used. Coatings in the B's statistically show no difference in percent inhibition. Also seen in Figure 4.19 is that as the PEG-based segment of the triblock is increased the average percent inhibition becomes more random. Coatings were only pre-leached at NDSU for 14 days rather than 30 days, which may account for the higher growth inhibition observed with these plates.

The mean amount of biomass on the test surfaces after 8 days growth is depicted in Figure 4.20. The RFU values are directly proportional to biomass. Sporeling biomass was similar on most of the control and test coatings, but particularly lower on coatings B2, C1, C2, D1 and D2.

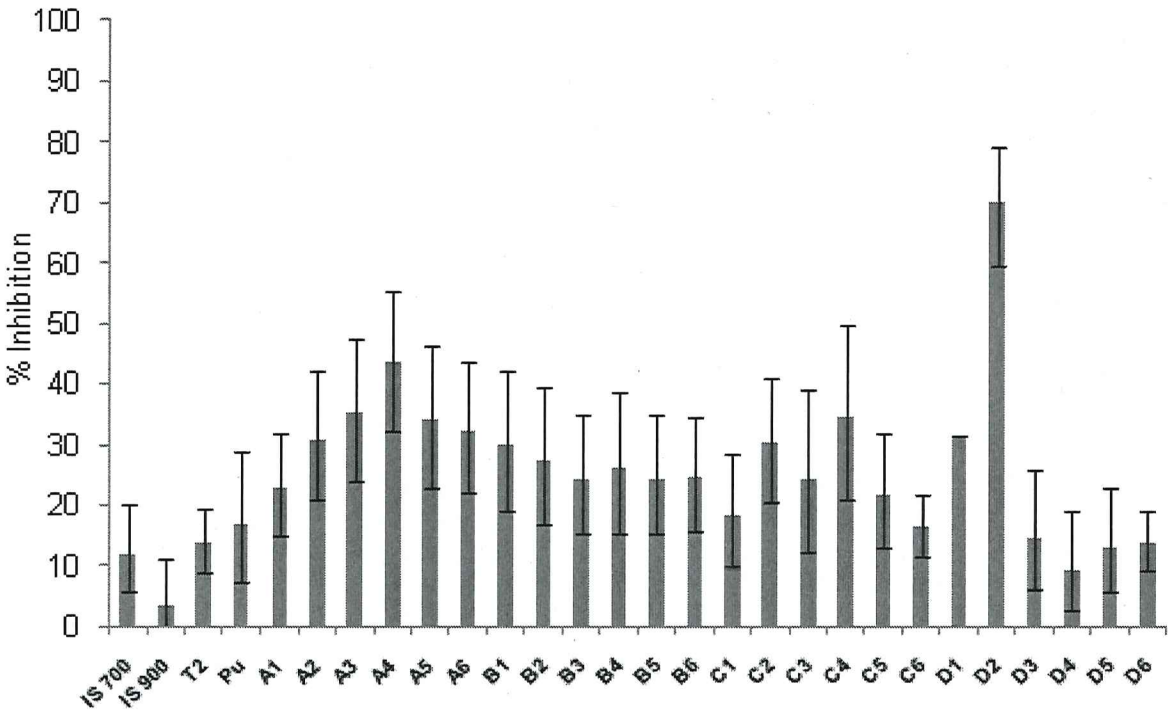

Figure 4.19. Percentage inhibition of *Ulva* sporeling growth in leachates collected over 18 hours on amphiphilic acrylic-polyurethane coatings, polyurethane control, commercial fouling release coatings and silicone standard. Each point is the mean of 6 replicates. Error bars show 95% confidence limits derived from arcsine transformed data.

Development of sporelings on this plate was checked microscopically and it was observed that the length of sporelings was much shorter than on the other test plates or standards. Images of the sporelings are presented in Figure 4.21.

The sporelings on D2 were significantly shorter when compared to the silicone control (T2). Coating C1 was used as an example of normal growth of sporelings. The problem that might arise from the smaller growth is the hydrodynamic removal of sporelings from D2 which may be affected since smaller plants generate lower hydrodynamic forces making them more difficult to remove.[49]

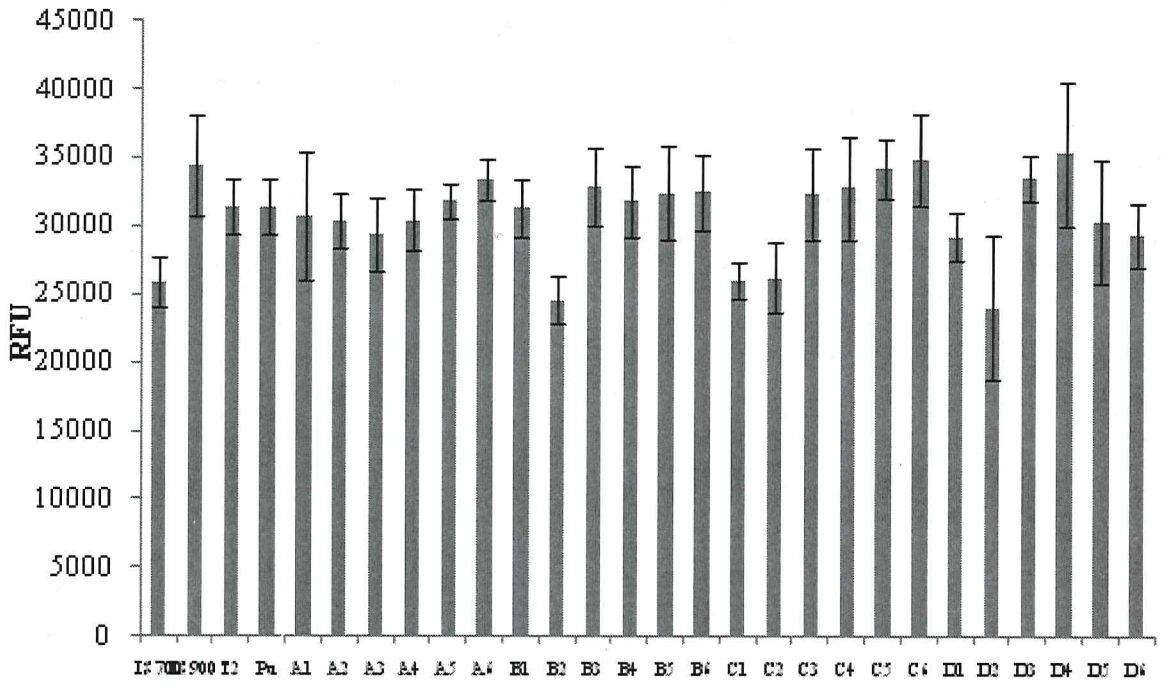

Figure 4.20. Biomass of *Ulva* sporeling before jetting presented as RFU values measured as extracted chlorophyll amphiphilic acrylic-polyurethane coatings, polyurethane control, commercial fouling release coatings and silicone standard. Each point is the mean of 6 replicates. Error bars show 95% confidence limits.

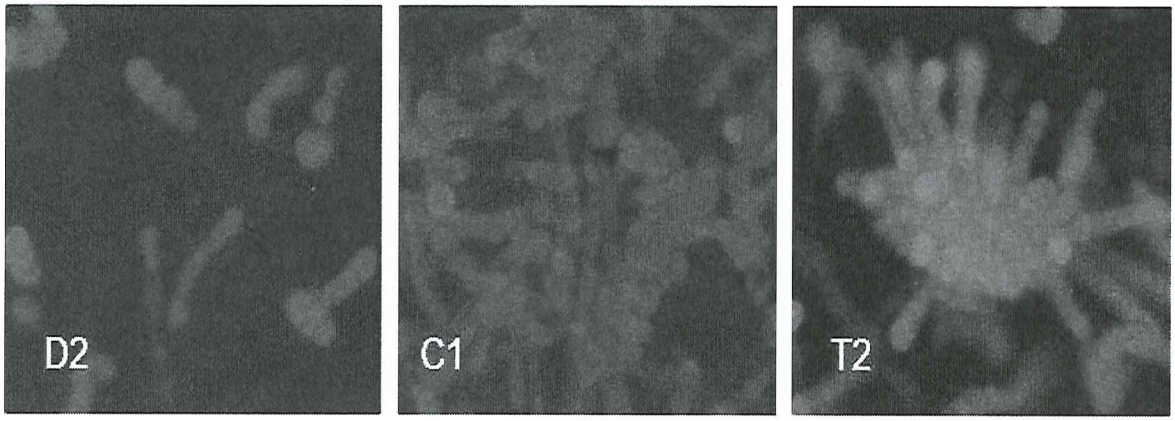

Figure 4.21. Growth of *Ulva* sporelings after 7 days on experimental coatings D2, C1, and Silicone control T2.

Percentage biomass removal after spin-jet washing at the highest pressure of 152 kPa impact pressure is illustrated in Figure 4.22. Coatings A3, A4, C1, D1,

and D6 showed the greatest removal (40-55%), which was comparable to Intersleek 700 and Intersleek 900. Interestingly, it seems that SE doesn't play a large factor in percent removal since A3 and A4 has SE that resembles PDMS and C1 and D1 SE are similar to PEG, so composition seems to be more important in overall percent removal. Coatings A3 and A4 had the highest percent removal of the sporelings, however, from Figure 4.19, A3, A4 and D1 had the highest percent of inhibition of *Ulva* sporelings which might lead to a higher observed percent removal. A general trend that is observed is that all coatings that were formulated with PDMS with a molecular weight of 3800 (coatings labeled with a 2) showed the highest average percent removal when compared to the other formulations. When taking into account the PEG-based component of the coatings, MEOMA, and the oligomeric PEG copolymers performed the best regardless of the molecular weight of the PDMS, this is because BAPTMDS, as well as the higher molecular weight PDMS showed similar *Ulva* sporeling percent removal. Coatings were analyzed for the barnacle reattachment assay after 14 days of water immersion and daily feeding with brine shrimp. A hand held digital force gauge, mounted to an automated stage, was used to measure the peak force of release for each barnacle (lbs). Adhesion strength in shear was calculated by dividing the measured force required to remove the barnacle by the basal area and reported in Megapascals (MPa). Each data point is the mean value of nine individual barnacle measurements. Error bars represent one standard deviation of the mean.

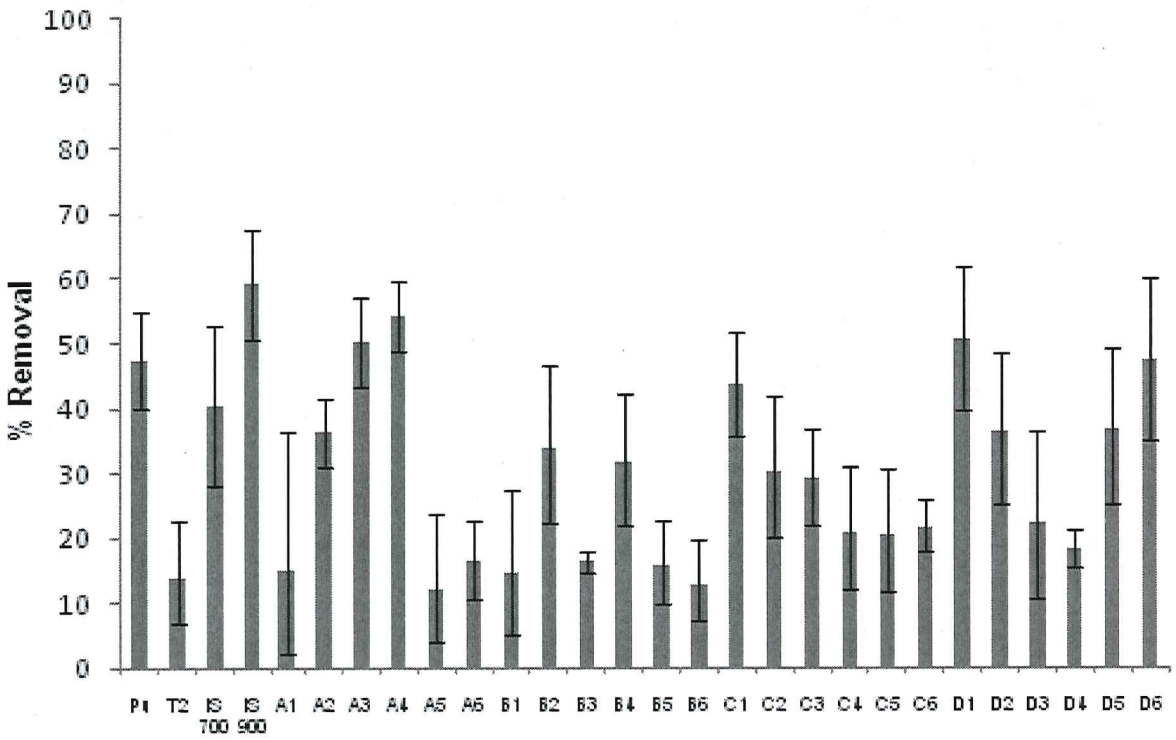

Figure 4.22. Percentage removal of *Ulva* sporelings after 8 days growth amphiphilic acrylic-polyurethane coatings, polyurethane control, commercial fouling release coatings and silicone standard using an impact pressure of 152 kPa with the water spin-jet. Each point is the mean of 6 replicates. Error bars show 95% confidence limits derived from arcsine transformed data.

In Figure 4.23, the ratio above each data point equals the number of measured barnacles to the number of broken barnacles. Broken barnacles indicate that the barnacle shell or baseplate broke or fractured before failure of the barnacle adhesive to the coating surface which is typical for poor fouling-release surfaces such as polyurethane. As illustrated in Figure 4.23, several experimental coatings failed the barnacle reattachment assay and all experimental coatings showed some amount of barnacle breakage. There is no real trend for the failures of the coatings since several examples from each formulation using PDMS and the PEG-based copolymers were unsuccessful in removal of the barnacles. It is

clearly evident from Figure 4.23 that only C6 showed barnacle removal adhesive force of 0.20 MPa, comparable to the silicone control (T2), nonetheless, only 2 barnacles were successfully removed from the coating. None of the coatings were comparable to the commercial fouling-release coatings, which had removal force of 0.05 MPa for IS 900, and 0.13 MPa for IS 700. Coatings A3, C6, and D5 demonstrated removal adhesive force better or comparable to the polyurethane control, with values ranging from 0.20-0.30 MPa, polyurethane adhesive force was 0.33 MPa. It is necessary to mention that coatings C6 and D5 had only 2 barnacles that were successfully removed from the coating, the polyurethane control had 1 barnacle that was successfully removed from the surface of the

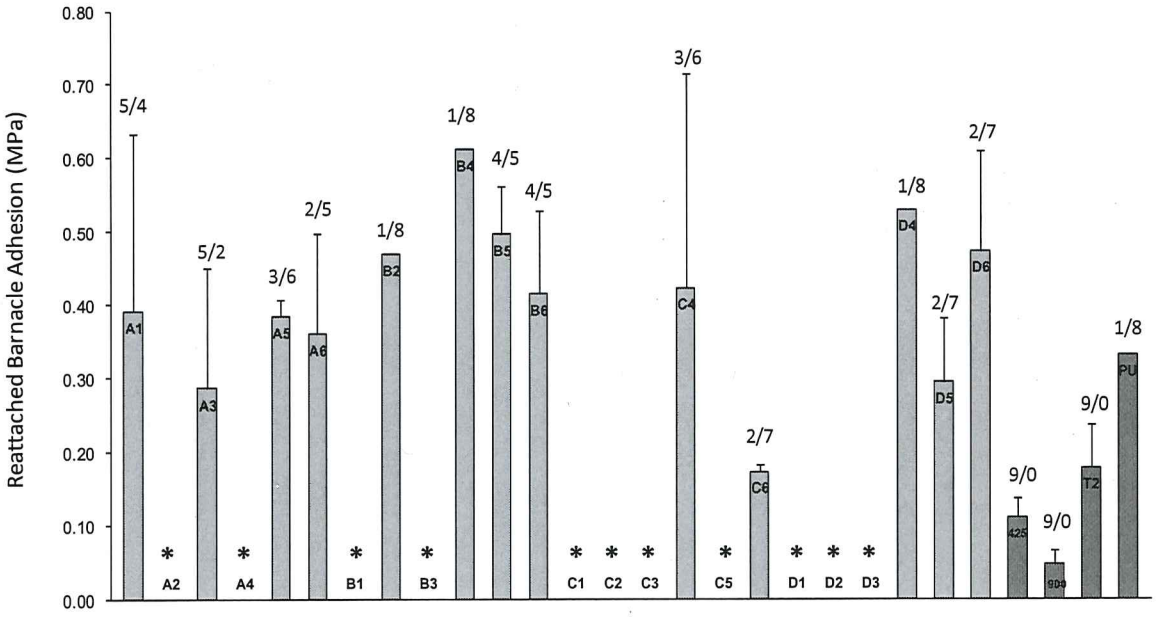

Figure 4.23. Reattachment barnacle adhesion of amphiphilic acrylic-polyurethane coatings, polyurethane control, commercial fouling-release coatings and silicone control coatings. Error bars represent one standard deviation of the mean. (*Asterisk indicates all 9 barnacles broke or fractured before failure of barnacle adhesive*)

coating. Overall, the coatings did not perform very well in the barnacle reattachment assay indicating that the surface of the amphiphilic coatings are not suited for the easy removal of barnacles.

4.4. Conclusions

The effects of amphiphilic copolymers based on PDMS molecular weight and the addition of PEG based polymer blocks on the properties of acrylic-urethane coatings were explored. Amphiphilic acrylic-urethane coatings were formulated, deposited, and screened for key properties. The key properties screened were surface energy, determined by contact angle measurements using water and methylene iodide and dynamic water contact angle (initial and after 30 days of water immersion), pseudo-barnacle adhesion properties, Coatings were generally stable and showed an increase in water contact angle following water immersion. AFM imaging showed the majority of the coatings contained micro tracks (ripple-like) formations on the surface. After water immersion the coatings, in general, had lower pseudo-barnacle adhesion due to possible surface rearrangement. Coatings were also evaluated against several marine bacteria (*H. pacifica, C. lytica*), barnacle reattachment (*A. amphitrite)*, diatom *N. incerta* bioassays, and *Ulva* sporelings. In general, the coatings formulated with higher molecular weight PDMS performed better or comparable to the commercial fouling-release coatings for the marine bacteria, diatom, and *Ulva* sporeling assays, especially using lower water jet pressure. The barnacle reattachment assay results showed the majority of the coatings were unsuccessful in removing the barnacles from the surface of the coatings without breaking and only a few had

removal values better or comparable to the silicone control. Overall, we were successful in synthesizing a library of amphiphilic copolymers that were formulated into acrylic-urethane coatings resulting in 24 amphiphilic polyurethane coatings for possible marine application.

4.4. References

1. Clark, E. A.; Sterritt, R. M.; Lester, J. N. *Environ. Sci. Technol.* **1988**, 22, 600-604.
2. Callow, M. E. *Biodeterioration Abstr.* **1996**, 10, 411.
3. Swain, G. E. *Paint Coatings Europe* **1999**, 18-25.
4. Vreeland, V.; Waite, J. H.; Epstein, L. *J. Phycol.*, **1998**, 34, 1.
5. Kamino, K.; Inoue, K. Maruyama, T.; Takamatsu, N. Harayama, S.; Shizuri, Y. *J. Biol. Chem.* **2000**, 275, 27360.
6. Stanley, M. S.; Callow, M. E.; Callow, J. A. *Planta*, **1999**, 210, 61.
7. Callow, J. A.; Callow, M. E.; Ista, L. K.; Lopez, G.; Chaudhury, M. K. *J. R. Soc. Interface* **2005**, 2, 319-325.
8. Smith, A.; Callow, J. A. Eds. *Biological Adhesives*. Springer: New York, 2006, 63-203, 257-279.
9. De Gennes, P.-G.; Brochard,-Wyart, F.; Quere. Capillarity: Deformable Interfaces. *Capillarity and Wetting Penomena*. Springer: New York, 2004.
10. Brady, R. F., Jr.; Singer, I. L. *Biofouling* **2000**, 16, 301-309.
11. Ekin, A.; Webster, D. C. *J. Polym. Sci., Part A: Polym. Chem.* **2006**, 44(16), 4880-4894.

12. Ekin, A.; Webster, D. C.; Daniels, J. W.; Stafslien, S. J.; Casse, F.; Callow, J. A.; Callow, M. E. *J. Coatings Tech. & Res.* **2007**, 4(4),435-451.

13. Majumdar, P.; Webster, D. C. *Macromolecules* **2005**, 38, 5857-5859.

14. Majumdar, P.; Webster, D. C. *Polymer* **2006**, 47, 4172-4181.

15. Schultz, M. P.; Finaly, J. A.; Callow, M. E.; Callow, J. A. *Biofouling* **2003**, 19 (Supplement), 17-26.

16. Chaudhury, M. K.; Finlay, J. A.; Chung, J. Y.; Callow, M. E.; Callow, J. A. *Biofouling*, **2005** 21, 41-48.

17. Holland, R.; Dugtale, T. M.; Wetherbee, R., Brennan, A. B.; Finaly, J. A.; Callow, J. A.; Callow, M. E. *Biofouling* **2004**, 20, 323-329.

18. Terlizzi, A.; Conte, E.; Zupo, V.; Mazzella, L. *Biofouling*, **2000**, 15, 327-342.

19. Brady, R. F. Jr. *Prog Org. Coat.* **1999**, 35, 31-35.

20. Schmidt, D. L.; Brady, R. F. Jr.; Lam, K. L.; Schmidt, D. C.; Chaudhury, M. K. *Langmuir* **2004**, 20, 2830-2836.

21. *Gudipati, C.S., Finlay, J.A.,* Callow, J.A., Callow, M.A., Wooley, K.L. *Langmuir **2005**, 21, 3044-3053.*

22. Pullin, R. A.; Nevell, T. G.; Tsibouklis, J. *Matter. Lett.* **1999**, 39, 142-148.

23. Curtis, A.; Wilkinson, C. *Biochem. Soc. Symp.* **1999**, 65, 15-26.

24. Granhag, L. M.; Finlay, J. A.; Jonsson, P. R.; Callow, J. A.; Callow, M. E. *Biofouling* **2004**, 20, 117-122.

25. Hoipkemeier-Wilson, L.; Schumacher, J. F.; Carman, M. L; Gibson, A. L.; Feinberg, A. W.; Callow, M. E.; Finaly, J. A.; Callow, J. A.; Brennan, A. B. *Biofouling* **2004**, 20, 53-63.

26. Berglin, M.; Lönn, N.; Gatenholm, P. *Biofouling* **2003**, 19 (Supplement.), 63-69.

27. Brady, R. F., Jr.; Singer, I. L. *Biofouling* **2000**, 15, 73-81.

28. Stein, J.; Truby, K.; Darkangelo-Wood, C.; Takemori, M.; Vallance, M.; Swain, G.; Kavanagh, C.; Kovach, B.; Schultz, M.; Wiebe, D.; Holm, E.; Monemarano, J.; Wendt, D.; Smith, C.; Meyer, A. *Biofouling* **2003**, 19, 87-94.

29. Pieper, R. J. PhD. Dissertation, Chapter 3, North Dakota State University, 2010.

30. Majumdar, P.; Ekin, A.; Webster, D. C. *ACS Symposium Series* **2007**, 957, 61-75.

31. Verkholantsev, V.; Flavian, M. *Prog.Org. Coat.* **1996**, 29(1-4), 239-246.

32. Vink, P.; Bots, T. L. *Prog.Org. Coat.* **1996**, 28(3), 173-181.

33. Benjamin, S.; Carr, C.; Walbridge, D. J. *Prog.Org. Coat.* **1996**, 28(3), 197-207.

34. Carr, C.; Wallstoem, E. *Prog.Org. Coat.* **1996**, 28(3), 161-171.

35. Walbridge, D. J. *Prog.Org. Coat.* **1996**, 28(3), 155-159.

36. Webster, D. C.; Bennett, J.; Kuebler, S.; Kossuth, M. B.; Jonasdottir, S. *JCT Coatings Tech.* **2004**, 1, 34-39.

37. Webster, D. C. *JCT Coatings Tech.* **2005**, 2, 24-29.

38. Michael, A. *J. Prakt. Chem.* **1887**, 35, 379.

39. Bergmann, E. D.; Gingberg, D.; Pappo, R. *Org. React.,* **1959**, 10, 179.

40. Owens, D.K.; Wendt, R.C. *Journal of Applied Polymer Science* **1969**, 13 (8), 1741-7.

41. Chisholm, B.J.; Webster, D.C.; Bennett, J.W.; Berry, M.; Christianson D.A.; Kim, J.; Mayo, B.; Gubbins, N.J. *Rev. Sci. Instr.* ***2007,*** **78**, 072213.

42. Cassé, F.; Stafslien, S.J.; Bahr, J.A.; Daniels, J.; Finlay, J.A.; Callow, J.A.; Callow, M.E. *Biofouling* **2007**, 23 (2), 121-130.

43. Stafslien, S.J.; Daniels, J.; Mayo, B,; Christianson, D.; Chisholm, B.; Ekin, A.; Webster, D.C.; Swain, G. *Biofouling* **2007**, 23(1/2), 45-54.

44. Cassé, F.; Ribeiro, E.; Ekin, A.; Webster, D.C.; Callow, J.A.; Callow, M.E. *Biofouling* **2007**, 23 (3/4), 179-192.

45. van Oss, C. J.; Good, R. J.; Busscher, H. J. *J. Disp. Sci. Tech.* **1990**, 11, 75.

46. Childs, M. A.; Yasar, B.; Suzer, S.; Baysal, B. M. *Langmuir* **1997**, 13, 5484-5493.

47. van Oss, C. J.; Chaudhury, M. K.; Good, R. J. *Adv. Coll. Interface Sci.*, **1987**, 28, 35.

48. Vargo, T. G.; Hook, D. J.; Gardella, D. J. Jr.; Eberhardt, M. A.; Meyer, A. E.; Baier, R. E. *J. Polym. Sci., Part A: Polym. Chem.* **1991**, 29, 535-545.

49. Finlay, J. A.; Fletcher, B. R.; Callow, M. E.; Callow, J. A. *Biofouling* **2008**, 24(3), 219-225.

50. Fang, H.; Feng, L.; Wu, L. *Chinese J. Polym. Sci.* **2009**, 27(3), 327-334.

CHAPTER 5. DESIGN, FORMULATION, AND CHARACTERIZATION OF ZWITTERIONIC/AMPHIPHILIC PENTA-BLOCK COPOLYMER ACRYLIC-POLYURETHANE COATINGS

5.1. Introduction

The rapid, undesirable accumulation of biofouling on marine surfaces is well-known[1] and has required the use of efficient antifouling coating systems. Currently, research efforts are now being expended on developing various environmentally friendly alternatives.[2-7] As described in Chapter 3, to date, the most effective nonbiocidal commercially available technologies are fouling-release coatings based on siloxane elastomers.[7-11] More recently, researchers have incorporated polydimethylsiloxane into polyurethanes. These coatings made use of a self-stratifying mechanism in which the low surface energy PDMS preferentially migrated to the surface of the coating whiles the bulk of the coating remained as the polyurethane. These PDMS-based coatings performed well with some species, such as *Ulva*, which were easily removed from hydrophobic surfaces,[12-13] however others, such as diatoms showed strong adhesion to hydrophobic surfaces.[14-15] Because of this, it appears that a single substrate chemistry cannot be utilized alone in designing multipurpose marine coatings for all forms of biofouling, including *Ulva* and diatoms.[16] A great deal of effort has been made to battle this problem with use of amphiphilic substances that are designed to have both hydrophobic and hydrophilic moieties on one compound. They have gain popularity for use in non-fouling biomaterials based on the idea that surfaces with amphiphilic compounds will form nanoscale heterogeneities, creating a surface topography that is unsuitable for the proliferation and adsorption

of proteins and marine micro-foulers.[17-29] Chapter 4 described the design of a chemically bound amphiphilic copolymer comprised of PEG-based monomers and PDMS and subsequently formulated into polyurethane coatings with the idea that these coatings would self-stratify.

However, in addition to PEG-based materials, it has also been recognized in the research community that zwitterionic based materials are also commonly used as nonfouling materials because of their protein resistance properties.[30-38] One type of zwitterionic material that belongs to the polybetaine polymers is sulfobetaine polymers, in which both cationic and anionic groups are on the same monomer residue.[39] It is believed that the nonfouling properties of a surface are from their functional groups and their surface packing.[20,22,30] Chang and coworkers designed diblock copolymers with fixed polypropylene backbones and a range of chain lengths of polysulfobetaine synthesized via atom transfer radical polymerization (ATRP). The copolymers were absorbed on to methyl (CH_3) - terminated self-assembled monolayers (SAM) and nonspecific protein absorption was compared.[30] In another study done by Cheng and coworkers long chain poly(SBMA) were grafted on to SAMs via ATRP and studied for long term and short term protein adsorption as well as biological evaluation of SAMs surface properties over time. These new materials make it possible to develop environmentally benign, effective, durable, and low-cost zwitterionic-based ultralow fouling coatings. It should be pointed out that previous studies have focused on materials and surfaces to resist nonspecific protein adsorption from single-protein solutions or human plasma. However, controlling biofouling in

marine environments poses great challenges because of the variety of fouling organisms, the complexity of the environment, and the need for a long-life coating.

In this work, zwitterionic/amphiphilic (z/a) pentablock copolymers were prepared using a series of reactions including Michael Addition and ATRP. The general structure of the amphiphilic copolymer illustrated in Figure 5.1, was the product of reacting a PEG-functionalized monoacrylate with PDMS in a 2:1 ratio via Michael Addition reaction. In general, the PEG functionalized acrylate reacts with an amine terminated siloxane via nucleophilic addition at the primary amine site of the siloxane and the unsaturated carbonyl of the acrylate. Thus, the

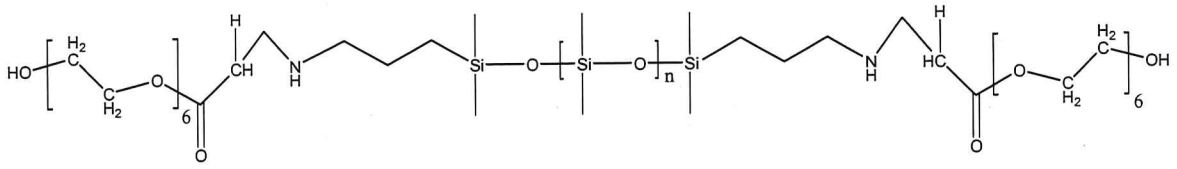

Figure 5.1. General structure of amphiphilic copolymer comprised of a middle block of PDMS and side blocks of PEG-based acrylate monomer.

resulting pentablock copolymer contains a secondary amine linker between each block which can be used as a crosslinking site when formulated into the polyurethane coatings.

The amphiphilic copolymer was reacted further to form the macroinitiator for the ATRP synthesis by bromoination of the hydroxy end groups. Figure 5.2 depicts the general structure of the amphiphilic macroinitiator.

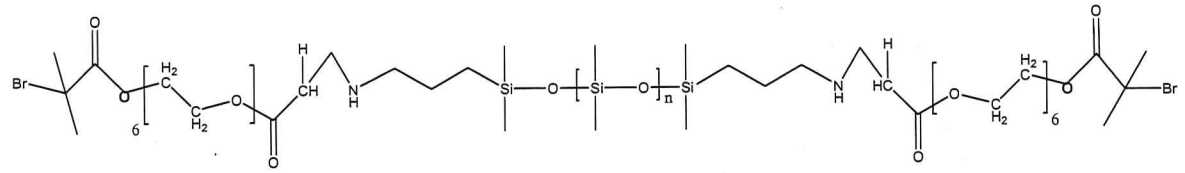

Figure 5.2. General structure of the amphiphilic macroinitiator.

Figure 5.3 illustrates the general structure of the z/a pentablock copolymer which was prepared by the ATRP of the PDMS-PEO-BR macroinitiator and SBMA monomer. The illustration depicts the reaction sites for the Michael addition as well as the ATRP synthesis. Three different shapes represent the three reacting components of the pentablock copolymer. The shapes are triangles, circles and squares for SBMA, APT-PDMS polyethylene glycol monoacrylate, respectively.

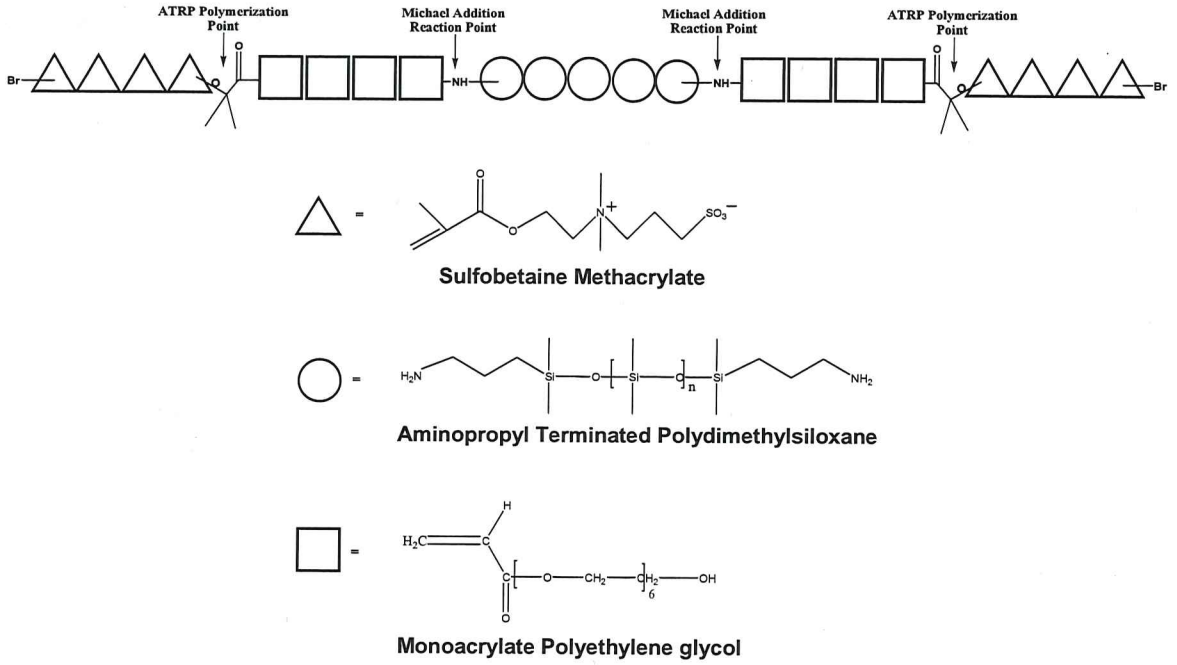

Figure 5.3. Illustration showing atom transfer radical polymerization reactants and zwitterionic/amphiphilic pentablock copolymer product.

It is challenging to design a practical coating system for underwater use that contains either polyethylene oxide or poly(SBMA). Typically, the coating is too hydrophilic and swells excessively when immersed in water. Excessive swelling results in a coating that has poor mechanical properties, thus not providing the durability needed for the coating application.

The objective of this preliminary study was to incorporate the z/a pentablock copolymer into an acrylic-polyurethane coating and determine if the coating system undergoes a self-stratification mechanism similar to the siloxane acrylic-polyurethane system. Since the components of the z/a pentablock are chemically bound, the low surface energy PDMS segment will carry the other segments up to the surface separating into a z/a top layer and a tough, durable polyurethane lower layer. The amount of z/a copolymer was based on 10% siloxane (from the pentablock) by weight per experimental coating. Therefore, 4 experimental coatings were designed to explore the effects on the addition of z/a pentablock copolymers on the coatings fouling-release properties using a combinatorial workflow consisting of automated characterization systems.[40-42]

The final coatings were screened based on their initial surface properties, pseudobarnacle adhesion properties, and their performance was evaluated against several bioassays including marine bacteria (*H. pacifica, C. lytica*), barnacle reattachment (*A. amphitrite)* and a diatom, *N. incerta*.

5.2. Experimental

5.2.1. Chemicals and reagents

Amino propyl terminated polydimethylsiloxanes (APT-PDMS) with average molecular weight of 875 (A-11) and 3000 (A-15) were purchased from Gelest, Inc. and used as received. Polyethylene glycol monoacrylate (Bisomer PEA6) was obtained from Cognis and used as received. [2-(Methacryloyloxy) ethyl] dimethyl-(3-sulfopropyl) ammonium hydroxide, sulfobetaine (SBMA, 97%), 2-bromoisobutyryl bromide (BIBB, ≥97%), 2,2'-bipyridine (Bpy, ≥99%), ethyl 2-

bromoisobutyrate (EBIB, 98%), methyl 2-bromopropionate (MBP, ≥99.5%) and triethylamine were purchased from Aldrich and used as received. Tetrahydrofuran (THF, 99.8%), toluene (purified, 99.5%), and N-methyl pyrrolidone (NMP) were purchased from VWR and used as received. Methanol (MeOH, 98%) was obtained from VWR and degassed prior to reaction. Alloy 102 copper beads were obtained from McMaster-Carr. An acrylic polyol composed of 80% butyl acrylate and 20% 2- hydroxyethyl acrylate was prepared by solution polymerization, as reported in Chapter 3. n-Butyl acrylate (BA), and 2-hydroxyethyl acrylate (HEA) were obtained from Aldrich. The free radical initiator, 2-azobis (2-methylbutanenitrile) (Vazo 67) was obtained from DuPont. Dibutyl tin diacetate (DBTDAc) and 2,4-pentanedione were purchased from Aldrich. IDT (Tolonate IDT 70B, 70% in butyl acetate) isocyanate was received from Rhodia. IDT is a triisocyranurate resin of isophorone diisocyanate. Polyurethane grade methyl n-amyl ketone (MAK) was supplied by Eastman Chemical. Dow Corning T-2 Silastic and DC was received from Ellsworth Adhesives. DC and T2 Silastic were solvent reduced with MIBK and used as silicone controls. Intersleek ®700 and ®900 were obtained from International Paint Ltd and used as the fouling-release controls. The polyurethane (PU) standard was composed of polycaprolactone and polyisocyanate and was used as a standard for the bioassays.

5.2.2. Amphiphilic copolymer synthesis and characterization

The typical protocol for the amphiphilic copolymer synthesis was as follows. A simple Michael Addition reaction[44-45] was carried out using calculated amounts of APT-PDMS (PDMS, MW 875 and 3000) and Bisomer PEA6 monomer based on

a reaction ratio of 2:1 (PEG:PDMS). The reagents were dispensed into 20 mL glass vials, capped, heated to 90°, and stirred via magnetic stirring overnight. ^{1}H Nuclear Magnetic Resonance (NMR) spectroscopy measurements were done using a Varian Unity/Inova-400NB (400-MHz) NMR spectrometer coupled with an autosampler accessory. The sample concentration was 25 mg/ml and D_2O was used as the solvent. Data acquisition was done using 16 scans with a 0.3 s delay time.

5.2.3. Synthesis and characterization of macroinitiator

The typical amphiphilic macroinitiator synthesis was as follows. The amphiphilic copolymer was dissolved in THF at 0°C in the presence of triethylamine in a round bottom flask in an ice bath. BIBB was added to an addition funnel along with THF (1:10 molar eq.), fitted to the RB flask, and added dropwise over 30 minutes. A white gas was evolved which was most likely hydrogen bromide (HBr), but with the addition of Et_3N acting as a base the HBr combined with the Et_3N to form the salt triethylamine hydrobromide (triethylammonium bromide). The resulting mixture was stirred for an additional 12 hours at 20°C. The final product was purified by extraction with 1% NaCl and H_2O three times and dried in a vacuum oven overnight. The dried product was characterized by Fourier Transform Infrared (FTIR) spectroscopy was performed using a Bruker Vertex 70 with HTS-XT accessory. The samples (3%w/w) were prepared in DI water, 5-µl samples were deposited on a 96-position silicon wafer using an Eppendorf pipette and placed in an oven at 80 °C to evaporate the solvent. The samples were run in absorbance mode with a resolution of 4 cm^{-1}

and 6 scans per sample. The absence of the -OH band confirms the successful completion of the macroinitiator.

5.2.4. ATRP synthesis of zwitterionic/amphiphilic copolymer

A typical protocol for the ATRP synthesis of the z/a copolymer using PDMS-PEA6-Br macroinitiator was as follows. The macroinitiator (2.46 g, 0.8 mmol), SBMA (4g, 0.8 mmol, target DP_n=18) and methanol (7500 µL) were added to a 4oz. glass jar. The mixture was stirred for 5 minutes with a magnetic stir bar to allow for the macroinitiator to go into solution. 4 Cu beads were then added to the jar and the Bpy solution (0.6247 g in 25 mL MeOH) was dispensed into the jar. The polymerization components for the ATRP synthesis are described in Table 5.1. In Table 5.1, the A-11 Cu beads (column 1-4) and the A-15 Cu Beads (column 5 and 6) are polymerizations of the same pentablock copolymer. The pentablock copolymers were combined for the formulations due to the amount of respective pentablock copolymer that was needed per formulation. The first two columns (A-11 Cu Bead) were the initial ATRP polymerizations using Cu beads, after the successful initial polymerizations, the respective ATRP polymerizations were done on a larger scale to allow for more product which in turn would allow for a larger quantity of coating formulations. The z/a pentablock copolymer ATRP polymerizations were performed at room temperature for 16 h. After polymerization the product was washed with MeOH to remove any residual monomer and rotovaped and placed in the vacuum oven overnight to remove any remaining MeOH. The z/a pentablock copolymers were also synthesized with the catalyst copper bromide instead of copper beads following the similar reaction

protocol as above; the amounts of the polymerization components using CuBr are shown in Table 5.1. Several variations of the ATRP polymerization of the z/a copolymer were performed and designated by a batch. As illustrated in Table 5.1, Batch 1 and 2 used the macroinitiator synthesized using commercial APT-PDMS with a MW of 875 (A-11) using a copper bead as the ATRP catalyst. Batch 1 and 2 were the initial ATRP polymerization and were performed on a small-scale. The initial ATRP polymerization was successful and subsequently Batch 3 and 4 were simply a scaled-up synthesis of batch 1 and 2. Batch 5 and 6 used commercial APT-PDMS with a MW of 3000 (A-15) for the macroinitiator and used copper beads as the catalyst for the scaled-up ATRP polymerization. Batch 7 had the same composition as batch 4, but copper bromide was used as the ATRP catalyst. Similarly, batch 8 had the same composition as batch 6, but used copper bromide as the ATRP catalyst.

Table 5.1. Polymerization components for atom transfer radical polymerization of zwitterionic/amphiphilic pentablock copolymer.

	Batch 1	**Batch 2**	**Batch 3**	**Batch 4**	**Batch 5**	**Batch 6**	**Batch 7**	**Batch 8**
SBMA, g	2	2	4	4	4	4	4	4
A-11 Macroinitiator, g	0.62	0.64	2.475	2.41	0	0	2.41	0
A-15 Macroinitiator, g	0	0	0	0	5.88	5.88	0	5.88
No. of Cu Beads	1	1	4	4	4	4	0	0
CuBr-Bpy, mL	0	0	0	0	0	0	10	10
Bpy, mL	10	10	10	10	10	10	0	0
MeOH, mL	30	30	30	30	30	30	30	30
Total, mL	40	40	40	40	40	40	40	40

The final product was characterized using ^{1}H NMR (400 MHz, D_2O). NMR peak assignments (ppm): 0.1, CH3, -Si(C)C; 1.85, CH2, -Si(=O)(=O), Np (C)C; 1.9, CH, -C(=O)OR; 2.65, CH2, -Si(=O)(=O), -C; 2.7, CH3, -Np(C)C; 2.8, NH; CH2, -O-C. The final product was also characterized using FTIR. Key absorbencies are observed at (cm^{-1}): 3441, NH; 2963, CH; 1727, C=O; 1196, Si-O; 1040, SO_3^-, and 964, C-O, indicative of the groups expected to be present in the final z/a pentablock copolymer product.

5.2.5. Solvent compatibility study for zwitterionic/amphiphilic copolymer

A solvent compatibility study was done on the z/a product in order to find a suitable solvent or solvent blend that dissolved or partial dissolved the product so it could be added to the coating formulation. For the study, 0.05 g of the z/a product was added to an 8 ml glass vial to which 2 ml of the respective solvent was added. The mixture was magnetically stirred at room temperature initially and then at an elevated temperature of 50 °C overnight. A large selection of solvents, which varied in polarity, were used as possible candidates for the solubility study and are depicted in Table 5.2 along with their respective dielectric constants. Solvents with dielectric constants with less than 15 are generally considered to be nonpolar. Those solvents with dielectric constants greater than 15 are generally considered polar and can be further divided into protic and aprotic. Protic solvents are solvents that solvate anions (negatively charged solutes) strongly via hydrogen bonding. Formic acid, acetic acid and ethanol are examples protic solvents. Aprotic solvents such as acetone, THF, DMF, and DMSO tend to have large dipole

moments (separation of partial positive and partial negative charges within the same molecule) and solvate positively charged species via their negative dipole.[46]

Table 5.2. Solvents and dielectric constants used in the solubility study for zwitterionic/amphiphilic pentablock copolymers.

Solvent	Dielectric Constant
Hexane	1.9
Ethyl 3-Ethoxypropionate (EEP)	2.4
Butyl Acetate	5.0
Methyl n-Amyl Ketone (MAK)	11.6
Dimethylformamide (DMF)	38
Ethanol	30
Acetic Acid	6.2
Formic Acid	58
Sulfuric Acid (97%)	8.6
Acetonitrile	37.5
Tetrahydrofuran (THF)	7.5
Acetone	21
Toluene	2.4
Dimethyl Sulfoxide (DMSO)	46.7
n-Methylpyrrolidone (NMP)	32.2

After each solvent was tried the results of the study were described as either not soluble, partially soluble, or soluble.

Table 5.3 illustrates the solvent blend successful in solubilizing the z/a pentablock copolymer. The solvent compatibility of the z/a pentablock copolymer consisted of a 5:1 ratio of toluene and NMP, respectively. The z/a pentablock copolymer was weighted out into glass 20 mL vials and the appropriate amounts of solvent were added to the vials. The mixture was allowed to stir magnetically overnight at 45 °C and continued stirring until needed for formulation.

Table 5.3. Solvent Compatible Mixtures for zwitterionic/amphiphilic pentablock copolymers.

	A-15 Cu Bead	A-15 CuBr	A-11 Cu Bead	A-11 CuBr
Pentablock Copolymer, g	0.7	0.7	2.42	2.42
Toluene, mL	4.15	4.15	2.86	2.86
NMP, mL	0.83	0.83	0.6	0.6

5.2.6. Formulation of zwitterionic/amphiphilic pentablock coatings.

Table 5.4 lists the polyurethane coating formulations containing the zwitterionic/ amphiphilic penta-block copolymer. Designation of the batches are as follows: for the Batch 1 coating formulation, the pentablock copolymer used the macroinitiator synthesized from the A-15 commercial APT-PDMS and Cu bead as the ATRP catalyst, batch 2 used the same APT-PDMS (A-15), but instead used CuBr for the ATRP catalyst, batch 3 formulation used commercial A-11 APT-PDMS and Cu bead was used as the catalyst, and batch 4 used A-11 APT-PDMS and CuBr as the catalyst. A control formulation not containing the pentablock copolymer was prepared and is labeled "acrylic-urethane". The dispensing of all components for the coating formulations was done using an Eppendorf repeat pipette. The ratio of isocyanate to other functional groups (amine or hydroxyl) was kept at 1.1:1.0. The amount of catalyst DBTDAc was 0.075% on solids, and the amount of pentanedione varied from 10-15% based on solids and reactivity of the specific coating sample. All coatings were prepared by adding the z/a pentablock copolymer from Table 5.4 into the formulation.

Table 5.4. Zwitterionic/amphiphilic pentablock polyurethane coatings formulations.

	Batch 1	Batch 2	Batch 3	Batch 4	Acrylic-polyurethane
Acrylic Polyol (20% HEA, 80% BA, 50% solids), mL	1.8	1.8	3.5	3.5	8.75
XIDT 70B(70% solids), mL	2.2	2.2	1.5	1.5	3.75
DBTDAc (0.001% in MAK), mL	0.2	0.2	0.2	0.2	0.25
Pentablock Copolymer-solvent, mL	5.68	5.68	5.88	5.88	0
Pentanedione	0.75	0.75	0.75	0.75	1.875

The z/a pentablock copolymer polyurethane coatings were formulated by first adding the non-reactive compounds into a glass 20 mL vial. The non-reactive components consisted of the acrylic polyol (50% solids in toluene), pentanedione, and the z/a pentablock copolymer solvent mixture (25% solids). The non-reactive components were stirred by magnetic stirring for 30 minutes at room temperature. The reactive components (isocyanate, 70% solids and DBTDAc) were added to the 20 mL vial and stirred for 30 minutes. An additional hour was allowed for an adequate viscosity for drawdowns. The coatings were drawdown on full panels (one coating per panel) with a wet film thickness of 8mils.

5.2.7. Zwitterionic/amphiphilic pentablock coatings deposition

The coating formulations were drawndown on standard 4"x8" aluminum panels (4"x8", Q-panel, 0.6 mm thickness, type A: alloy 3003 H14) and aluminum panels with Intergard 264 primed surface at a wet thickness of 8 mils. The formulations were also dispensed on stamped primed aluminum panels, and 24-well microtiter plates for further characterization. After completion of the application of all the coatings, the panels were allowed to ambient cure overnight

in dust free drying racks. After the overnight cure, the panels were placed in ovens at 80 °C for one hour, after compete cure they were placed back into the drying racks until needed for further testing and characterization

5.2.8. Zwitterionic/amphiphilic pentablock coatings characterization

The Symyx surface energy system measures and averages contact angles of various liquids and calculate the surface energy. The system receives a 4"x8" coated panel. The images of three droplets of each test liquid are taken by a CCD camera, and the static contact angles are determined using automated image analysis. Water and methylene iodide (MI) are used as test liquids, and the surface energies are calculated using the Owens-Wendt method.[47] Dynamic contact angles with water and MI were measured with the same automated surface energy measurement unit. Advancing contact angle was measured by dispensing additional liquid over a droplet of liquid placed on the surface. Receding contact angle was measured during the withdrawing of the liquid. Liquids were dispensed and aspirated at a rate of 0.2 µl/sec.

The Symyx pull-off adhesion system was used for the pseudo-barnacle pull-off adhesion analysis.[48] The adhesion system can be used to either determine the adhesive strength of a coating on the substrate or the adhesive strength of an epoxy to the coating surface (pseudo-barnacle). The instrument can receive two 4X8 inch coating array panels. First, the two array panels were placed onto the holders of the adhesive application system by applying a vacuum underneath the panels. Then, a plastic template was placed on top of the coatings using pins on the substrate holder for alignment. The plastic sheets have three 7 mm diameter

holes over each coating on the array panel. Then Loctite Hysol® Epoxy 1C-LV glue was spread on the coatings through the custom made plastic sheets, resulting in the placement of three 7-mm spots of adhesive on each coating. The plastic sheet was removed and the panels were removed from the adhesion preparation station and placed into clamping jigs. After the panels were clamped, three aluminum studs per coating sample were placed into the clamping jig on top of the applied glue. Weighted foam blocks were placed on top of the studs and the epoxy glue was cured overnight. The next day, the clamped panels with the holders still attached to them were placed into the holders of the automated adhesion system. A pull-off head removes each test stud and the maximum force at failure is recorded and saved in a database. The three values are then averaged.

5.2.9. Evaluation with the marine bacterium *Cellulophaga lytica*

Bacterial analysis was carried out after 14 and 28 days of water immersion. Leachate toxicity was assessed by introducing the bacterium into overnight extracts (artificial sea water with nutrients (ASW)) of each coating and evaluating growth after 24 hours via a crystal violet colorimetric assay. Growth in coating leachates was reported as an absorbance ratio (600 nm) to a growth control.

A series of negative growth controls (medium + bacteria + triclosan) was also included in the analysis. [TC15= triclosan 15 μg, TC6= 6 μg, and TC3= 3 μg.] *C. lytica* biofilm retention and retraction analysis was assessed by a crystal violet colorimetric assay. A 5% suspension of *C. lytica* in ASW + nutrients (~107 cells.ml^{-1}) was prepared and 1ml was added to each well of the coating plate. Plates were incubated statically at 28 °C for 24 hours to facilitate bacterial

attachment and colonization. Plates were rinsed three times with DI water and stained with crystal violet. Images were taken after staining, and then the crystal violet was extracted in 33% acetic acid and the resulting eluates were measured for absorbance at 600nm. Biofilm retention was reported as the mean absorbance value of three replicate samples. Biofilm retraction was assessed by determining percent coverage calculations from digital images taken of each coating plate using an automated software tool. Biofilm retraction was reported as the mean percent coverage value of three replicate samples.

5.2.10. Evaluation with the marine bacterium *Halomonas pacifica*

Bacterial analysis was carried out after 14 and 28 days of water immersion. Leachate toxicity was assessed by introducing bacterium into overnight extracts (artificial sea water with nutrients) of each coating and evaluating growth after 24 hours via a crystal violet colorimetric assay. Growth in coating leachates was reported as an absorbance ratio (600 nm) to a growth control. A negative growth control (medium + bacteria + triclosan) was also included in the analysis. *H. pacifica* biofilm retention analysis was assessed by a crystal violet colorimetric assay. A 10% suspension of *H. pacifica* in ASW + nutrients (~108 cells.ml^{-1}) was prepared and 1ml was added to each well of the coating plate. Plates were incubated statically at 28 °C for 24 hours to facilitate bacterial attachment and colonization. Plates were rinsed three times with DI water and stained with crystal violet. Images were taken after staining, and then the crystal violet was extracted in 33% acetic acid and the resulting eluates were measured for absorbance at 600nm. Biofilm retention was reported as the average crystal violet absorbance

value of three replicate samples. Water jet adhesion was carried out after 24 hrs of bacterial biofilm growth. The first column of each plate was not treated and served as the measure of biofilm growth before water jetting. The second and third column of each coating was jetted for 5 seconds at a pressure of 15 psi and 25 psi, respectively. Biofilm adhesion was reported as the percent removal for each pressure indicated above.

5.2.11. Evaluation with the marine microalgae *Navicula incerta*

Algal analysis was carried out after an overnight pre-equilibration in artificial sea water. Leachate toxicity was assessed by introducing algae into overnight extracts (artificial sea water with nutrients) of each polymer and evaluating growth after 48 hours via fluorescence of chlorophyll. Growth in polymer leachates was reported as a fluorescence ratio to a growth control. A series of negative growth controls (medium + bacteria + triclosan) was also included in the analysis. For the assessment of biofilm growth, algae were diluted to an OD of 0.03 at 660 nm in ASW supplemented with nutrients. 1 ml was added to each well of the plate and allowed to incubate statically for 48 hours. Algal biofilm growth was determined by fluorescence measurement of DMSO extracts. Biofilm growth was reported as fluorescence intensity (relative fluorescence units). Water jet adhesion was carried out after 24 hrs of algal cell growth. The first column of each plate was not treated and served as the measure of cell growth before water jetting. The second and third column of each coating was jetted for 5 seconds at a pressure of 15 psi and 25 psi, respectively. Algal cell attachment was reported as the percent removal for each pressure indicated above.

5.2.12. Evaluation with the marine fouling barnacle *Amphibalanus amphitrite.*

Adult barnacles were allowed to attach to sample coatings surfaces for two weeks. Coatings were analyzed after 2 weeks of water immersion and daily feeding of the barnacles with brine shrimp. A hand held digital force gauge, mounted to an automated stage, was used to measure the peak force of release for each barnacle using the protocols described in ASTM D5618-94. Adhesion strength in shear was calculated by dividing the measured force required to remove the barnacle by the basal area and reported in megapascals (MPa). Each data point is the mean value of nine individual barnacle measurements.

5.2.13. Evaluation with the marine algae *Ulva linza* sporelings leachate toxicity, growth and removal.

Biological screening involving *Ulva linza* was completed at the University of Birmingham, U.K. For the *Ulva* sporelings study microtiter plates were leached in a recirculating distilled water tank fitted with a carbon filter for a total of eight weeks and placed in seawater to equilibrate two hours before the start of the experiment. Three replicate microtiter plates were incubated in trays with a suspension of *Ulva* zoospores for three hours in the dark.[13, 49-50] After washing to remove unattached zoospores, the panels with settled spores were cultured in enriched sea water for 7 days. After 7 days, the settled spores had germinated and the surface of the panels was covered with young plants. The panels were subjected to impact pressures of 18 kPa, 67 kPa, 111 kPa, and 152 kPa from a water jet [47], percentage removal was estimated visually.

After leaching the coatings in distilled water for 48 h, 1 ml of artificial seawater was added to one row of each coating (6 replicates) and plates were gently shaken (60 movements/min) for 18 h. One ml of each leachate was then deposited in a well of untreated Costar® 24-well plates. To each well, 1 ml *Ulva* spore solution adjusted to 5 x 10^5 spores ml^{-1} in double strength enriched seawater medium was added. The plates were incubated for 2 h in darkness at room temperature before being transferred to an illuminated incubator at 18°C with a 16:8 light: dark cycle (photon flux density 44 $\mu mol.m^{-2}.s^{-1}$). After 7 days growth, the seawater medium was removed from the wells and the chlorophyll extracted from the attached biomass. The mean (6 replicates) percentage inhibition compared to a seawater control was calculated. Chlorophyll was determined in a Tecan plate reader.

5.3. Results

The general objective of this study was to explore a practical and clever design of a fouling-release coating having a zwitterionic/amphiphilic surface. More specifically, this was a preliminary study to determine if self-stratification can be used to generate a novel robust coating with a z/a surface.

The experiment started with the design and subsequent synthesis of the amphiphilic triblock copolymer. The synthesis of the amphiphilic triblock copolymers, described in scheme 5.1, consisted of the reaction of the PEG functionalized acrylate with the amine terminated siloxanes via nucleophilic addition using the Michael Addition reaction. Since the primary amine is a good nucleophile it easily adds to the alpha, beta unsaturated carbonyl of the

methacrylate under mild conditions. The resulting triblock copolymer has both the hydrophobic properties of the PDMS and the hydrophilic properties of the PEG-based acrylate providing a chemically bonded triblock copolymer that has unique amphiphilic characteristics.

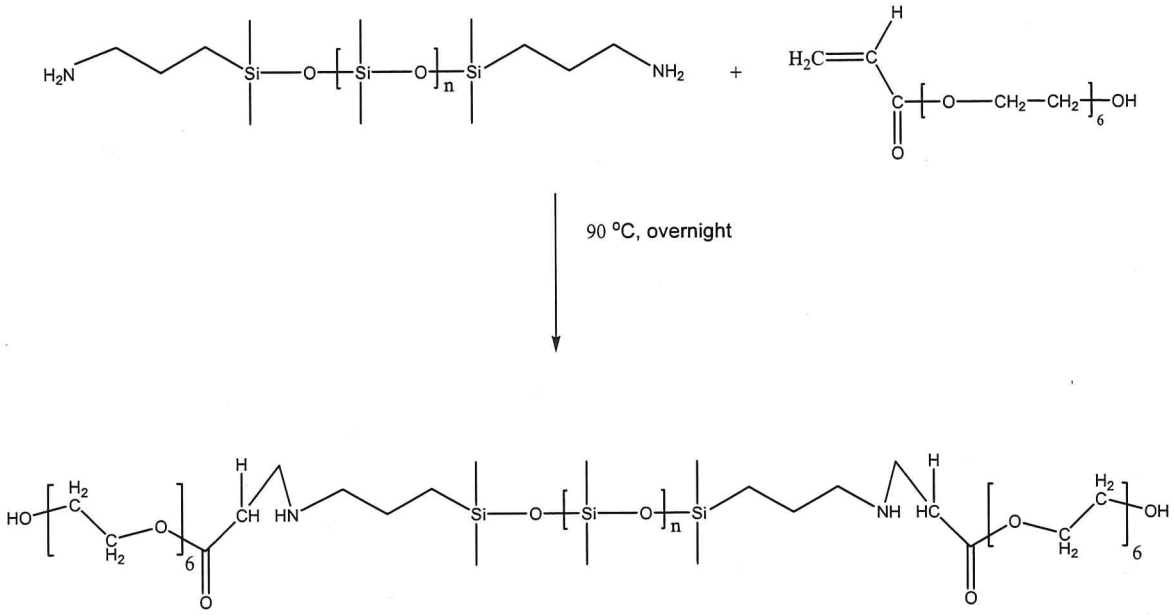

Scheme 5.1. Reaction scheme for Michael Addition of APT-PDMS and Polyethylene glycol Monoacrylate.

Characterization of the amphiphilic triblock copolymer was completed by ^{1}H NMR. Figure 5.4(a) depicts the initial reaction mixture of the APT-PDMS and Bisomer PEA6 components. The NMR spectrum from the beginning of the reaction clearly shows the presence of the 1-ethylene peaks from the PEG-based acrylate and the protons adjacent to the primary amines on the APT-PDMS.

The completion of the Michael addition reaction was illustrated in Figure 5.4(b) by the disappearance of the two doublets and the triplet of the 1-ethylene peaks, as well as, the protons adjacent to the primary amines on the APT-PDMS.

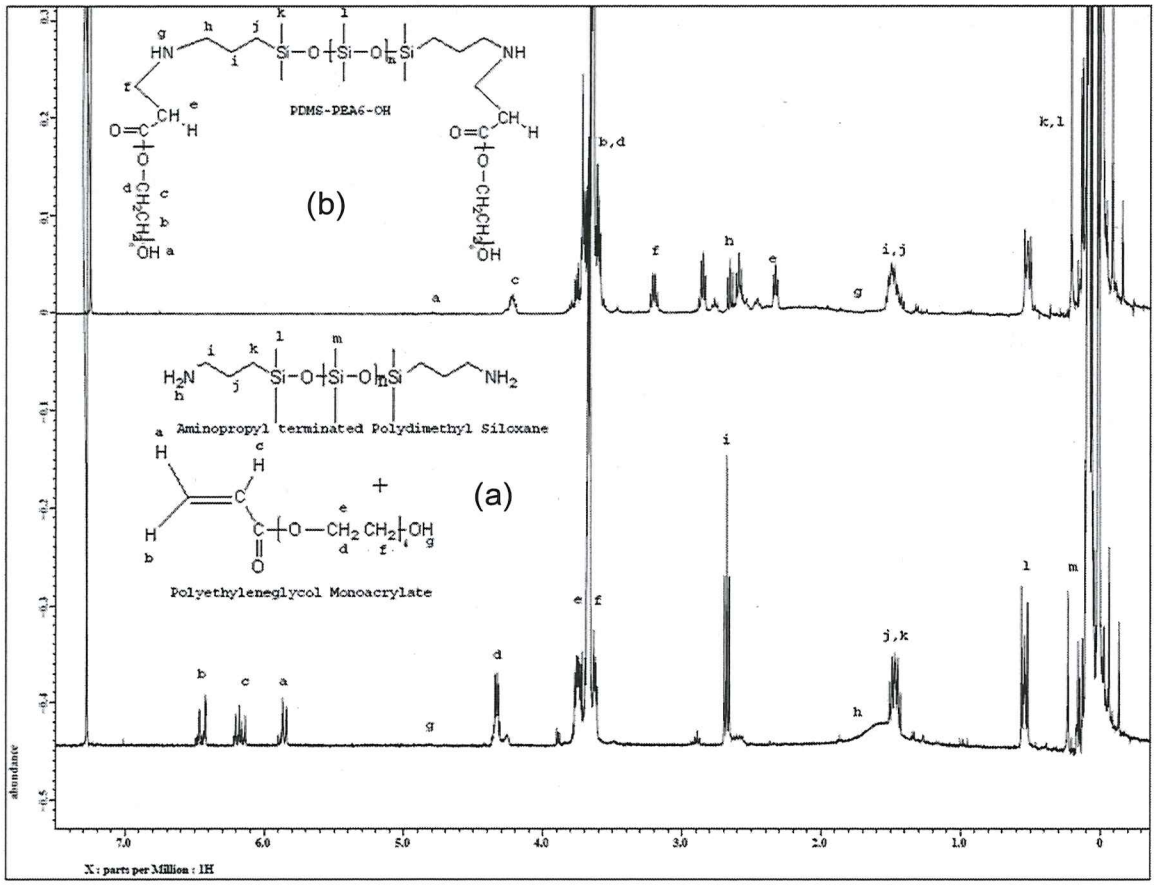

Figure 5.4. ^{1}H NMR spectrum of (a) beginning of Michael Addition reaction of amino propyl terminated polydimethylsiloxane and polyethylene glycol monoacrylate and (b) completion of Michael Addition reaction.

In addition, the appearance of the protons adjoining to the secondary amine on the APT-PDMS and the carbonyl of the PEG-based acrylate further demonstrates the completion of the Michael Addition reaction and the successful synthesis of the amphiphilic copolymer.

As previously described in section 5.2.3, the amphiphilic copolymer was further reacted to form the amphiphilic macroinitiator. Illustrated in Scheme 5.2, the general reaction where the macroinitiator was synthesized by a halogenation

reaction where the amphiphilic copolymer product from the Michael Addition reacted with BIBB in the presence of THF and triethylamine at 0°C.

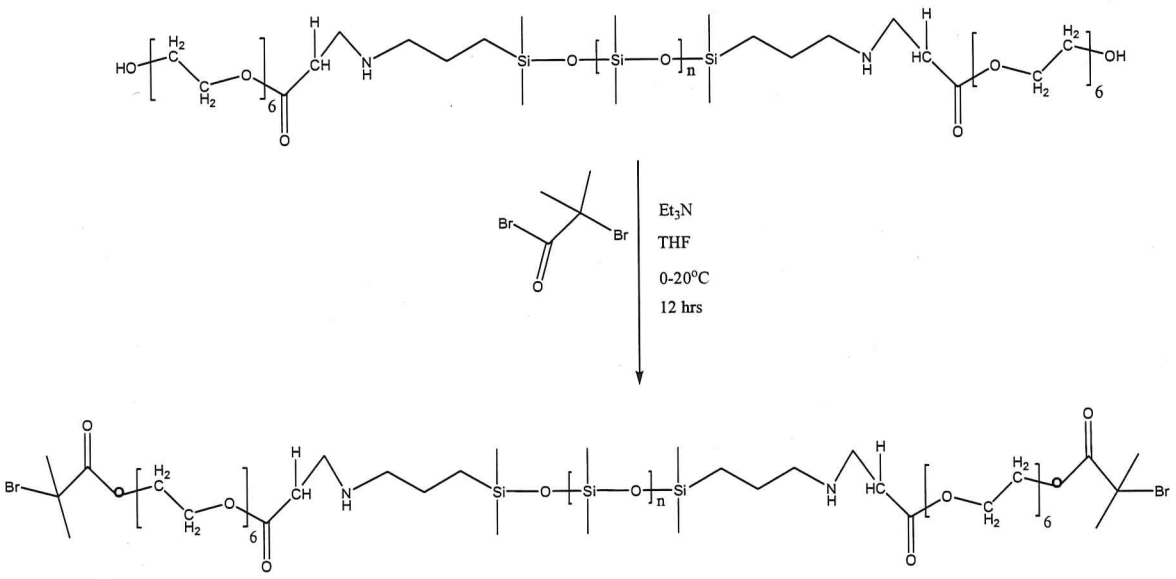

Scheme 5.2. Reaction scheme for the macroinitiator synthesis of polydimethylsiloxane-polyethylene glycol with 2-bromoisobutyryl bromide.

The z/a pentablock copolymers were then synthesized by ATRP using the difunctional macroinitiators. It should be pointed out that because of the problems and concerns with polymer purification and removal of the more common copper catalysts used in ATRP polymerizations;[51-59] Cu beads were used for this study.[60] As a control, copper bromide was also used in additional ATRP polymerization of the z/a pentablock copolymer. The z/a pentablock copolymer ATRP polymerization was performed at room temperature for 16 hrs. After completing of the ATRP polymerization the product was washed with MeOH to remove any residual monomer and rotovaped and placed in the vacuum oven overnight to remove any remaining MeOH. The final product was a light green colored grainy

solid. The target molecular weight for the z/a pentablock copolymer was calculated to 5000 kDa. Figure 5.5 illustrates the general structure of the final z/a pentablock copolymer.

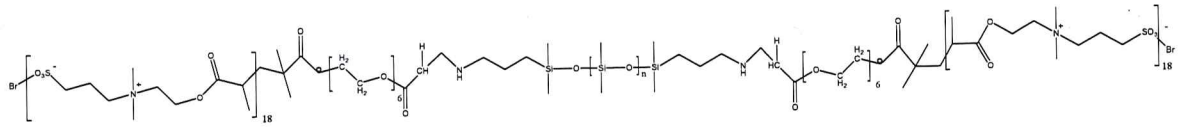

Figure 5.5. General structure of the target zwitterionic/amphiphilic pentablock copolymer.

The structure of the target z/a pentablock shows the hydrophobic PDMS middle block, the hydrophilic PEG-based acrylate blocks adjoined via the secondary amine junction to the PDMS block, and the zwitterionic polySBMA block adjoined via the methyl isobutyryl junction to the PEG-based acrylate blocks. Through the process of multiple reactions, the final z/a pentablock copolymer was successfully polymerized.

The final product was characterized using FTIR and the spectrum is illustrated in Figure 5.6. Key absorbencies are observed at (cm^{-1}): 3441, NH; 2963, CH; 1727, C=O; 1196, Si-O; 1040, SO_3^-, and 964, C-O, indicative of the groups expected to be present in the final z/a pentablock copolymer product.

The final product was also characterized using ^1H NMR (400 MHz, D_2O). NMR peak assignments (ppm): 0.1, CH3, -Si(C)C; 1.85, CH2, -Si(=O)(=O), Np (C)C; 1.9, CH, -C(=O)OR; 2.65, CH2, -Si(=O)(=O), -C; 2.7, CH3, -Np(C)C; 2.8, NH; CH2, -O-C. The absorbencies and peak assignments by FTIR and ^1H NMR, respectively, confirms the successful polymerization of the z/a pentablock copolymer.

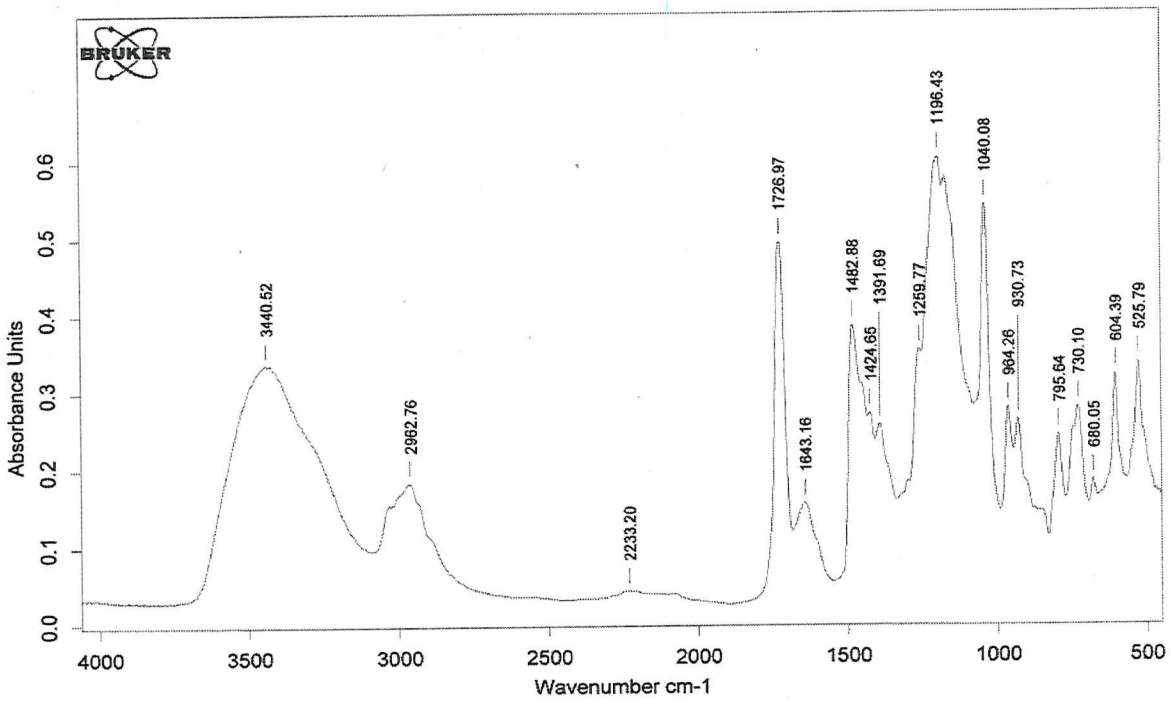

Figure 5.6. FTIR spectra of zwitterionic/amphiphilic pentablock copolymer product.

Due to the difficulty of finding a suitable solvent(s) that solubilize the z/a product, gel permeation chromatography (GPC) could not be completed due to the lack of the z/a product being soluble in THF (THF is the mobile phase of the GPC).

Because of the chemical complexity of the z/a pentablock copolymer, a suitable solvent or solvent blend that dissolved or partial dissolved the product had to be prepared. Since the final product was a grainy solid it had to be dissolved in a solvent/blend in order to utilize it in the formulation of the polyurethane coatings. Small amounts of the pentablock copolymers were added to 15, 8 ml vials and 2 ml of each respective solvent were added to the separate vials. The vials were stirred magnetically at room temperature for 4 hrs and then heated to 50°C overnight. Table 5.5 illustrates the solvents used in the study and the solubility

result. As the results show, most solvents were unable to solubilize the z/a pentablock copolymer regardless if the solvent was polar or nonpolar.

Table 5.5. Solvent solubility results for zwitterionic/amphiphilic pentablock copolymers

Solvent	Solubility Result
Hexane	Not soluble
Ethyl 3-Ethoxypropionate (EEP)	Not soluble
Butyl Acetate	Not soluble
Methyl n-Amyl Ketone (MAK)	Not soluble
Dimethylformamide (DMF)	Not soluble
Ethanol	Not soluble
Acetic Acid	Not soluble
Formic Acid	Not soluble
Sulfuric Acid (97%)	Not soluble
Acetonitrile	Not soluble
Tetrahydrofuran (THF)	Not soluble
Acetone	Not soluble
Toluene	Partially soluble
Dimethyl Sulfoxide (DMSO)	Not soluble
n-Methylpyrrolidone (NMP)	soluble

It was found that the z/a pentablock copolymer was fully soluble in NMP, a polar aprotic solvent. However, using NMP in coatings is problematic since the low volatility with a boiling point of 202-204 °C would make it difficult to fully remove the NMP from the coating during the curing process. However, toluene, a nonpolar solvent, also had partial solubility of the z/a product. From the solvent compatibility study, it was determined to use a solvent combination of NMP and toluene.

The solvent combination used a ratio of 5:1 (toluene: NMP), this was found to be the minimum amount of NMP in addition to toluene, that could successfully solubilize the product. For the formulations of the z/a polyurethane coatings, the appropriate amounts of the solvent and z/a pentablock copolymer, previously described in Table 5.3, were weighed out and added to 20 ml glass vials and magnetically stirred at 45°C. The mixture continued to stir at elevated temperatures until needed for the formulation.

As previously described, the z/a pentablock copolymers were incorporated into acrylic-polyurethane coatings based on a 10% load of siloxane by weight per experimental coating depicted in Table 5.4. The resulting 4 unique z/a pentablock acrylic-polyurethane experimental coatings were then applied to substrates and were characterized after ambient curing overnight and heat curing at 80°C for one hour.

The experimental coatings that were prepared were screened for their surface energy using contact angle measurements, dynamic water contact angle, and pseudo-barnacle adhesion, as well as biological screening including *C. lytica*, *H. pacifica*, *N. incerta*, *Ulva linza*, and *A. amphitrite* to check their performance with marine organisms to help understand these systems better and make a correlation between analytical techniques and biological screening.

To better understand the bioassays graphical results on this coating system Table 5.6 illustrates the z/a pentablock acrylic-polyurethane coatings and the polyurethane control coating formulations abbreviated by the numbers on the

bioassay graphs. Coatings were preleached for two weeks and four weeks, represented on the graphs by a -2 or -4, respectively.

Table 5.6. Description of zwitterionic/amphiphilic polyurethane formulations abbreviations as represented on subsequent graphs of performance properties.

Label on Graphs	1	2	3	4	5
APT-PDMS (MW)	A-15 =3000	A-15 =3000	A-11 =950	A-11 =950	X
ATRP Initiator	Cu Bead	CuBr	Cu Bead	CuBr	X
polySBMA Block Length	5000 MW	5000 MW	5000 MW	5000 MW	X
					Acrylic-Urethane Control

The z/a pentablock acrylic-polyurethane coatings were characterized using static water contact angle measurements. As shown in Figure 5.7, most of the pentablock copolymer polyurethane coatings show a hydrophobic nature with water contact angles greater than 90°.

The high water contact angle tends to indicate that the surface is enriched with PDMS. This possibly indicates that by chemically bonding the protein resistant zwitterionic/amphiphilic moiety to the low surface energy PDMS component, the PDMS component self-stratified to the coating surface bringing the z/a component to the surface as well. However, even with the complexity of the z/a copolymer, the hydrophobic PDMS segment leads to the WCA of the experimental coatings ≥90°C.

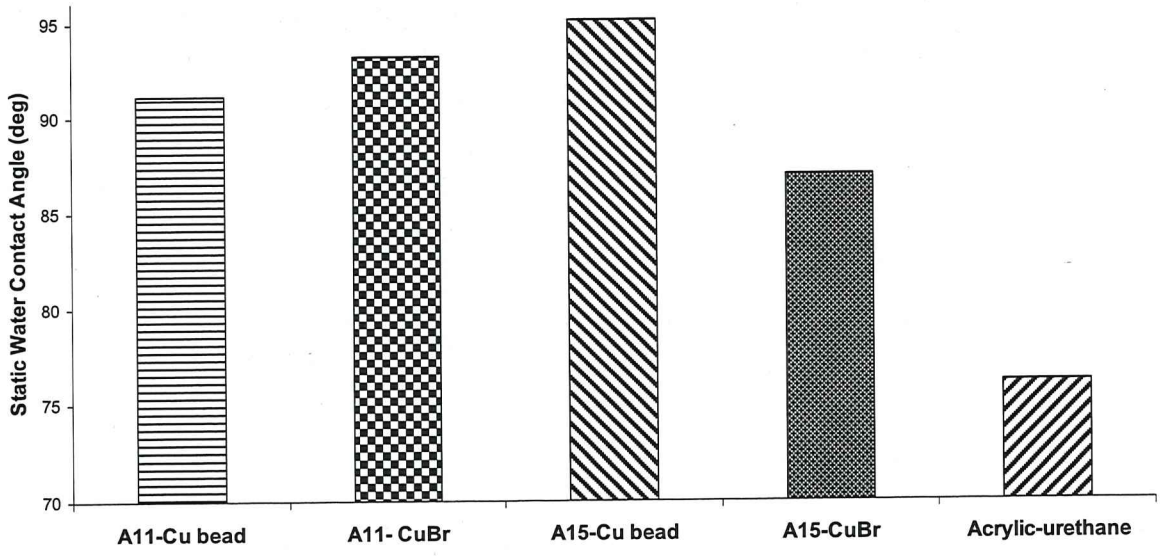

Figure 5.7. Static water contact angle of zwitterionic/amphiphilic polyurethane coatings and acrylic urethane control.

The water contact angles for all of the pentablock copolymer containing polyurethanes are higher than the acrylic-urethane control, indicating that the surface composition has been modified by the incorporation of the z/a pentablock copolymer.

The experimental coatings were subjected to the pseudo-barnacle adhesion test. In this test a metal stud is glued to the surface of the coating using an epoxy adhesive. After curing the force required to remove the stud from the surface is recorded. In Figure 5.8, the pseudo-barnacle adhesion (average force at release) vs. experimental and control coatings formulations is plotted. It is seen that all four zwitterionic/amphiphilic pentablock urethane coatings have very low average force of release, below 10N. The value of 10N for the experimental coatings shows that the surfaces have very low surface energy which suggests that the siloxane component of the formulation contributed to the low initial force of release.

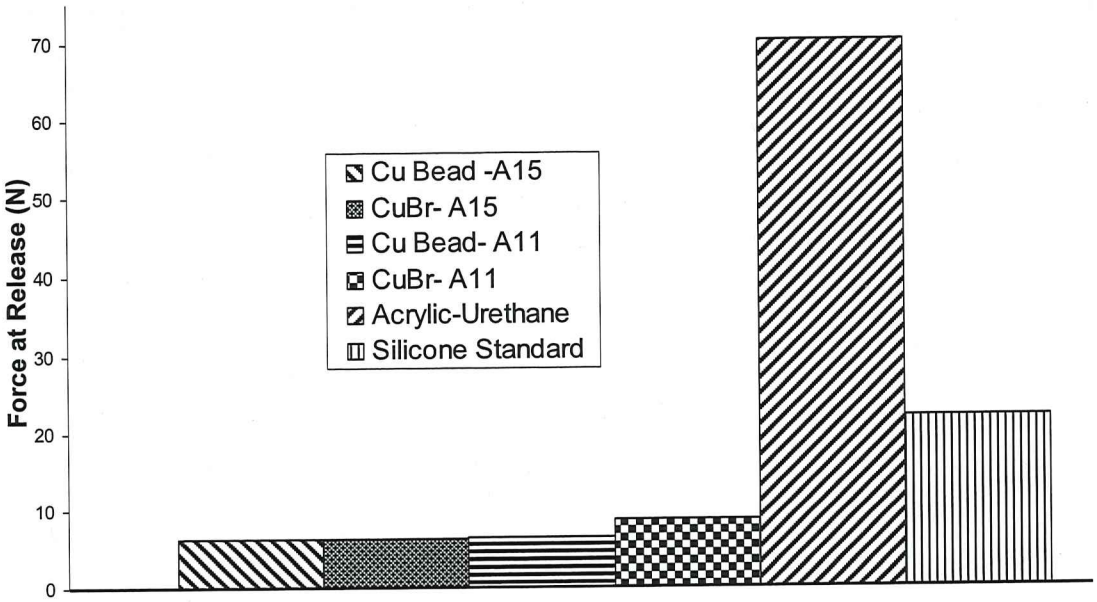

Figure 5.8. Pseudo-barnacle adhesion results of zwitterionic/amphiphilic polyurethane experimental coatings, acrylic urethane control coating, and silicone standard.

However, the silicone standard used in this study had an initial force of release of 20N, nearly twice the force of the z/a pentablock polyurethane experimental coatings. In addition, the acrylic-polyurethane control coating had an initial force of release above 60N, which is consistent with values for coatings with higher surface energies. A slight trend seen is that as the molecular weight of the PDMS is increased (875 MW to 3000 MW) the force of release tend to decease. It is observed from the results that the ATRP amphiphilic macroinitiator and PDMS molecular weight do not have a significant effect on the initial pseudo-barnacle adhesion results.

Figure 5.9 shows the dynamic water contact angle (DWCA) of the z/a pentablock copolymer polyurethane coatings and the acrylic polyurethane control coating.

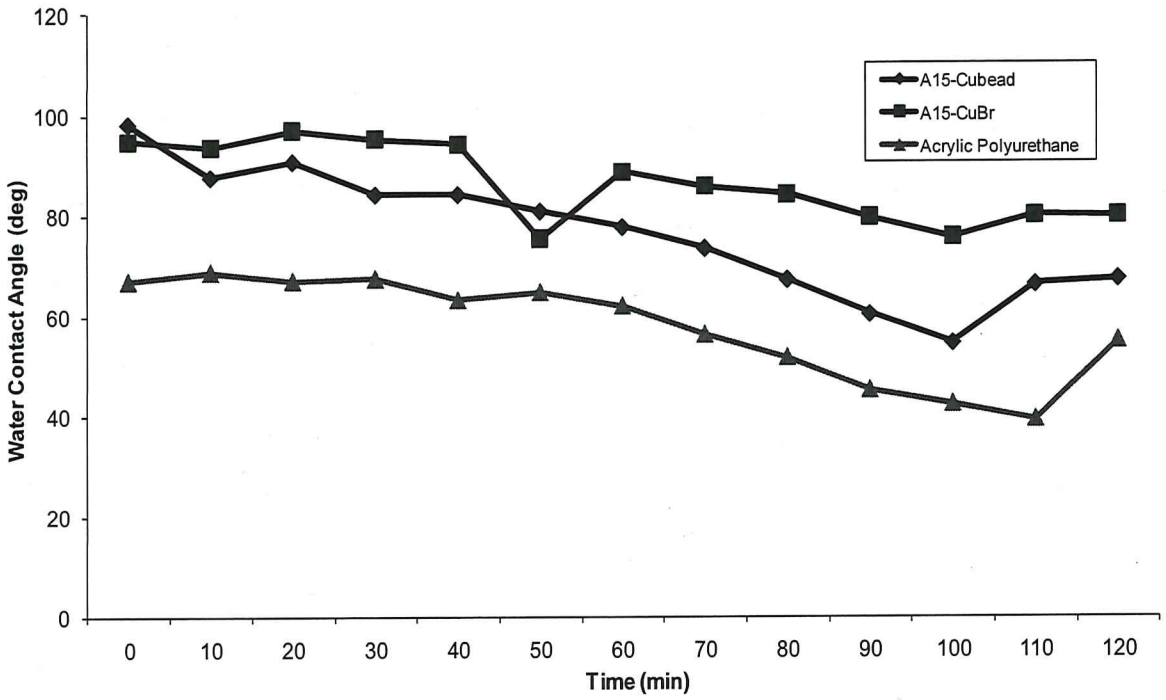

Figure 5.9. Dynamic Water Contact angle of zwitterionic/amphiphilic polyurethane coatings and acrylic polyurethane control.

Dynamic water contact angle is a general indicator of surface chemical and morphological stability and is known to be attributed to one of several effects such as surface roughness, chemical heterogeneity, surface deformation, surface configuration change, adsorption/desorption mechanisms, or some combination of these effects. In general, the dynamic water contact angle can be used as an indication of the degree of surface instability resulting from wetting of the surface. From the data in Figure 5.9, a very general trend of decreasing water contact angle over time can be seen for all experimental coatings. The DWCA data indicates that the water contact angle of the zwitterionic/amphiphilic pentablock copolymer-containing polyurethane coatings begins at a high value, indicating that the coating is initially hydrophobic as a result of the self-stratification of the z/a

pentablock containing PDMS migrating to the surface. The contact angle decreases during the experiment indicating that the hydrophilic segment of the z/a pentablock copolymer is switching with the PDMS segment at the surface as a result of being in contact with the water droplet. The polyurethane control coating was hydrophilic throughout the experiment which was expected. Overall, the z/a pentablock copolymer polyurethane coatings demonstrate surfaces with amphiphilic behavior.

Bacterial biofilm assays using marine bacteria are used as a screening tool to further characterize the coatings. Leachate toxicity was assessed by introducing the bacterium into overnight extracts (artificial sea water with nutrients) of each coating and evaluating growth after 24 hours via a crystal violet colorimetric assay. Growth in coating leachates was reported as an absorbance ratio (600 nm) to a growth control. A series of negative growth controls (medium + bacteria + triclosan) at three different concentrations were also included in the analysis. Figure 5.10 represents the leachate toxicity of the experimental coatings using the marine bacteria *C. lytica* after two weeks and four weeks of water immersion. Experimental coating 3 showed leachate toxicity after two weeks and four weeks, interestingly, the toxicity increased with longer preleach time. This trend was seen for experimental coatings 4 and 5 as well which showed some slight leachate toxicity after four weeks of water immersion. The leachate toxicity observed is likely due to residual copper catalyst from the synthesis of the z/a pentablock copolymer. Overall, most experimental coatings were similar to the growth control

after two weeks of preleaching. *C. lytica* biofilm retention analysis, illustrated in Figure 5.11, was assessed by a crystal violet colorimetric assay.

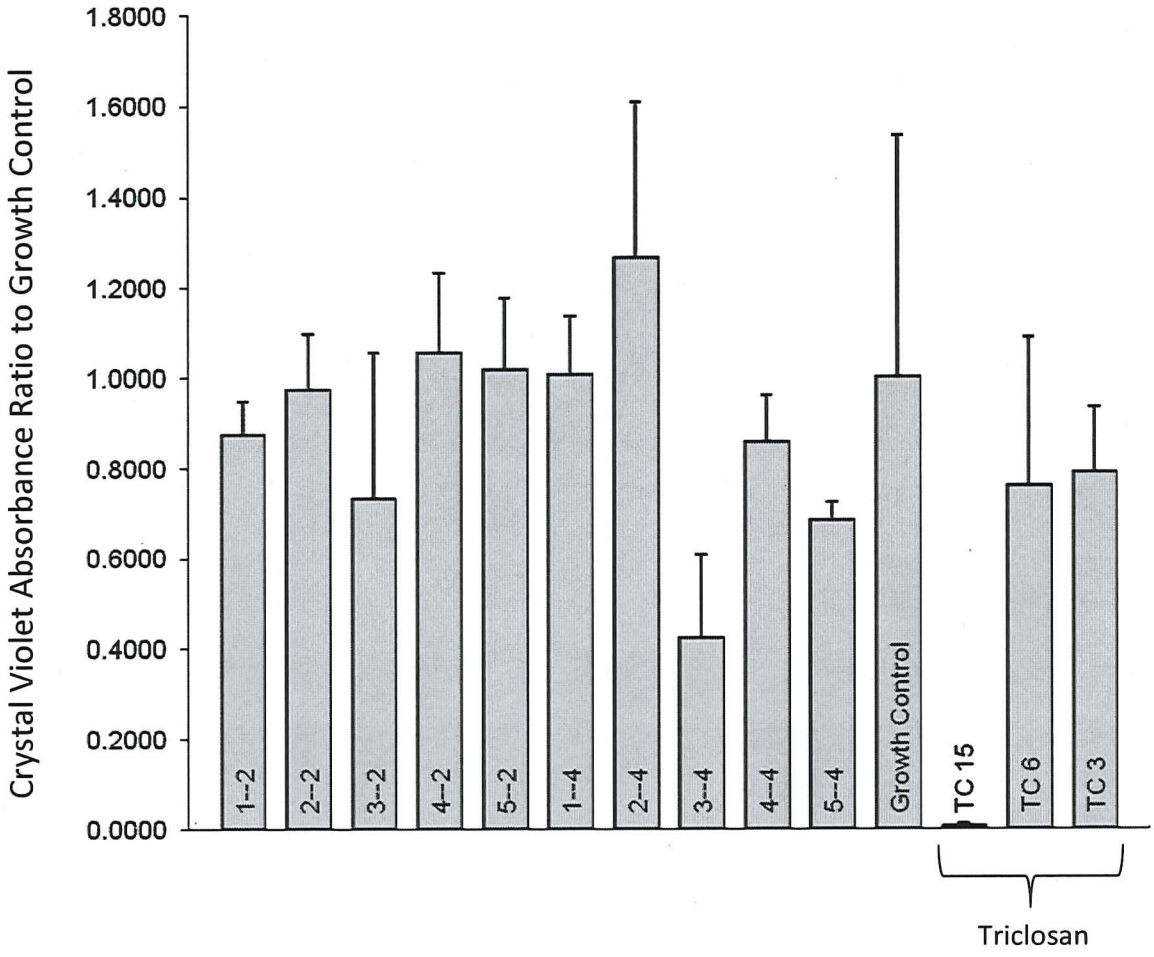

Figure 5.10. Leachate toxicity using *C .lytica* of zwitterionic/amphiphilic polyurethane coatings, polyurethane control and triclosan controls. Error bars represent one standard deviation of the mean.

A 5% suspension of *C. lytica* in ASW + nutrients (~10^7 cells.ml^{-1}) was prepared and 1ml was added to each well of the coating plate. Plates were incubated statically at 28°C for 24 hours to facilitate bacterial attachment and colonization. Plates were rinsed three times with DI water and stained with crystal

violet. Images were taken after staining, and then the crystal violet was extracted in 33% acetic acid and the resulting eluates were measured for absorbance at 600nm. Biofilm retention was reported as the mean absorbance value of three replicate samples. The absorbance value reported is directly proportional to the amount of biofilm retained on the coatings' surface. A series of additional control coatings were utilized in this study to gauge performance of experimental coatings. The control coating was Intersleek 700, a commercial fouling-release coating manufactured by International Paint and was represented by "700" in the bioassay figures. Intersleek 900, a commercial fouling-release coating manufactured by International Paint and was represented by "900" in the bioassay figures. Silastic T-2 and DC-4 are commercial silicone elastomers manufactured by Dow Corning, represented by T2 and DC-4, respectively in the bioassay figures. Polyurethane made from polycaprolactone and a polyisocyanate was represented by "PU" in the bioassay figures.

As seen in Figure 5.11, all coatings, with the exception of coating 4-4, were determined to retain less of the *C. lytica* biofilm, which was better or comparable to the commercial fouling-release coatings and silicone elastomer controls. In terms of the fouling process this is significant because it shows that the biofilm actually avoids, or deters, settlement on the surface of the experimental coatings, theoretically stalling or even stopping the microfouling stage (for marine organisms that need a conditioning layer to adhere) of the process and thus impeding continuation of the biofouling process on the experimental coatings surface.

Biofilm retraction was assessed by determining percent coverage calculations from digital images taken of each coating plate using an automated software tool. Biofilm retraction was reported as the mean percent coverage value of three replicate samples.

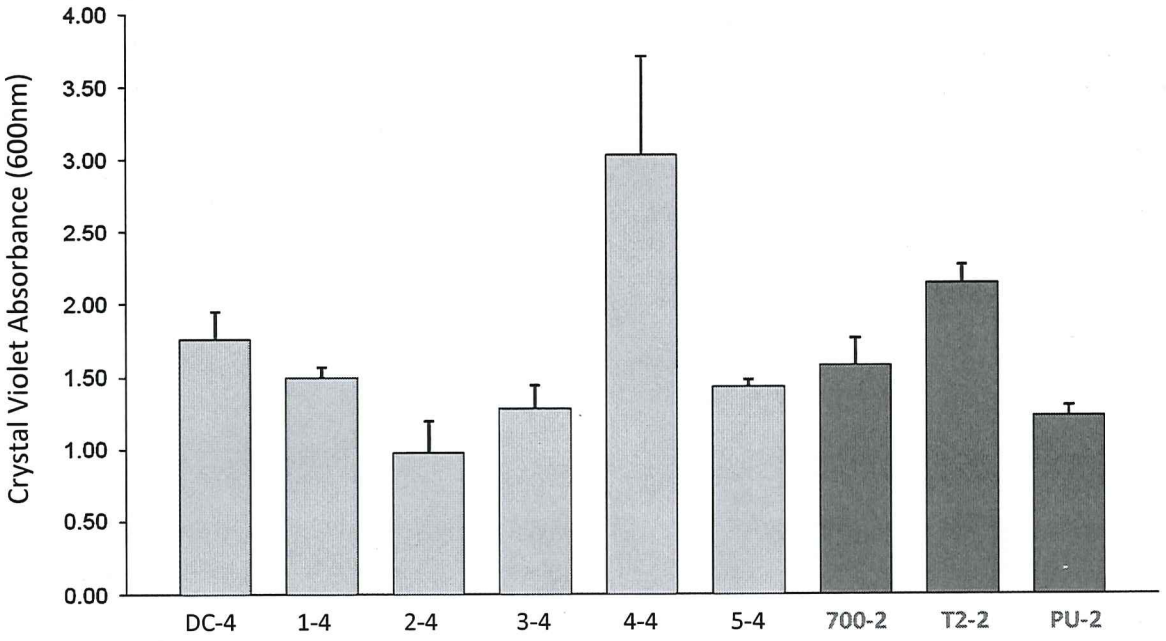

Figure 5.11. *C. lytica* biofilm retention of zwitterionic/amphiphilic polyurethane coatings, acrylic-polyurethane control, commercial fouling-release coatings, and silicone control coatings. Error bars represent one standard deviation of the mean.

Figure 5.12 depicts the biofilm retraction of the novel z/a pentablock polyurethane coatings and the control coatings. Experimental coating 4 could not be analyzed due to crystal violet staining of the coating. Experimental coating 2-4 showed biofilm retraction result of only 5% surface coverage, which shows that the biofilm does not want to wet or spread on the coating surface. Coating 1-4 showed 30% surface coverage and coating 3-4 showed about 60% surface

coverage, which was still better than the control coatings surface coverage which ranged from 95% to full surface coverage (100%).

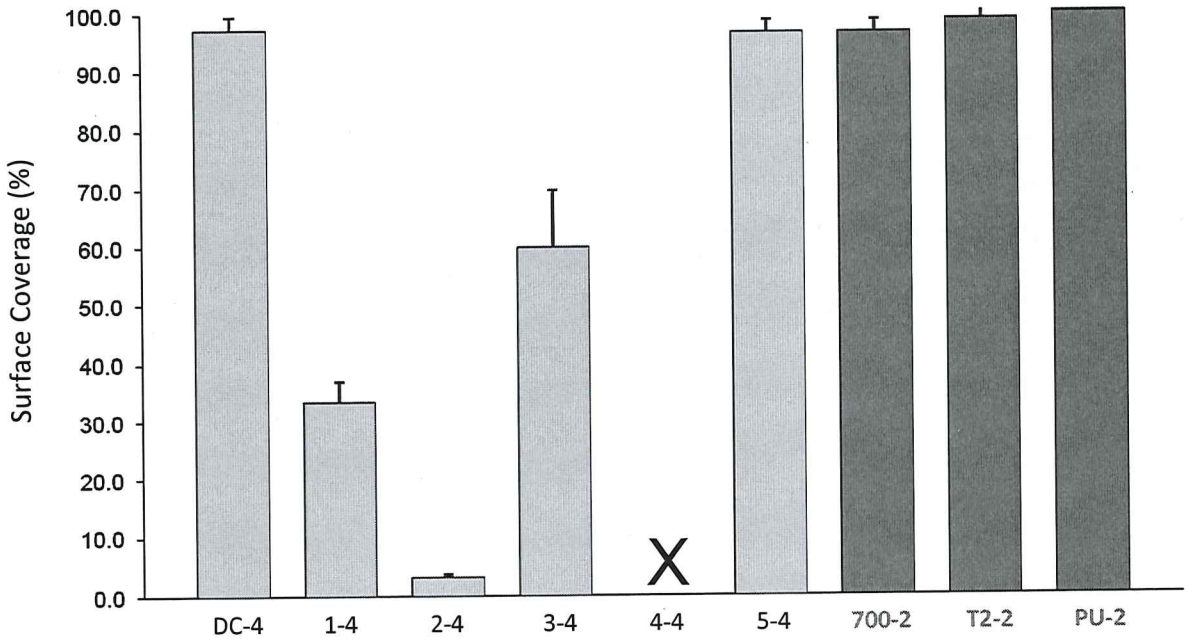

Figure 5.12. *C. lytica* biofilm retraction on zwitterionic/amphiphilic polyurethane coatings, acrylic-polyurethane control coating, commercial fouling-release coatings, and silicone standards. Error bars represent one standard deviation of the mean

Overall, the results indicate that the biofilm surface coverage on the experimental coatings are significantly less than that of the control coatings, indicating that the bacteria are not adhering or are adhering weakly to the z/a pentablock experimental coatings.

Figure 5.13 represents the leachate toxicity using the marine bacteria *H. pacifica* after two weeks and four weeks of water immersion. Experimental coatings 2-2, 3-2, and 4-2 showed leachate toxicity after two weeks of water

immersion. After four weeks of water immersion Coating 3 still showed significant slight leachate toxicity when compared to the growth control. As with the previous leachate assay, the leachate toxicity observed is likely due to residual copper catalyst from the synthesis of the z/a pentablock copolymer.

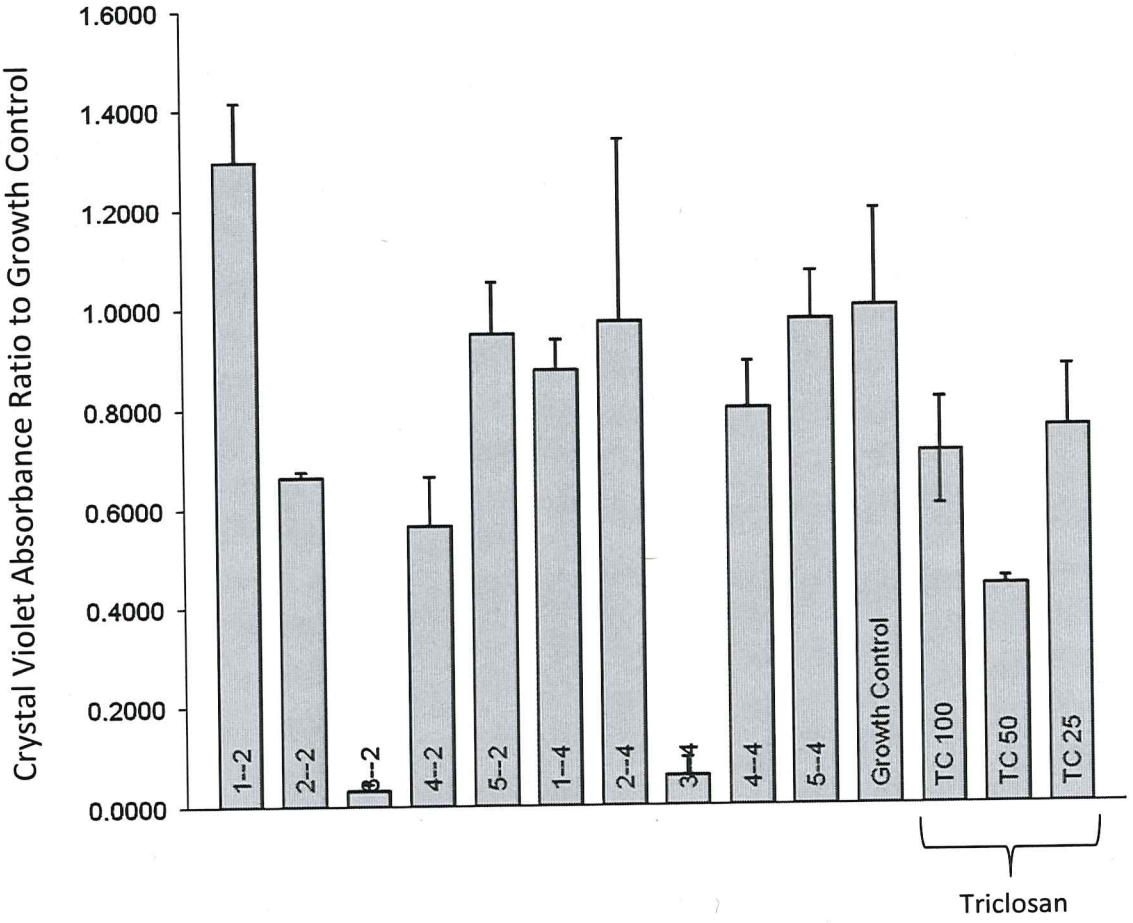

Figure 5.13. Leachate toxicity using *H. pacifica* of zwitterionic/amphiphilic polyurethane coatings, polyurethane control and triclosan controls. Error bars represent one standard deviation of the mean.

Biofilm retention analysis using marine bacteria, *H. pacifica* is shown in Figure 5.14. Z/a pentablock polyurethane coating 3 could not be analyzed due to crystal violet staining of the coating.

It can be observed in Figure 5.14 that the two week preleach retention results indicate that the amounts of biofilm on the z/a pentablock copolymer polyurethane coatings are similar or slightly less than that on the control coatings with the exception of coating 4-2.

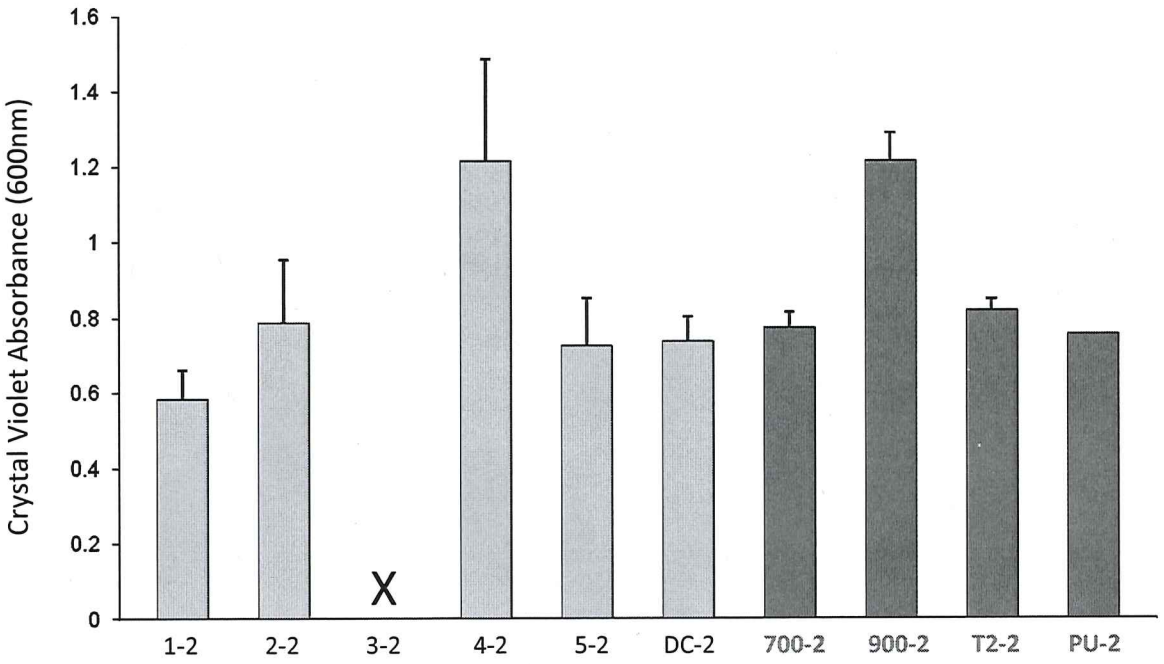

Figure 5.14. *H. pacifica* biofilm retention after two weeks of preleach of zwitterionic/amphiphilic Urethane coatings, acrylic-polyurethane control, commercial fouling-release coatings, commercial fouling-release coatings, and silicone control coatings. Error bars represent one standard deviation of the mean.

Experimental coatings 1 and 2 retained the least amount of biofilm compared to any of the experimental or control coatings. This low retention of biofilm on the surface of the novel coatings is indicative of non-fouling behavior attributed to the zwitterionic/amphiphilic nature of the coatings.

Figure 5.15 shows the four week preleach results for the *H. pacifica* biofilm retention indicating that the amounts of biofilm on the zwitterionic/amphiphilic

pentablock copolymer polyurethane coatings are similar or slightly less than that on the control coatings with the exception of coating 4.

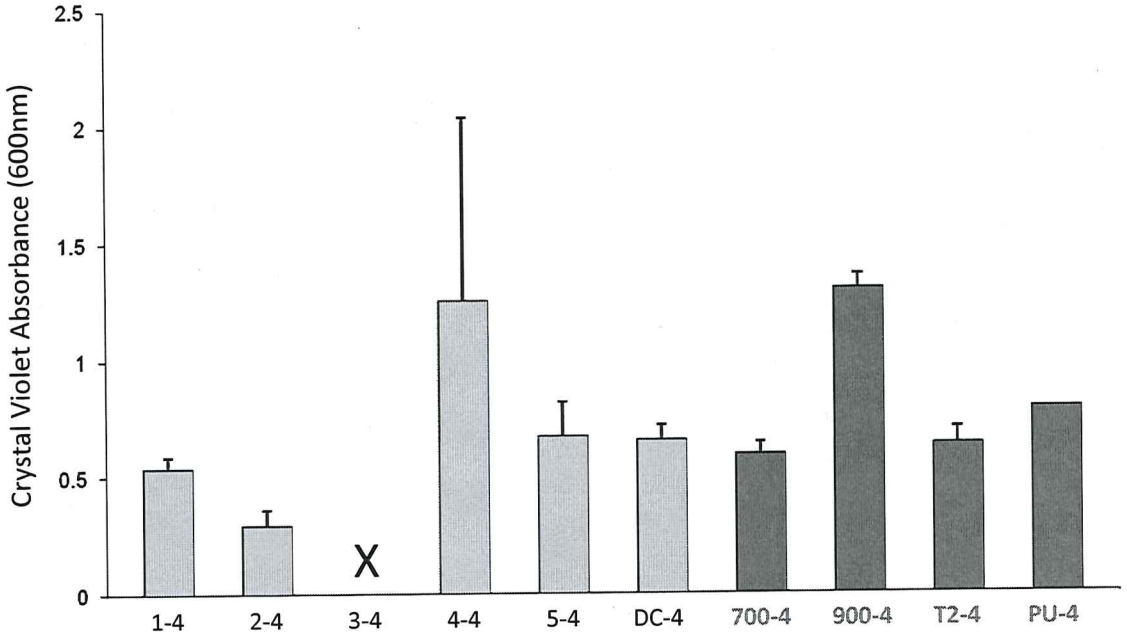

Figure 5.15. *H. pacifica* biofilm retention after four weeks of preleach of zwitterionic/amphiphilic polyurethane coatings, acrylic-polyurethane control, commercial fouling-release coatings, and silicone control coatings. Error bars represent one standard deviation of the mean.

Experimental coating 1-4 and 2-4 retained the least amount of biofilm compared to any of the experimental or control coatings. There was little change in the retention results when comparing two weeks preleach to 4 weeks preleach. The exception was experimental coating 2, which showed a decrease in biofilm retention when comparing Figure 5.14 to Figure 5.15.

Water jet adhesion of the *H. pacifica* biofilm was carried out after 24 hrs of bacterial biofilm growth. Each coating was jetted for 5 seconds at a pressure of 15 psi and then a new set of each coating was jetted at a pressure of 25 psi and

biofilm adhesion is represented by percent removal. In Figure 5.16, *H. pacifica* cell percent removal results for the coatings treated with a water jet pressure of 15 psi and 25 psi after two weeks preleach are shown. As previously reported in Chapter 3, *H. pacifica* had been known to adhere poorly to polyurethane.

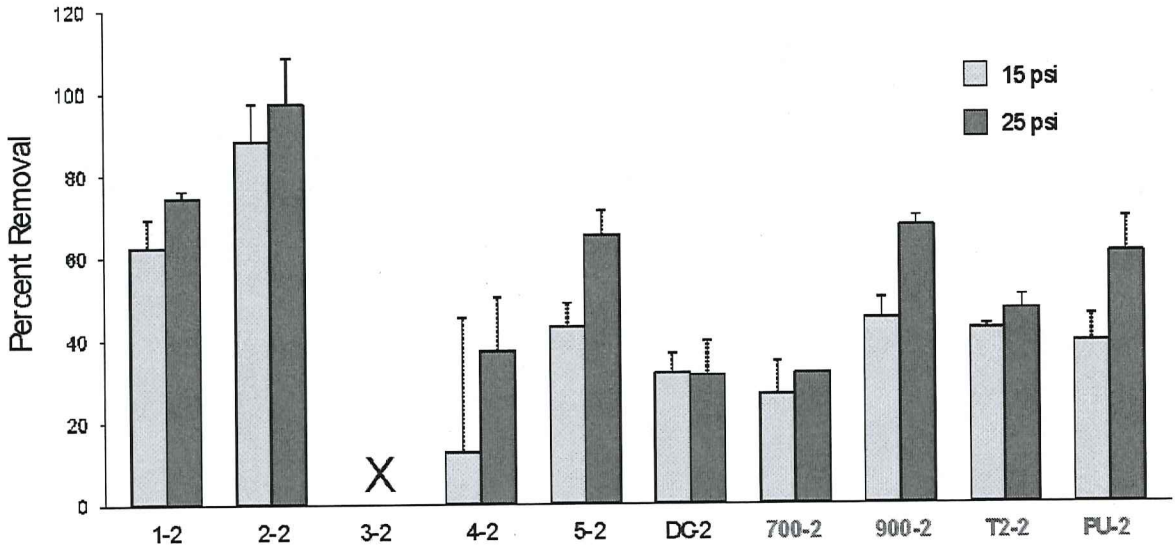

Figure 5.16. *H. pacifica* biofilm adhesion after two weeks preleach of Zwitterionic/amphiphilic polyurethane coatings, acrylic-polyurethane control, commercial fouling-release coatings, and silicone control coatings using water jet at 15 psi and 25 psi. Error bars represent one standard deviation of the mean.

After two weeks of water immersion, z/a pentablock copolymer polyurethane coatings 1 and 2 showed that the bacteria biofilm could be more easily removed than the control coatings. Experimental coating 1 showed approximately a 60% removal at the water jet pressure of 15 psi and 75% removal when the water jet pressure was increased to 25 psi. Experimental coating 2 showed removal of approximately 90% at 15 psi and almost 100% removal when the water jet pressure was increased to 25 psi. These results would indicate that the surface of

the coatings 1 and 2 are polyurethane-like since *H. pacifica* adhered weakly to the coatings surfaces. Coating 5, which is the acrylic polyurethane control had removal results similar to the control PU with removal of 40% at 15 psi and 60% at 25 psi water jet pressure. Overall, experimental coatings 1 and 2 preformed better than the control coatings after two weeks of preleach.

After four weeks of preleach the z/a pentablock copolymer polyurethane coatings were subjected to *H. pacifica* cell percent removal with a water jet pressure of 15 psi and 25 psi. Figure 5.17 depicts the experimental coatings results of the percent removal of *H. pacifica* after four weeks preleach. Experimental coatings 1 and 2 showed that the bacteria biofilm could be more easily removed than the control coatings. Experimental coating 1 showed approximately a 80% removal at the water jet pressure of 15 psi and 90% removal when the water jet pressure was increased to 25 psi. Experimental coating 2 showed removal of approximately 90% at 15 psi and 85% removal when the water jet pressure was increased to 25 psi. When comparing the results from two weeks preleach to four weeks preleach there was an increase in removal for experimental coating 1, but little change in percent removal for the other experimental coatings, as well as the control coatings. The removal results for coatings 1 and 2 would, once again indicate that the surface is PU-like since there was very high removal of *H. pacifica* biofilm at both 15 psi and 25 psi water jet pressure.

Overall, experimental coatings 1 and 2 performed better than the control coatings including the PU control, which indicates that experimental coatings formulated with z/a pentablock copolymers can successfully remove *H. pacifica* from the coatings surface.

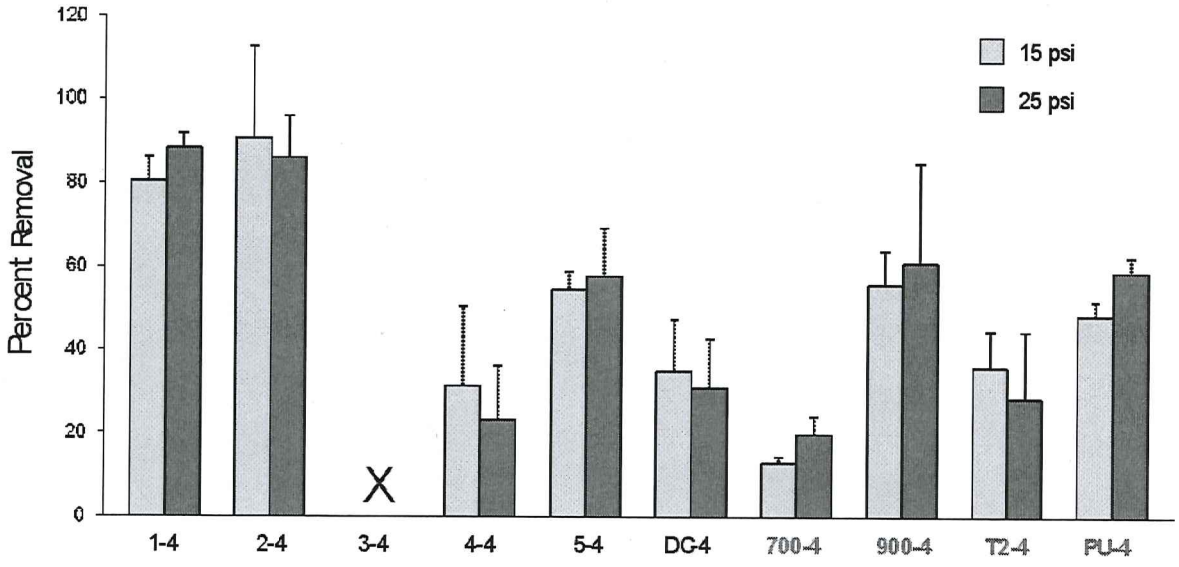

Figure 5.17. *H. pacifica* biofilm adhesion after four weeks preleach of zwitterionic/ amphiphilic polyurethane coatings, acrylic-polyurethane control, commercial fouling-release coatings and silicone control coatings using water jet at 15 psi and 25 psi. Error bars represent one standard deviation of the mean

Navicula incerta algal leachate toxicity was reported as a fluorescence ratio to a growth control. A series of negative growth controls which included triclosan was included in the analysis. Shown in Figure 5.18, experimental coatings 1, 2, and 4 showed no leachate toxicity after two weeks and four weeks of water immersion, indicated by the fluorescence ratio to the growth control having values at or higher than the growth control. However, coating 3 was leachate toxic after two and four weeks of water immersion. The toxicity of experimental coating 3 is

most likely due to residual copper catalyst from the atom transfer radical polymerization of the zwitterionic/amphiphilic pentablock copolymer.

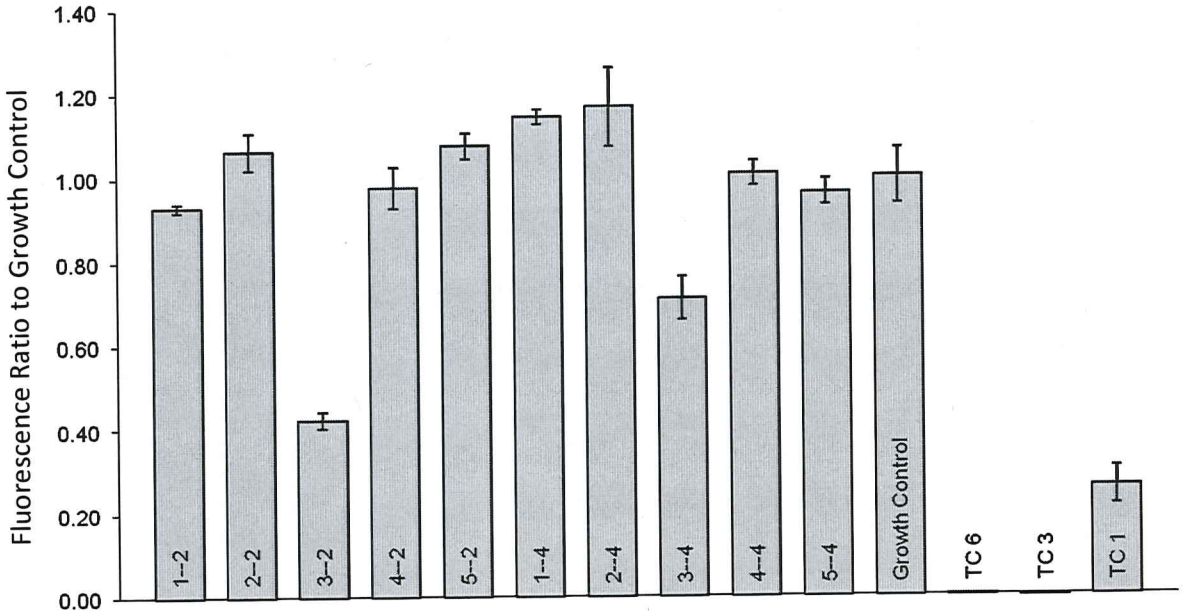

Figure 5.18. Leachate toxicity using *N. incerta* of Zwitterionic/amphiphilic polyurethane coatings, polyurethane control and triclosan controls. Error bars represent one standard deviation of the mean.

Figure 5.19 illustrates the *N. incerta* cell attachment on the experimental coatings after pleaching two weeks and four week of *N. incerta* algae assessed before water jet adhesion analysis. Algae were diluted to an OD of 0.03 at 660 nm in artificial sea water (ASW) supplemented with nutrients. 1 ml was added to each well of the plate and allowed to incubate statically for 2 hours (cell attachment). Algal cell attachment was measured by fluorescence measurement of DMSO extracts. Attachment was reported as fluorescence intensity (relative fluorescence units). The absorbance value reported is directly proportional to the amount of cell attachment on the coatings surface.

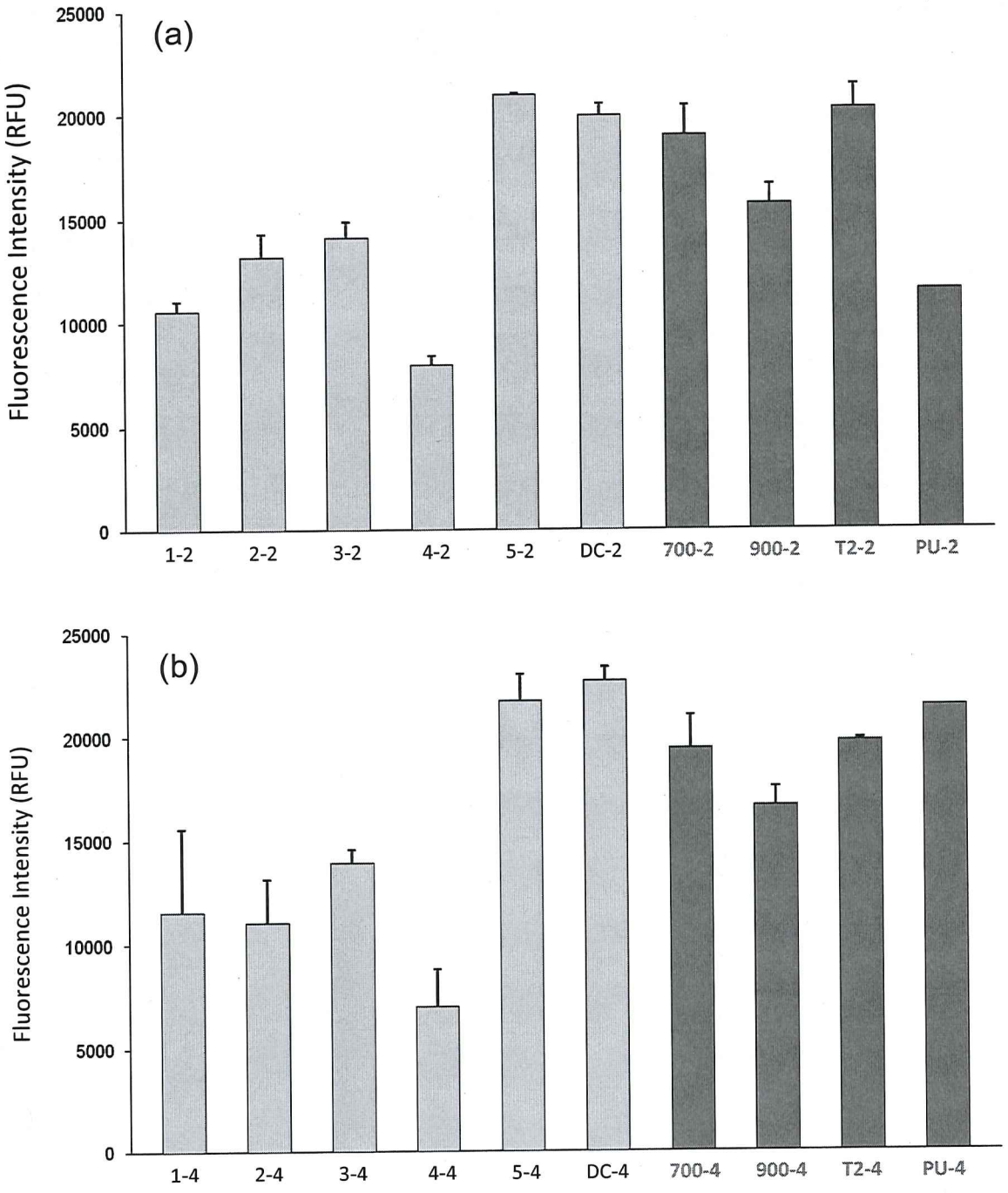

Figure 5.19. *N. incerta* cell attachment after two weeks (a) and four weeks (b) of preleach of Zwitterionic/amphiphilic polyurethane coatings, acrylic-polyurethane control commercial fouling-release coatings and silicone control coatings. Error bars represent one standard deviation of the mean.

A general trend shown In Figure 5.19 (a) was that the cell attachment of *N. incerta* after two weeks of water immersion is lower for the experimental coatings 1-2, 2-2, 3-2, and 4-2 than the control coatings after a two week water immersion. This observation indicates the experimental coatings have a surface that deters the attachment of the bacteria cells, which is consistent with zwitterionic and amphiphilic surfaces creating surface topography unsuitable for the proliferation and adsorption of marine microfoulers. The cell attachment results after four weeks of preleach, illustrated in Figure 5.19 (b), show the experimental coatings changed very little compared to the two week preleach results. Experimental coating 2-4 showed a lower cell attachment which could indicate that with longer water immersion the complex surface chemistry rearranged to form a surface with non-fouling behavior consistent with the nature of zwitterionic/amphiphilic surfaces. Overall, the low cell attachment on the surface of the experimental coatings indicates good correlation with previous studies that involved non-fouling coating surface behavior due to the nature of z/a material. Also, the experimental z/a coatings demonstrated excellent hydrolytic and surface stability since there was no dramatic change in the results for the cell attachment from two weeks to four weeks preleach.

Water jet adhesion was carried out after 2hrs of initial cell attachment. The coatings were jetted for 10 seconds at a pressure of 10 psi and then a new set of each coating was jetted at a pressure of 20 psi. Algal adhesion was reported as the percent removal for each pressure indicated above. Figure 5.20 illustrates *N. incerta* cell adhesion after two weeks (a) and four weeks (b) preleach of the z/a

polyurethane experimental coatings, polyurethane control, silicone elastomers control, and commercial fouling-release coatings using water jet at 10 psi and 20 psi.

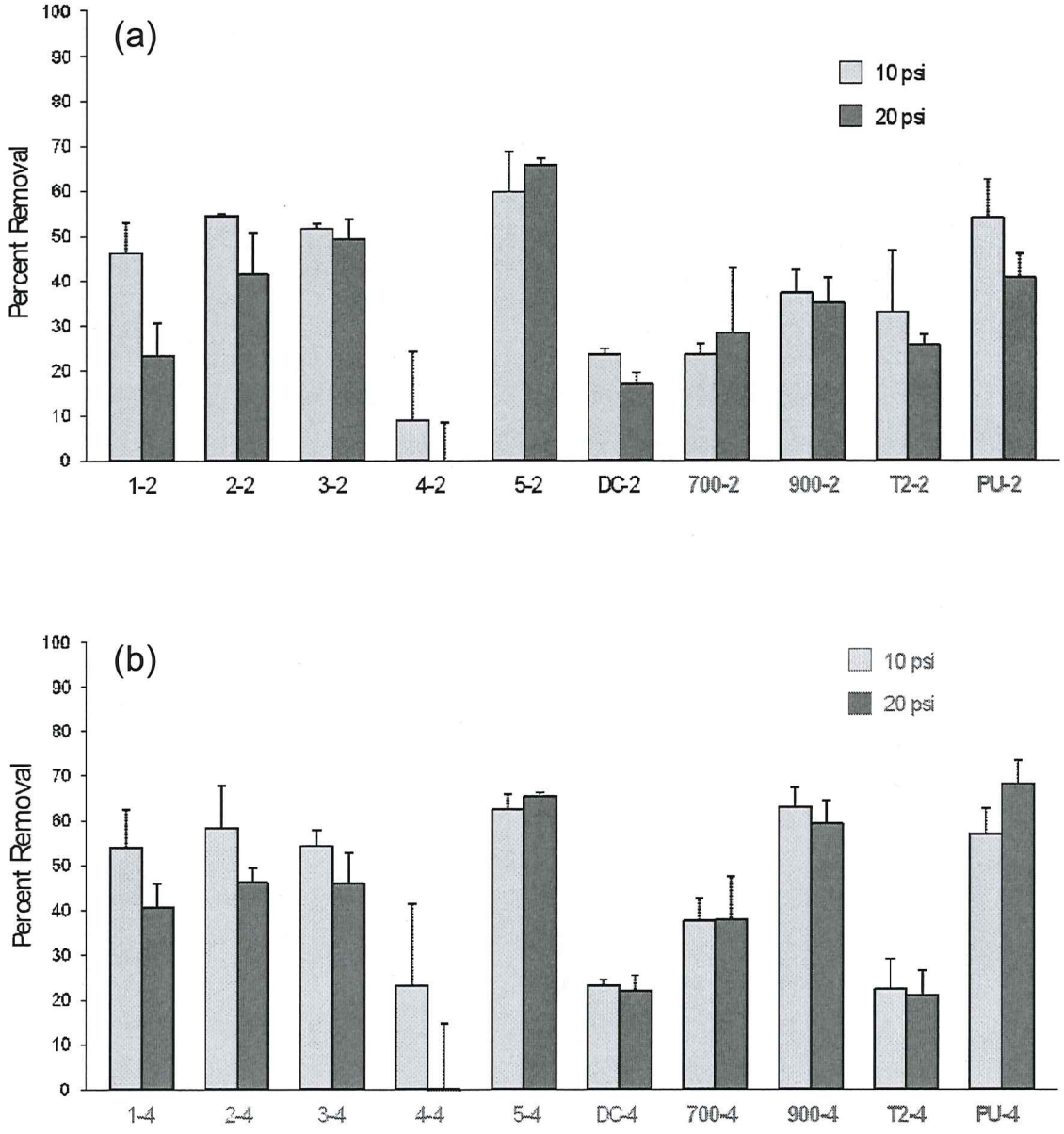

Figure 5.20. *N. incerta* cell adhesion after two weeks (a) and four weeks (b) preleach of zwitterionic/amphiphilic polyurethane coatings, acrylic-polyurethane control, commercial fouling-release coatings and silicone control coatings using water jet at 10 psi and 20 psi. Error bars represent one standard deviation of the mean.

Previous studies have shown that *N. incerta* attaches very well to PDMS and releases from polyurethane coatings. As a result, it is not surprising that the removal for polyurethane coatings 5-2 and PU-2 were good while the removal from the silicone control coatings and the commercial fouling-release coatings were poor. A trend observed after two weeks of water immersion, with the exception of 4-2, shows the z/a pentablock copolymer polyurethane coatings 1-2, 2-2, and 3-2 showed the biofilm removed better than the silicone control coatings, and approached the removal results of the polyurethane controls (5-2, PU-2). These results would indicate that after water immersion the coatings surfaces rearrange so that the z/a segments are at the surface and the PDMS segments are either buried into the surface or not as prevalent at the surface compared to the amount of z/a segments. The biofilm removal after four weeks of water immersion in Figure 5.20 (b) shows the experimental coatings continue to have removal better than the silicone standards and have removal comparable to the polyurethane control coatings. Commercial fouling-release coating, Intersleek 900, had much better removal after the four weeks of preleach which could be due to the surface chemistry of the coating. Overall, the majority of the experimental coatings performed well compared to the controls in the removal of *N. incerta* biofilms indicating a surface unsuitable for cell proliferation and adhesion.

Growth and release measurements of *Ulva* sporelings from the experimental coatings were conducted at the University of Birmingham, UK. The control coatings for the test were Intersleek 700 (IS 700) and Intersleek 900 (IS 900), Dow Corning Silastic-T2 (T2) and polyurethane (PU). Coatings were applied

to 24-well microtiter plates (one coating per plate). The sample coatings were pre-leached at NDSU for 14 days. All 24-well plates were equilibrated in artificial seawater for 2 h in Birmingham, after leachate collection, before the start of the *Ulva* experiment. The *Ulva* spore inoculum was adjusted to 0.05 OD at absorbance 660 nm (5 x 10^5 spores ml^{-1}). Spores settled on the plates were grown for 8 days inside an illuminated incubator at 18°C with a 16:8 light: dark cycle (photon flux density 44 $\mu mol \cdot m^{-2} \cdot s^{-1}$) with renewal of nutrients every 48 hours. After 8 days growth, the plates were sprayed at 18 kPa, 67 kPa, 111 kPa, and 152 kPa impact pressure with the water spin-jet.

Leachate toxicity was performed on the coatings prior to the *Ulva* sporelings release measurements. After leaching the coatings in distilled water for 48 h, 1 ml of artificial seawater was added to one row of each coating (6 replicates) and plates were gently shaken (60 movements/min) for 18 h. One ml of each leachate was then deposited in a well of untreated Costar® 24-well plates. To each well, 1 ml *Ulva* spore solution adjusted to 5 x 10^5 spores ml^{-1} in double strength enriched seawater medium was added. The plates were incubated for 2 h in darkness at room temperature before being transferred to an illuminated incubator at 18°C with a 16:8 light: dark cycle (photon flux density 44 $\mu mol \cdot m^{-2} \cdot s^{-1}$). After 7 days growth, the seawater medium was removed from the wells and the chlorophyll extracted from the attached biomass. The mean (6 replicates) percentage inhibition compared to a seawater control was calculated. The results of the leachate toxicity assay are depicted in Figure 4.19 in terms of sporeling inhibition. Results presented in Figure 5.21 show that there was some inhibition of the growth of *Ulva*

sporelings when cultured in leachate from a number of the coatings. Experimental coatings 2 and 3 showed the greatest percent inhibition of *Ulva* with values of 33% and 22%, respectively. This may be due to the zwitterionic and PEG-based components of the z/a pentablock copolymer rearranging at the surface, inhibiting the growth of the *Ulva* sporelings.

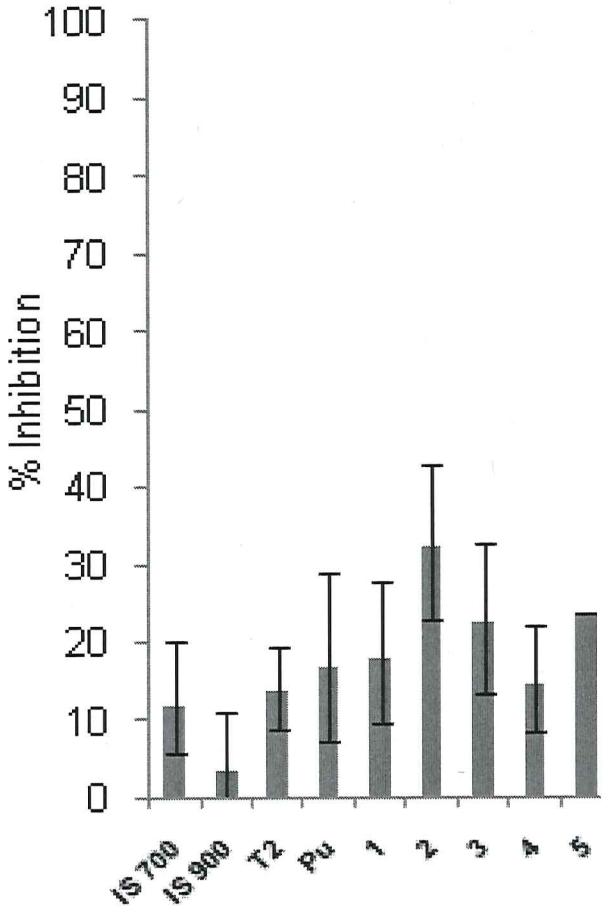

Figure 5.21. Percentage inhibition of *Ulva* sporeling growth in leachates collected over 18 hours. Each point is the mean of 6 replicates. Error bars show 95% confidence limits derived from arcsine transformed data.

Coatings were also only pre-leached at NDSU for 14 days rather than 30 days, which may account for the higher growth inhibition observed. Residual copper catalyst in the coating may also effect the growth of the *Ulva* sporelings.

The mean amount of biomass on the test surfaces after 8 days growth is depicted in Figure 5.22. The RFU values are directly proportional to biomass. Sporeling biomass was similar on most of the control and test coatings, but particularly lower on experimental coatings 3 and 4.

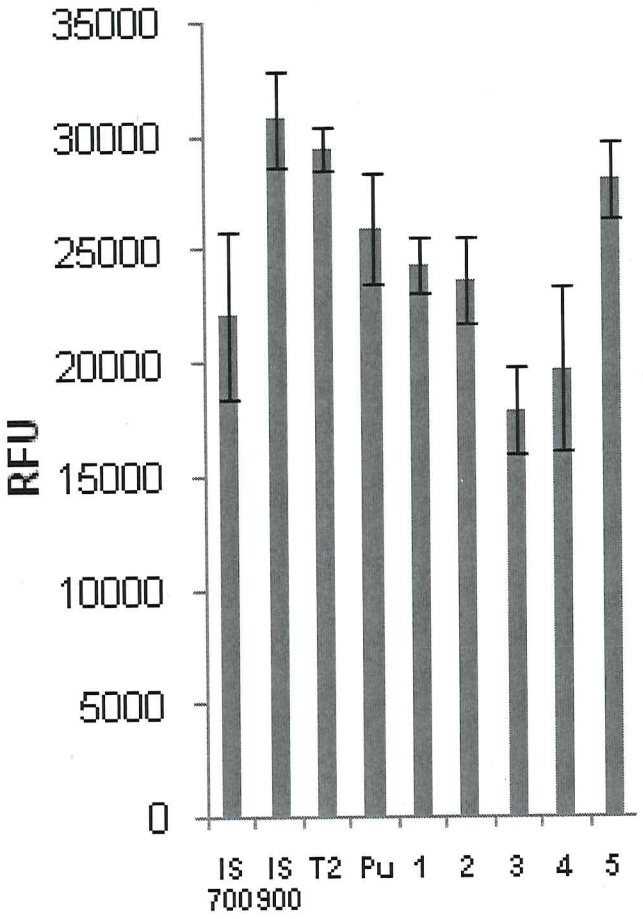

Figure 5.22. Biomass of *Ulva* sporeling before jetting presented as RFU values measured as extracted chlorophyll. Each point is the mean of 6 replicates. Error bars show 95% confidence limits.

Since experimental coatings 3 and 4 used lower molecular weight PDMS (Mn=875) in the synthesis of the amphiphilic macroinitiator, this may have allowed for the zwitterionic and PEG-based segments to rearrange at the surface of the experimental coatings and inhibit the proliferation of the sporelings. This observation can also correlate with coatings 1 and 2 as well, however, because the molecular weight of the PDMS was 3000 kDa there is a likely hood that the PDMS segment is more prominent at the surface when compared with the amount of zwitterionic and PEG-based segments based purely on the size of each segment. Overall, the z/a pentablock copolymer polyurethane coatings had biomass values equal to or better than the control coatings, including the commercial fouling-release coatings.

Percentage biomass removal after spin-jet washing at the pressures of 111 kPa (a) and152 kPa (b) impact pressure is illustrated in Figure 5.23. The removal results at 111 kPa (Figure 5.23(a)) showed that the experimental coatings didn't perform as well as the commercial fouling-release coatings. Experimental coating 2 performed the best of all experimental coatings with removal of 48%, but statically it was comparable to Intersleek 900 and T2. This is probably due to the PDMS segment of the pentablock copolymer being predominately on the surface of coating 2. Coatings 1 and 3 had statistically comparable removal of 30% and 28%, respectively. Coating 4 had the least amount of removal of about 5%, this is most likely due to poor coating integrity as it was noticed that the coatings had cracked. When the water jet pressure was increased to 152 kPa (Figure 5.23(b))

experimental coatings 1, 2, and 3 had removal statistically similar to Intersleek 700 with coating 3 having the greatest removal at 36%.

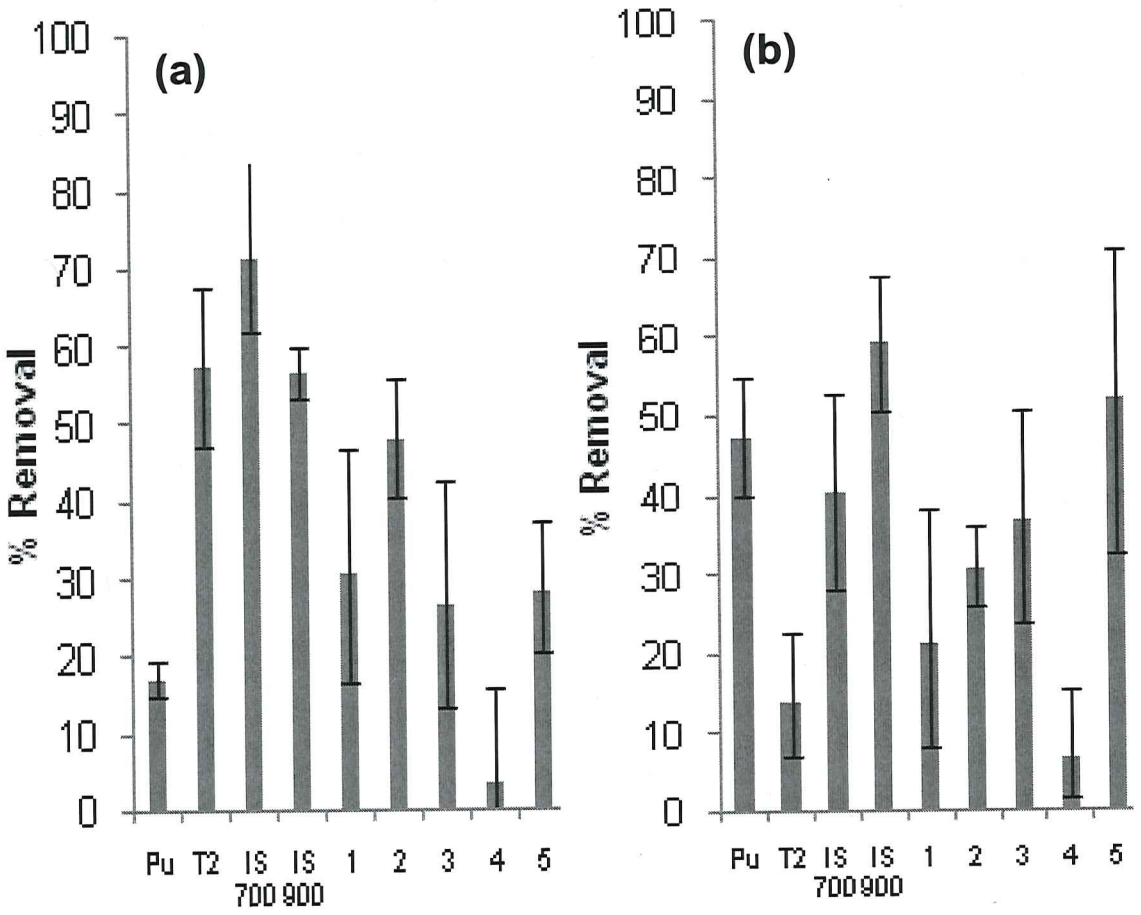

Figure 5.23. Percentage removal of *Ulva* sporelings after 8 days growth using an impact pressure of (a) 111 kPa and (b) 152 kPa with the spin-jet. Each point is the mean of 6 replicates. Error bars show 95% confidence limits derived from arcsine transformed data.

The polyurethane control as well as coating 5 showed an increase in removal with an increase in the water jet pressure with both having about 50% removal. Intersleek 900 showed the best removal at 152 kPa with a value of 60%

which was slightly higher than what was observed at 111 kPa. T2 showed a decrease in removal at 152 kPa which may be due to the lack of durability of the silicone elastomer when water jet washed. Overall, the experimental coatings statistically had removal better than T2 and similar removal to Intersleek 700 indicating that even with a complex surface of z/a segments, the coatings could remove *Ulva* sporelings effectively.

Figure 5.24 illustrates experimental coatings that were analyzed for the barnacle reattachment assay after two weeks and four weeks of water immersion and daily feeding of the barnacles with brine shrimp. A hand held digital force

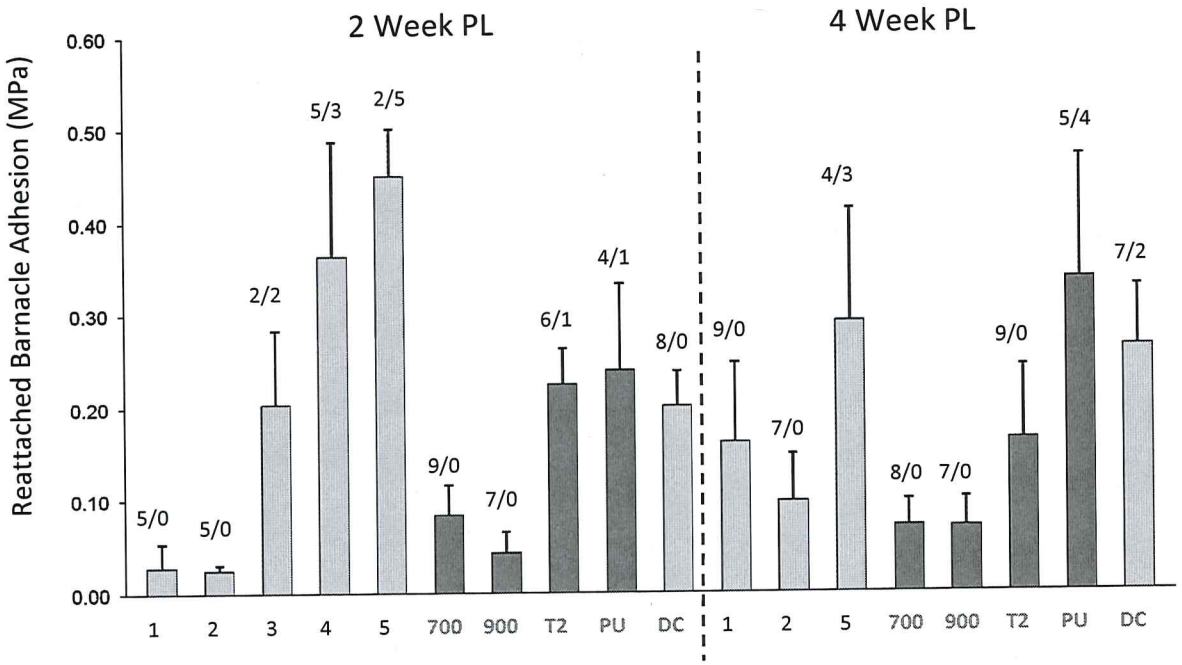

Figure 5.24. Reattachment barnacle adhesion of zwitterionic/amphiphilic urethane coatings, acrylic-polyurethane control, commercial fouling-release coatings and silicone control coatings. Error bars represent one standard deviation of the mean.

gauge was used to measure the adhesion strength of the barnacle by dividing the measured force of release for each barnacle by the basal area and reported in Megapascals (MPa).

Each data point is the mean value of nine individual barnacle measurements. The ratio above each data point equals the number of measured barnacles to the number of broken barnacles. Broken barnacles indicate that the barnacle shell or baseplate broke or fractured before failure of the barnacle adhesive to the coatings surface. This is typical for poor fouling-release surfaces such as polyurethanes. As shown in Figure 5.24, the experimental coatings have low values of barnacle adhesion after two weeks of preleach, with experimental coating 1 having a value of approximately 0.04 MPa and coating 2 having a value of 0.03 MPa. The values for coatings 1 and 2 are lower than the commercial fouling-release controls, Intersleek 700 and 900. This indicates that coatings 1 and 2 have surfaces that are not just PDMS, but likely contain some of the PEG-SBMA after two weeks of water immersion. However, after four weeks of water immersion the values for coatings 1 and 2 increased to 0.15 MPa and 0.10 MPa, respectively, which suggest that the coatings surfaces may be rearranging. Overall, the experimental coatings synthesized with higher molecular weight PDMS segments in the z/a pentablock copolymer (coatings 1 and 2) performed equal or better than the commercial fouling-release control coatings and better than the silicone elastomer controls.

5.4. Discussion

Experimental coatings designed with novel z/a pentablock copolymers were successfully formulated into polyurethane coatings. The static WCA results showed that all experimental coatings had hydrophobic surfaces. Taking the composition and the synthetic route of each experimental coating and comparing the performance results many correlations could be expressed. It was observed that formulation 2 (pentablock consisted of 3000 MW APT-PDMS and CuBr as the ATRP catalyst) had low biofilm retention and retraction for the marine bacteria *C. lytica* and *H. pacifica* as well as good biofilm removal for *H. pacifica* and *N. incerta*. Also, formulation 2 demonstrated good removal of *Ulva* sporelings compared to the commercial foul-release control coatings. Formulation 1 (pentablock consisted of 3000 MW APT-PDMS and copper beads as the ATRP catalyst) had similar results indicating that the surface properties using higher MW of the APT-PDMS on the amphiphilic block of the pentablock copolymer played a large role on performance properties of the experimental coating. Formulations 3 and 4 (pentablock consisted of 875 MW APT-PDMS and copper beads or CuBr as the ATRP catalyst, respectively) showed reasonable performance properties with the same bioassays, but not as good as the formulations with higher MW APT-PDMS concluding that the performance of the coatings may be more directed towards the MW of the PDMS.

5.5. Conclusions

In the present invention, the synthesis of a new amphiphilic macroinitiator via Michael Addition reaction of APT-PDMS and PEA-6 and subsequent reaction

with ATRP initiator produced the macroinitiator for the synthesis of a novel zwitterionic/amphiphilic pentablock copolymer. The copolymer was polymerized by ATRP using uniformly sized Cu beads as the transition metal for the reversible redox reaction (e.g.- Cu(0)/Cu(I)/Cu(II)), an amphiphilic macroinitiator and ligand, which provides the CRP properties of the reaction. The z/a pentablock copolymer was then reacted with acrylic polyol (80% butyl acrylate, 20% 2-hydroxyethyl acrylate) and an aliphatic isocyanate to form a crosslinked coating system. The incorporation of the protein and microfoulers resistance properties of sulfobetaine and PEG-based monomers and the low surface energy of PDMS compounds into a single copolymer make for an excellent candidate for a non-fouling marine coating. The data from all of the biological assays indicates that the novel coatings are able to resist fouling and have low fouling adhesion for the broad variety of fouling organisms tested. While fouling adhesion to silicone coatings is low for organisms such as barnacles and marine bacteria, adhesion by diatoms is known to be high, the experimental coatings . Thus, these novel coatings are able to resist fouling by marine bacteria, marine algae, and also barnacles.

5.6. References

1. Schultz, M. P. *Biofouling* **2007**, 23, 331-341.
2. Year, D. M.; Kiil, S.; Dam-Johansen, K. *Prog. Org. Coat.* **2004**, 50, 75-104.
3. Krishnan, S.; Weinman, C. J.; Ober, C. K. *J. Mater. Chem.* **2008**, 18, 3405-3413.
4. Chambers, L. D.; Stokes, K. R.; Walsh, F. C.; Wood, R. J. K. *Surf. Coat. Technol.* **2006**, 201, 3642-3652.

5. Genzer, J.; Efimenko, K. *Biofouling* **2006**, 22, 339-360.

6. Vladkova, T. *J. Univ. Chem. Technol. Metall.* **2007**, 42, 239-256.

7. Webster, D. C.; Chisholm, B. J.; Stafslien, S. J. *Biofouling* **2007**, 23, 179-192.

8. Ekin, A.; Webster, D. C. *J. Polym. Sci., Part A: Polym. Chem.* **2006**, 44(16), 4880-4894.

9. Ekin, A.; Webster, D. C.; Daniels, J. W.; Stafslien, S. J.; Casse, F.; Callow, J. A.; Callow, M. E. *J. Coatings Tech. & Res.* **2007**, 4(4),435-451.

10. Majumdar, P.; Webster, D. C. *Macromolecules* **2005**, 38, 5857-5859.

11. Majumdar, P.; Webster, D. C. *Polymer* **2006**, 47, 4172-4181.

12. Schultz, M. P.; Finaly, J. A.; Callow, M. E.; Callow, J. A. *Biofouling* **2003**, 19 (Supplement), 17-26.

13. Chaudhury, M. K.; Finlay, J. A.; Chung, J. Y.; Callow, M. E.; Callow, J. A. *Biofouling*, **2005** 21, 41-48.

14. Holland, R.; Dugtale, T. M.; Wetherbee, R., Brennan, A. B.; Finaly, J. A.; Callow, J. A.; Callow, M. E. *Biofouling* **2004**, 20, 323-329.

15. Terlizzi, A.; Conte, E.; Zupo, V.; Mazzella, L. *Biofouling*, **2000**, 15, 327-342.

16. Brady, R. F. Jr. *Prog Org. Coat.* **1999**, 35, 31-35.

17. Finlay, J. A.; Sitaraman, K,; Callow, M. A.; Callow, J. A.; Rong, D.; Asgill, N.; Wong, K.; Kramer, E. J.; Ober, C. K. *Langmuir*, **2008**, 24(20, 503-510.

18. Gudipati, C.S., Finlay, J.A., Callow, J.A., Callow, M.A., Wooley, K.L. *Langmuir*, **2005**, 21, 3044-3053.

19. Harris, J. M. *Poly(ethylene glycol) chemistry: biotechnical and biomedical applications;* Plenum Press: New York, 1992.

20. Zheng, J.; Li, L.; Jiang, S.; Chen, S. *Langmuir*, **2004**, 20, 8931-8938.

21. Horbett, T. A.; Brash, J. L. ACS Symposium Series 602; American Chemical Society: Washington D. C., 1995.

22. Ostuni, E.; Champman, R. G.; Holmlin, R. E.; Takayama, S.; Whitesides, G. M. *Langmuir,* **2001**, 17, 5605-5620.

23. Kane, R. S.; Deschatelets, P.; Whitesides, G. M. *Langmuir,* **2003**, 19, 2388-2391.

24. Iwasaki, Y.; Ishihara, K. *Anal. Bioanal. Chem.* **2005**, 381, 534-546.

25. Senaratne, W.; Andruzzi, L.; Ober, C. K. *Biomacromolecules*, **2005**, 6, 2427-2448.

26. Zheng, J.; Li, L.; Jiang, S.; Chen, S. *Langmuir*, **2004**, 20, 8931-8938.

27. Li, L.; Chen, S.; Zheng, J.; Ratner, B.; Jiang, S. *J. Phys. Phys. B* **2005**, 109, 2934-2941.

28. Zheng, J.; Li, L.; Tsao, H. K.; Sheng, Y. J.; Chen, S.; Jiang, S. *Biophys. J.* **2005**, 89, 158-166.

29. Zhang, Z.; Chen, S.; Chang, Y.; Jiang, S. *J. Phys. Chem. B* **2006**, 110, 10799-10804.

30. Chang, Y.; Shengfu, C.; Zhang, Z.; Jiang, S. *Langmuir*, **2006**, 22, 2222-2226.

31. Cheng, G.; Zhang, Z.; Shengfu, C.; Bryers, J.D.; Jiang, S. *Biomaterials*, **2007**, 28, 4192-4199.

32. Chen, S.; Zheng, J..; Li, L.; Jiang, S. *J. Am. Chem. Soc.* **2005**, 127, 14473-14478.

33. Lewis, A. L. *Colloids Surf., B* **2000**, 18, 261-275.

34. Chang, Y.; Shengfu, C.; Yu, Q; Zhang, Z.; Bernards, M; Jiang, S. *Biomacromolecules* **2007**, 8, 122-127.

35. Cho, W. K.; Kong, B.; Choi, I. S. *Langmuir* **2007**, 23, 5678-5682.

36. West, S. L.; Salavage, J. P.; Lobb, E. J.; Armes, S. P.; Billingham, N. C.; Lewis, A. L.; Hanoln, G. W.; Llyod, A. W. *Biomaterials* **2004**, 25, 1195-1204.

37. Zheng, Z.; Chao, T.; Chen, S.; Jiang, S. *Langmuir* **2006**, 22, 10072-10077.

38. Zheng, Z.; Finlay, J. A.; Wang, L.; Gao, Y.; Callow, J. A.; Callow, M. E.; Jiang, S. *Langmuir* **2009**, 25(23), 13516–13521.

39. Lowe, A. B.; McCormick, C. L. *Chem. Rev.* **2002**, 102, 4177.

40. Walbridge, D. J. *Prog.Org. Coat.* **1996**, 28(3), 155-159.

41. Webster, D. C.; Bennett, J.; Kuebler, S.; Kossuth, M. B.; Jonasdottir, S. *JCT Coatings Tech.* **2004**, 1, 34-39.

42. Webster, D. C. *JCT Coatings Tech.* **2005**, 2, 24-29.

43. Pieper, R. J. PhD. Dissertation, Chapter 3, North Dakota State University, 2010.

44. Michael, A. *J. Prakt. Chem.* **1887**, 35, 379.

45. Bergmann, E. D.; Gingberg, D.; Pappo, R. *Org. React.,* **1959**, 10, 179.

46. Lowry, T. H.; Richardson, K. S. *Mechanism and theory in organic chemistry 3rd ed.* New York: Harper& Row Publishers**1987**, 177-183.

47. Owens, D.K.; Wendt, R.C. *Journal of Applied Polymer Science* **1969**, 13 (8), 1741-7.

48. Chisholm, B.J.; Webster, D.C.; Bennett, J.W.; Berry, M.; Christianson D.A.; Kim, J.; Mayo, B.; Gubbins, N.J. *Rev. Sci. Instr.* ***2007,*** **78**, 072213.

49. Stafslien, S.J.; Daniels, J.; Mayo, B,; Christianson, D.; Chisholm, B.; Ekin, A.; Webster, D.C.; Swain, G. *Biofouling* **2007**, 23(1/2), 45-54.

50. Cassé, F.; Ribeiro, E.; Ekin, A.; Webster, D.C.; Callow, J.A.; Callow, M.E. *Biofouling* **2007**, 23 (3/4), 179-192.

51. Kamigaito, M.; Ando, T.; Sawamoto, M. *Chem. Rev.*, **2001**, 101(12), 3689-3745.

52. Braunecker, W.A., Matyjaszewski, K. *Prog. Polym. Sci.*, **2007**, 32(1), 93-146.

53. Matyjaszewski, K. *Prog. Polym. Sci.*, **2005**, 30(8-9), 858-875.

54. Matyjaszewski, K., Xia, J. *Chem. Rev.*, **2001**, 101(9), 2921-2990.

55. Coessens, V., Pintauer, T., Matyjaszewski, K. *Prog. Polym. Sci.*, **2001**, 26(3), 337-377.

56. Percec, V., Gulishvili, T., Ladislaw, J.S., Wistrand, A., Stjernadahl, A., Sienkowska, M.J., Monteiro, M.J., Sahoo, S. *J. of Am. Chem. Soc.*, **2006**, 128, 14156-14165.

57. Percec, V., Gulishvili, T., Popov, A.V. *Journal of Polymer Science, Part A: Polymer Chemistry,* **2005**, 43(9), 1948-1954.

58. Percec, V., Gulishvili, T., Popov, A.V., Ramirez-Castillo, E., Hinojosa-Falcon, L.A. *Journal of Polymer Science, Part A: Polymer Chemistry*, **2005**, 43(8), 1660-1669.

59. Johnson, R.M., Ng, C., C.C.M., Fraser, C.L. *Macromol.* **2000**, 33(23), 8618-8628.

60. Nasrullah, M.J., Sonalkar, V.V., Koralage, T., Webster, D.C. *Polymer Preprints*, **2008**, 49(2), 113-114.

CHAPTER 6. OVERALL CONCLUSIONS

The overall goal of the work reported in this dissertation was to address the development of novel non-toxic, non-leaching, and durable fouling-release coatings systems. The exploration of numerous variables involved in the design of novel crosslinked siloxane-polyurethane, amphiphilic-polyurethane, and zwitterionic/amphiphilic coatings were carried out using combinatorial and high throughput methods.

In Chapter 2, the design, synthesis via batch and semi-batch solution free radical polymerization and characterization of acrylic polymers using combinatorial high-throughput and automated parallel reactor methods was explored. With the use of the Chemspeed Autoplant 100™ for the polymerization, variations in process parameters, i.e. – reaction temperature, rate of monomer and initiator addition, percent solvent, etc were conducted. Details of the methodology were discussed with respect to the process of writing the program for the synthesis to carrying out the syntheses with the automated reactor system. It was demonstrated that acrylic polyols can be synthesized by free radical polymerization with combinatorial high-throughput and automated parallel reactor system and that there was good correlation among the replicates. The progress of the polymerization could be followed by sampling the reactor contents periodically, providing valuable information regarding conversion and molecular weight as a function of time. The acrylic polyols were characterized by R-GPC for molecular weight and polydispersity information, DSC was used for glass transition

temperature data, and percent solids and percent conversion was used for tracking completion of the reaction.

In Chapter 3, the objective was to explore the effect of variations in the bulk properties on the surface and fouling-release properties of the siloxane-polyurethane coating system. An acrylic polyol library of systematically varying composition was synthesized, characterized, and formulated into a siloxane-acrylic-polyurethane coating. The coatings were screened for key properties to determine if there were significant trends. The T_g data showed that the bulk properties of the coatings varied independently of the surface properties. The contact angle data showed evidence that the acrylic-polyurethane coatings went from a hydrophilic surface to a hydrophobic surface when the PDMS was incorporated into the polyurethane formulation. Key laboratory screening properties were surface energy and pseudobarnacle pull-off adhesion. Coatings were also subjected to laboratory screening using two important marine fouling algae, a diatom *Navicula* and sporelings (young plants) of the green seaweed *Ulva*. In addition, the siloxane acrylic-polyurethane coatings were also screened using several assays developed to challenge the coatings with marine bacteria. Coatings that were based on a low T_g polyol containing butyl acrylate and 20 percent hydroxyethyl acrylate formed siloxane acrylic-polyurethane coatings having low bioadhesion with respect to *Ulva* spores.

In Chapter 4, a novel approach to the design of amphiphilic polyurethane crosslinked coatings was explored using combinatorial and high throughput methods. A library of 24 amphiphilic PDMS/ PEG copolymers were synthesized to

systematically explore the compositional space by adjusting the molecular weight of the PDMS and the PEG blocks. The amphiphilic copolymers were characterized and formulated into a crosslinked polyurethane coatings system. The key properties screened were surface energy, determined by contact angle measurements using water and methylene iodide and dynamic water contact angle (initial and after 30 days of water immersion), and pseudo-barnacle adhesion properties. Coatings were generally stable and showed an increase in water contact angle following water immersion. AFM imaging showed the majority of the coatings contained micro tracks (ripple-like) formations on the surface. These coatings were also evaluated against several marine bacteria (*H. pacifica, C. lytica*), barnacle reattachment (*A. amphitrite)*, diatom *N. incerta* bioassays, and *Ulva* sporelings. It was reported that the coatings formulated with higher molecular weight PDMS performed better or comparable to the commercial fouling-release coatings for the marine bacteria, diatom, and *Ulva* sporeling assays, especially using lower water jet pressure. These 24 amphiphilic polyurethane coatings could be useful for possible marine application.

In Chapter 5, the synthesis of a new amphiphilic macroinitiator via Michael Addition reaction of APT-PDMS and PEA-6 and subsequent reaction with ATRP initiator produced the macroinitiator for the synthesis of a novel zwitterionic/ amphiphilic penta-block copolymer. The copolymer was polymerized by ATRP using uniformly sized Cu beads as the transition metal for the reversible redox reaction (e.g.- Cu(0)/Cu(I)/Cu(II)), an amphiphilic macroinitiator and ligand, which provides the controlled radical polymerization properties of the reaction. The

penta-block copolymer was then reacted with acrylic polyol (80% butyl acrylate, 20% 2-hydroxyethyl acrylate) and an aliphatic isocyanate to form a crosslinked coating system. The incorporation of the protein-resistance properties of sulfobetaine and poly(ethylene glycol) compounds and the low surface energy of PDMS compounds into a single copolymer made for an excellent candidate for a non-fouling marine coating. The data from all of the biological assays indicates that the novel coatings were able to resist fouling and had low fouling adhesion for the broad variety of fouling organisms tested. These novel coatings were able to resist fouling by marine bacteria, marine algae, and also barnacles and could be useful as a non-toxic, non-leaching fouling-release coating.

CHAPTER 7. FUTURE WORK

A lot of progress was made on the development of fouling-release coatings for marine applications. Novel crosslinked siloxane-polyurethane, amphiphilic-polyurethane, and zwitterionic/amphiphilic coatings were designed, successfully formulated, and performance properties were investigated against several bioassays. Even though the novel fouling-release coatings performed well, future work can be done.

In Chapter 3 of this dissertation, fouling-release coatings prepared from 10K molecular weight 3-aminopropyl poly(dimethyl siloxane) oligomers (APT-PDMS), acrylic polyols consisting of different ratios of butyl acrylate, butyl methacrylate, and 2-hydroxy acrylate and aliphatic polyisocyanate HDT were studied in detail. It will be interesting to study the effect of coating performance using various terminated PDMS with this coating system such as hydroxylalkyl or dihydroxyalkyl carbamate terminated PDMS or hydride terminated PDMS macromers resulting in brush-like structures when reacted with organic molecules that have 2-3 allyl groups and hydroxyl groups. An additional direction in future research in this coating system can be the incorporation of silicone oil. The addition of the silicone oil to this siloxane-urethane coating will produce a dynamic surface by slowly leaching silicone oil while maintaining good adhesion to the primer, superior mechanical properties, and durability, solving the problems often associated with primarily using silicone oil.

In Chapter 4, the amphiphilic coating composition consisted of APT-PDMS and PEO was studied in detail. However, follow up studies are needed which

would help understand the system better. Aliphatic polyisocyanate HDT was using as the isocyanate crosslinker in all experiments described in Chapter 4. It will be interesting to study the effect of different types of isocyanate crosslinkers on the coating system and the possible formation of a mircotopographical surface. In addition, future research can adjust the weight percent of the amphiphilic copolymer in the coating formulation to study the effect on coating performance.

In Chapter 5, there are many studies which will make it more complete. The current coating formulation uses sulfobetaine as the zwitterionic component, APT-PDMS as the hydrophobic component and poly(ethylene oxide) (PEO) as the hydrophilic component. More design space is needed to be explored in the synthesis of the zwitterionic/amphiphilic pentablock copolymer (z/a) considering different types of zwitterionic monomers such as carboxy- or phospho-betaine, molecular weight of APT-PDMS block, and molecular weight of PEO block. During formulation with these copolymers, studying the effect of using different polyols such as polyesters, polyethers and polycarbonates, as well as, different polyisocyanates such as aromatic isocyanate and cycloaliphatic isocyanate will be useful. In addition, studying the effects of the weight percent of the z/a component in the coating composition will also be useful.

It would also be beneficial to employ surface characterization techniques to better understand the surfaces of these novel coatings. Under

water Atomic Force Microscopy (AFM) could be used to observe the effects of water immersion on possible surface rearrangements, where these results could be compared to the common AFM technique in air. Other techniques that could

be used to study topographical and morphological characterization are X-ray Photoelectron Spectroscopy (XPS) and Scanning Electron Microscopy (SEM). With these techniques, chemical composition of the surface could be mapped out as well as patterns and textures in high resolution.